NASA CONTRACTOR REPORT 166258

(NASA-CR-166258) STUDY OF VTOL IN GROUND-EFFECT FLOW FIELD INCLUDING TEMPERATURE EFFECT Final Report (Grumman Aerospace Corp.) 179 p HC A09/MF A01 CSCL 01A G3/01

N82-25170

Unclas 28025

# STUDY OF VTOL IN-GROUND-EFFECT FLOW FIELD INCLUDING TEMPERATURE EFFECT

W.G. Hill
R.C. Jenkins
S.G. Kalemaris
M.J. Siclari

CONTRACT NAS2- 10645
April 1982

NASA

NASA CONTRACTOR REPORT 166258

# STUDY OF VTOL IN-GROUND-EFFECT FLOW FIELD INCLUDING TEMPERATURE EFFECT

W.G. Hill
R.C. Jenkins
S.G. Kalemaris
M.J. Siclari
Grumman Aerospace Corporation
Bethpage, New York 11714

Prepared for
Ames Research Center
Under Contract NAS2-10645

NASA
National Aeronautics and
Space Administration

Ames Research Center
Moffett Field California 94035

CONTENTS



PRECEDING PAGE BLANK NOT FILMED

CONTENTS (contd)

## ILLUSTRATIONS

ILLUSTRATIONS (Cont.)

# VTOL IN GROUND EFFECT FLOWS FOR CLOSELY SPACED JETS WITH TEMPERATURE

W.G. Hill, R.C. Jenkins, S.G. Kalemaris and M.J. Siclari

Grumman Aerospace Corporation
Bethpage, New York

## 1 - SUMMARY

The primary purpose of this study was to obtain detailed pressure, temperature, and velocity data for twin-fan configurations in-ground-effect and to develop flow models to aid in predicting pressures and upwash forces on aircraft surfaces. For the basic experiments, 49.5mm-diameter jets were used, oriented normal to a simulated ground plane, with pressurized, heated air providing a jet. The experimental data consisted of: (1) the effect of jet height and temperature on the ground, model, and upwash pressures and temperatures, (2) the effect of simulated aircraft surfaces on the isolated flow field, (3) the jet-induced forces on a three-dimensional body with various strakes, (4) the effects of non-uniform coannular jets.

For the uniform circular jets, temperature was varied from room temperature (24°C) to 232°C. Jet total pressure was varied between 9,300 Pascals and 31,500 Pascals. For the coannular jets, intended to represent turbofan engines, fan temperature was maintained at room temperature while core temperature was varied from room temperature to 437°C. Fan and core total pressures were chosen to match the power settings most frequently used during the large-scale tests of Reference 1.

In general, the test data correlate well with the induced forces presented in Reference 1. No scale effects were found, and jet temperature and pressure did not affect the nondimensionalized induced lift. The induced lift in-ground-effect was found to be higher for the uniform circular jets than for the simulated fan jets.

Modifications to an existing wall-jet transition model adequately predict the trends with height above ground of upwash temperatures and pressures. The addition of a recirculation model is necessary to predict upwash temperatures in the presence of an aircraft.

## 2 - INTRODUCTION

Lift and control for V/STOL aircraft operating in-ground-effect present a critical condition in sizing the propulsion system. Ground proximity effects can result in large jet-induced lift losses or produce positive fountain lift, depending on the aeropropulsion configuration. The complexity of the resulting flow field and the sensitivity to many design parameters give rise to a large body of experimental data which model various aspects of the flow field. The primary purpose of this study was to expand the existing data base for a twin-fan V/STOL aircraft by exploring the effects of temperature and non-uniformities (temperature and pressure) in the jet. These effects were then added to an existing computerized prediction method.

Of almost equal importance, and possibly greater interest to the typical reader, this effort also investigated scale effects on jet-induced characteristics. To this end, the model used was a 1/24-scale replica of a TF 34-powered, large-scale model tested recently at NASA-Ames (Reference 1).

## 3 - SYMBOLS

| | | |
|---|---|---|
| A | = | Area; nozzle exit area |
| b | = | Thickness of viscous layer |
| D | = | Diameter; nozzle exit diameter |
| f | = | Analytic functions respresenting viscous profiles |
| F | = | Force; radial flux deflection function |
| $\Delta F$ | = | Interference force (total force on body minus thrust) |
| h | = | Nozzle height above ground |
| H | = | Heat; distance to ground |
| M | = | Mach number; momentum |
| NPR | = | Nozzle pressure ratio relative to ambient |
| NTR | = | Nozzle temperature ratio relative to ambient |
| P | = | Static pressure |
| q | = | Dynamic pressure |
| r | = | Jet radius; ground radius coordinate |
| $r_o$ | = | Ground impingement radius |
| R | = | Radius from one jet impingement point |
| S | = | Jet spacing |
| T | = | Temperature; static temperature |
| V | = | Velocity |
| X | = | Distance perpendicular to Y and Z |
| Y | = | Distance from midpoint of line joining jet centerline |
| Z | = | Distance above ground; vertical jet or ground coordinate |
| Z' | = | Distance downward from nozzle exit |
| $\alpha$ | = | Exponent of profile function |
| $\gamma$ | = | Isentropic exponent; ratio of specific heats |
| $\delta$ | = | Boundary layer thickness |
| $\Delta$ | = | Difference between local and ambient conditions |
| $\zeta$ | = | Non-dimensional wall thickness |
| $\eta$ | = | Thrust efficiency factor; nondimensional thickness |
| $\theta$ | = | Angular orientation around one jet impingement point |
| $\rho$ | = | Density |
| $\Upsilon$ | = | Angle in ground polar |

## SUBSCRIPTS

| | | |
|---|---|---|
| a, A | = | Ambient |
| B | = | Body |
| C | = | Core nozzle exit conditions; potential core |
| F | = | Flux, fan nozzle exit conditions |
| FD | = | Fully-developed |
| g | = | Value at ground effect height |
| H | = | Half value |
| J | = | Nozzle value; jet exit conditions for open circular nozzle |
| m, M | = | Maximum value; viscous layer |
| N | = | Nozzle |
| PC | = | Potential core |
| rec | = | Recirculation |
| S | = | Stagnation value; static |
| T | = | Thermal layer; total; stagnation |
| u | = | Upwash |
| V | = | Velocity layer |
| W | = | Wall jet |

## 4 - EXPERIMENTAL BACKGROUND

### 4.1 Test Facility

The experiments conducted under this contract were performed in the Grumman Environmental Test Facility (ETF). This facility performs a wide range of system and component testing for Grumman and has two compressor systems capable of supplying heated air: the ram air system for pressures to 110 kPag and temperatures to 232°C, and the bleed air system for pressures to 3.45 MPag and temperatures to 760°C. A general overview of the installation in this facility is given in Figure 1; a detailed photo of the test arrangement is presented in Figure 2.

### 4.2 Air Supply

For most of the tests, the air was compressed by a Rootes-type blower (referred to in this facility as the "ram air compressor"). Compression heating of the flow was removed and the flow divided into two piping systems. One system was then heated by a controlled resistance electrical heating system with a maximum temperature of 249°C. Both the hot and cold flows were piped to the test site by 20.3-cm diameter insulated piping systems. Supply pressure was controlled by a feedback control system at the compressor control panel and a second control valve at the user's outlet area (Figure 3). For the experiments with core temperatures above 232°C, air was supplied by a piston-type compressor and gas and electric heaters in series (bleed-air systems).

### 4.3 Settling Chamber

The settling chamber for the fan nozzle was a cylindrical steel tank of 76.2-cm diameter and 218.4-cm length, adapted from underwater flow research. (See Figure 4). The first 91.4 cm of this chamber are occupied by a diffuser to spread the flow from the 20.3-cm diameter inlet evenly over the chamber cross-section. This is followed by a tube bundle of 9.5-cm diameter stainless steel tubes and two fine mesh screens. The heated air supply for the core flow enters through the bottom of the chamber after a combined turn and transition from a single 20.3-cm pipe to a pair of separate 5.1-cm tubes. This supply is con-

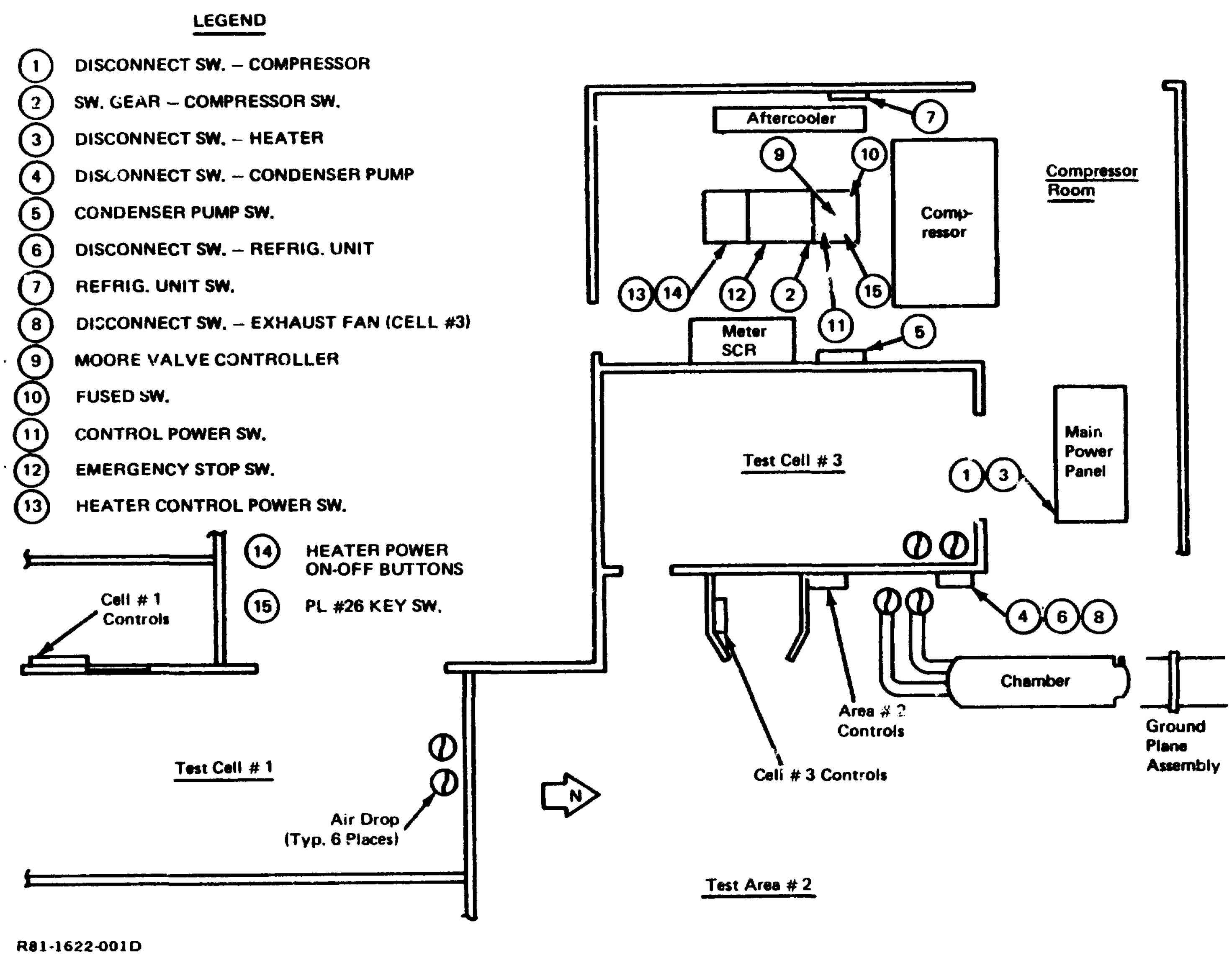


Figure 1 - Ram air system location plan, Plant 31.

ORIGINAL PAGE
BLACK AND WHITE PHOTOGRAPH

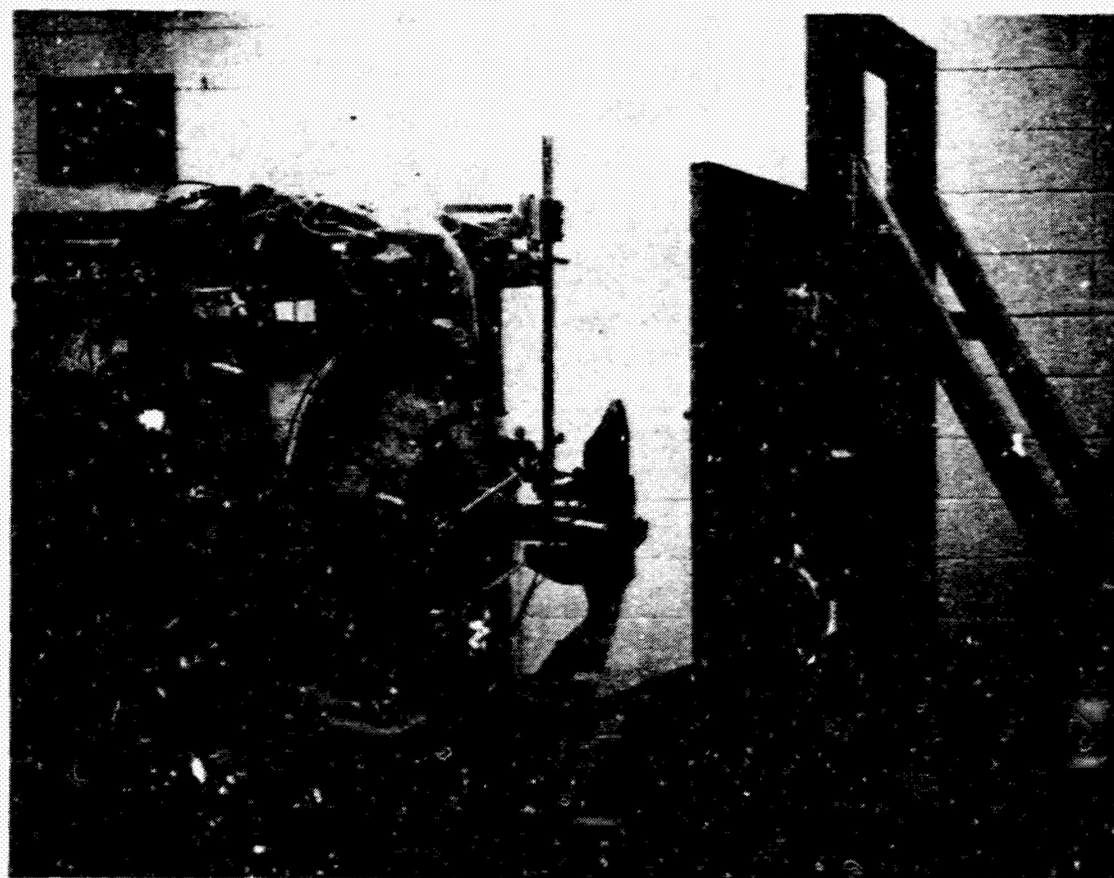

R81-1622-041D

Figure 2 - Test arrangement.

tinued inside the chamber by flexible, insulated pipes to the nozzle entrances. For the open-jet experiments, this tubing system was entirely removed and the piping system was changed to bring heated air in through the diffuser inlet.

## 4.4 Nozzles

The outer fan nozzle, which is also the hardware for the open-circular-jet experiments, is an ASME elliptical profile flow metering contour with an inside diameter of 5.0 cm. (Figure 5). This nozzle is continued as a straight tube for 30.5 cm in a tradeoff of boundary layer growth and heat transfer in the nozzle flow against the need to separate the model from the front face of the chamber, thus preventing the chamber from interfering with the recirculation flow field. The inner core nozzle for the heated flow begins with a contraction from the 5.1-cm flexible supply tubes beginning 5.1 cm before the fan flow

ORIGINAL PAGE IS
OF POOR QUALITY

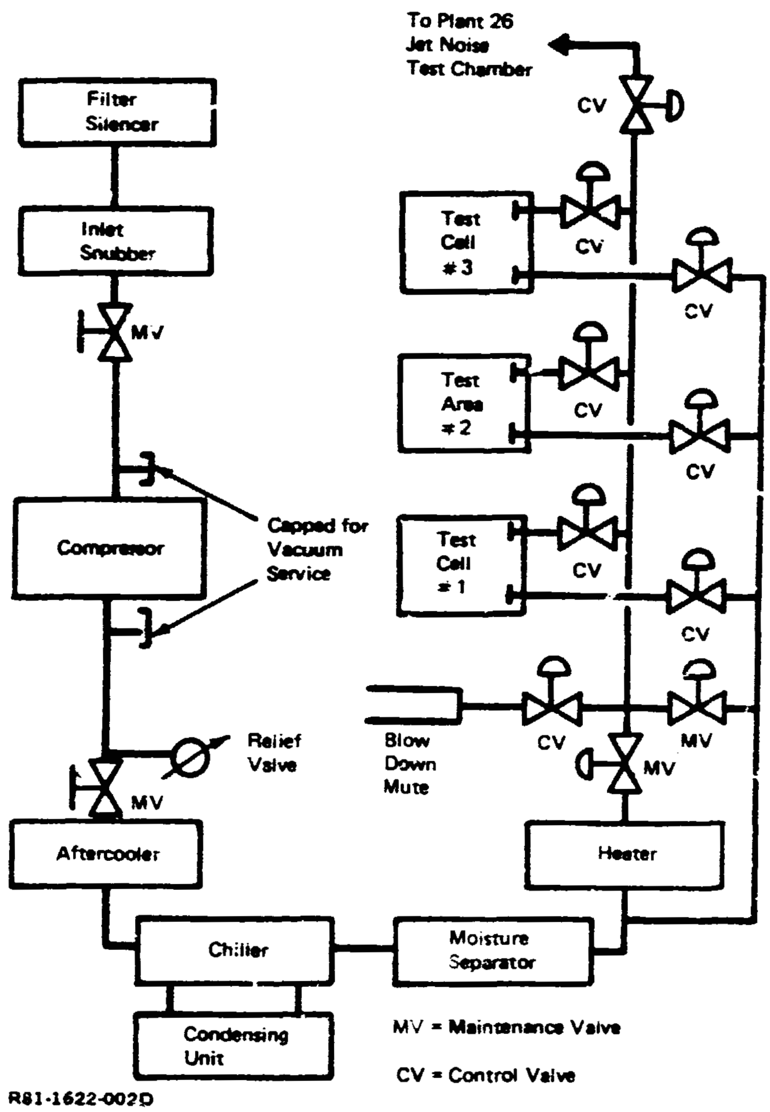


Figure 3 - Ram air system schematic.

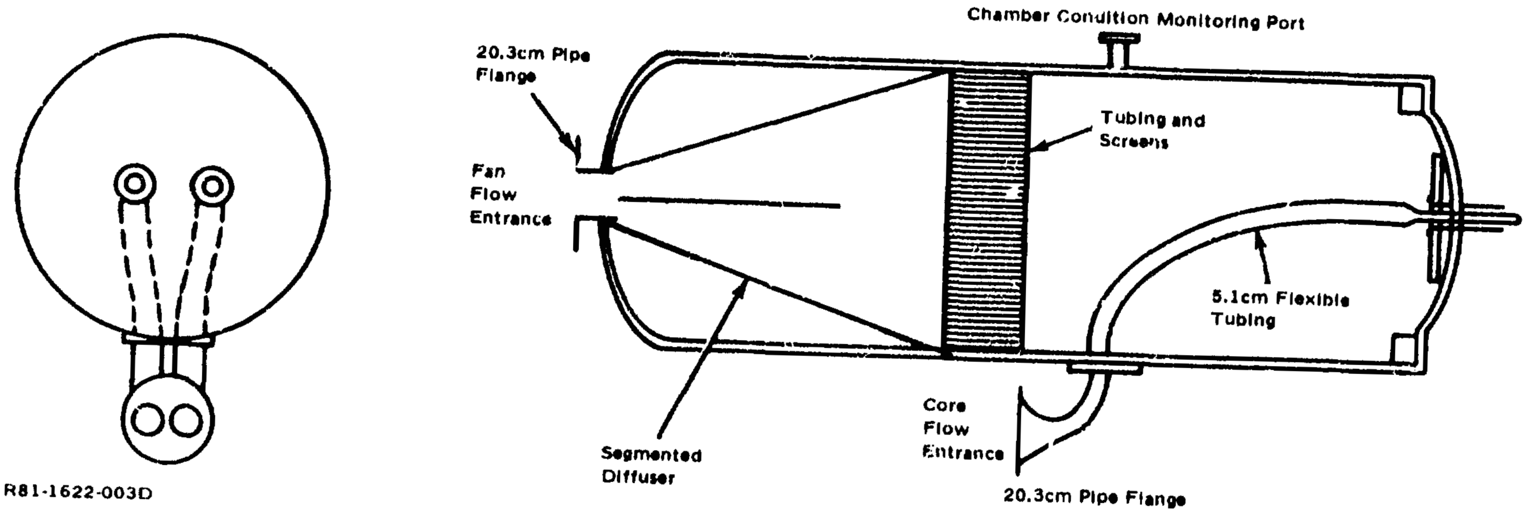


Figure 4 - Settling chamber arrangement.

ORIGINAL PAGE
BLACK AND WHITE PHOTOGRAPH

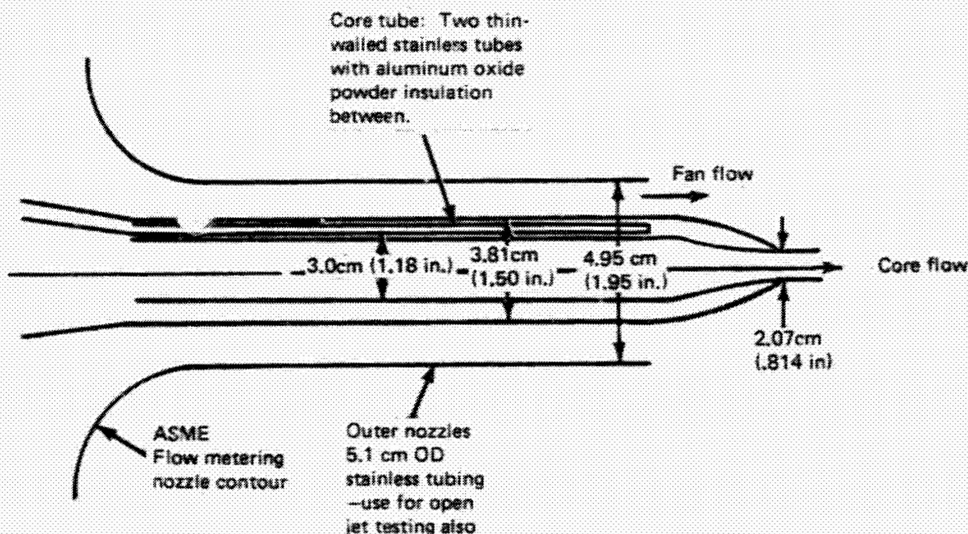


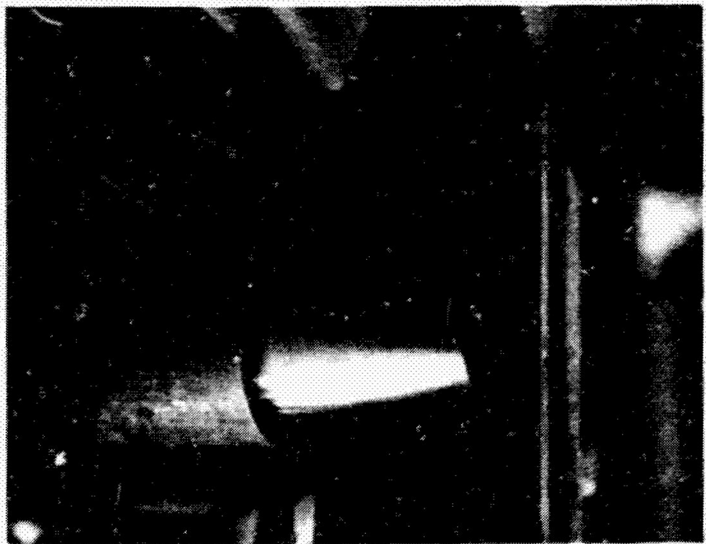

R81-1622-042D

Figure 5 - Fan-jet nozzle simulation.

nozzle entrance. This contraction connects to a double wall tubing system with an outer diameter of 3.8 cm (the scale centerbody diameter) and an inner diameter of 3.0 cm. The area between the two walls of this contraction section and the constant area section running to the final core nozzle contraction were insulated with aluminum oxide powder. The final contraction to the 20.7-mm core exit diameter and the core centerbody outer profile are accomplished in one solid machined segment. The core-flow tube is held in place by a machine screw in the simulated core pylon, and three thin finger-type supports near the nozzle entrance.

### 4.5 Ground Plane

The simulated ground plane consists of a 2.5-cm thick aluminum plate 121.9-cm square, with a circular insert of steel for the pressure tap and wall jet probe mountings. (Figure 6a). This plate was mounted on a framework which rode on rails that were aligned parallel to the nozzles. The ground plane was moved by a screw that was driven by a variable speed motor/controller. The instrumentation locations are shown in Figure 6b, c, and d, (pressure taps, surface temperature thermocouples and wall jet rakes). Numbering of the instrumentation locations matches that of the full-scale ground plane (Ref. 1), with additional instrumentation designated by "R".

### 4.6 Aircraft Model

The model (Figure 7) was a 1/24 scale reproduction of the Grumman Design 698-411B tested in the NASA-Navy-Grumman full-scale demonstrator program. This model was constructed of a partially-hollow high-temperature-plastic fuselage section housing the balance and pressure/temperature lines, a metal bottom plate for pressure and temperature instrumentation, metal strakes at the fuselage chines, and separately attachable plastic wings and empennage.

### 4.7 Instrumentation

4.7.1 Pressure. - Pressures were measured with Validyne model DP15 or DP103 transducers, powered by single channel CD-15 or MC1-10 multichannel systems using CD18 or CD19 carrier demodulators. Transducers were calibrated versus an oil filled manometer, either singly (transducers used for probe measurements) or in groups with the manometer calibration pressure applied through a manifold (ground plane or aircraft surface).

ORIGINAL PAGE
BLACK AND WHITE PHOTOGRAPH

a) Test set-up

R81-1622-043(1/3)D

Figure 6 - Ground plane.

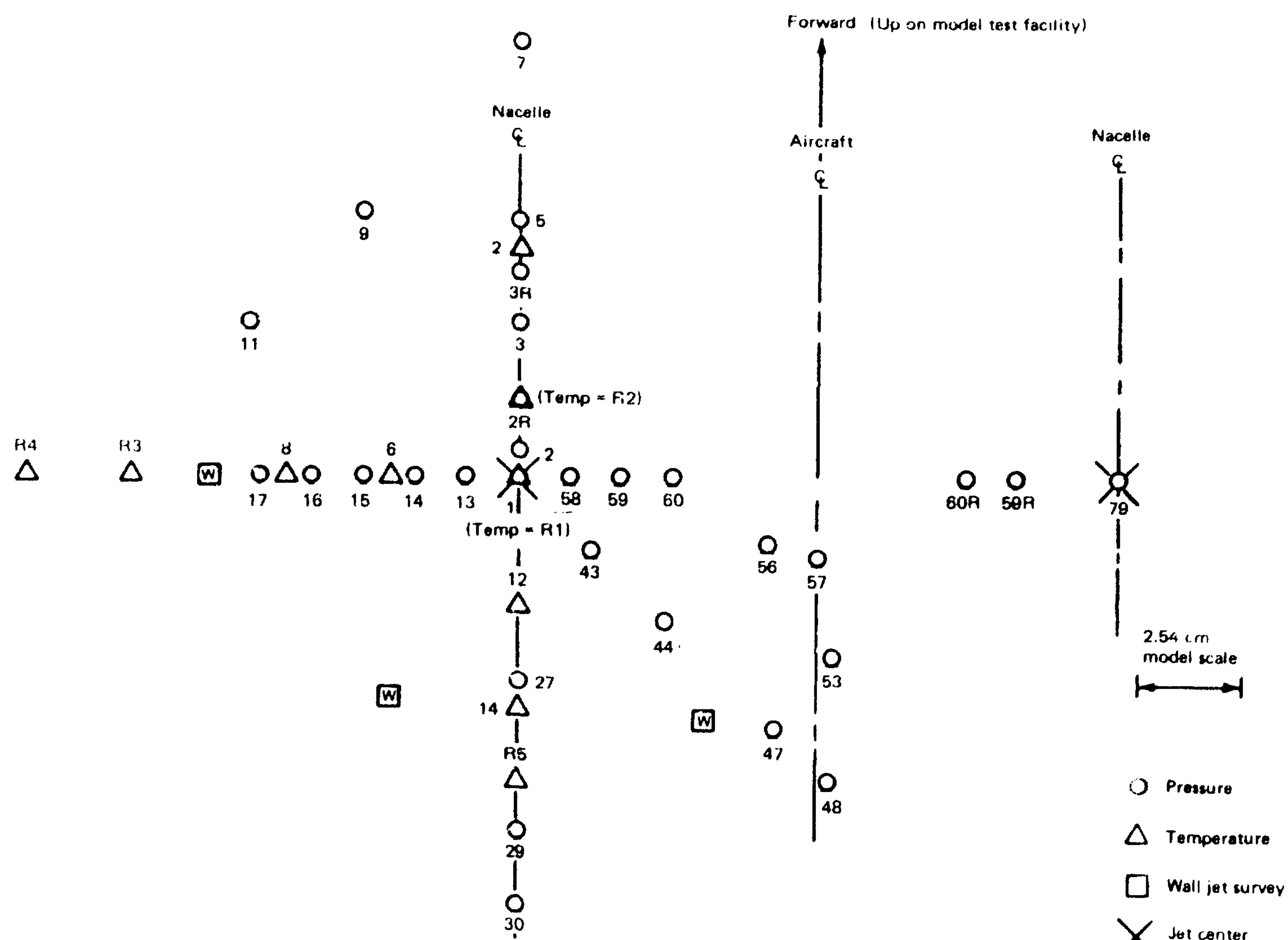


b) Ground plane instrumentation locations

R81-1622-043(2/3)D

Figure 6 - (Continued.)

ORIGINAL PAGE
BLACK AND WHITE PHOTOGRAPH

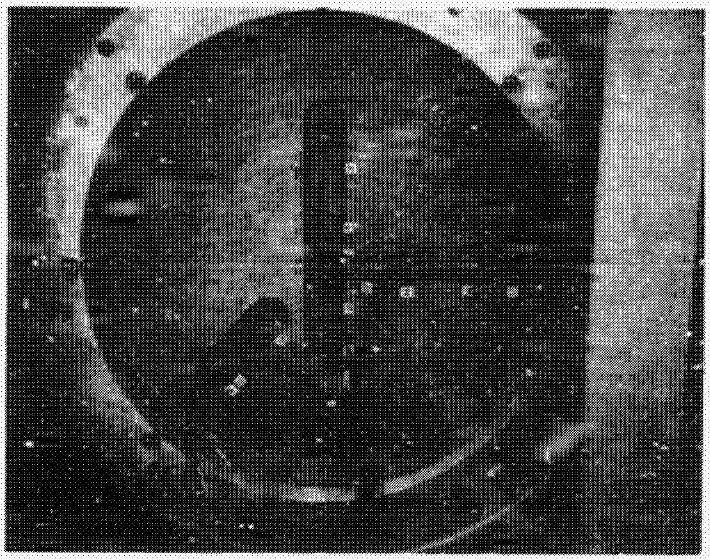

c) Thermocouple installation

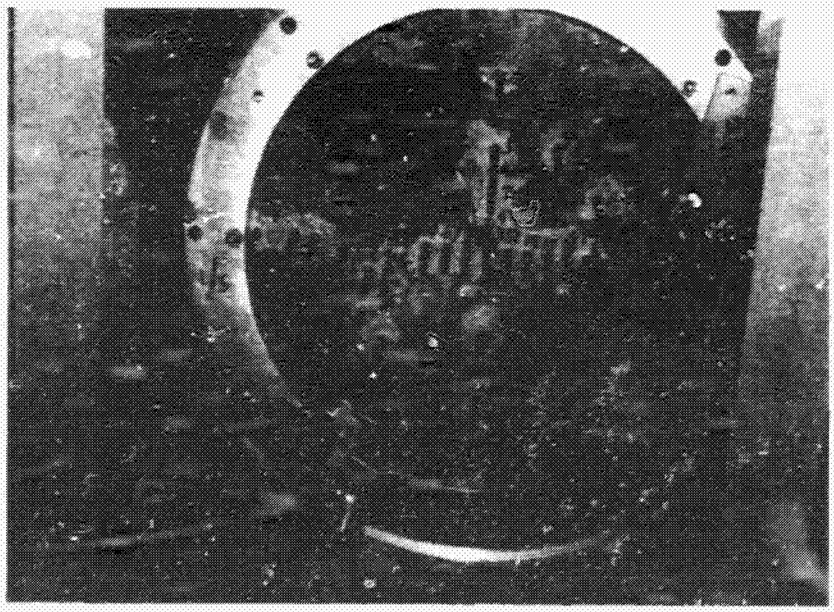

d) Pressure and wall jet instrumentation

R81-1622-043(3/3)D

Figure 6 - Concluded.

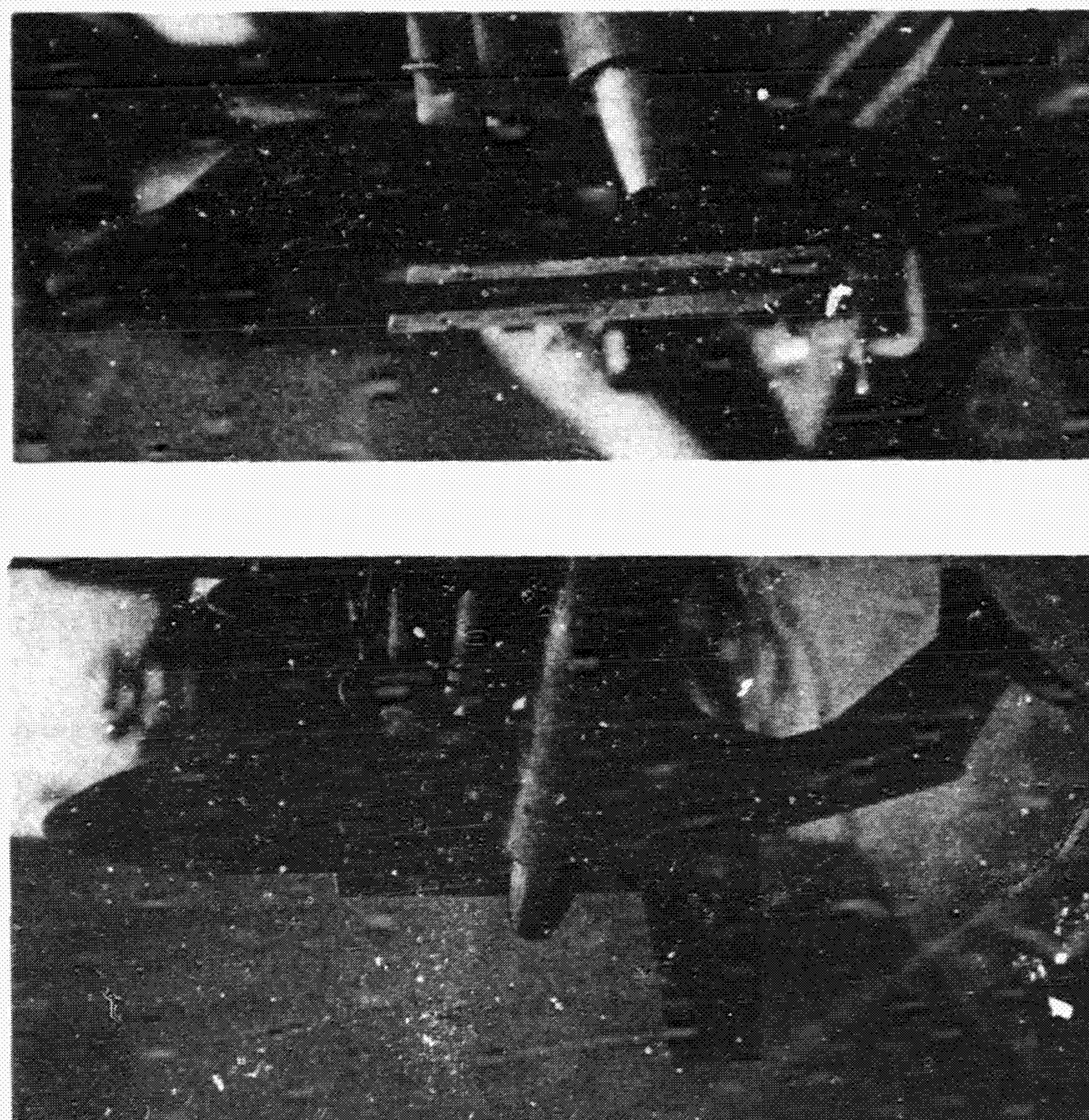

R81-1622-044D

Figure 7 - 1/24 scale model.

Pressure tap locations on the ground plane are discussed in Section 4.5. Full-scale locations on the line connecting the nozzle impingement centerline, at 90° to the line through one jet-centerline, and at 45° were used, with a few additional locations added. The full-scale tap identification numbers were used for the model tests to aid comparisons.

Pressure tap locations on the aircraft model are shown in Figure 8. Full scale locations were matched for many of these taps, but some taps were relocated so that temperature (thermocouple) instrumentation could be added.

4.7.2 Temperature. - All temperature measurements were made with chromel-alumel (Type k) thermocouples connected by a multi-connection switch box to either an Omega model 2175A or a Fluke model 2166A linearized thermocouple readout amplifier. The ground plane surface temperatures and those on the flat segment of the aircraft bottom were measured with thermocouples spot welded to thin (0.4 mm) stainless steel areas. On the aircraft, the entire flat bottom was formed from one thin piece of stainless steel, and thicker pieces were spot-welded in areas for pressure tap installation. (Figure 8). The 30.5-cm diameter ground plane insert was 4.2-cm thick, and the areas for temperature measurement were machined to the 0.4-mm thickness for a distance of at least 1.3 cm from all thermocouples. (See Figure 6c). The thin skin allows greater spatial resolution in temperature measurements, which is important in small-scale testing.

4.7.3 Probes. - Three separate probe assemblies were used for measurements in the free jet, wall jet, and upwash flows (Figure 9). In each probe assembly the temperature data were taken by a bare thermocouple probe protruding from a 1.5-mm diameter stainless steel sheath that was located close to one of the pressure probes. Bare thermocouples were chosen, rather than a more conventional shielded thermocouple probe, in order to obtain good spatial resolution and time response and to avoid flow disturbances that would be associated with a housed probe. Temperature measurements with bare thermocouples require correction to account for radiation losses. Temperature corrections were acquired for the thermocouple probes in each assembly by recording output in a flow field of known temperature over a wide temperature range. We used the open jet nozzle configuration for this work. Each probe assembly was placed on the centerline of one nozzle shortly downstream of the exit and a housed thermocouple probe (United Sensor type KT-12-C/A) was placed at a corresponding point in the flow from the other nozzle.

The probe assembly used for free-jet data (Fig. 9a) consisted of 1.6-mm O.D. sharp-lipped pitot tube with a 0.5-mm diameter thermocouple displaced 2.5 mm laterally from the tip of the pitot tube. Wall jet data were taken with a

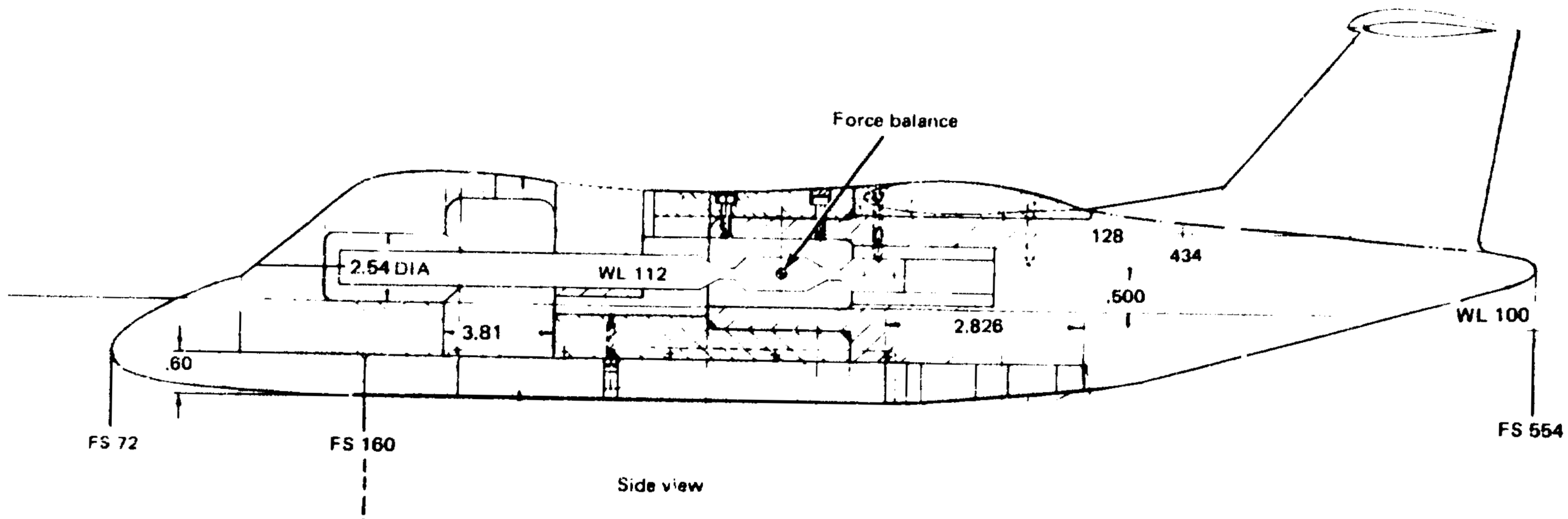


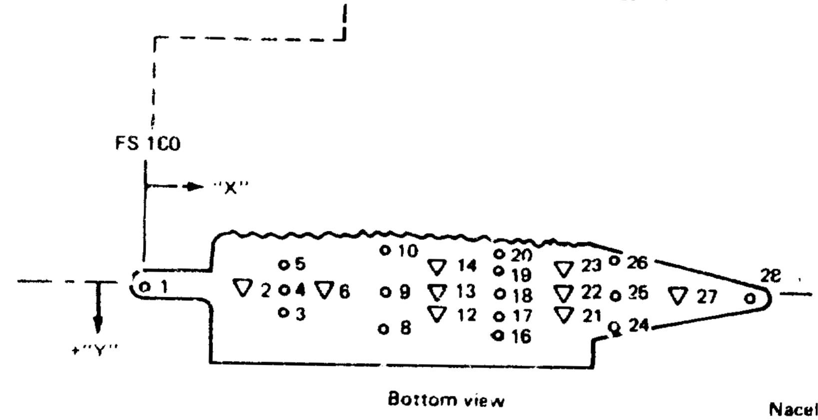


| ○ PRESS<br>△ TEMP | NO. | FUSE STA | SENSOR COORDINATES "X" | SENSOR COORDINATES "Y" |
|---|---|---|---|---|
| ○ | 1 | 160 | 0 | 0 |
| ▽ | 2 | 200 | 4.22 | 0 |
| ○ | 3-5 | 215 | 5.82 | .71, 0, -.81 |
| ▽ | 6 | 238 | 8.26 | 0 |
| ○ | 8-10 | 255 | 10.0 | 1.57, 0, -1.57 |
| ▽ | 12-14 | 280 | 12.7 | .79, 0, - 79 |
| ○ | 16-20 | 300 | 14.7 | 1.52, .76, 0, -.81, -1.68 |
| ▽ | 21-23 | 325 | 17.5 | 1.4, 0, -1.45 |
| ○ | 24-26 | 345 | 19.6 | 1.4, 0, -1.45 |
| ▽ | 27 | 370 | 22.2 | 0 |
| ○ | 28 | 400 | 25.4 | 0 |

NOTE: All dimensions in centimeters

R81-1622-052D

Figure 8 - Model instrumentation.

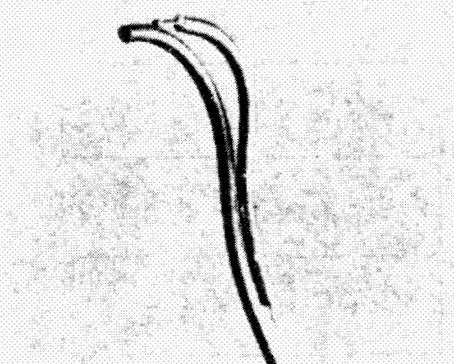

a) Free-jet probe

b) Wall-jet probe

c) Upwash probe

R81-1622-053D

Figure 9 - Flow field probes.

1.3-mm O.D. pitot tube (Fig. 9b) that was flattened to 9.5 x 1.5-mm dimensions at the tip, with a 0.5-mm diameter thermocouple that was displaced laterally 1.8 mm. The probe assembly for upwash measurements consisted of a 3.0-mm O.D. Kiel probe with a 1.6-mm O.D. static tube displaced 4.3 mm on one side, and 0.5-mm diameter thermocouple displaced 3.0 mm on the other side of the Kiel probe (Figure 9c).

The free-jet probe assembly and the upwash probe assembly were supported by a motor-driven traverse that was mounted on the same rails as the ground plane carriage. Probes were traversed in the plane containing the two jet centerlines, along paths perpendicular to those centerlines.

The support for the wall-jet probe assembly passed through a hole in the ground plane and attached to a manually driven screw traverse that was fastened to the back of the ground plane (Figure 10). The probe location relative to the wall was measured from the voltage output of a thin film linear resistance transducer that was attached to the screw drive.

## 4.8 Experimental Techniques

All experiments were conducted under steady or pseudo-steady operating conditions. After initial startup time (approximately one hour) changes in pressure operating conditions took only a few minutes. Total temperature changes were much slower, primarily because of the heat capacity of the supply piping.

Under most of the operating conditions for this contract, we utilized the techniques we developed earlier (Refs. 2, 3 and 4) of continuously recording test variables versus input parameters in an analog form on an X-Y recorder. This allowed a constant monitoring of test results. Operating conditions could be changed to allow for results observed (such as gradients or fluctuations). The most frequent examples of this are the recording of interference force, ground-plane pressures, and vehicle surface pressures versus height above ground, or probe temperature and pressures versus probe position.

Probe and ground plane position were converted to voltage by a cable-

BLACK AN[illegible] [illegible] PHOTOGRA[illegible]H

R81-1622-045D

Figure 10 - Wall-jet traversing system.

driven rotary potentiometer (Figure 11) for most cases, and a linear potentiometer for the wall-jet measurements (Figure 10). Voltage was supplied by Hewlett Packard Model 6216A D.C. power supplies and adjusted so that a "calibrated" scale setting could be used on the recorder (allowing changes in scale with ease). Position was controlled by a variable speed DC motor/controller and a screw drive.

For the aspects of the experiments requiring many measurements simultaneously (such as ground plane and aircraft surface pressures) data were recorded simultaneously by an on-site minicomputer (Hewlett-Packard Model 1000(X) through A/D converters.

The aircraft force measurements were taken on separate runs from the pressure and temperature measurements because of force interference from the pressure and temperature leads which could not be eliminated. The instrumented lower surface and the instrumentation leads attached to it were removed for the force tests. A plain lower surface was fabricated to match the external contours of the instrumented lower surface and used to cover the cavity in the fuselage during the force tests.

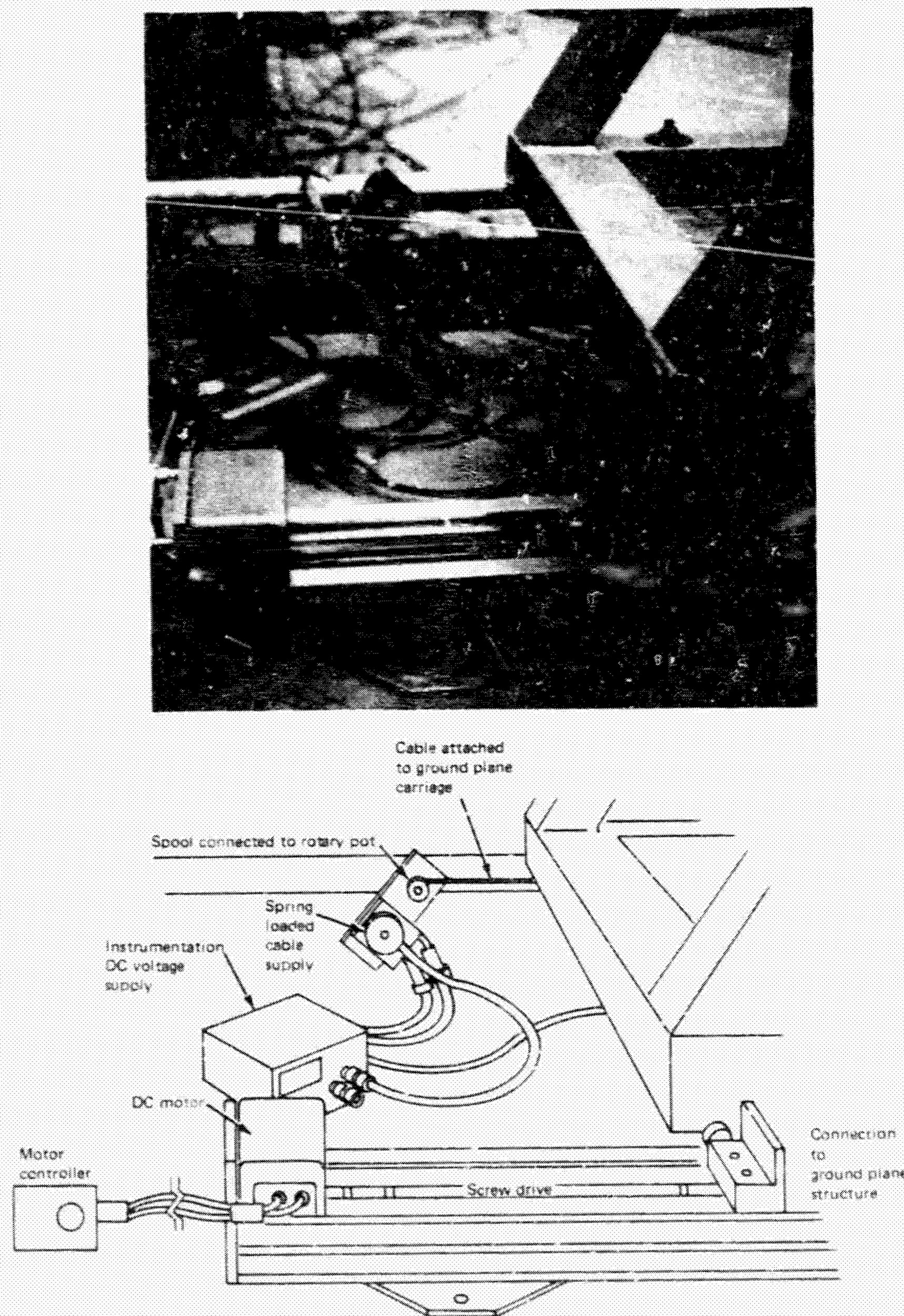


Figure 11- Position readout system.

## 5 - RESULTS

### 5.1 Fan-Jet Nozzles

The sketch of fan-jet impingement geometry in Fig. 12 illustrates the co-ordinate system used to describe probe and nozzle locations. All data were taken with the spacing between nozzles scaled to the full-scale model of Reference 1, with the jets normal to the ground and with the aircraft model present.

5.1.1 Nozzle Flow. - Figures 13 and 14 show pressure profiles taken across the fan and nozzle exit, with baseline pressure conditions and a 24°C total temperature in both flows. The total-pressure profile at the core exit is quite flat. The profile across the fan exit shows a well-defined maximum near the center of the annulus. The maximum value of the pitot pressure at the exits was used to define the nozzle pressure ratios (1.103 for the core and 1.195 for the fan at baseline conditons). Most of the fan-jet impingement data were taken with these nozzle pressure ratios, chosen to match those conditions most frequently used in the full-scale experiments. After the initial series of experiments, during attempts to compare full-scale and model results, it was discovered that the full-scale conditions to be matched were based on area averaged total pressures. Additional tests were conducted at the most critical conditions with the correct pressures. Non-dimensional results were found to have very little dependence on the total pressure.

Integration of the pressure profiles in Figures 13 and 14 (assuming axial symmetry) gives a value of 36.5 N thrust for one fan-jet nozzle. However, this approach provides only an approximation of the thrust because the fan flow is not truly axially symmetric (engine support pylon blockage on one side of the fan duct) and because this method of determining thrust does not account for pressure forces on the outer cowl of the core nozzle (centerbody).

A more accurate determination of nozzle thrust was made by measuring the impingement on a 0.914-meter square ground-plane plate that was instrumented with three strain beams. With baseline pressure conditions, the thrust produced by one nozzle was found to be 36.2 N. Maintaining pressure within 5% of the baseline conditions, the core exit temperature was raised from 24° to

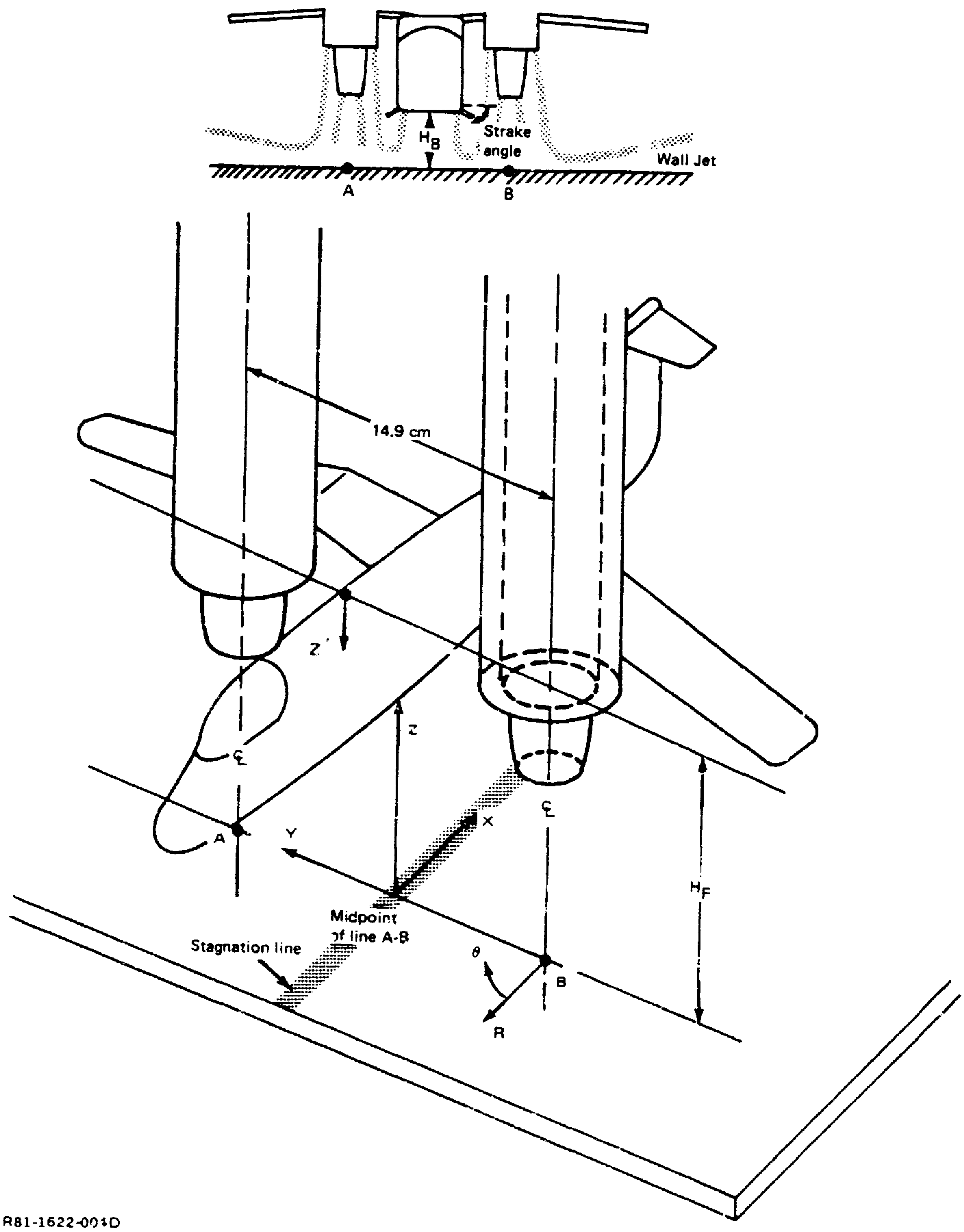


Figure 12 - Coordinate system and nomenclature.

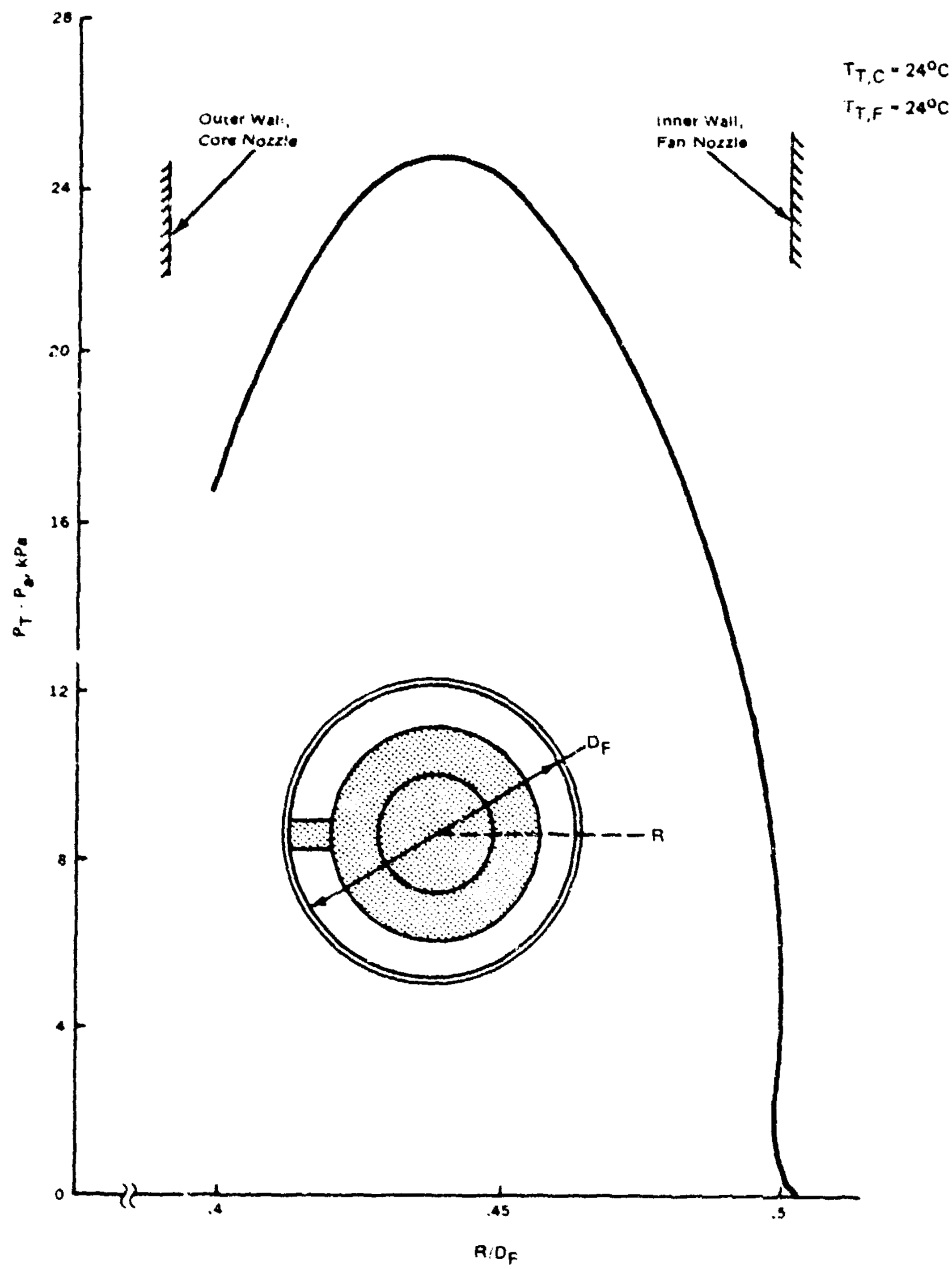


R81-1622-005D

Figure 13 - Pitot pressure profile at fan nozzle exit, baseline pressure operation.

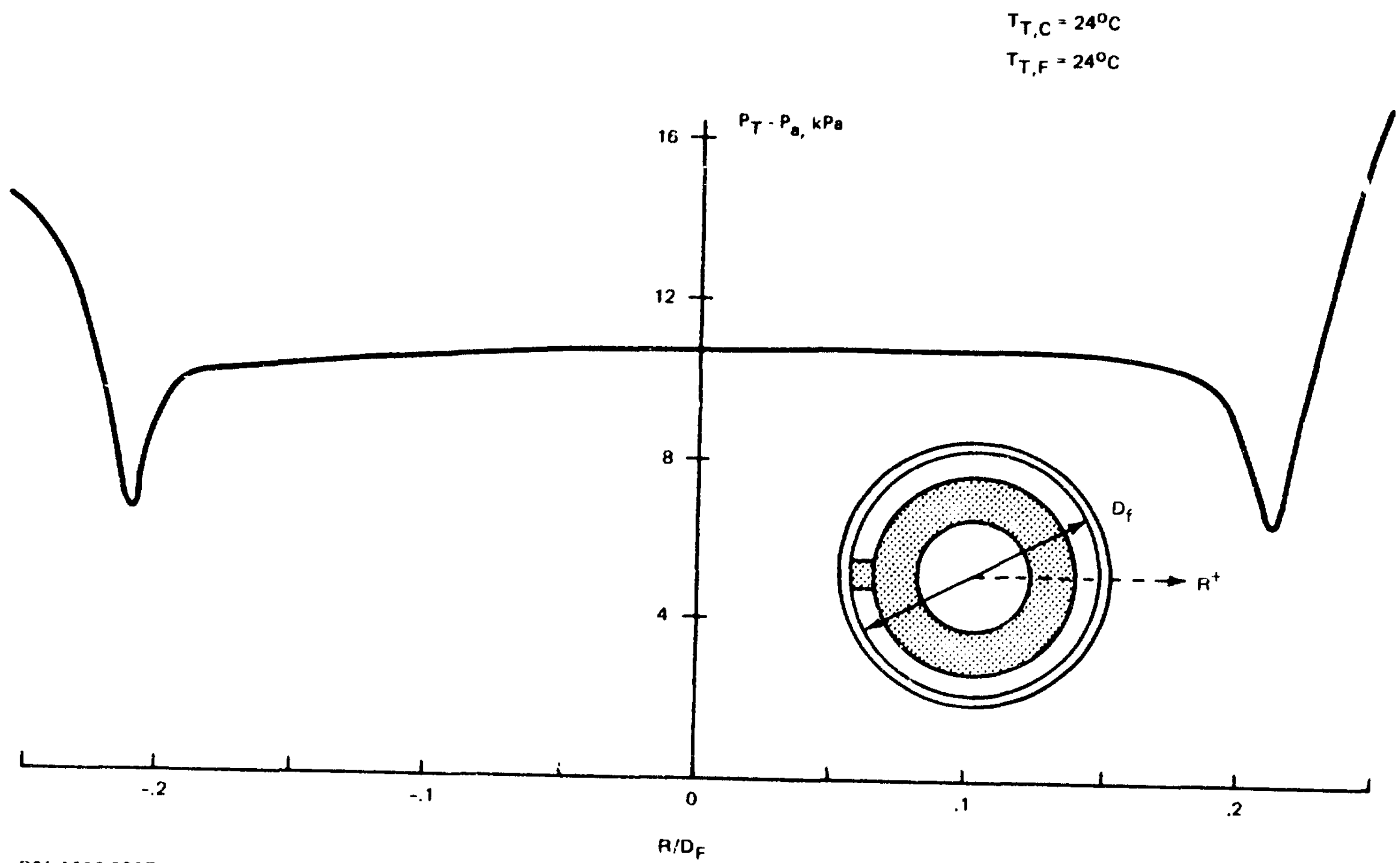


R81-1622-006D

Figure 14 - Pitot pressure profile at core nozzle exit, baseline pressure operation.

$168^{o}C$. As shown in Figure 15, there was a negligible variation in nozzle thrust over this range of core exit temperatures when minor variations in total pressure at the core exit and the fan exit were taken into account.

The thrust of a fan-jet nozzle was measured for a range of both core and fan nozzle total pressures. The thrust was found to be a linear function of fan and core pressures (Figure 16). This is true over a range of pressures exceeding those used in this study. An empirical fit of the data yields $F = 1.55\, q_{fan,\, avg.} + 0.719\, q_{core} - 0.445$, in which q is in kilopascals and F is in Newtons. As an indication of the origin of this equation, the following relationship was assumed: (1)

$$F = \left(K_1 + K_2\right)\ 2q_{fan}A_{fan} + K_3 2q_{core}A_{core} \quad (2)$$

where $K_1$ and $K_3$ represent the relative thrust efficiencies and $K_2$ refers to the drag of the core centerbody in the fan flow. For the nozzles used in the study, $A_{fan} = 7.8\ cm^2$ and $A_{core} = 3.37\ cm^2$

From integration of the core nozzle exit profiles, $K_3$ was found to be 0.0962. Combining the terms relative to the core, $\left(K_1 + K_2\right) \times 2\ A_{fan} = K_4$ we have the relationship

$$F = K_4 \times q_{fan} + 0.650\ q_{core}. \quad (3)$$

Solving for $K_4$ with room-temperature, baseline condition data yields $K_4 = 1.46$. Substituting, we find

$$\Delta F = 1.46\ q_{fan,\ avg.} + 0.650\ q_{core,\ avg} \quad (4)$$

This agrees quite closely with the empirical relation of Eq. (1)

Figure 17 shows free-jet total-pressure profiles that were taken (with both fan jet nozzles operating) at successive axial stations for a total temperature at the exit of $24^{o}C$. The lack of symmetry in each of the fan flows can be attributed to the core pylon blockage in the fan nozzles. The apparent convergence of the two flows, indicated by measurement on these profiles of center-to-center distance between the two flows at several axial stations, was

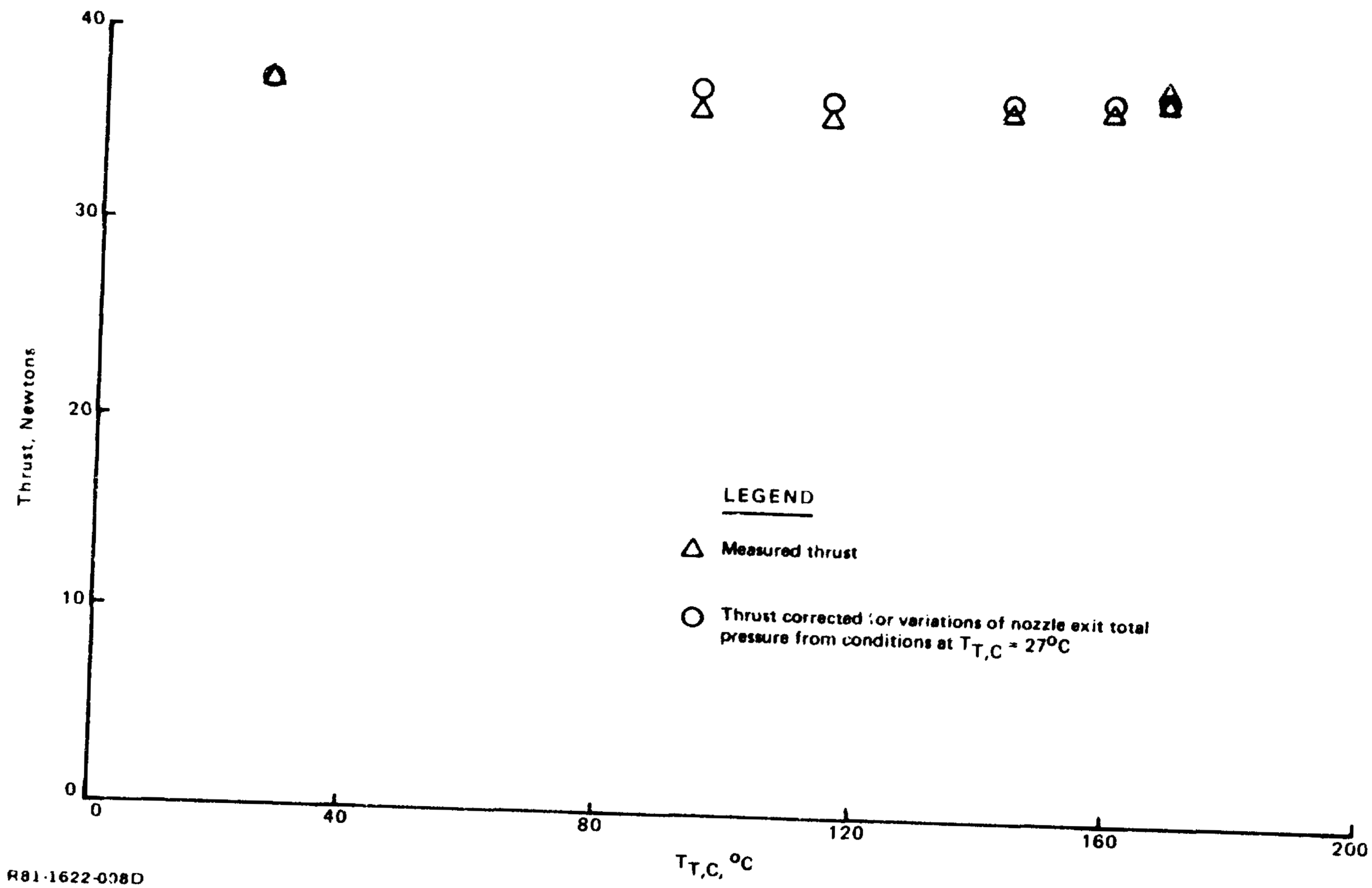


Figure 15 - Variation of nozzle thrust with core exit temperature for baseline nozzle pressure conditions.

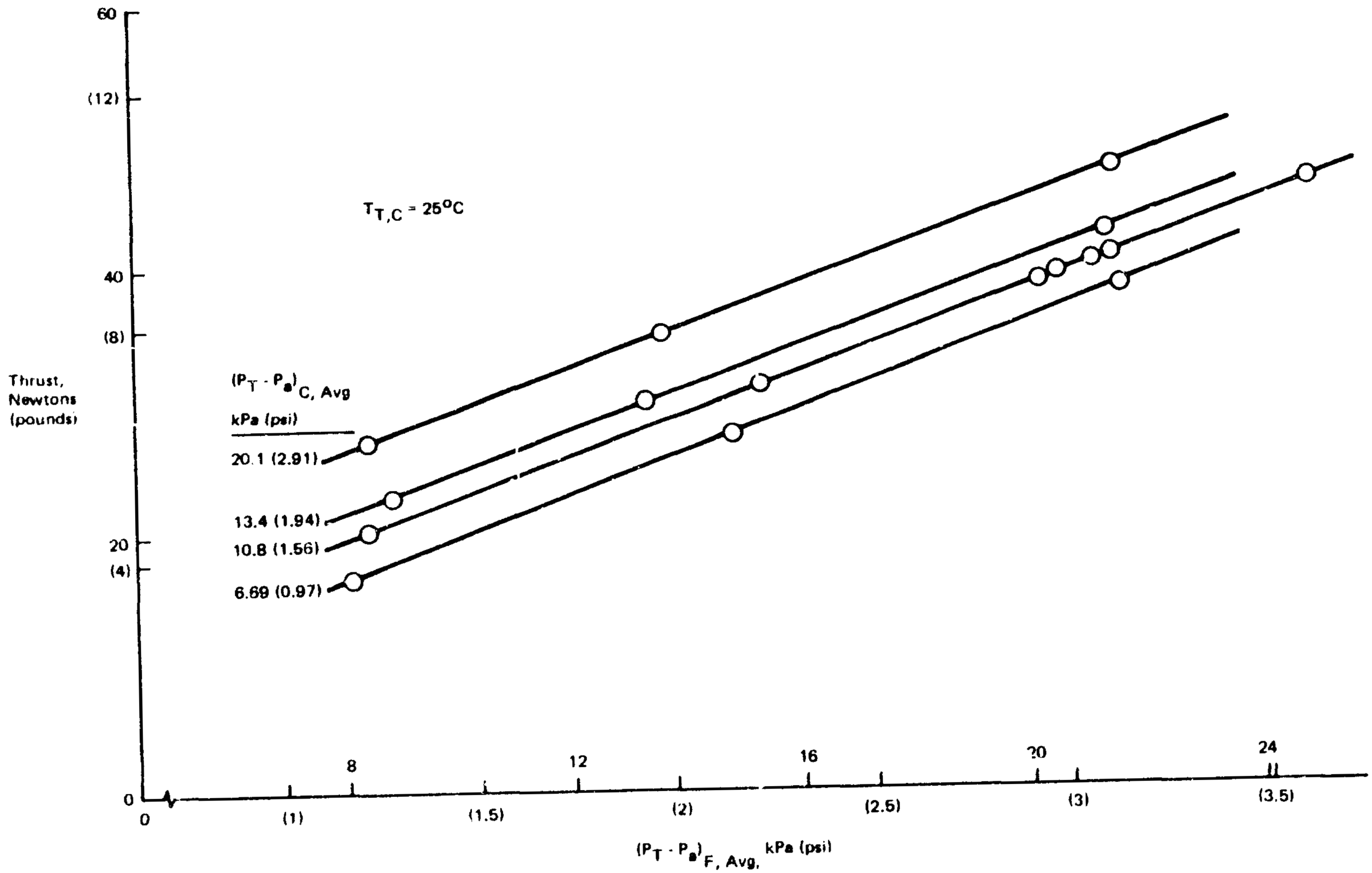


R81-1622-007D

Figure 16 - Effect of fan and core total pressure on nozzle thrust.

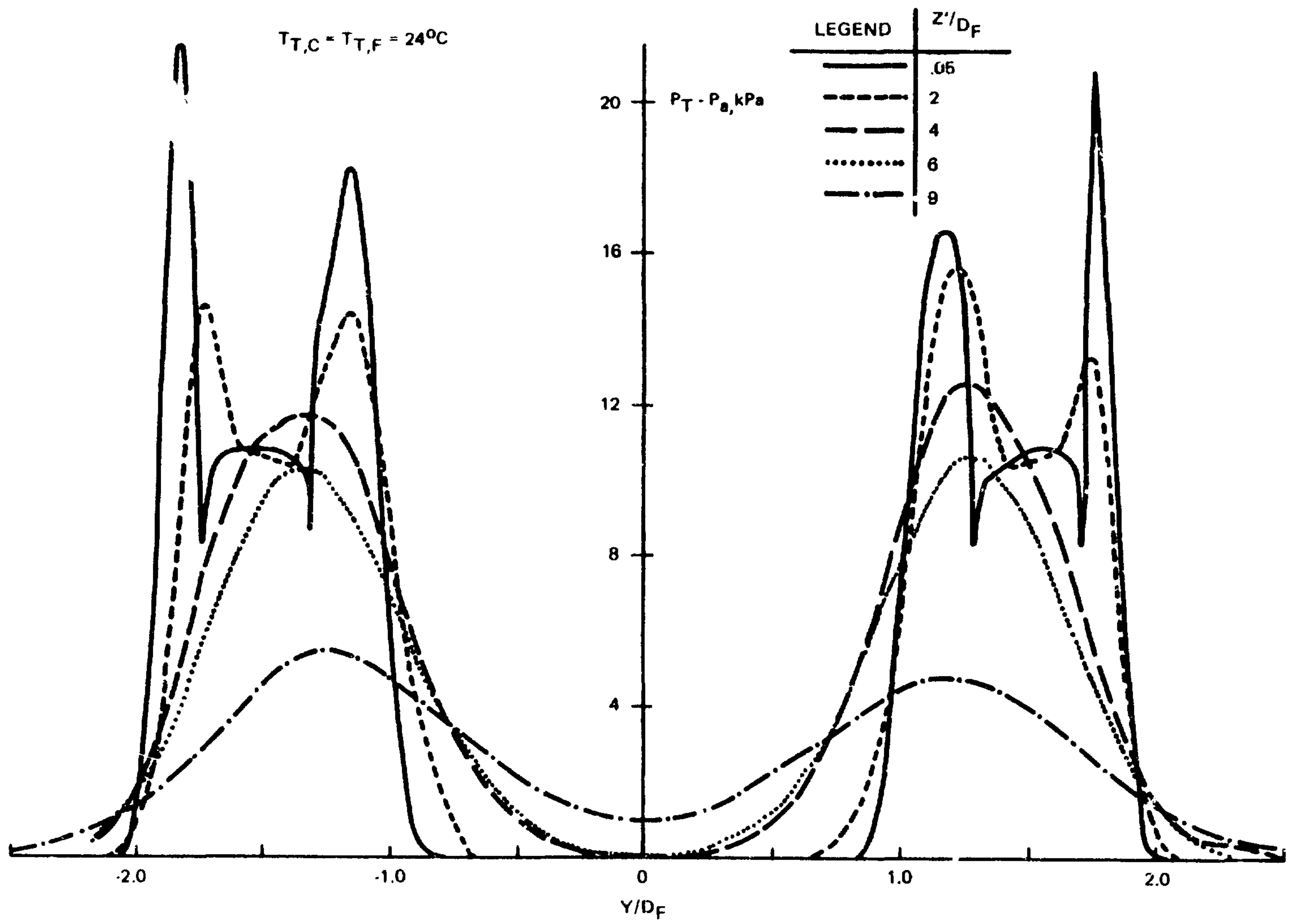


Figure 17 - Free-jet pitot pressure profiles, baseline operation.

not caused by actual convergence of either the fan or core nozzle hardware. The reason for this characteristic of the free-jet pitot pressure profiles is still under active investigation, but it is assumed to be due to the pylon-induced asymmetries.

5.1.2 Ground Flow. - Pressures taken on the ground surface were recorded by a 30-channel A/D system connected to an HP-1000 minicomputer as the ground height was varied. In addition, some pressure data were taken at fixed ground heights as continuous profiles by displacing the ground plane in the y-direction. Figure 18 shows the variation of ground pressure along a line between the two jet impingement points for three body heights above ground. These ground pressure profiles were taken using baseline nozzle pressure conditions and 24°C core nozzle exit temperature. The maximum ground pressure in the stagnation line region (central section of the profiles) shows little variation with body height. The ground pressure in the impingement regions (outer sections of the profiles) shows an inward shift of the ground impingement center for each jet as ground height is increased, which is analogous to the convergence of the free jet centerlines illustrated by Figure 17.

Ground temperature measurements were taken at points around one jet impingement region for the same three heights above ground, using almost the same nozzle pressure conditions and a core exit temperature of 425°C. Figure 19 shows the ground temperature radial variation from one jet impingement point for three different angular orientations ($\theta$). A curve was faired through the round symbols, corresponding to $\theta = 90°$ (oriented in the wing spanwise direction). Note that, for $\theta = 0°$, the ground temperature was lower, and for $\theta = 180°$ the temperatures were higher, than this curve. The higher ground temperature under the wing may have been caused by blockage of air entrainment into the jet exhaust by the presence of the wing.

Figure 20 shows representative wall-jet profiles of total pressure and total temperature that were obtained by traversing a probe normal to the ground at the ground location scaled to rake number 6. Data were taken at the three ground heights corresponding to those run during the full-scale tests. Data were obtained at this ground location and at two other locations (rakes number

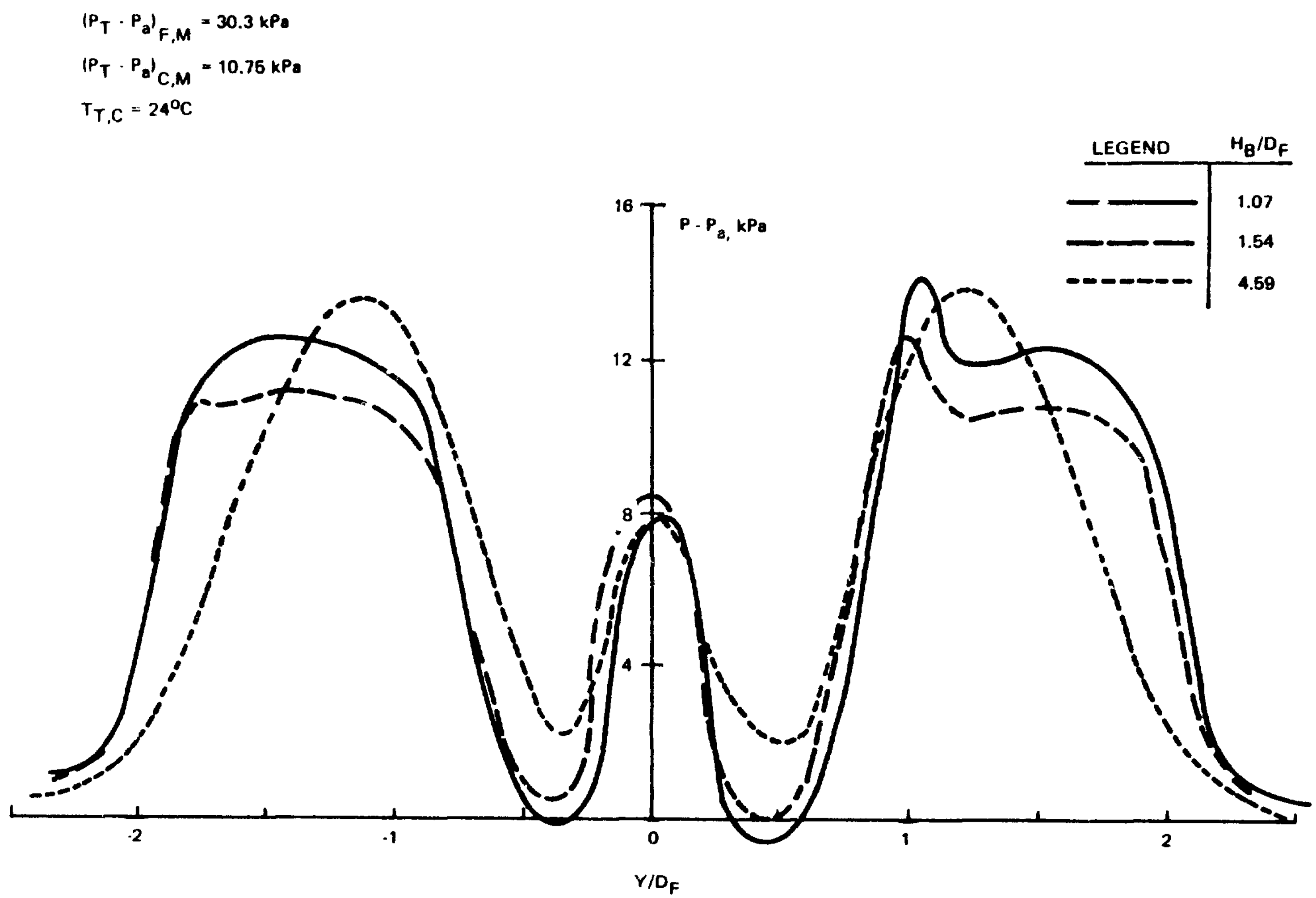


R81-1622-010D

Figure 18 - Ground pressure profiles, fan-jet impingement.

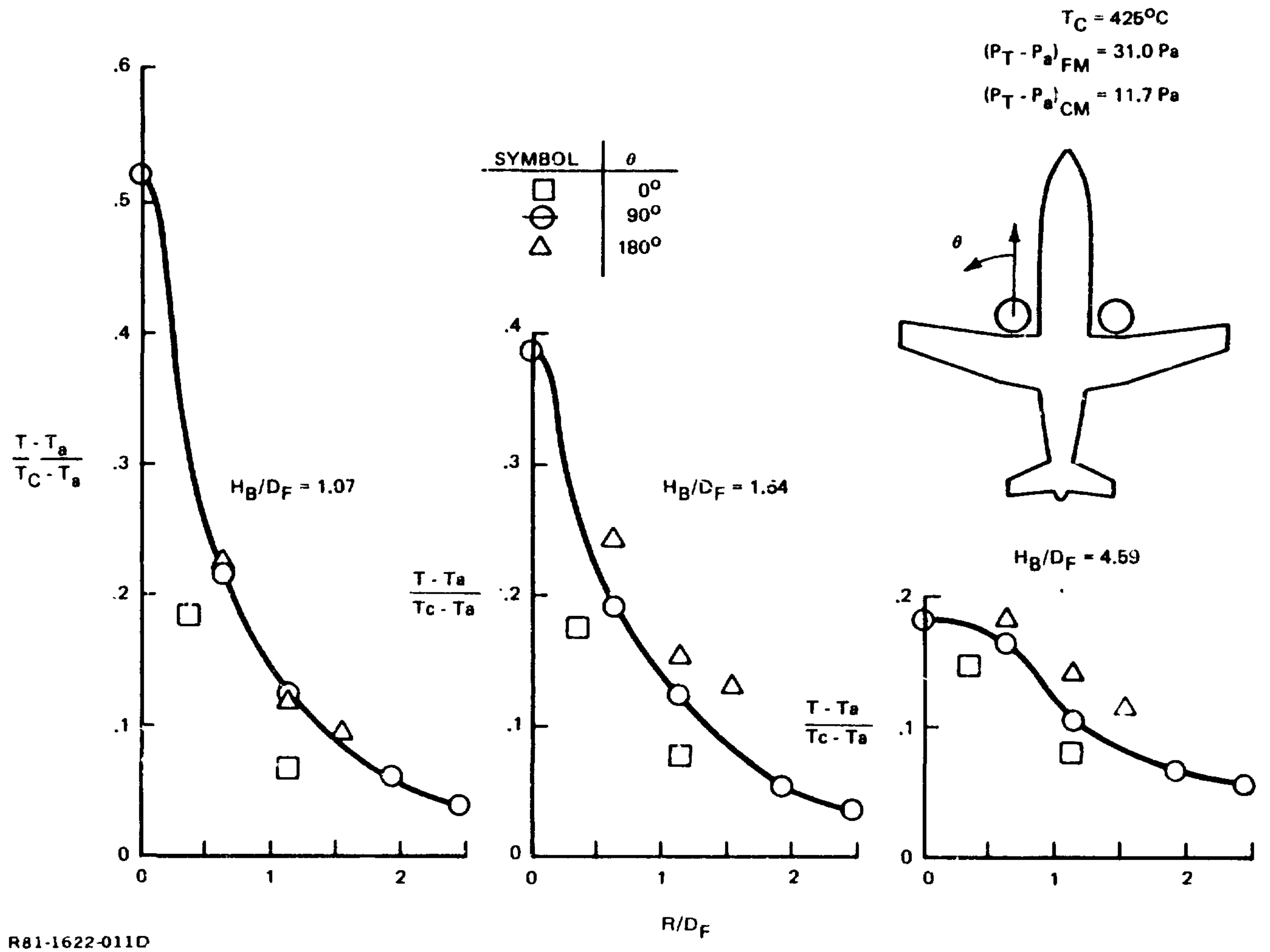


Figure 19 - Ground temperature measurements.

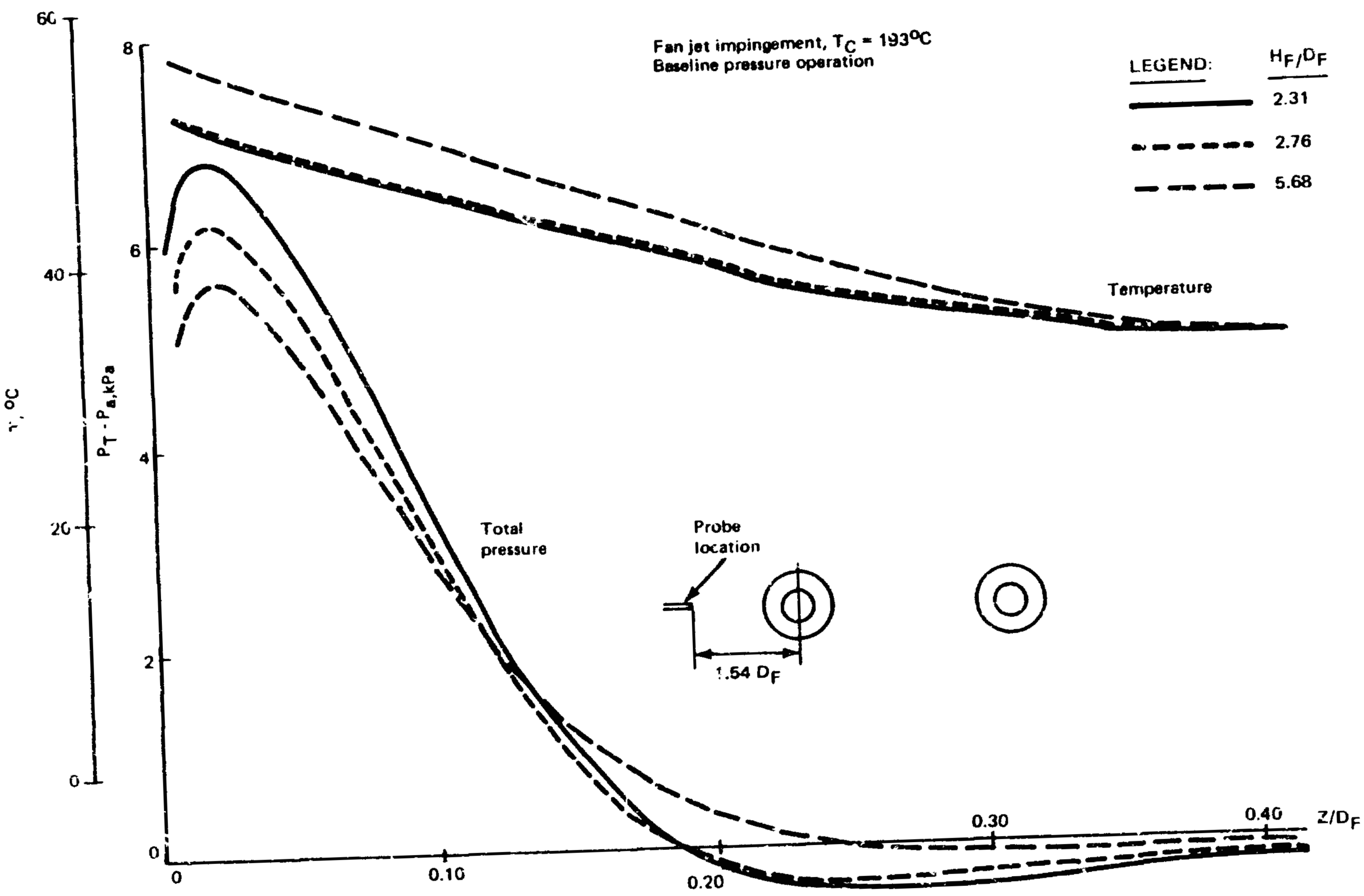


R81-1622-012D

Figure 20 - Wall jet temperature and total pressure profiles.

8 and 10). Figure 21 shows a tabulation of representative features of the pressure and temperature profiles taken at all three ground locations and three ground heights. In this figure, the maximum wall-jet total pressures have been normalized by the maximum total pressure at the fan exit and the wall-jet thickness (at one quarter the maximum profile dynamic pressure) has been normalized by fan-nozzle outside exit diameter.

The temperature data shown in Figure 20 were taken with a bare thermocouple that was located adjacent to the total pressure tube. These data must be corrected to account for radiation losses. The correction has been applied to the data listed in Figure 21.

5.1.3 Upwash Flow. - Flow properties in the upwash were measured by traversing a probe assembly through the centerline of the upwash in the y-direction with the model in place. The total pressure, static pressure and total temperature profiles were measured along a line .56D below the model lower surface, using baseline nozzle pressure conditions and core exit temperatures of 24°C, 128°C, and 192°C. Data could not be taken at the lowest body height tested full-scale (1.07D) because the probe would have been in the upwash formation region. For the greatest full-scale body height (4.59D), the upwash was not recorded because the level was too low. Data were taken at the intermediate full-scale body height (1.54D), Figure 22, and at a somewhat higher body height (1.99D), Figure 23.

Figures 22 and 23 show the variation of total pressure and of the difference between total and static pressures across the upwash for the lowest and highest core temperatures. It was found that the upwash pressure profiles were well-centered around the midpoint between the nozzle centerlines and that they were essentially independent of core exit temperature. The temperature across the upwash was almost constant and can be represented by the centerline values plotted in Figure 24.

5.1.4 Model Forces. - Ground-induced interference forces were measured for both the 15° and 45° strake angle configuration for several nozzle pressures and temperatures. The first example, varying fan total pressure with core temperature equal to fan temperature (approximately 24°C), is shown in Figure 25.

| $H_B/D_F$ | Wall Jet Station | $R/D_F$ | $\theta$ | $\frac{(P_T - P_a)_M}{(P_T - P_a)_{FM}}$ | $Z_{.25}/D_F$ | $\frac{(T_T - T_a)_M}{(T_T - T_a)_C}$ |
|---|---|---|---|---|---|---|
| 1.54 | 6 | 1.54 | 90° | .276 | .132 | .173 |
| 1.54 | 8 | 1.28 | 150° | .433 | .122 | .233 |
| 1.54 | 10 | 1.54 | 218° | .354 | .108 | .112 |
| 1.99 | 6 | 1.54 | 90° | .253 | .130 | .173 |
| 1.99 | 8 | 1.28 | 150° | .396 | .119 | .241 |
| 1.99 | 10 | 1.54 | 218° | .346 | .113 | .112 |
| 4.60 | 6 | 1.54 | 90° | 229 | .138 | .200 |
| 4.60 | 8 | 1.28 | 150° | .320 | .138 | .227 |
| 4.60 | 10 | 1.54 | 218° | .323 | .169 | .112 |

Notes: 1) Baseline pressure operation

2) $T_{T,C} = 193°C$

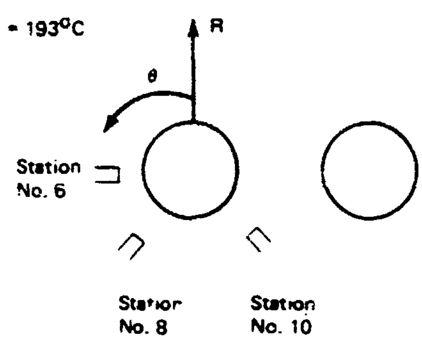


R81-1622-013D

Figure 21 - Data from wall jet profiles resulting from fan jet impingement.

For both the 15° and 45° strakes, changing fan total pressure with core total pressure held constant produced a progression of interference forces with no change in the qualitative behavior with height above ground. Note that, for all these cases, the fan total pressure was well above the core total pressure. The behavior may be changed if the core total pressure becomes equal to or larger than the fan total pressure because of changes in the impinging jet behavior.

A more meaningful view of the effects of the fan total pressure can be found in the non-dimensional presentation with interference force normalized by

ORIGINAL PAGE IS
OF POOR QUALITY

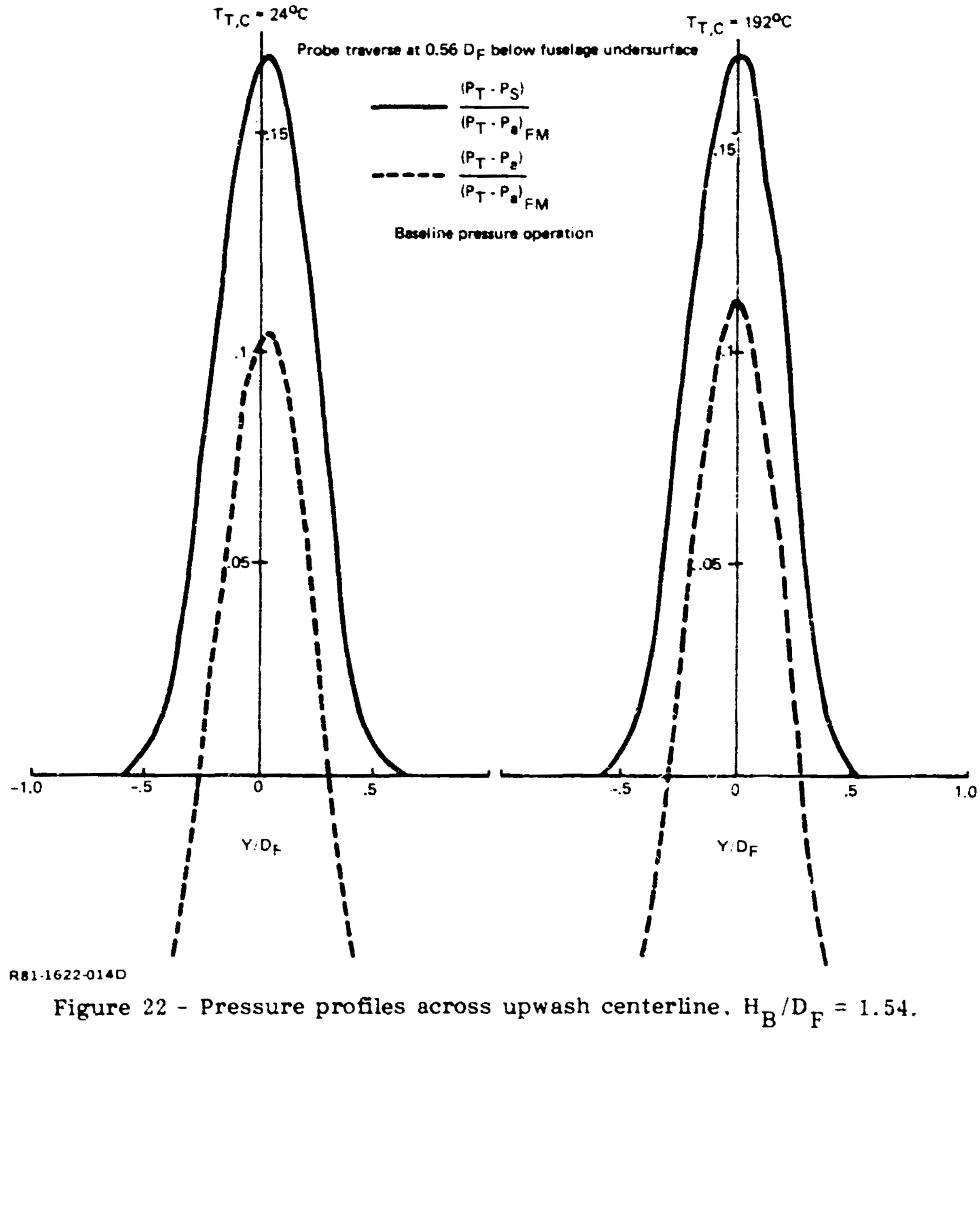


Figure 22 - Pressure profiles across upwash centerline. $H_B/D_F = 1.54$.

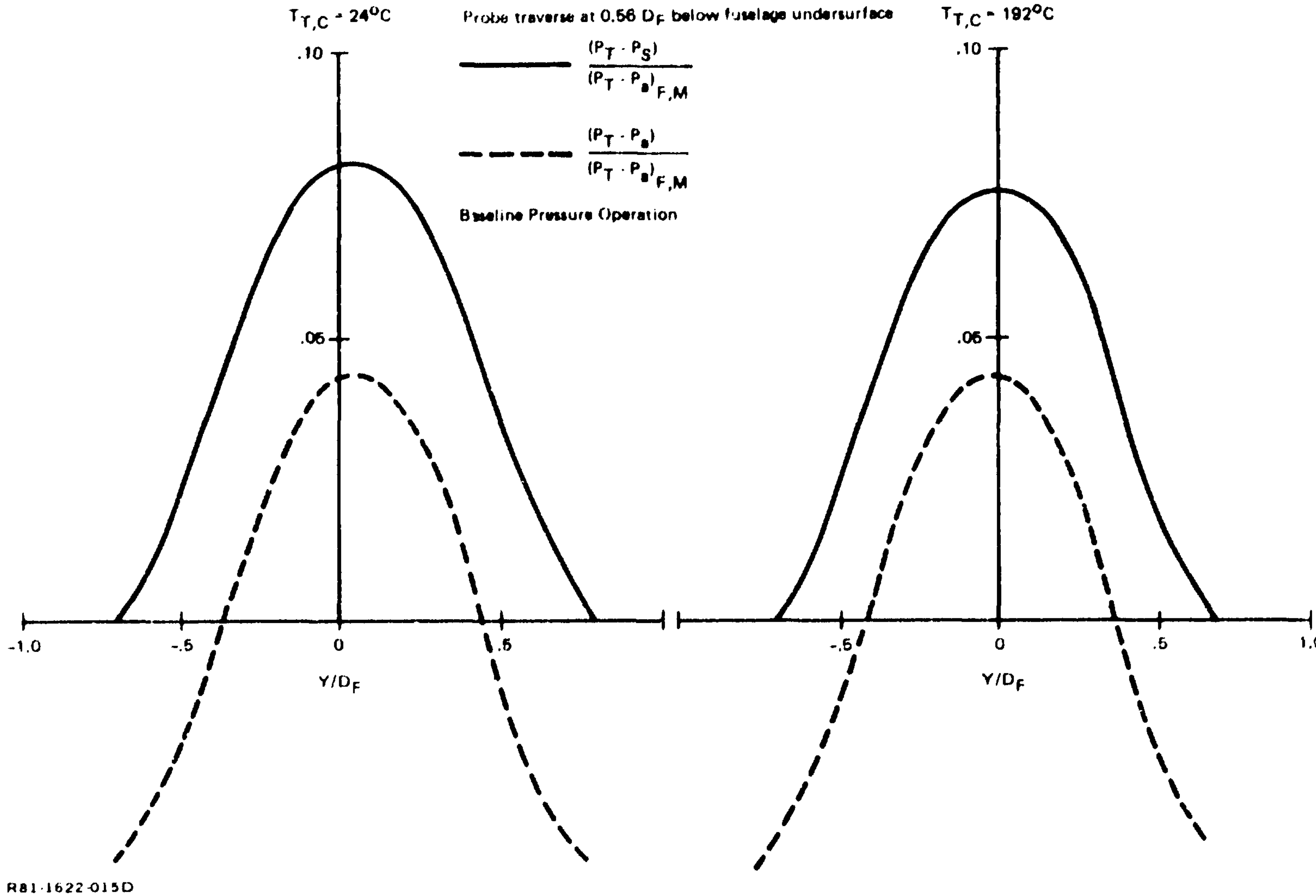


Figure 23 - Pressure profiles across upwash centerline, $H_B/D_F$ = 1.99.

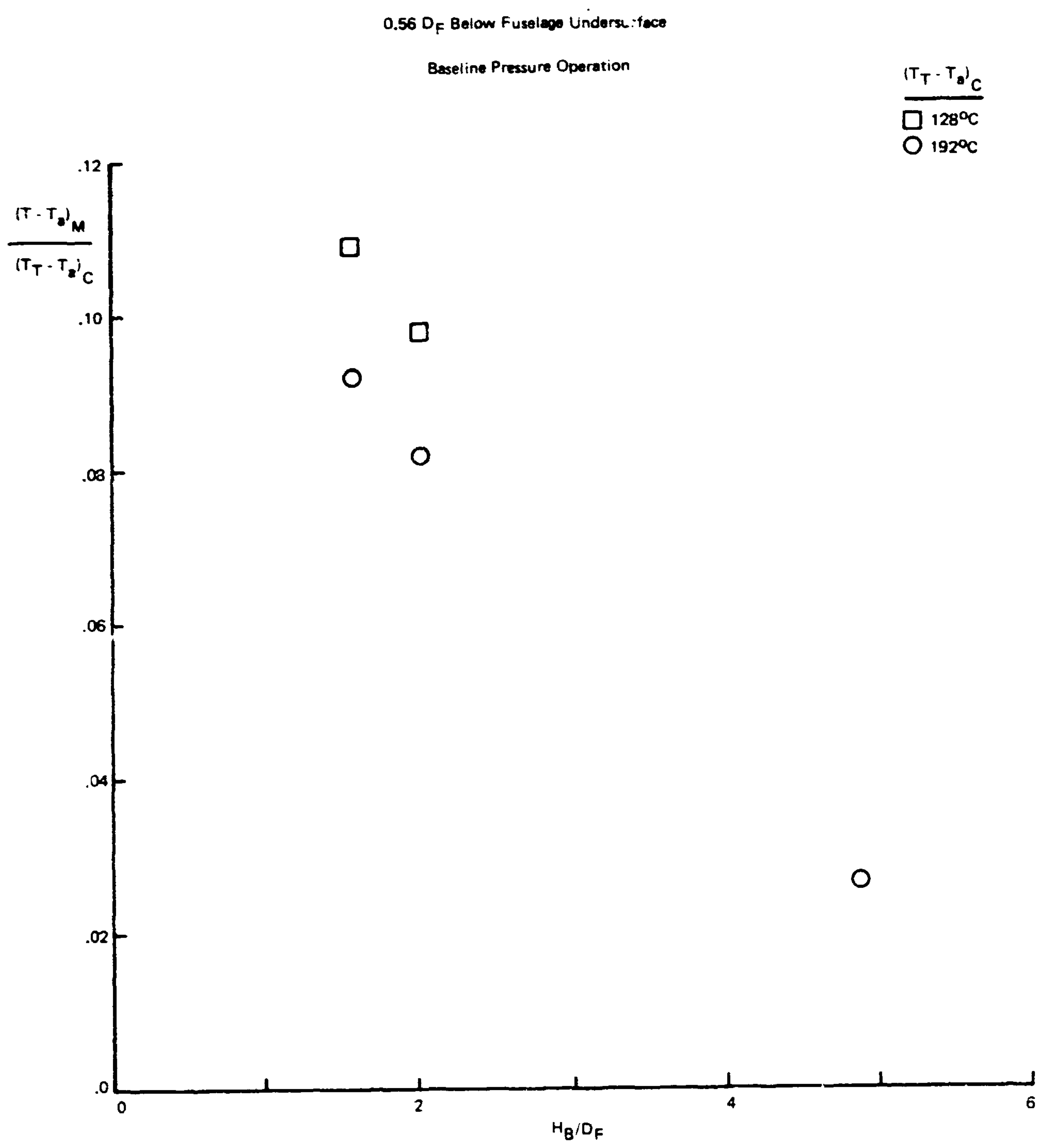


Figure 24 - Variation of centerline upwash temperature with ground height.

ORIGINAL PAGE IS
OF POOR QUALITY

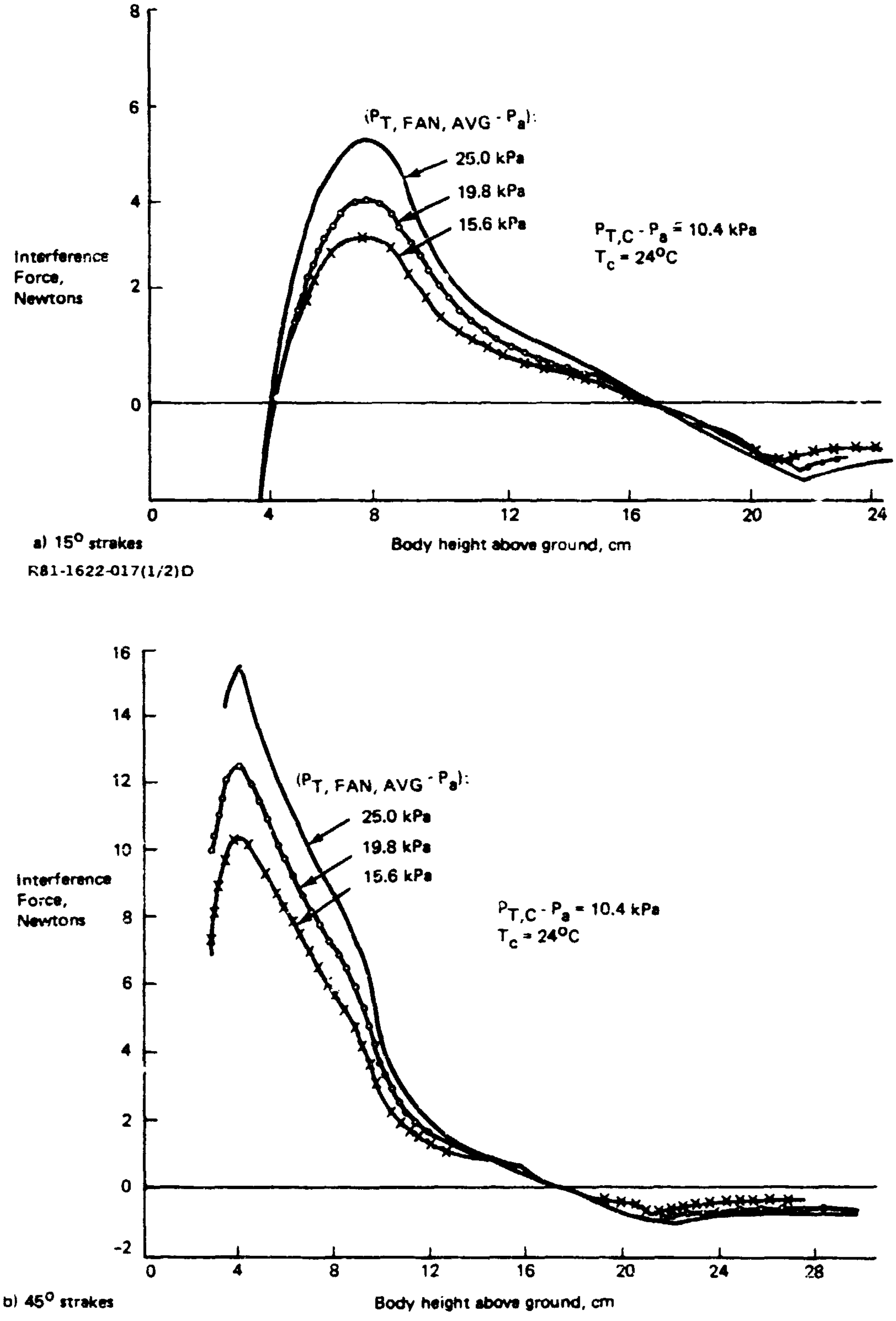


Figure 25 - Effect of fan pressure on interference forces.

the nozzle thrust shown in Figure 26. The total pressure level has no significant effect on the non-dimensional interference forces. Full scale data (from Ref. 1) are shown on this plot for reference.

At a fan average total pressure of 19.8 kPa gauge (and core total pressure, again, at 10.4 kPa gauge) five core total temperatures were run: 43°C, 104°C, 254°C, 322°C and 416°C. As shown in Figure 27, there is essentially no effect of temperature on the interference forces. Experiments were also conducted with the nozzle exit flow more closely matching the full-scale engine conditions. For a fan total pressure of 25 kPa gauge, model forces were measured with core exit temperature of 421°C and 43°C. Figure 27 shows these results compared to the full-scale data (Ref. 1). Again, there is a very small effect of temperature on interference forces. The close agreement between the model test results and the full-scale data indicates that good simulation of aircraft ground interference forces can be obtained with a 1/24th scale model even without core temperature simulation.

5.1.5 Model Surface Pressures and Temperatures. - Pressure and temperature measurements were taken on the model undersurface with the baseline nozzle pressure conditions and core nozzle exit temperatures of 128°C and 192°C. Figure 28 shows dimensionless temperature distributions along the model underside (x-direction) for three heights above ground. The temperature across the model surface (y-direction) showed little variation. Values of the surface temperature coefficient $((T-T_a)/(T_c-T_a))$ at station number 22 (0.54D aft of the nacelle centerline) are very close to values found with a probe on the upwash centerline at 0.56D below the model surface (Figure 24). This comparison provides some verification for the model surface temperature data, which were taken by thermocouples attached to the inner surface of the metallic underside of the model as described in Subsection 4.7.2. Figure 29 shows the variation of model temperature and pressure with body height above ground. The temperature was measured at station number 22 and the pressure at the midpoint between nozzles.

Model pressure and temperature data were also taken for a higher core temperature and a higher fan pressure that more closely matched the full-

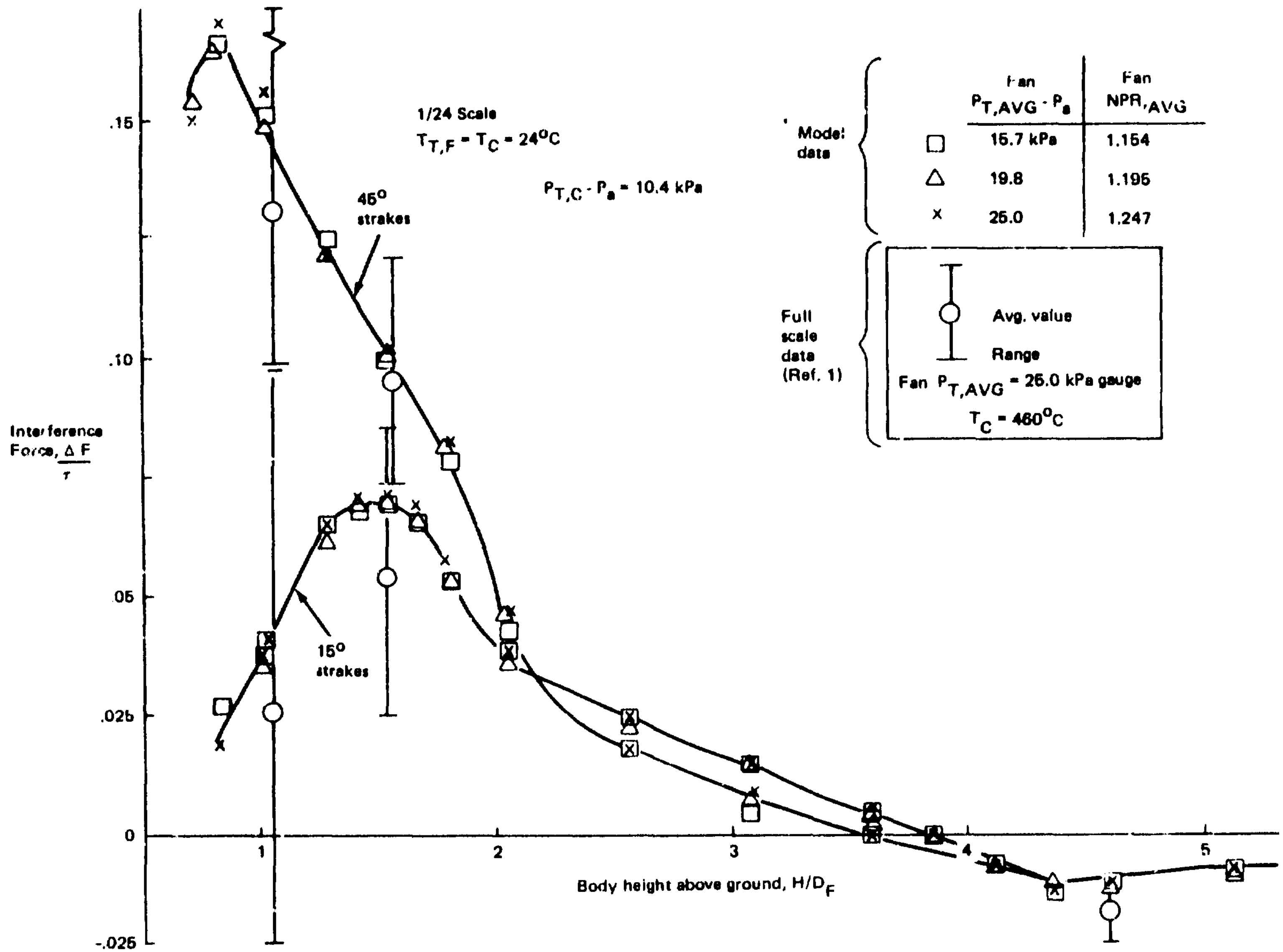


R81-1622-018D

Figure 26 - Effect of fan nozzle pressure on interference forces

ORIGINAL PAGE IS
OF POOR QUALITY

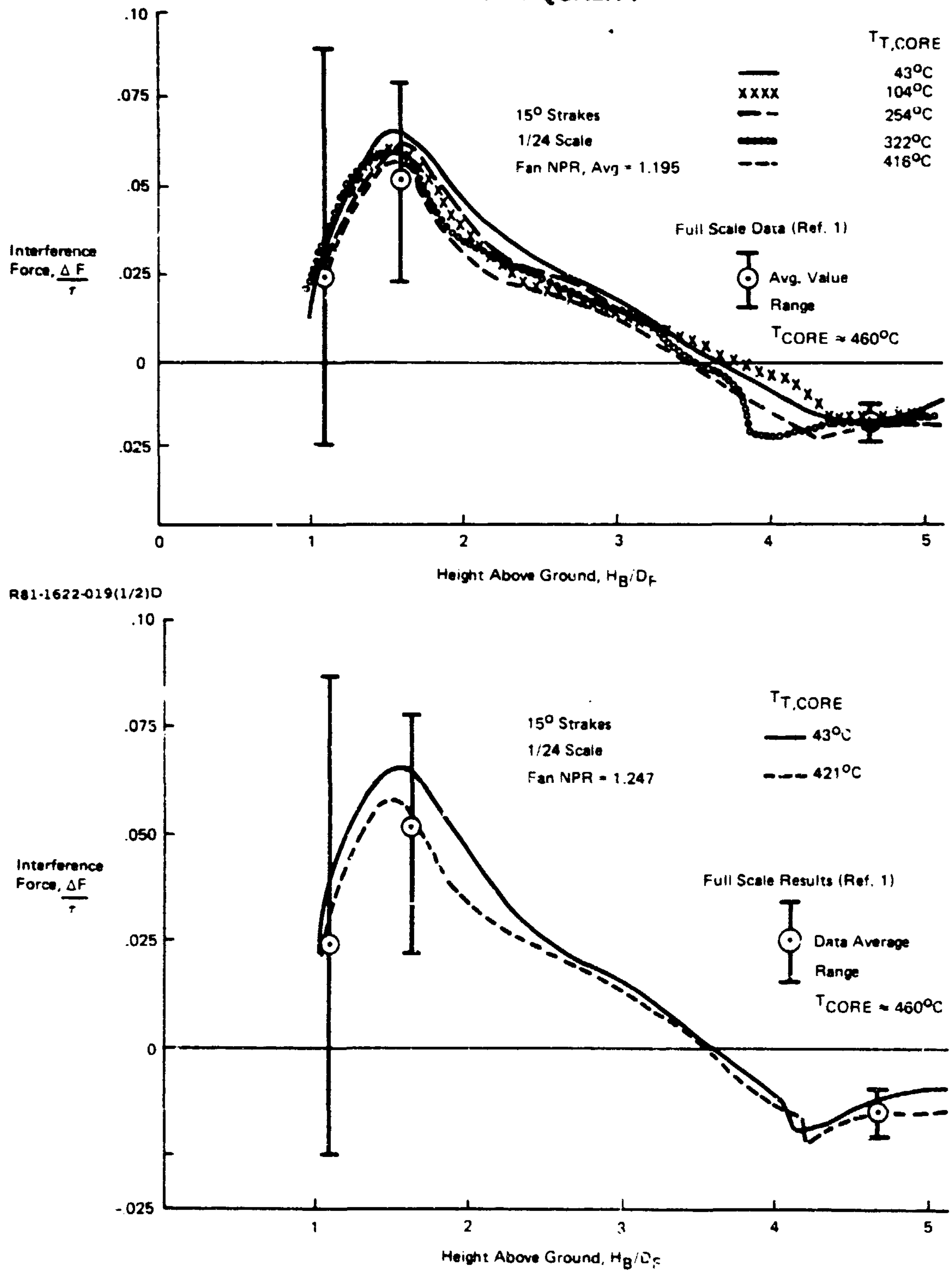


Figure 27 - Effect of core temperature and fan pressure ratio on interference forces. $T_{T,F} = 24^{o}C$.

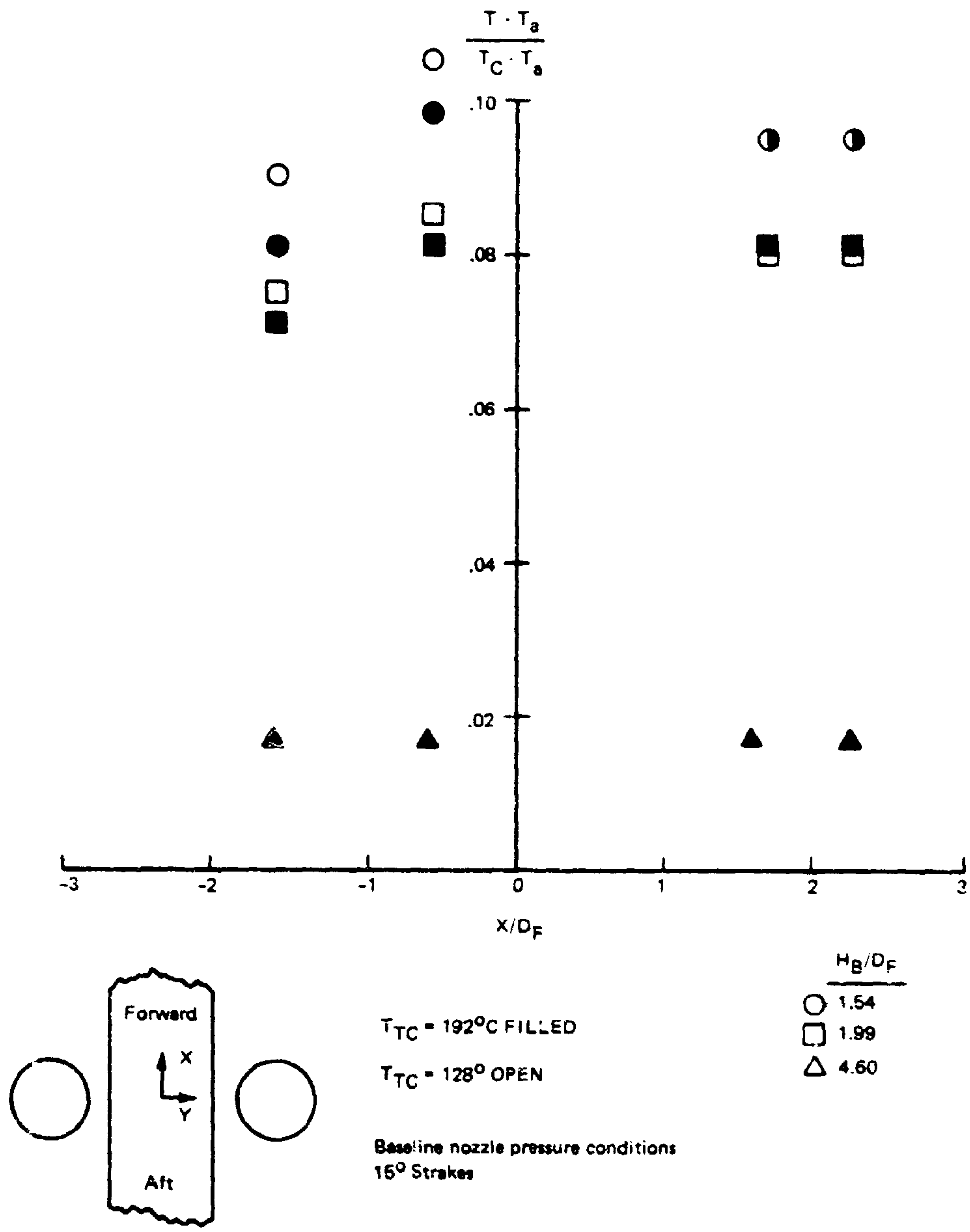

R81-1622-020D

Figure 28 - Temperature distribution along model underside.

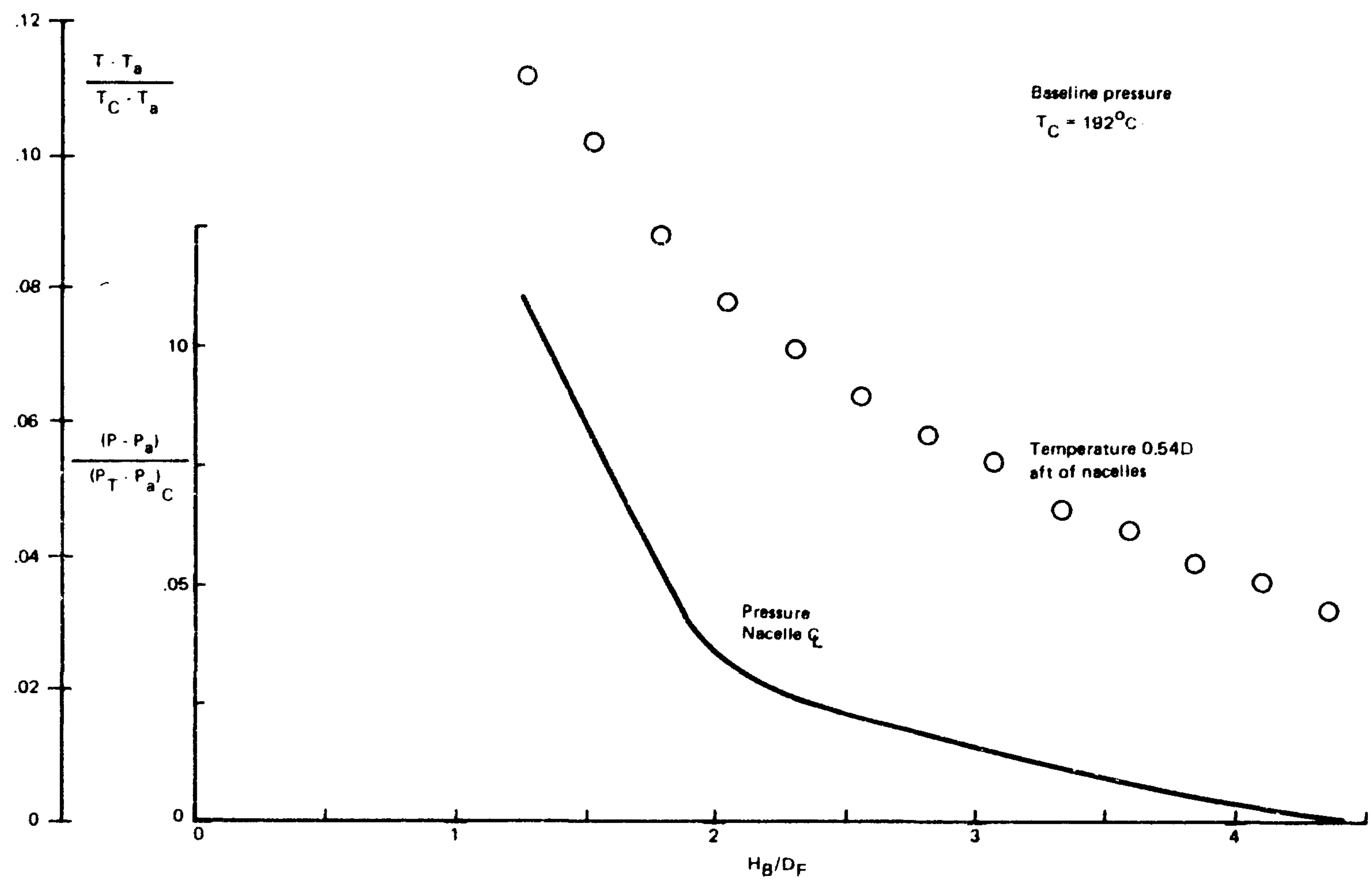


R81-1622-021C

Figure 29 - Variation of model pressure and temperature with ground height.

scale tests. Figures 30 and 31 show pressure and temperature measurements taken at three heights above ground for a core exit temperature of 427°C. The relatively low model surface temperatures shown at $X/D_F$ = 0.5 in Figure 31 are not due to faulty thermocouples. Temperatures on both sides (y-direction) of this centerline thermocouple showed the same values, which verified that the temperature profile along the model had a local minimum slightly forward of the nacelle centerline. The magnitude of this local minimum varied with height above ground. This distortion did not appear in the data taken at lower core temperature (Figure 28) because this centerline thermocouple and one of the side thermocouples were inoperative during the earlier tests.

Comparison of the data shown in Figure 31 with those shown in Figure 28 indicates that the model surface temperature does not scale well with wide variations in core exit temperature. The model surface temperature coefficient decreased by more than a factor of two when the core flow temperature was raised from 128°C to 421°C. The same poor temperature scaling appeared in probe temperature measurements on the upwash centerline (Figure 24). In this case, the local temperature coefficient in the flow decreased by 15 percent when the core exit temperature was raised from 128°C to 192°C.

Probe temperature surveys were made in the area corresponding to the inlets on the full-scale model ($1.8D_F$ above the model upper surface, close to the outer surface of the fan nozzles). It was found that the temperature in this region was very close to ambient, and fluctuating greatly. The maximum temperature rise observed for a nozzle total temperature of 192°C was approximately 2°C. The strakes apparently turn the flow enough to prevent any significant amount of upflow from reaching the inlet area. The inlet suction may affect the flow field to alter this behavior, but this is not expected to happen.

## 5.2 Open Circular Nozzles

5.2.1 Nozzle Flow. - Free jet data were taken with the ground plane removed, using settling chamber temperatures from ambient to 232°C, and a settling chamber pressure of 27.6 kPa above ambient. Total pressure and temperature profiles were recorded for probe traverses across both jet centerlines for dis-

ORIGINAL PAGE IS
OF POOR QUALITY

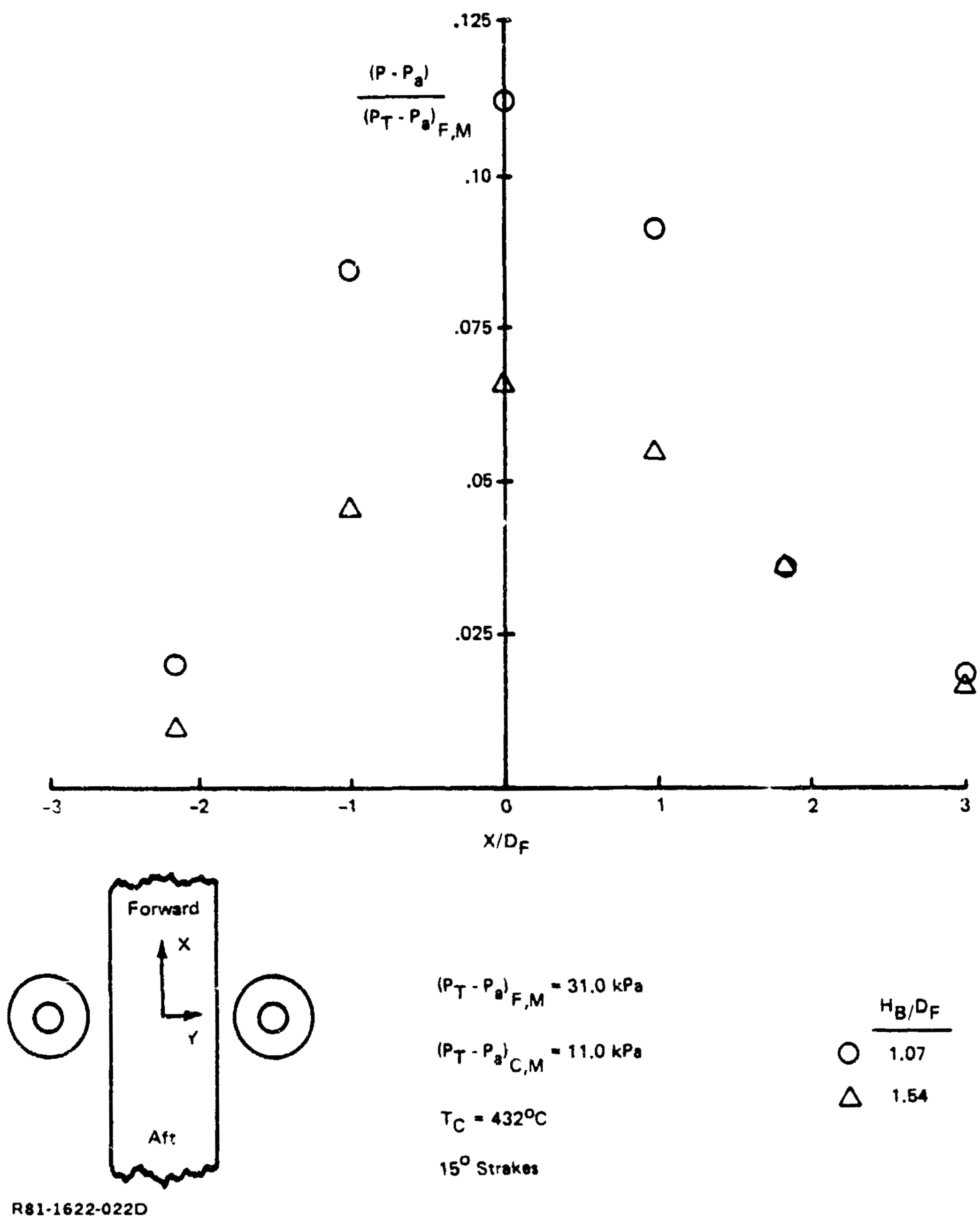


Figure 30a - Pressure distribution along model.

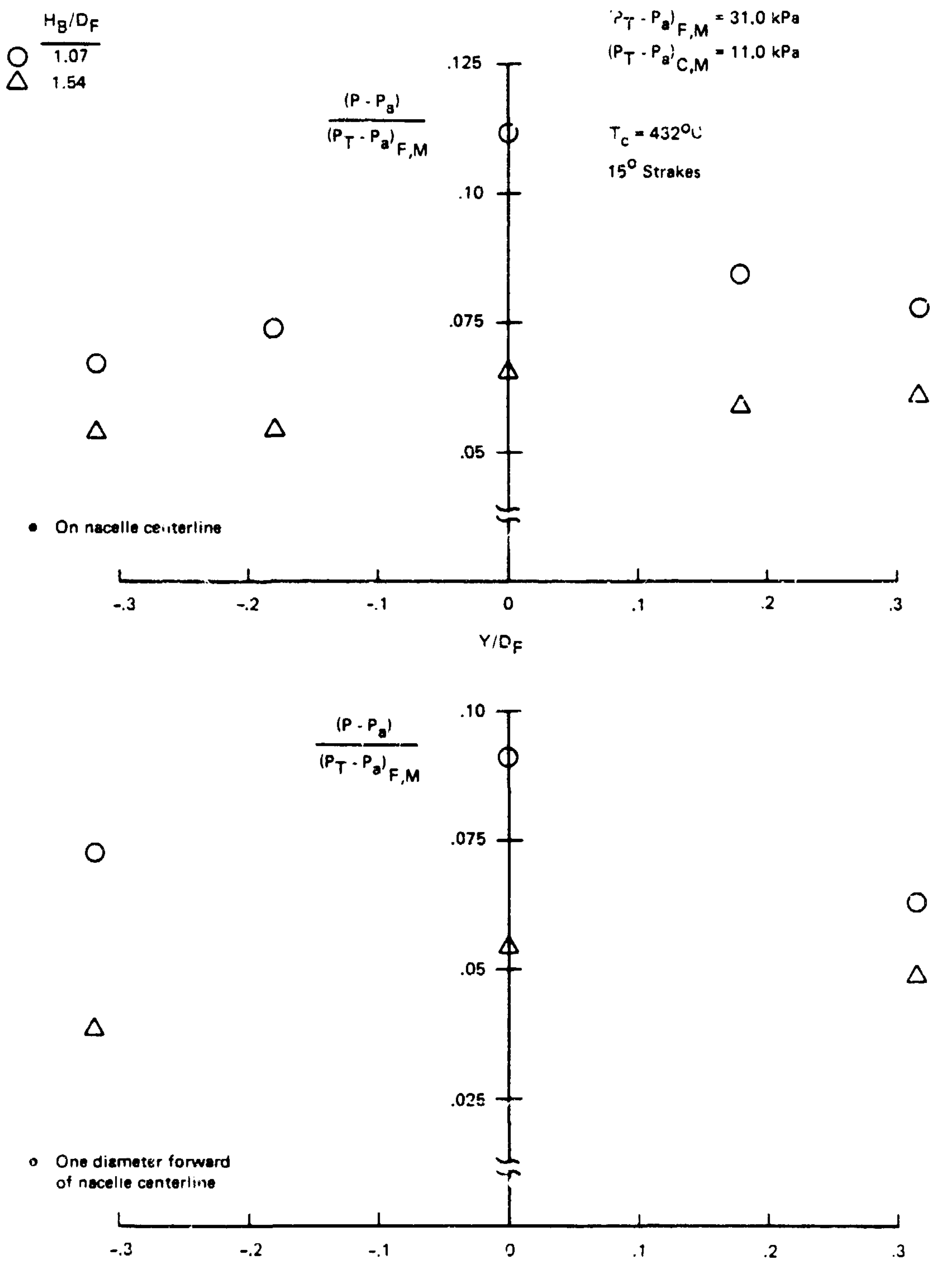


R81-1622-023D

Figure 30b - Pressure distribution across model.

Ol... OF P... QUALITY

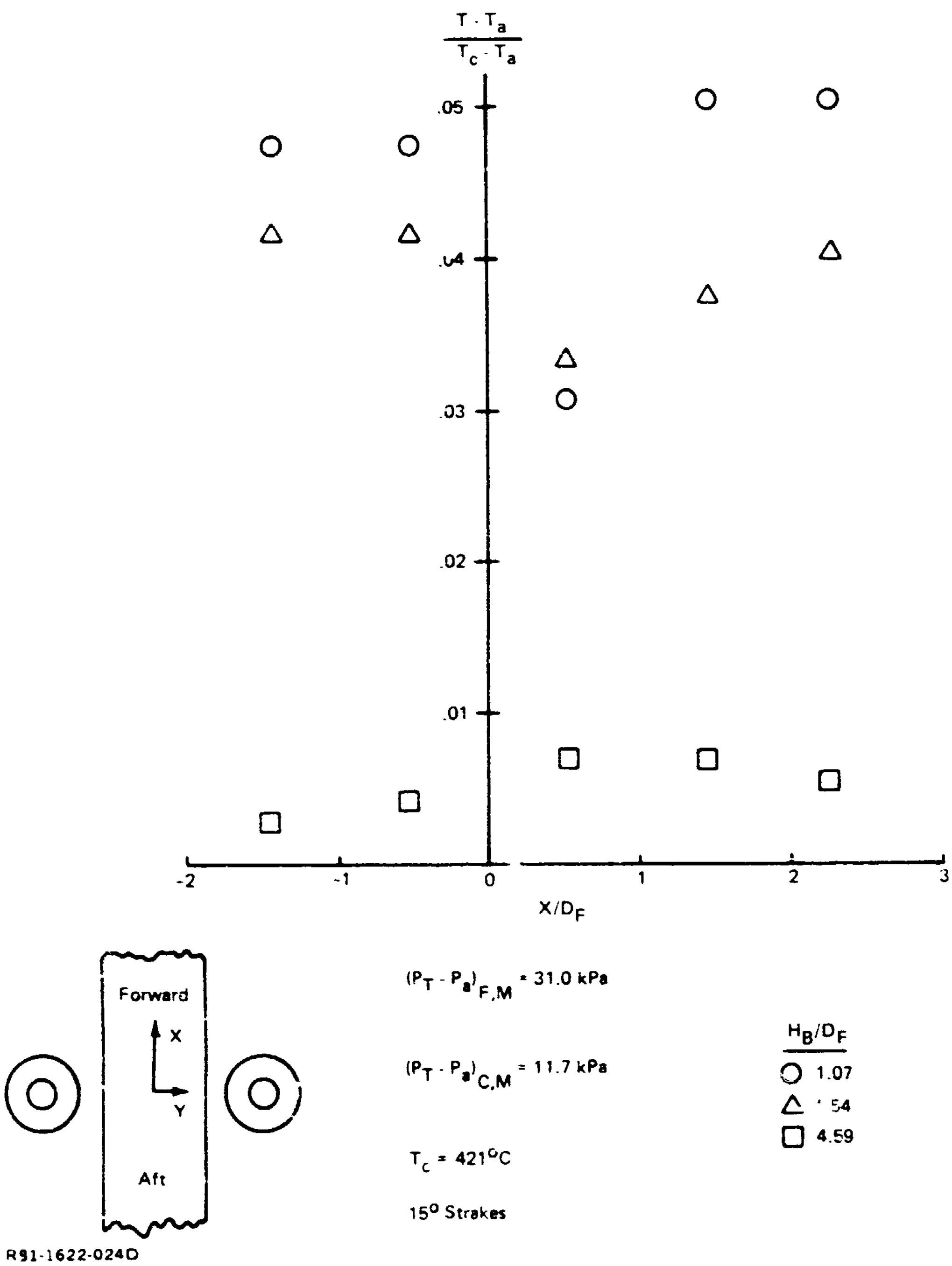


Figure 31 - Model temperature distribution.

tances (Z') from the jet exists up to 15 diameters. Figure 32 shows pitot pressure profiles obtained with a settling chamber temperature of 227$^{o}$C. Profiles taken close to the exit exhibit a flat-topped profile with a 1 percent ripple that was caused by fluctuations with time of the air supply pressure. Note that there is no inward shift of the maximum pitot pressure points at large values of Z' as occurred in the free-stream data obtained with fan-jet nozzles. The corresponding temperature profiles are shown in Figure 33. These temperature data were plotted directly from the thermocouple output and have not been corrected for radiation losses. (This correction was typically of the order of 10$^{o}$C.) The pressure profiles begin to merge about seven diameters from the nozzle exit. The temperature profiles show a greater radial spreading and begin to merge about five diameters from the nozzle exit.

Figure 34 shows data taken from profiles that were obtained with different settling chamber temperatures. The data show the decay of pitot pressure and temperature along one jet centerline with two jets in operation. The centerline pitot pressure decay is slightly greater for heated than for unheated jets. Several runs made with one nozzle blocked off showed no difference between the single- and dual-jet results in the centerline values of both pitot pressure and temperature out to Z' = 15 diameters. Hence, the decay in centerline properties obtained from two jet operation can be used to represent single-jet operation.

5.2.2 <u>Ground Flow without Model</u>. - Ground-pressure and wall-jet profiles were taken at three values of H/D corresponding to the full-scale test conditions. Ground pressure measurements were taken without the model to determine how closely the radial pressure distribution around one jet impingement point matched existing single-jet impingement data. Figure 35 shows the data taken along radial paths at two orientations around one jet centerline. The solid curve, taken from Ref. 2, represents an empirical approximation for the ground pressure distribution for a single jet with H/D between 2.0 and 5.0.

Wall-jet profiles (similar to those shown in Figure 20) were taken at the same values of H/D and the same ground locations used in the full-scale

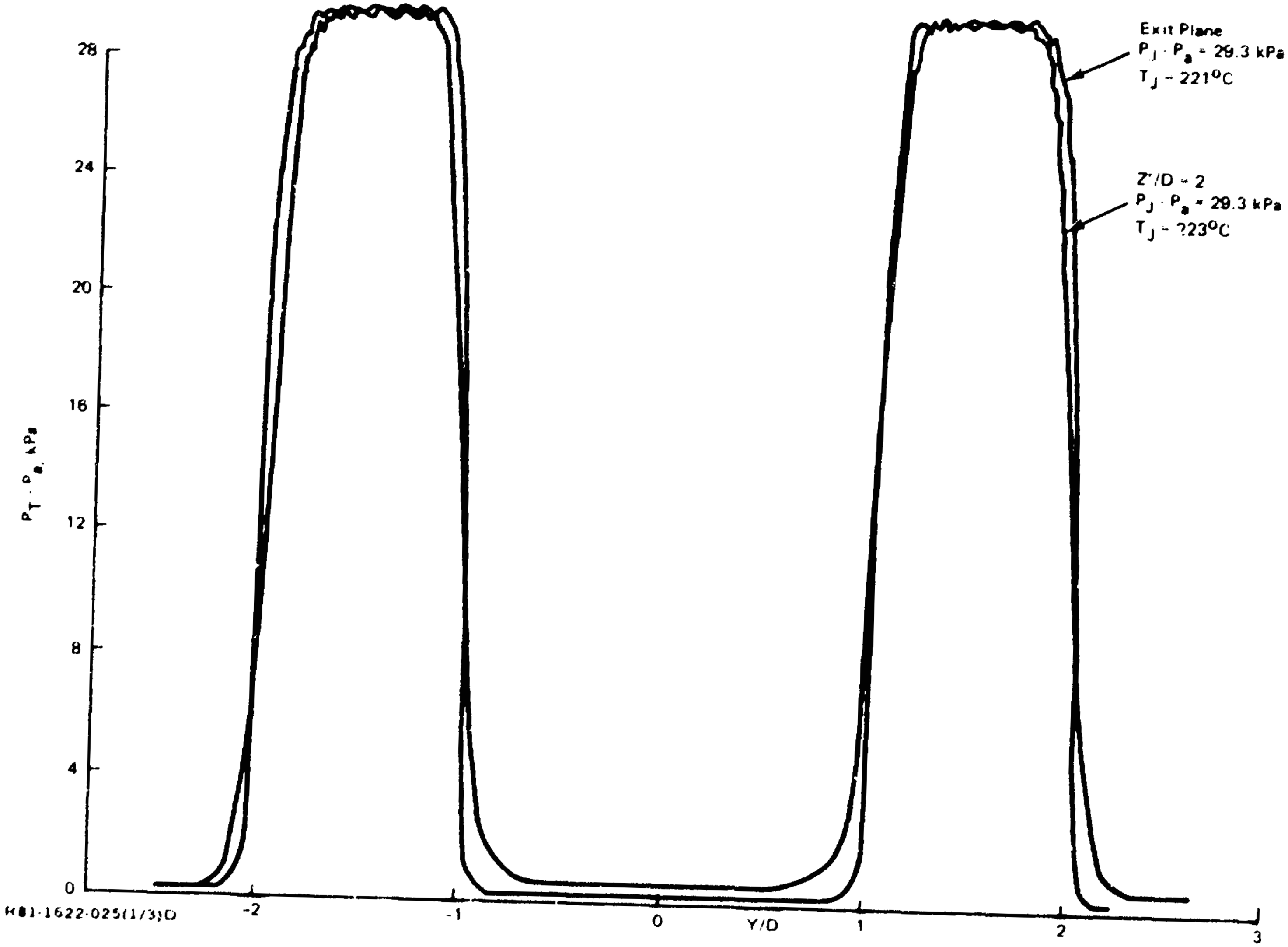


Figure 32 Free jet total pressure surveys, open circular nozzles.

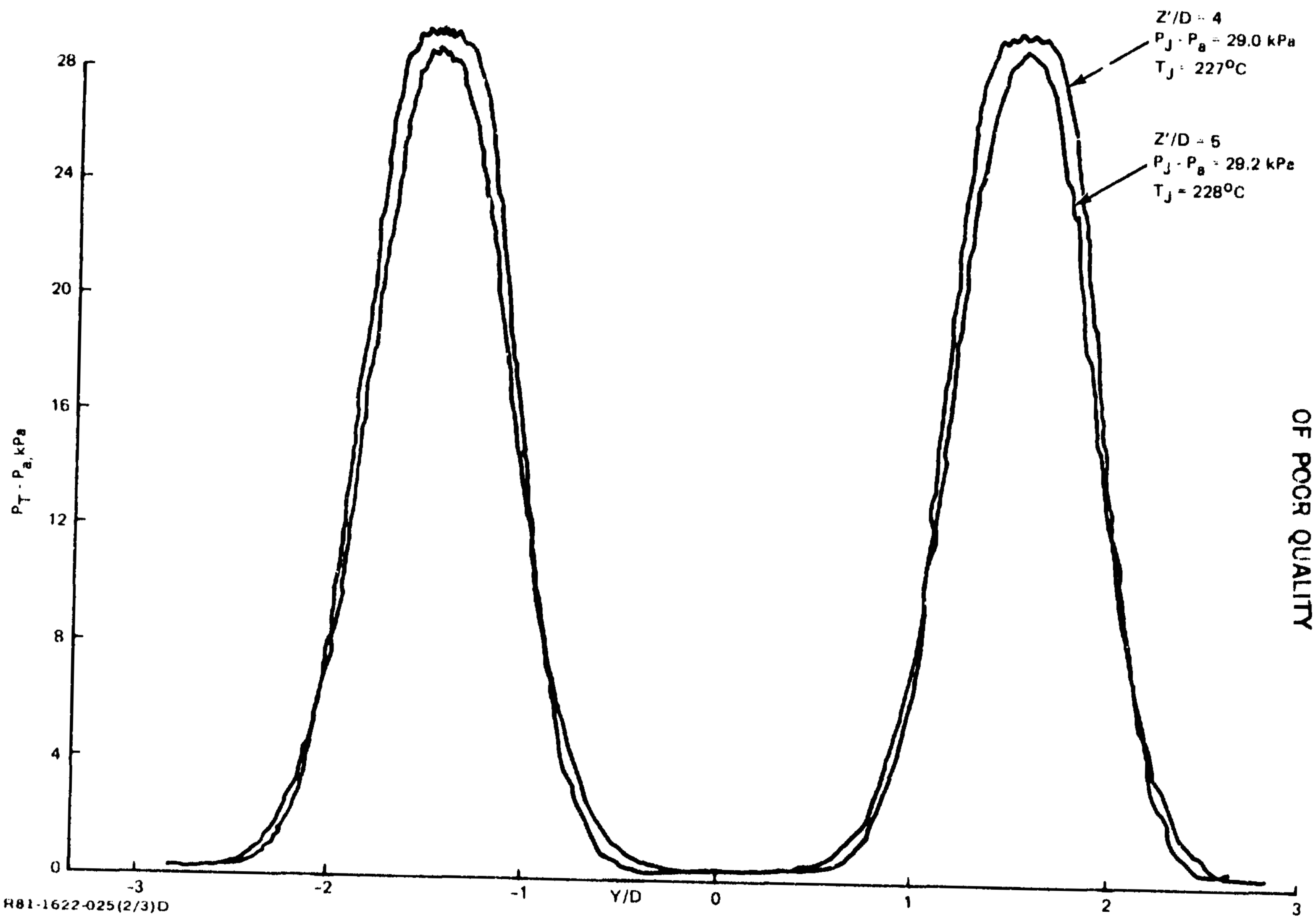


Figure 32 -- (Continued).

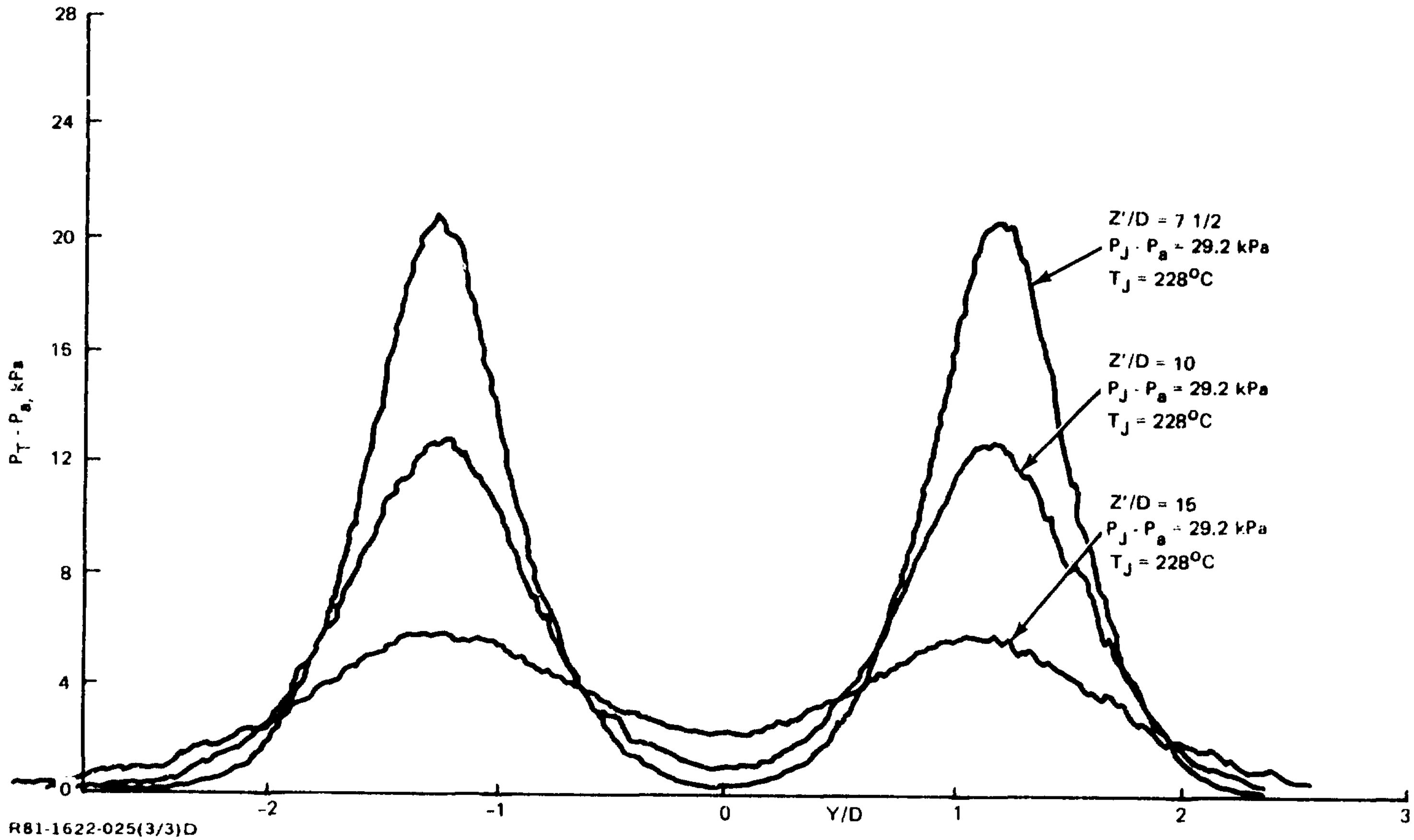


Figure 32 - (Concluded).

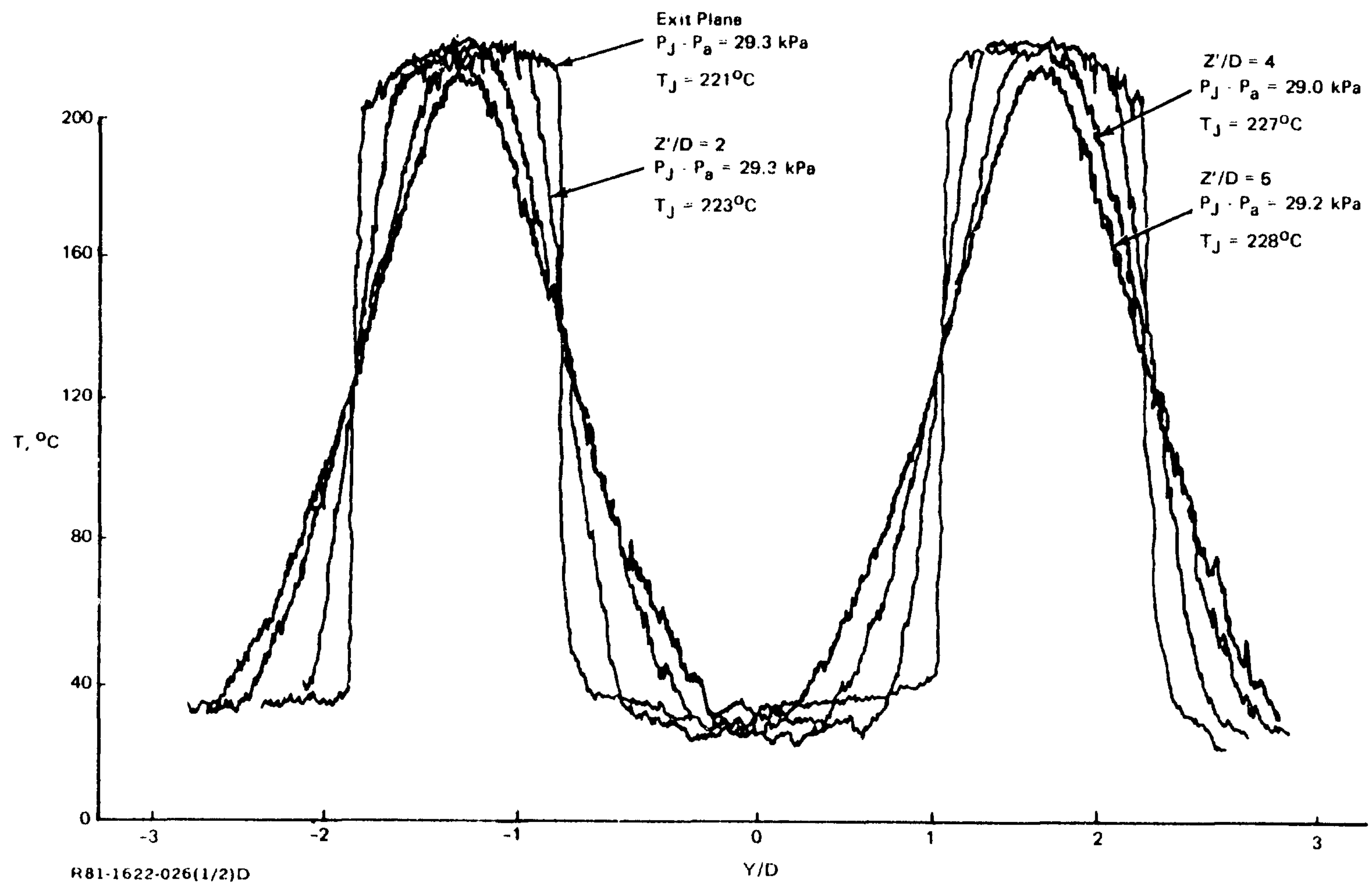


Figure 33 - Free jet total temperature surveys, open circular nozzles.

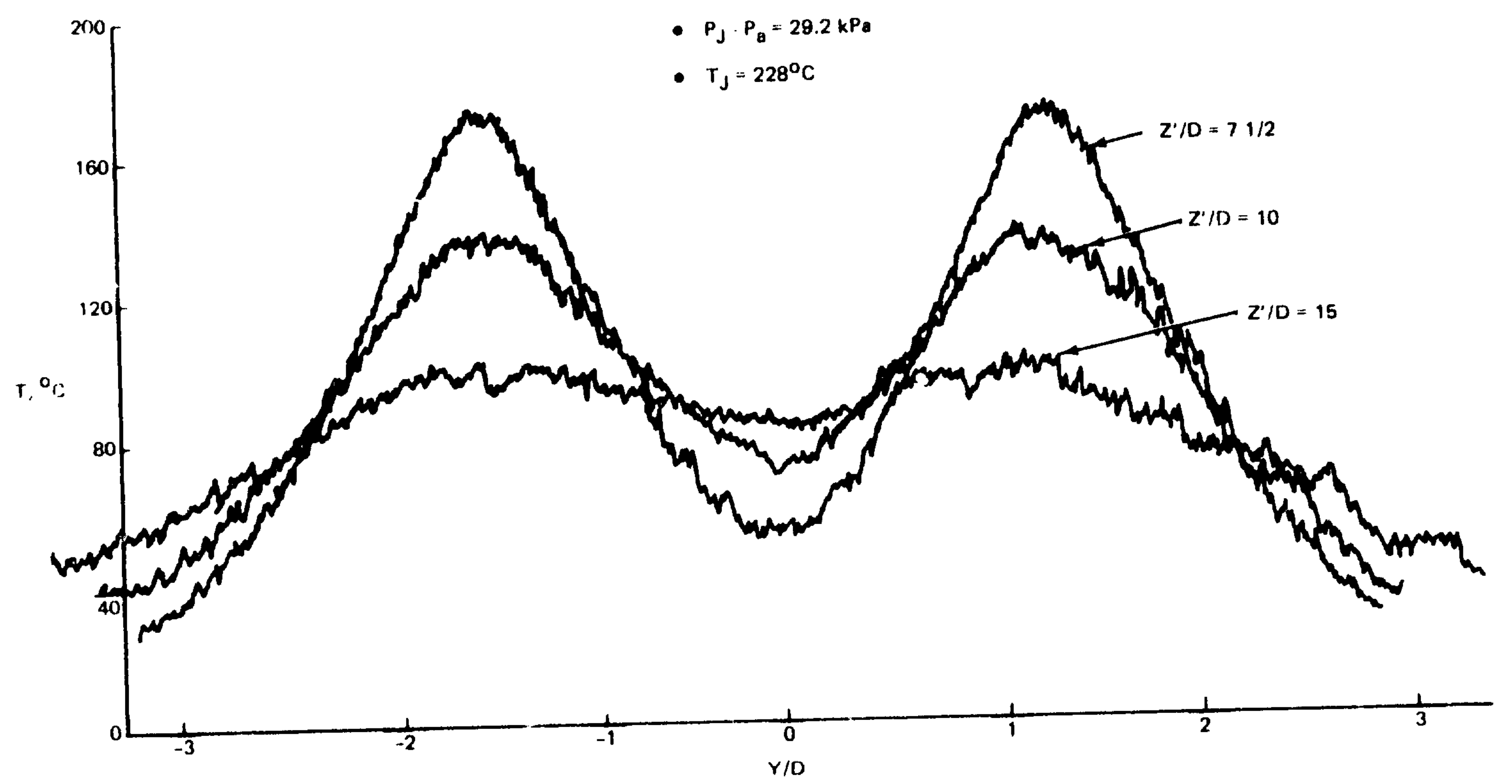


R81-1622-026(2/2)D

Figure 33 - (Concluded).

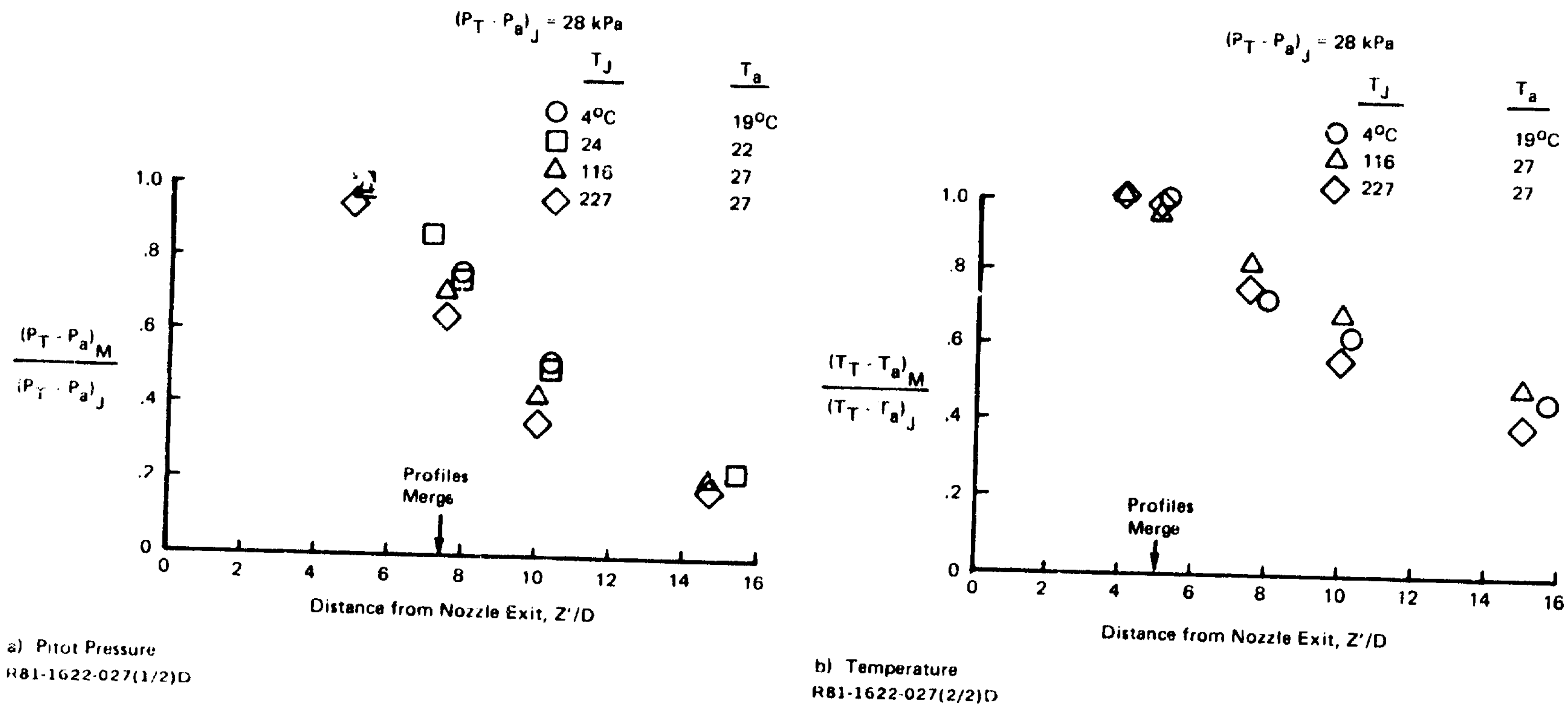


Figure 34 - Free jet properties along one flow centerline, two jets operating, open circular nozzles; data representative of single-jet operation.

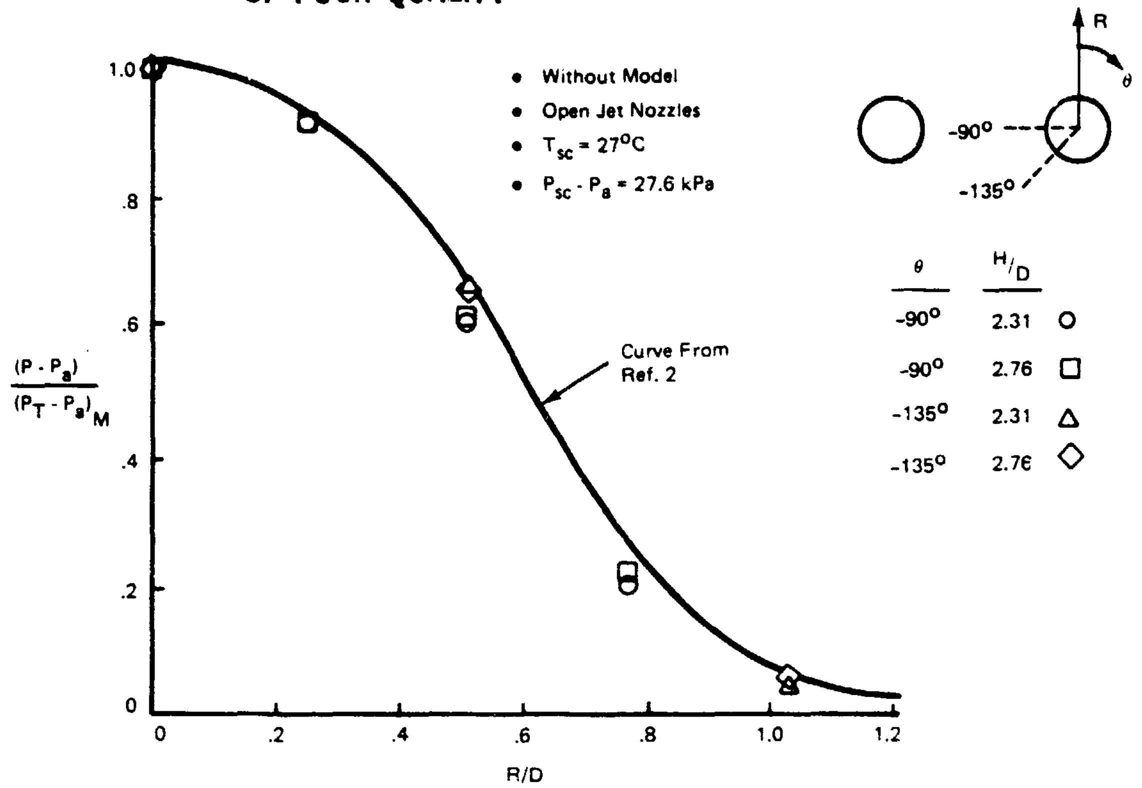


R81-1622-028D

Figure 35 - Radial ground pressure distribution around one jet impingement center.

fan-jet tests. These measurements, summarized by plots of maximum total pressure and thickness in Figure 36, show little influence of temperature on the wall-jet pressure data.

This figure suggests that the wall-jet flow was not axially symmetric around one jet impingement point. Wall-jet profiles taken at the same radius from the closest impingement center show that the flow directed toward the stagnation line has a higher peak total pressure and a greater thickness than the flow directed away from it. This trend occurs for all tested heights above the ground and all settling chamber temperatures. This apparent lack of symmetry in the wall jet data around one impinging jet is probably a real distortion of the ground flow caused by the impingement of the second jet, but may have been caused by interference of the probe support with the upwash formation region when it was located at Station No. 10 (see sketch in Figure 36).

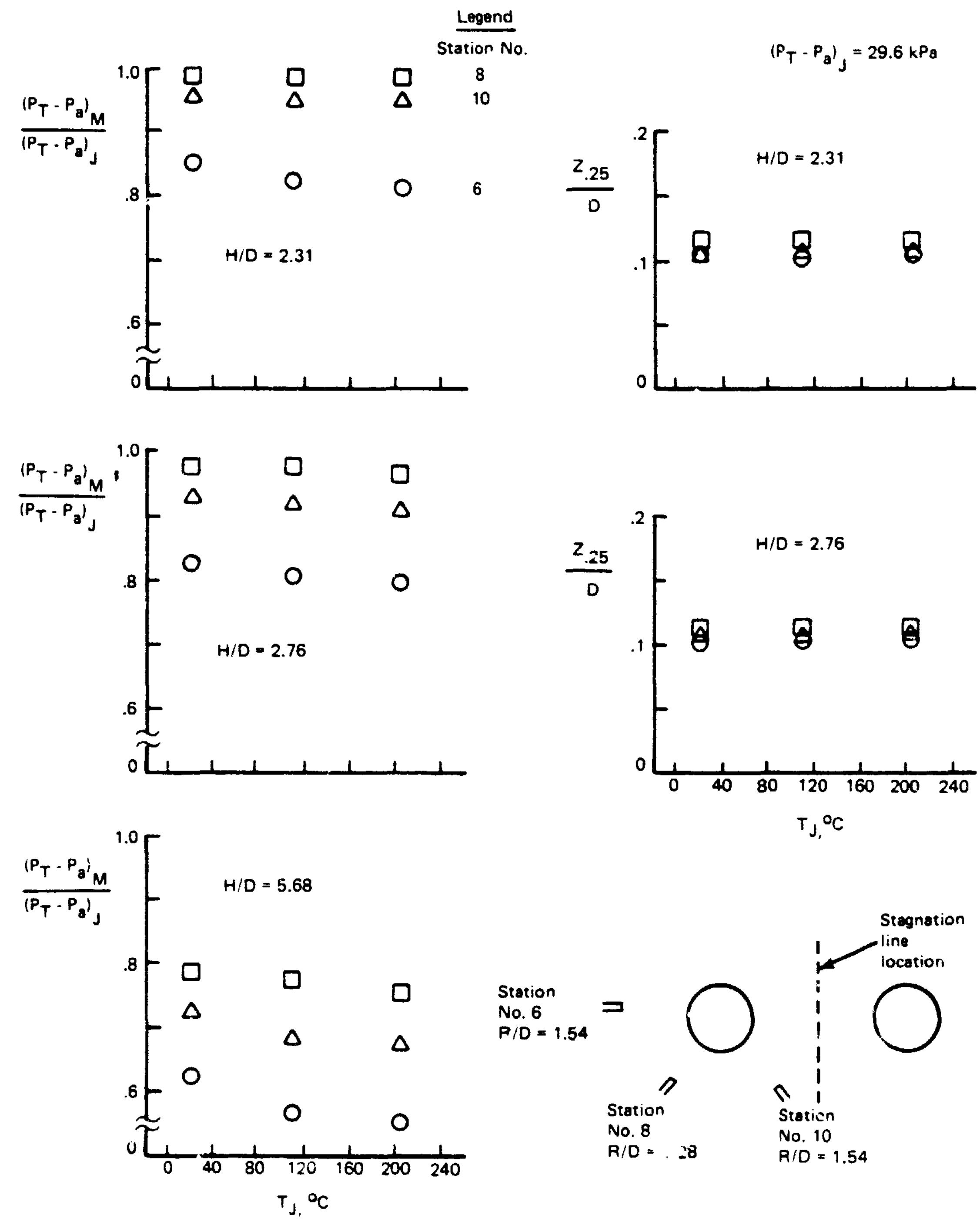


Figure 36 - Data from wall jet profiles, open jet impingement.

5.2.3 Upwash Flow without Model. - Measurements were taken in the upwash without the model to evaluate flow properties in the absence of model blockage effects. The probes were traversed through the upwash at the nozzle exit plane for several values of H/D and a range of settling chamber temperatures. The results are summarized by the centerline values of upwash properties at the nozzle exit plane that are plotted in Figure 37. The data obtained from the pressure probes were essentially unaffected by temperature. Temperature profiles across the upwash were almost flat, and the exit plane temperatures show little variation with ground height out to H/D = 4.

Additional upwash surveys were made at a fixed nozzle height above ground by traversing the probe through the upwash at various probe heights above ground. The results are summarized in Figure 38 which shows the variation of temperature and pressure along the upwash centerline for H/D = 3. These pressure plots also show little influence of jet exit temperature.

The effect of settling chamber pressure on upwash properties with jet temperature equal to ambient was investigated by conducting exit-plane probe traverses at various ground heights. Figure 39 shows that the centerline properties at the nozzle exit plane, for ground heights of 2-1/2 nozzle diameters or greater, vary linearly with settling chamber pressure over a wide range. Furthermore, these measurements agree with past data taken at this jet spacing in our low-pressure facility. The lack of pressure scaling at low ground heights may be caused by the influence of the ground interaction flow on nozzle exit conditions. As brought out in Ref. 3, the pressure distribution inside the nozzles close to the exit (for this jet spacing) becomes non-uniform when the ground is brought closer than 2-1/2 diameters to the nozzle exit.

The magnitude of the upwash pressure data shown in Figure 39 illustrates that the upwash flow at the nozzle exit plane can be treated as an incompressible flow for all of the nozzle exit conditions and all of the ground heights, even though the nozzle exit flow itself was in the compressible flow range. Flow with a dynamic pressure less than about 5 kPa (corresponding to airflow velocity less than 90 m/sec) can be considered incompressible without a loss in accuracy. Below this value, the dynamic pressure can be found from the difference between total and static pressures. Dynamic pressure much

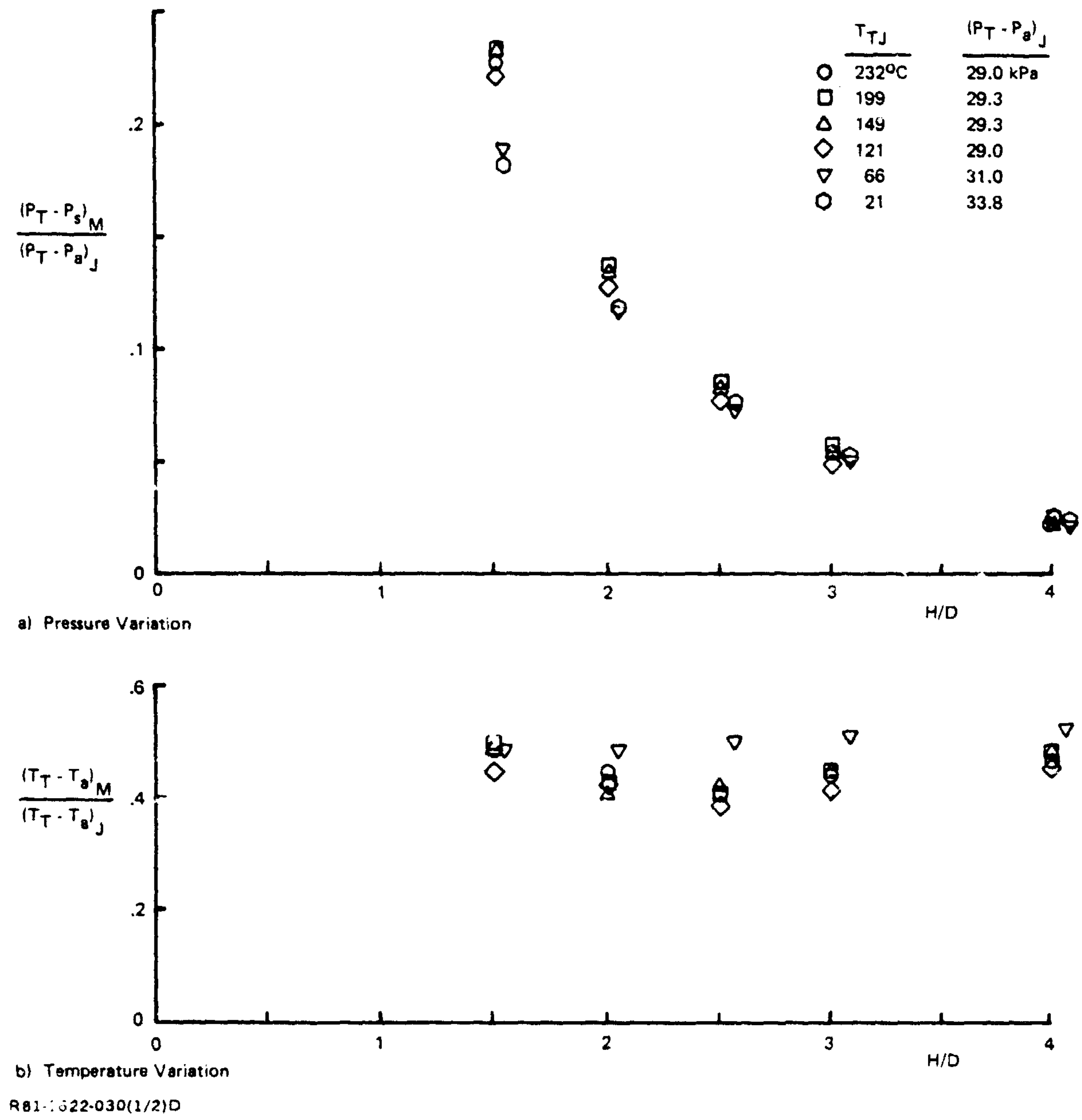


Figure 37 - Upwash properties at nozzle exit plane.

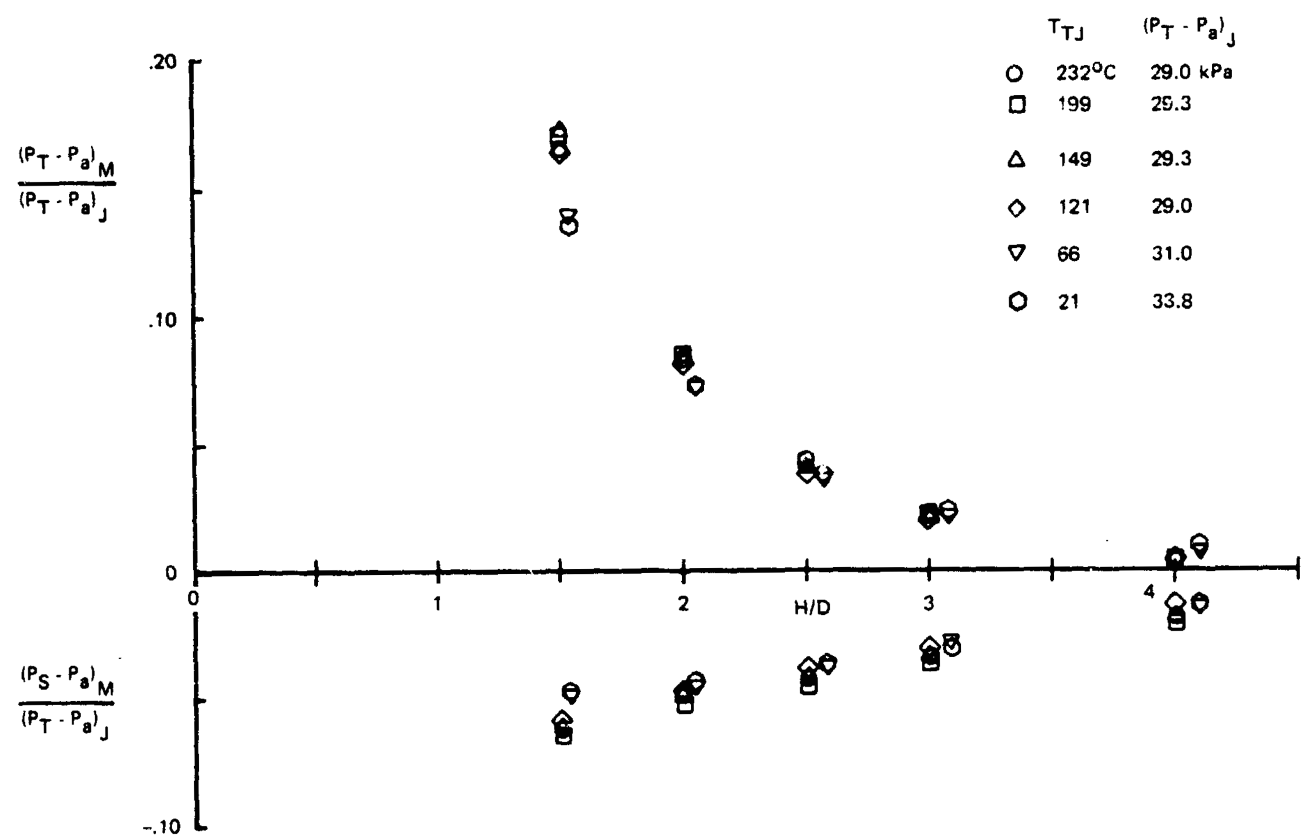


c) Total and Static Pressure

R81-1622-030(2/2)D

Figure 37 - (Concluded).

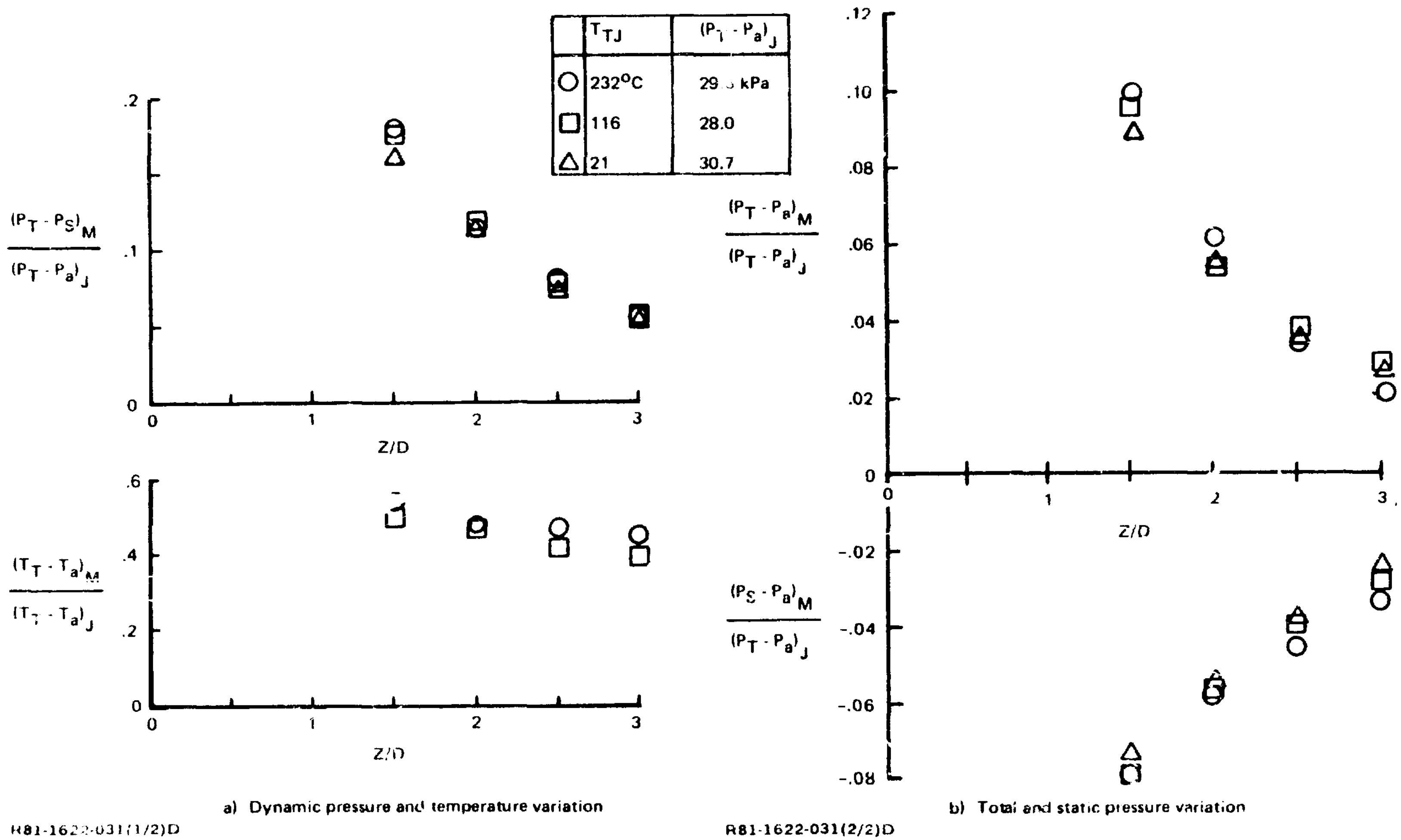


Figure 38 - Upwash properties between nozzle exit plane and ground, H/D = 3.

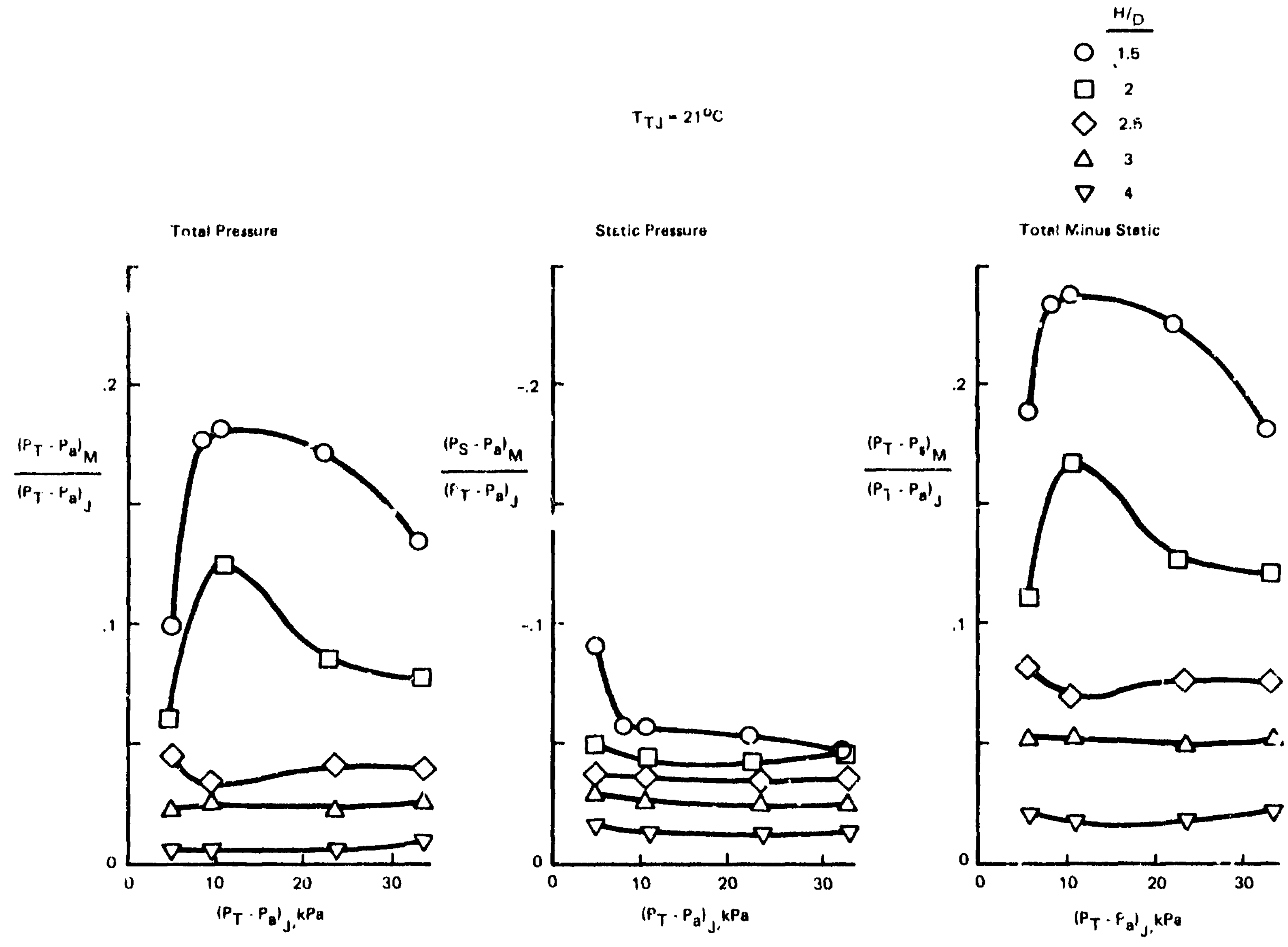


Figure 39 - Effect of settling chamber pressure on upwash properties at nozzle exit plane.

higher than this (somewhat arbitary) 5kPa level requires a compressible flow approach to determine dynamic pressure, since it cannot be found by subtracting static pressure from total pressure. Nozzle exit total pressure was greater than 5 kPa for almost all of our experimental work.

Therefore, for all of the data shown in Figure 39, the quantity $(P_T-P_S)$ represents the upwash dynamic pressure on the centerline at the nozzle exit plane, and the flow velocity corresponding to this dynamic pressure can be evaluated with incompressible flow relations. Total pressures were measured with a Kiel probe and static pressures with a static probe aligned with the mean flow direction (probe dimensions are given in Subsection 4.7.3). Traversing both probes through the flow simultaneously ( with fixed inter-probe distance, Y') provided direct plots of the total and static pressure profiles. When overlaid and shifted a distance, Y', one can trace a profile of $(P_T-P_S)$. Data shown as $(P_T-P_S)_M$ in Figure 37, 38 and 39 were all obtained from the peak value of such tracings.

5.2.4 Effect of Model on Ground Flow. - Ground pressure measurements taken with and without the model in place showed that the model had little influence on the pressure close to the stagnation line but did change the pressure in the jet impingement region. Figure 40 shows the distribution of ground pressure in one of the jet impingement regions along a line connecting the two jet centerlines. The solid curve represents an empirical approximation for the ground pressure distribution for single jet impingement. Comparison with data taken at the same locations without the model (Figure 24) shows that the model reduces the pressure in this part of the impingement region. Data in Figure 40 for different jet temperatures show no significant temperature effect.

5.2.5 Effect of Model on Upwash. - Probe traverses were taken across the upwash with and without the model in place to determine the influence of the model on upwash properties. The temperature profiles across the upwash presented in Figure 41 show that the presence of the model raises the temperature of the upwash approaching the model. The increased upwash temperature with the m del in place indicates a recirculating flow entrainment caused by model blockage.

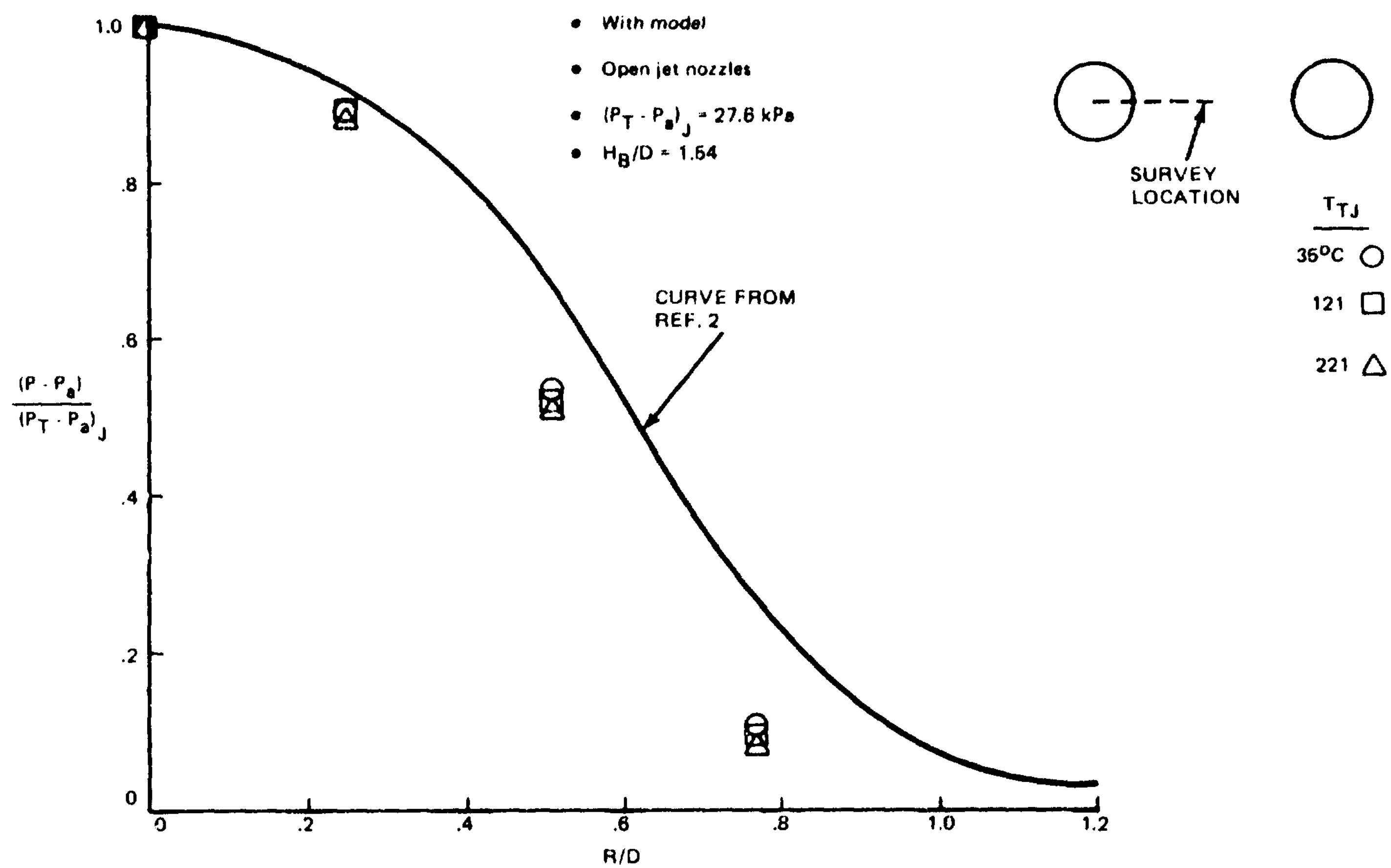


R81-1622-033D

Figure 40 - Radial ground pressure distribution around one jet impingement center.

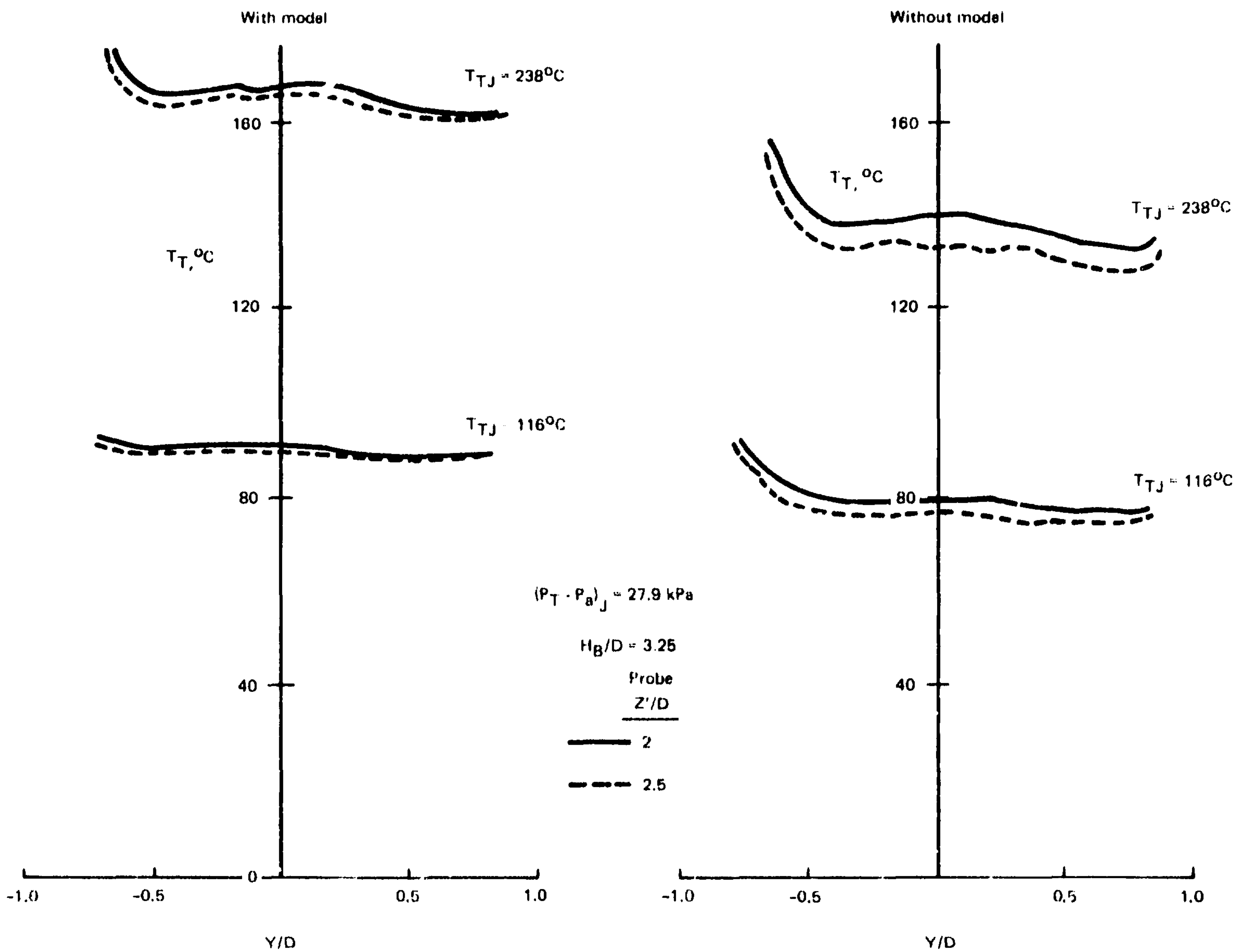


R81-1622-034D

Figure 41 - Effect of presence of body on upwash temperatures.

Figure 42 shows pressure profiles taken across the upwash with and without the model for the same nozzle height above ground. These profiles were taken far enough from the model undersurface so that the increased upwash dynamic pressure caused by the presence of the model was not a local flow disturbance involving flow around the model. The dynamic pressure (and hence flow velocity) throughout the entire upwash was affected by model blockage. This change is significant for flow modelling. The cause of this change is not understood at present. The data in Figure 42 were taken with a jet exit temperature of 238°C. Data taken at temperatures of 116°C and 24°C showed almost identical profiles with and without the model, again illustrating that jet exit temperature has little influence on the pressure measurements in the upwash.

5.2.6 Model Forces. - The thrust of one of the open circular nozzles was determined from the relation

$$\text{Thrust} = 2\, q\, \eta\, A \;,$$

where q is the dynamic pressure associated with the nozzle pressure ratio, A is the nozzle exit area and $\eta$ is a thrust efficiency factor that accounts for momentum loss in the nozzle boundary layer. Based on thrust measurements made earlier on this 5-cm diameter nozzle, we found $\eta = .90$ for the open circular nozzles.

Using $q = \frac{\gamma}{2} P M^2$ and $M^2 = 5\left[\left(\frac{P_T}{P_S}\right)^{2/7} - 1\right]$ for air.

the thrust developed by one circular nozzle can be found as a function of $P_{TJ}$ (settling chamber pressure):

$$\text{Thrust} = 6.30 \left[\left(\frac{P_{TJ}}{P_a}\right)^{2/7} - 1\right] A P_a$$

Force data taken with the open circular nozzles were normalized by twice the value of nozzle thrust.

Forces were measured on the model with 15° strakes for a range of settling-chamber temperatures and pressures. Figure 43 shows the variation of model interference force with height above ground for a settling chamber pressure of 27.6kPa gauge and jet temperatures of 24°C, 116°C and 240°C. These

ORIGINAL PAGE IS
OF POOR QUALITY

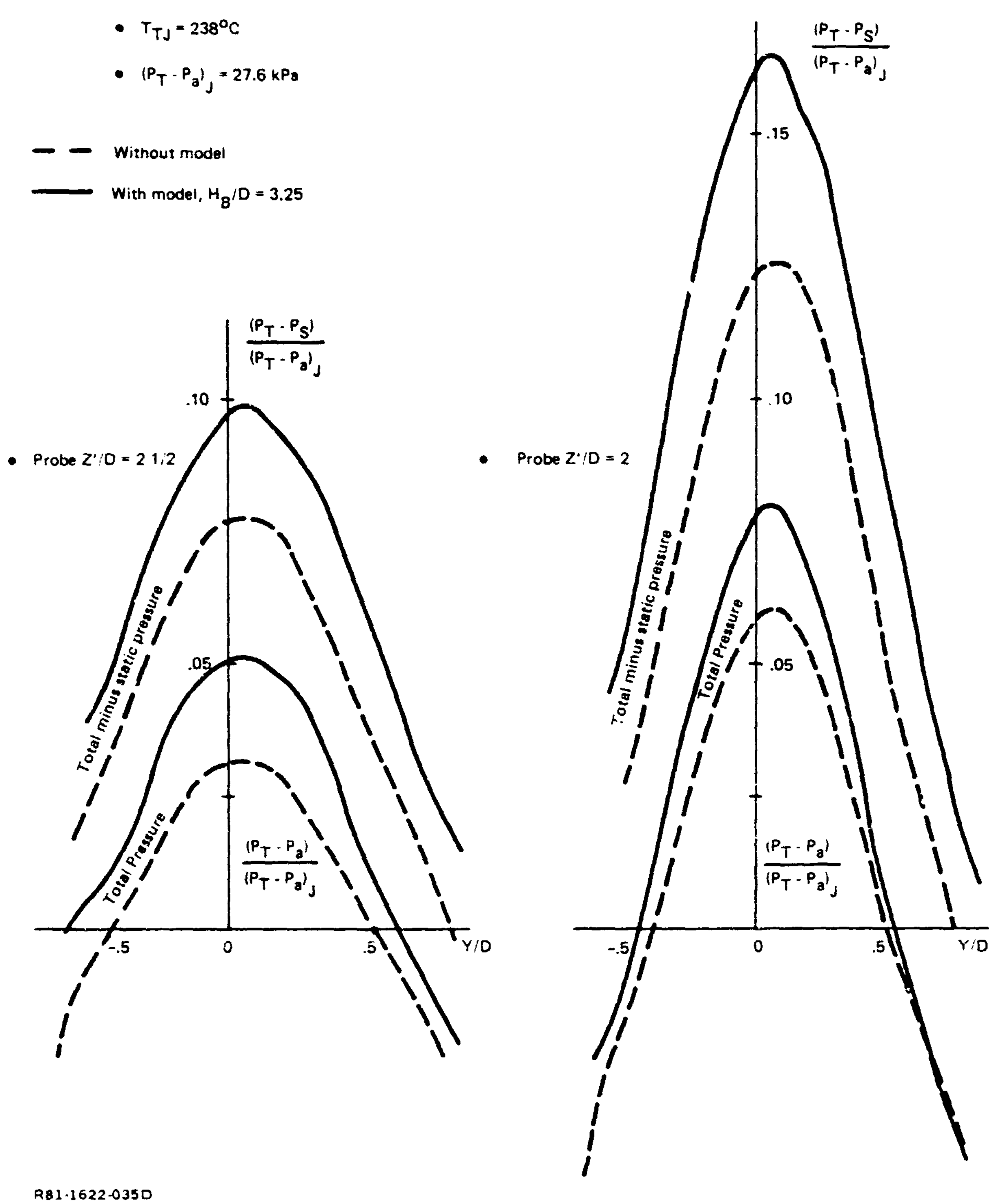


Figure 42 - Effect of presence of body on upwash pressures.

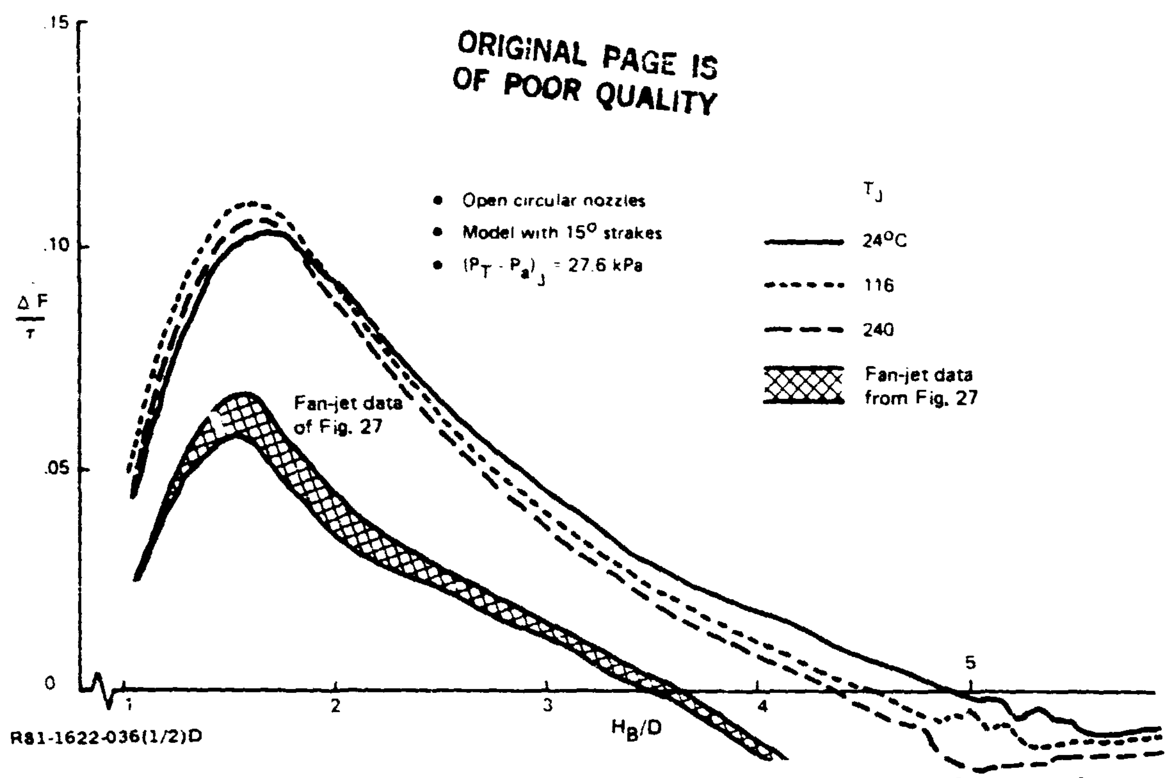


Figure 43 - Effect of nozzle exit temperature on ground interference forces.

three curves are quite similar, having small differences that appear to show a progression with temperature. Further investigation showed that differences in the force curves in Figure 43 are more likely to represent scatter attributable to slight differences in model alignment between runs. Subsequent measurements were taken at a fixed height above ground (H/D = 3.2) as the settling chamber temperature was raised from 24° to 221°C. Testing in this manner, essentially no change was found in interference force with jet exit temperature. The non-dimensional forces for the fan-jet simulation (Figure 27) are also shown and are much lower than those of the present section.

Figure 44 shows the variation of model force with height above ground for different settling chamber pressures and a jet ex[illegible]perature of 24°C. While these curves are qualitatively the same, they [illegible]me variation with settling chamber pressure. These data were all t[illegible] [illegible]t disturbing alignment between tests.

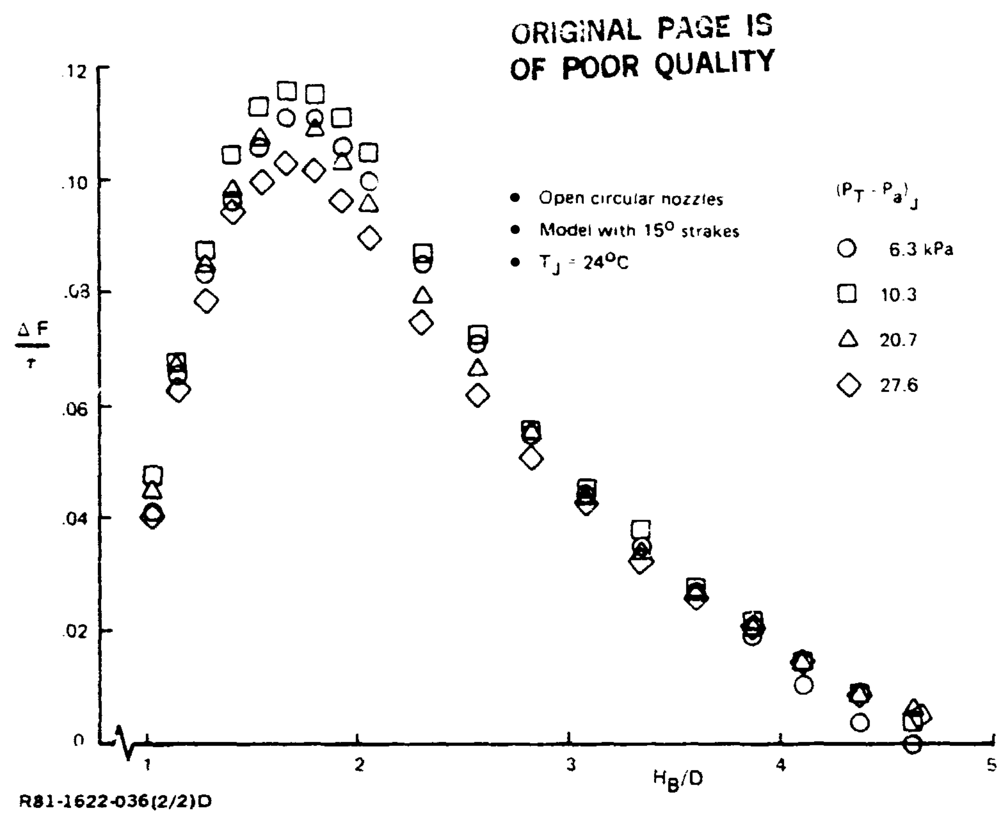


Figure 44 - Effect of nozzle stagnation pressure on ground interference forces.

5.2.7 Model Surface Pressure and Temperature. - Model surface pressures were measured with and without the 15° strakes for 24°C nozzle exit temperatures. At higher jet temperatures, the data were taken only with the strakes attached. Figure 45 shows the effect of the strakes on the pressure distribution along the fuselage undersurface. The pressure distribution across the model is shown in Figure 46. The presence of the strakes raises the surface pressure level and flattens the profile across the undersurface. Figure 47 shows the variation with height above ground of model pressure at three centerline taps for the model with strakes. The pressure on the fan nacelle centerline (from Figure 29) is shown for comparison, and is much lower. Figure 48 shows that the pressures along the model at a fixed height above ground are not significantly affected by jet temperature.

The temperature distribution along the model is shown in Figure 49. For H/D = 1.54, the temperature coefficient at a point between the nozzles was approximately 0.8, which is considerably higher than values measured with probes (range of 0.5) on the upwash centerline without the model (see Figures

ORIGINAL PAGE IS
OF POOR QUALITY

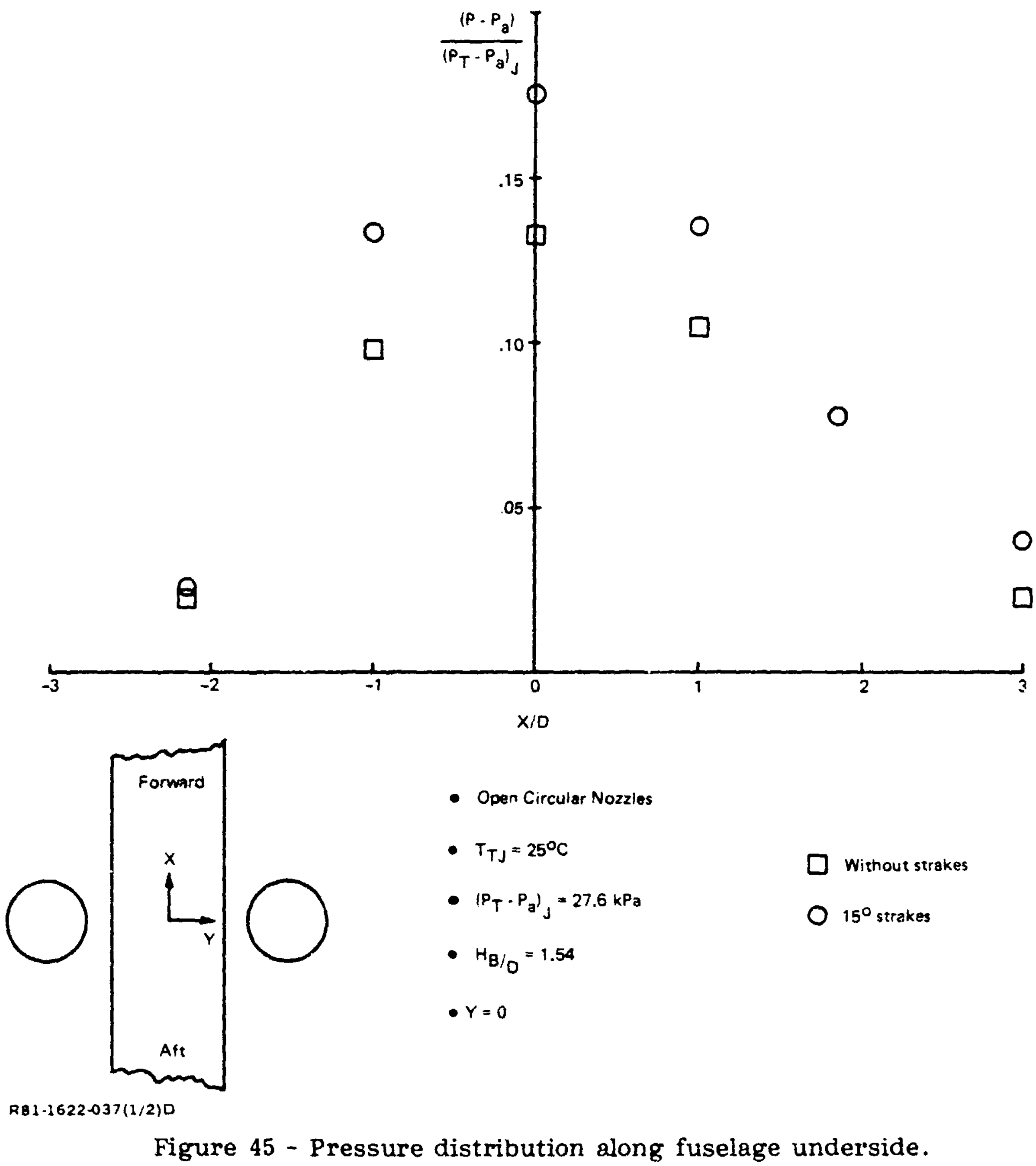


R81-1622-037(1/2)D

Figure 45 - Pressure distribution along fuselage underside.

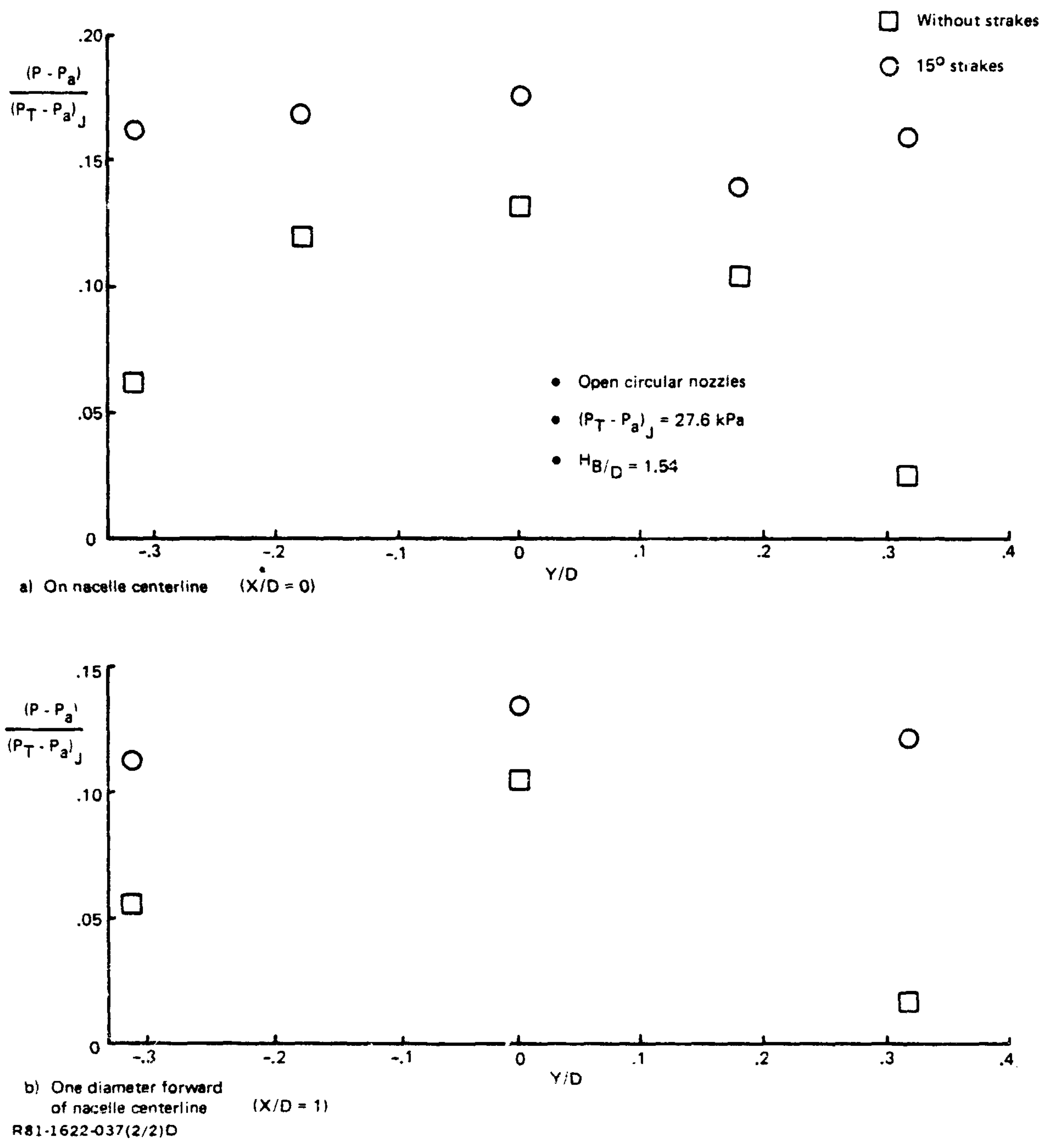


Figure 46 - Pressure distribution across fuselage underside.

ORIGINAL PAGE IS
OF POOR QUALITY

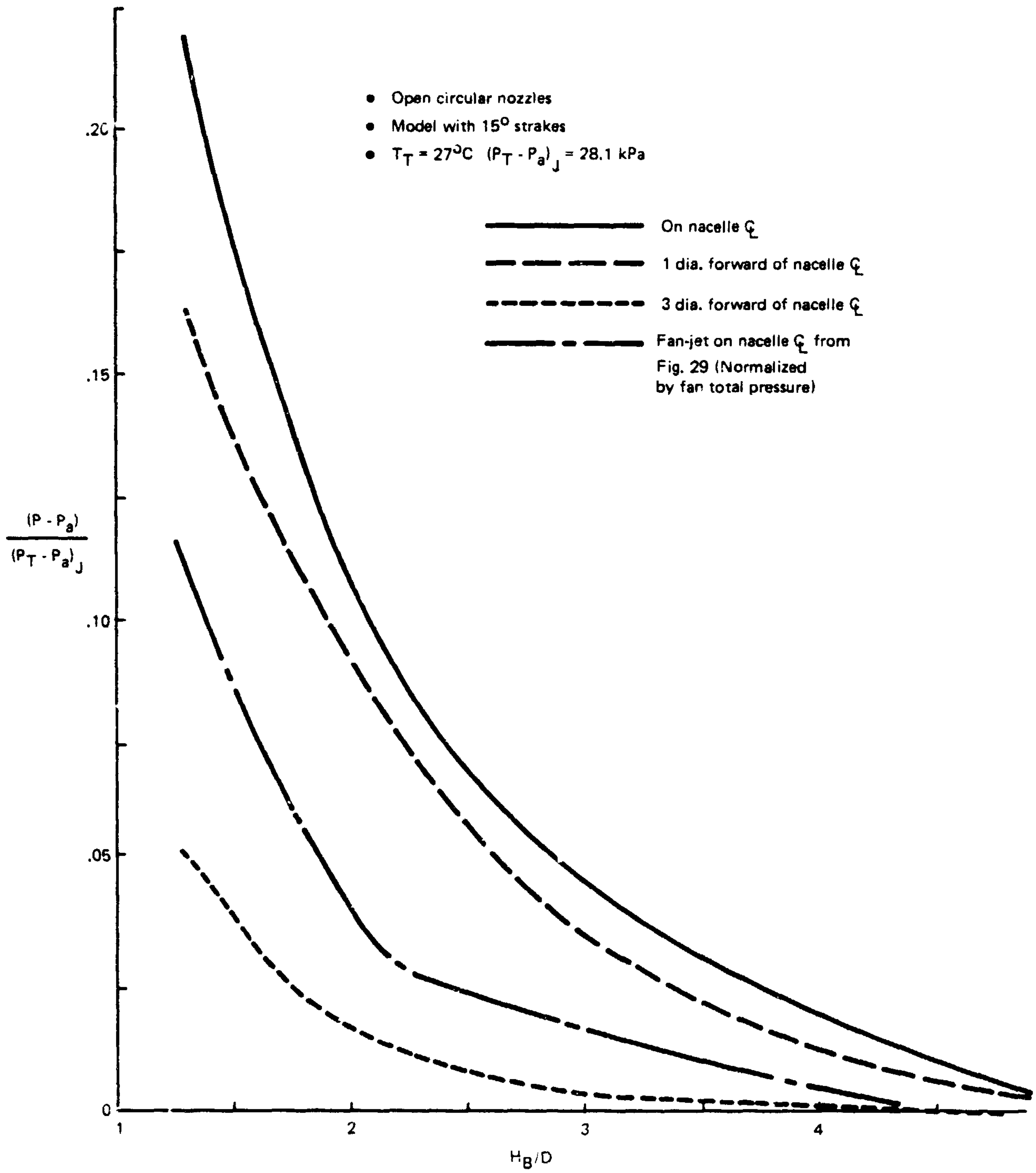


R81-1622-038D

Figure 47 - Variation of model pressure with height above ground.

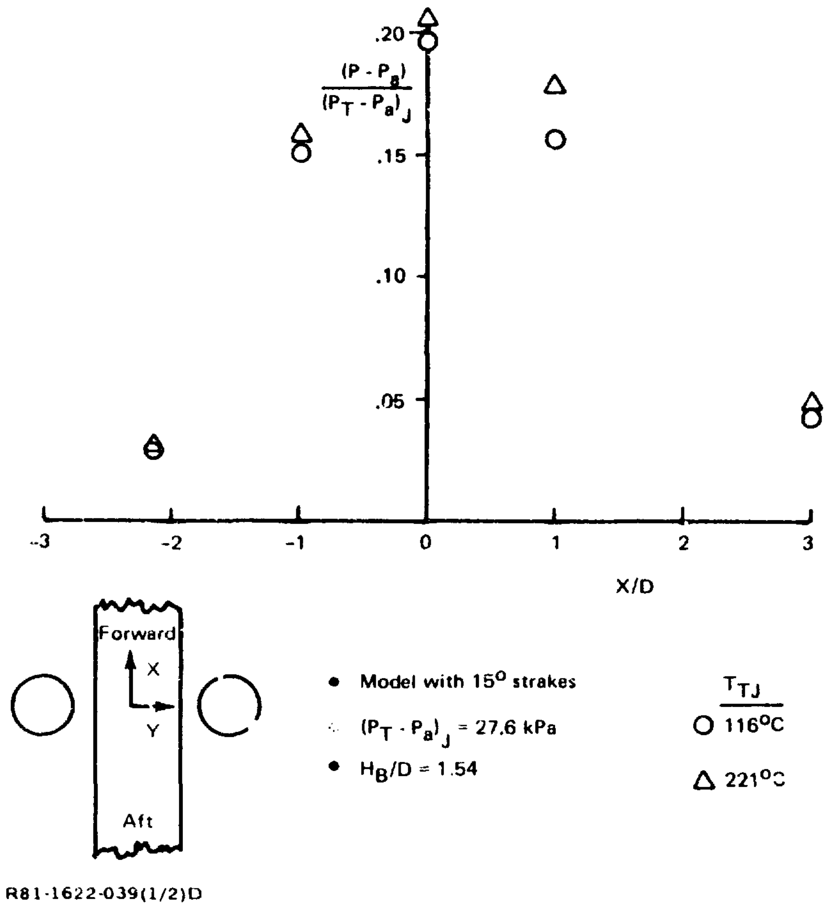


Figure 48 - Pressure distribution along fuselage underside.

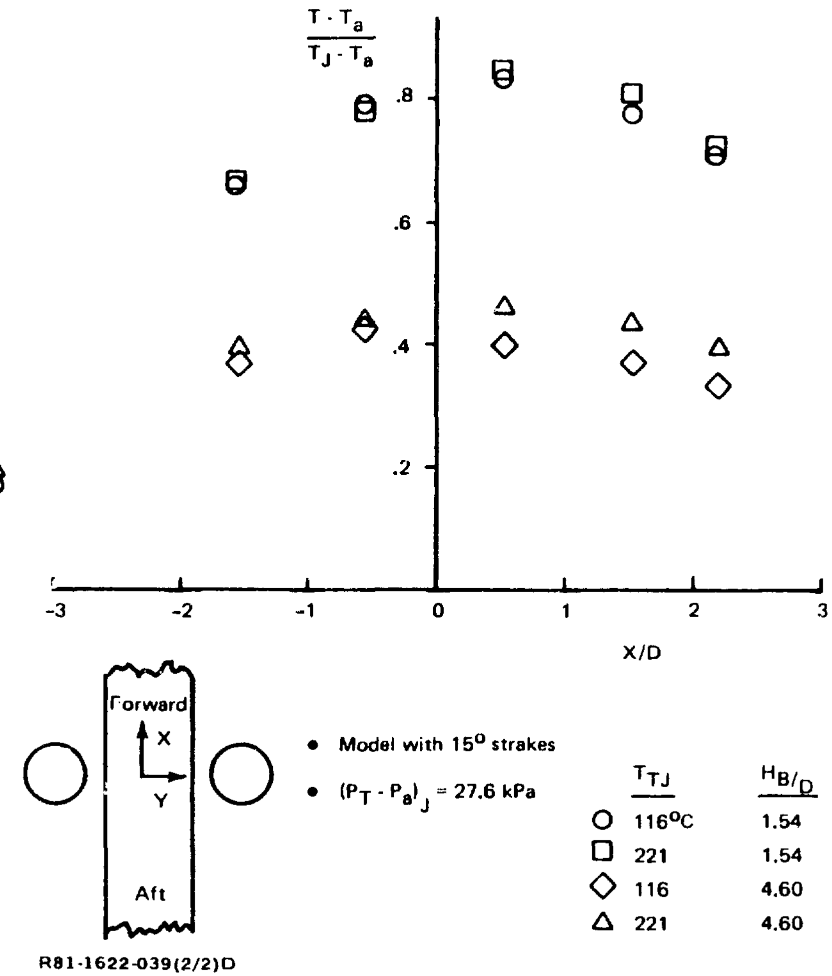


Figure 49 - Temperature distribution along fuselage underside

37b and 38a). The high model temperature appears to be caused by blockage of the entrainment flow brought about by the presence of the model. As discussed in Subsection 5.2.5, higher temperatures were measured in the upwash with the model in place than without it.

The model temperature distributions in Figure 49 do not show a local temperature minimum just forward of the nacelle centerline that was found using the fan jet nozzles (Figure 31). In addition, comparison of Figure 49 with Figures 31 and 28 shows that the model temperature coefficients appear to scale better with jet exit temperature using the open circular nozzles than using the fan-jet nozzles, where only the core flow was heated. Temperature data taken in the upwash using the open circular nozzles (Figure 37b and 38a) also showed better temperature scaling than the fan-jet data (Figure 24).

## 5.3 Conclusions

5.3.1 Fan-Jet Simulation. - The primary conclusion of this experimental study is that a geometrically correct small-scale model testing program can predict V/STOL aircraft hover performance quite well. Interference force results of the 1/24-scale experiments matched full scale results closely. Pressure ratio changes (in this case with subsonic jet exit conditions) produced a neglibible effect. Core nozzle exit temperature produced a small effect, easily compensated for by empirical scaling. Aircraft lower surface temperatures did not scale well with core nozzle exit temperature.

5.3.2 Open Circular Nozzles. - The normalized interference forces resulting from operation with open circular nozzles were much larger (approximately a factor of two) than those found with the fan jets. The qualitative behavior with height above ground was the same. As with the fan-jet nozzles, there was a small change in the force with changes in stagnation temperature. There was also a small change in normalized force with total pressure in the region of highest forces ($H/D \sim 1\frac{1}{2}$), which did not occur for the fan-jet case. Aircraft lower surface temperature did scale well with nozzle exit temperature, a different result than that obtained with the fan-jet nozzles.

The presence of the model was found to raise significantly the temperature in the upwash. Unexpectedly, model presence also raised the total pressure in the upwash.

## 6 - PREDICTION METHODOLOGY

The establishment of a vertical jet impingement model is the basis for the prediction of the behavior of two jets impinging on the ground plane. A sketch of the flow problem is shown in Figure 50. Figure 50a shows the vertical plane containing the jet stagnation points and the ground plane. Each jet impinges on the ground plane and deflects to form radial-wall jets. The wall jets then interact and form an upwash deflection zone where the wall jets collide and are turned upward on leaving the ground plane. The stagnation line lies on the ground in the vertical plane of symmetry between the two impinging jets. The maximum upwash stagnation pressure occurs at the midpoint of the line connecting the two jet stagnation points on the ground. The ground pressure then drops off with lateral distance along the stagnation line. Figure 50b shows the radial streamline pattern that has been observed (Ref. 5, 6 & 7) both in the ground plane and in the vertical upwash plane of symmetry between the two jets. This flow situation only exists when the jets are spaced far enough

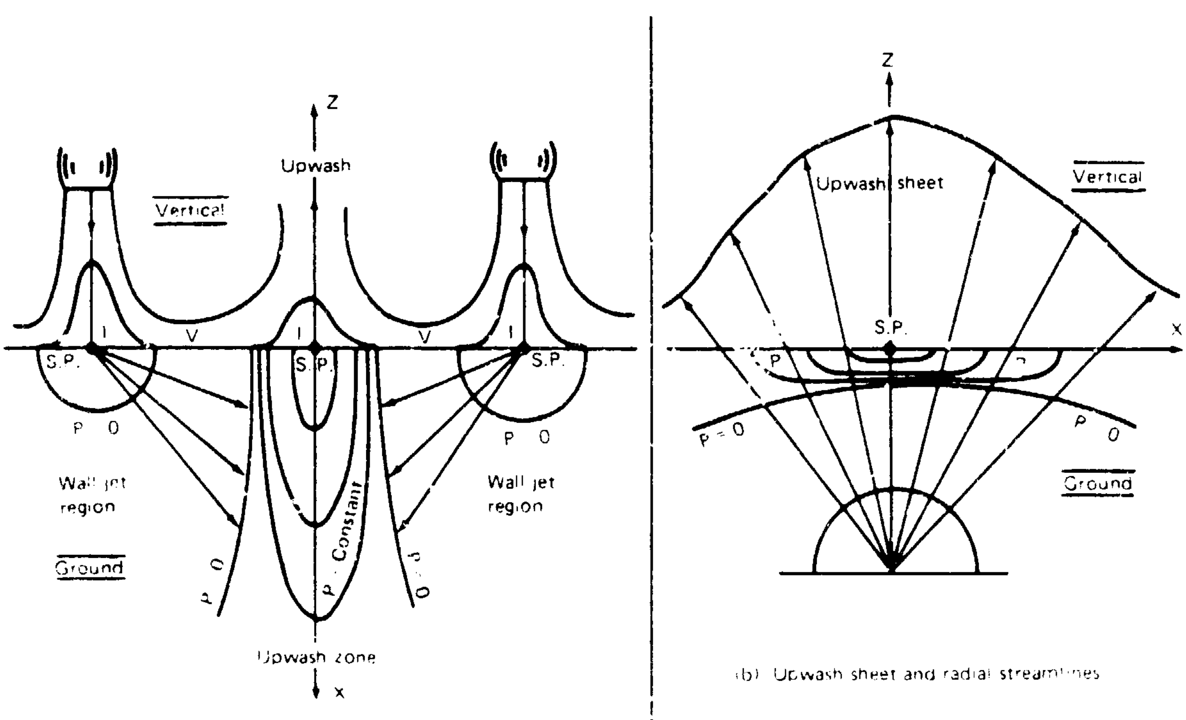


R81-1622-047D

Figure 50 - Two-jet interacting flows - negligible deflection zone interaction.

apart so that the jet impingement zone does not interact or has a negligible affect on the upwash deflection zone. (Ref. 3).

## 6.1 Theoretical Models for Non-Isothermal Jet Impingement

In Ref. 3, semi-empirical analytical models were formulated to simulate the global behavior of two incompressible jets impinging on a ground plane. Models were generated for the behavior of the free and wall jets and, finally, the upwash sheet generated by the interaction of the opposing wall jets. The effect of jet proximity is considered in Ref. 3, leading to the development of upwash momentum models.

These incompressible models are extended, in the present study, to include temperature or density effects. The flowfield is divided into three major regions where viscous or turbulent mixing effects dominate, being:

- Free jet
- Wall jet
- Upwash.

Subdomains of these regions include the jet and upwash deflection zones. In these smaller regions, the flow changes from an inviscid behavior to a shear flow along with streamline deflections, causing a change in static pressure due to the stagnation and acceleration of the flow.

## 6.2 General Temperature and Velocity Equations

The transport or diffusion of heat in a free jet is much like the transport of momentum. The viscous mixing and entrainment of ambient air causes a shear layer of momentum (velocity) and heat to occur. Schlicting (Ref. 8), in quoting the experimental and theoretical observations of Reichardt (Ref. 9), implies that the temperature profile distribution of a two-dimensional jet behaves like the square root of the velocity distribution. Taylor's Free Turbulence Theory, as quoted by Abramovich (Ref. 10), arrives at this result for the thermal layer by a turbulence theory that is based on vorticity transfer rather than momentum. In Ref. 10, the temperature profile in a jet is obtained by a "New Prandtl-Gortler Theory of Turbulence". The following relationship is obtained between the temperature and velocity:

$$\frac{\Delta T}{\Delta T_M} = \left( \frac{V}{V_M} \right)^{\frac{1}{\delta}} \qquad (1)$$

where $\delta$ is some constant. If $\delta = 1$, the dimensionless temperature and velocity profile coincide. It has been observed experimentally that this behavior does not hold. For $\delta = 2$, Taylor's analytical result is obtained as well as Reichardt's experimental observations.

Experimental observations indicate that the thermal layer spreads faster than the dynamic (velocity) layer. In order to establish an empirical value for $\delta$ in eq. (1), some non-isothermal profile data are plotted in Figure 51a for a circular jet. Similarity is not obtained if the temperature data are related to the velocity half widths as shown in Figure 51b. In addition, the data do not seem to confirm the square root of the velocity relationship. If, on the other hand,

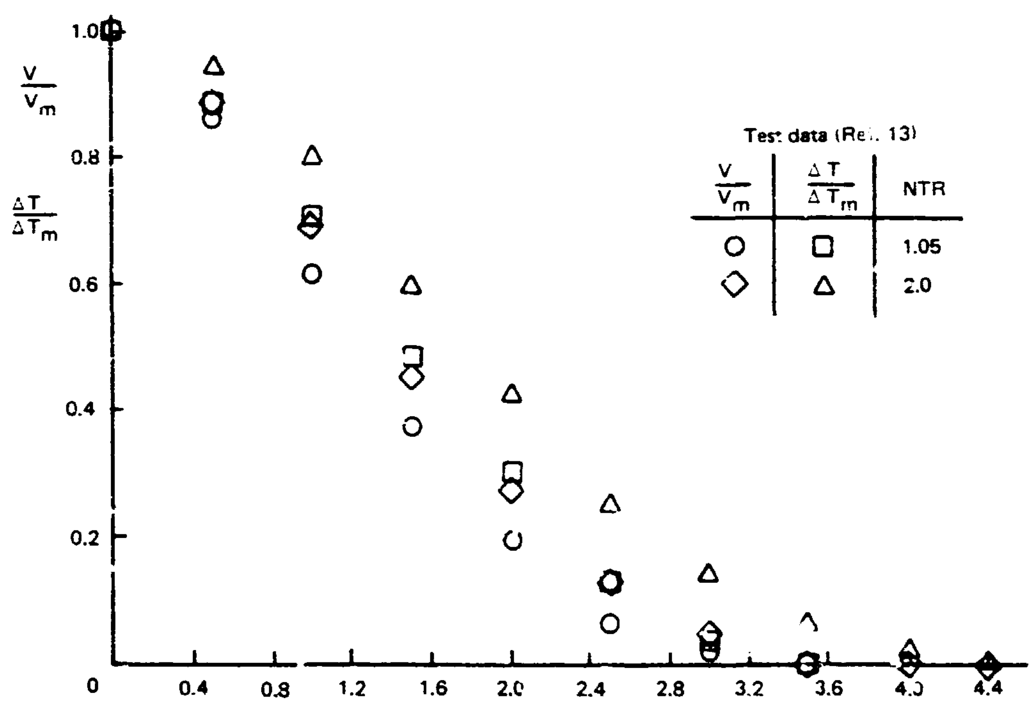


a) Related to jet radius.

.81-1622-040(1/3)D

Figure 51 - Dimensionless velocity and temperature difference profile data.

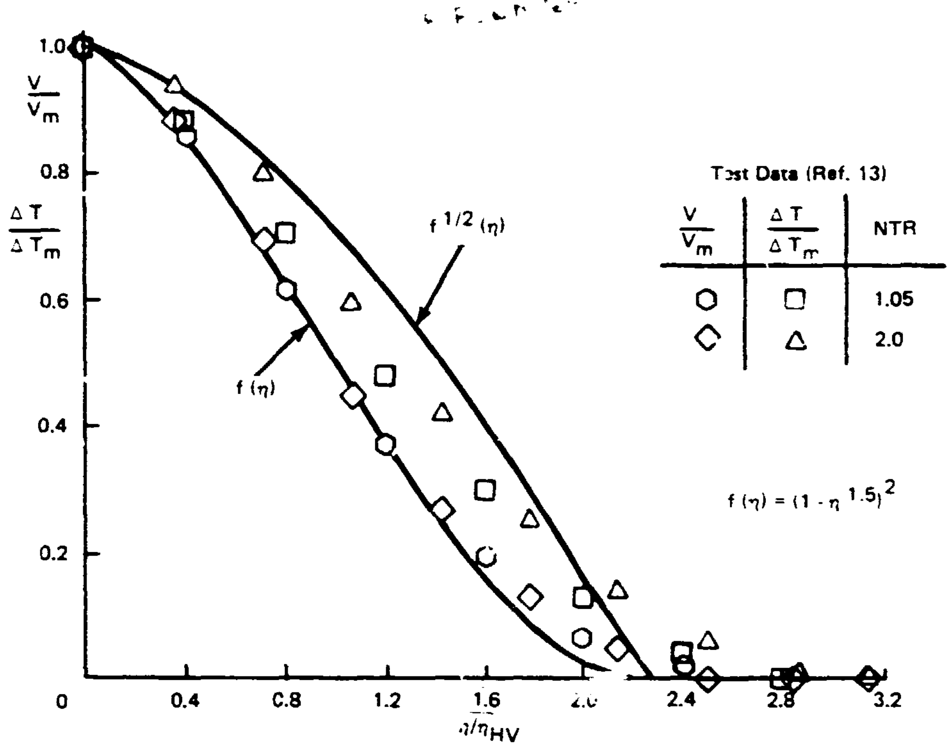


b) Related to jet radius non-dimensionalized by velocity half-width.
R81-1622-040(2/3)D

Figure 51 - (Continued).

the velocity and temperature difference data are plotted dimensionless to their respective half-velocity and half-temperature difference lengths, the data fall on one dimensionless curve as illustrated in Figure 51c. This result was also observed in Ref. 11 and in Ref. 12 for wall jets. It seems to be clear from the available data that the thermal layer persists beyond the point where a measurable velocity exists. The form of eq. (1) implies that the dynamic and thermal layers have the same scale length. If an exponential or infinite layer is assumed for the velocity profile and, hence, the thermal layer, then eq. (1) would yield results consistent with measured data. Indeed, if such a relationship as eq. (1) exists, the exponent may be a function of the nozzle thermal conditions.

In the models to be developed, it is more convenient to assume a finite thickness to the various layers to facilitate the various integrations involved in computing the velocity and temperature decay rates. Equation (1) is not

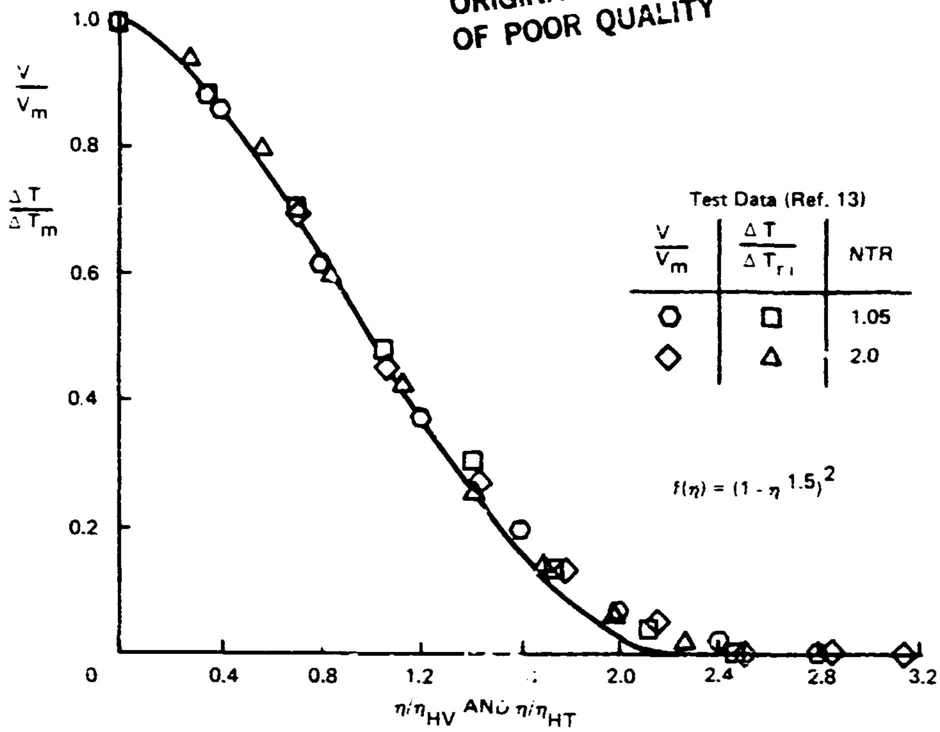


c) Related to jet radius non-dimensionalized by velocity and temperature half-widths.
R81-1622-040(3/3)D

Figure 51 - (Concluded).

used in the following models but the relationship depicted by Figure 51c is used instead:

$$\frac{T-T_A}{T_M-T_A} = f_T(\eta_T) \qquad\qquad (2)$$

$$\frac{V}{V_M} = f_V(\eta_V)$$

where $\eta_T = \frac{r}{b_T}$, $\eta_V = \frac{r}{b_V}$ and $f = \left(1 - \eta^{\alpha}\right)^2$

The dimensionless forms (i.e., velocity and temperature each have their own scale lengths, $b_V$ and $b_T$) of the velocity and temperature difference profiles as depicted in eq. (2) are assumed identical. The relationship between the thermal and dynamic (velocity) layers can be simply expressed by the ratio of the half widths of the two layers:

$$\lambda = \frac{b_{HT}}{b_{NV}} > 1 \tag{3}$$

Hence, the thermal and dynamic layers do not have the same scale. The velocity goes to zero while the temperature persists beyond a measurable velocity.

6.3 Conservation Equations

The basic governing equation to model the behavior of jets is the conservation of momentum equation. To account for non-isothermal or temperature effects, an additional equation is required. The conservation of excess heat content is used as the governing equation to account for heat diffusion or temperature effects. These two integral equations can be expressed as:

Momentum -

$$M_J = \rho_N V_N^2 A_N = \iint \rho V^2 dA \tag{4}$$

Heat Flux

$$H_F = \rho_N V_N (\Delta T_N) A_N = \iint \rho V \Delta T dA \tag{5}$$

where $\Delta T_N = T_N - T_A$, $T_N$ is the nozzle temperature, and $A_N$ is the nozzle area.

Equations (4) and (5) yield two expressions for the two unknowns, maximum centerline temperature and velocity. Unfortunately, more than two unknowns exist, namely, the profile shapes and growth rates of the various shear layers. These additional parameters must be given by empirical observations. The spreading models of Ref. 3 are used with the addition of eq. (5) and the further complication of the density or temperature occurring in eq. (4) which necessitates the simultaneous solution of eqs. (4) and (5).

6.4 Heated Free-Jet Model

The nozzle exit conditions of a free jet can be specified by two parameters, the nozzle exit stagnation pressure ratio (NPR) and temperature ratio (NTR). The exit Mach number of the jet is purely a function of NPR. A compressibility correction is included in the incompressible models, based upon an approximate Mach number computed using Bernoulli's equation.

$$M_N \sim \sqrt{\frac{2}{\gamma}(NPR-1)}$$

To be consistent with an incompressible approximation, the nozzle exit static temperature is assumed equal to the nozzle stagnation temperature, or

$$T_N \sim NTR$$

The free jet is subdivided into three regions, as shown in Figure 52:

- Potential core, Region I
- Transition, Region II
- Fully developed, Region III.

In order to solve eqs. (4) and (5), some information about the half-velocity boundary growth behavior must be assumed to be known from experimental data. To be consistent with the models of Ref. 3, and for the sake of simplicity, the jet radius model assumes a simple linear boundary growth in each region.

Region I: $$\frac{b_{VH}}{r_N} = a_1\left(\frac{Z}{r_N}\right)+1$$

Region II: $$\frac{b_{VH}}{r_N} = a_2\left(\frac{Z}{r_N}\right)+b_2$$

Region III: $$\frac{b_{VH}}{r_N} = a_3\left(\frac{Z}{r_N}\right)$$

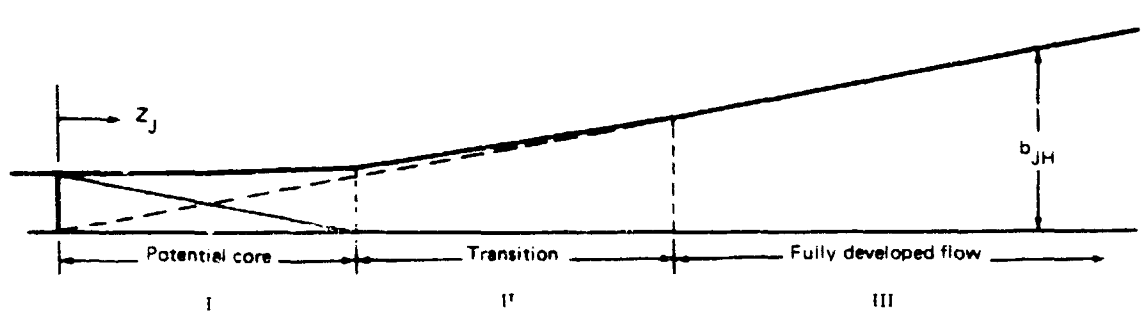


Figure 52 - Jet half-velocity width model.

The constants ($a_1$, $a_2$, $a_3$) governing the half-velocity boundary growth in the transition and fully-developed regions are determined empirically. The potential core length ($Z_{PC}$) and the exponent $\alpha_{FD}$ governing the shape of the shear profile in the fully developed region also must be specified. These constants vary slightly as functions of nozzle Mach number and temperature ratio. Suitable values have been determined as:

$$a_3 = .09 \left\{ 1 + \ln \left( \frac{2}{1 + \frac{1}{T_N} \beta_3} \right) \right\} \left\{ 1 - .16 \, M_N \right\}$$

where $\beta_3 \sim 0.50$.

The potential core length is approximated by:

$$\frac{Z_{pc}}{D} = \frac{8.55}{2} \left[ 1 + \frac{1}{T_N} \beta_c \right]$$

where $\beta_c \sim 0.75$, and is also slightly a function of the nozzle temperature ratio.

The growth constant of the half-velocity boundary in the potential core region is determined by matching the boundaries at the end of the potential core, yielding,

$$a_1 = \frac{(b_2 - 1)}{(Z_{pc}/r_N)} + a_2$$

In addition, a linear decay in potential core radius $r_c$, is assumed:

$$\frac{r_c}{b_V} = 1 - \frac{Z_J}{Z_{Pc}}$$

The beginning of the fully developed region of flow, denoted by the length parameter $Z_{FD}$, is determined by matching the boundaries between the transition and fully developed regions.

$$\frac{Z_{FD}}{r_N} = \frac{b_2}{(a_3 - a_2)}$$

The momentum and heat flux equations become, for a circular jet,

$$M_J = \frac{2\pi P_A}{R_G} \int \frac{V^2 r \, dr}{T} \tag{6}$$

$$H_F = \frac{2\pi P_A}{R_G} \int \frac{V \Delta T \, r dr}{T} \tag{7}$$

using $P_A = \rho R_G T$ to eliminate density.

The velocity and temperature profiles are represented by the following dimensionless self-similar quantities:

$$\frac{V}{V_M} = f_V(\eta_V) \; ; \; \eta_V = \frac{r}{b_V} \tag{8}$$

$$\frac{\Delta T}{\Delta T_M} = f_T \; (\eta_T) \; ; \; \eta_T = \frac{r}{b_T} \tag{9}$$

Since finite profile functions will be used in the modeling, the velocity and temperature scale lengths, as represented by $b_V$ and $b_T$, are not equal.

Substituting eqs. (8) and (9) into eqs. (6) and (7), and rearranging, yields,

Momentum
$$\frac{T_M}{T_N} = 2 \left(\frac{V_M}{V_N}\right)^2 \left(\frac{b_V}{r_N}\right)^2 \int_0^1 \frac{f_V{}^2 \eta_V d\eta_V}{\left[f_T + \frac{(1-f_T)}{\bar{T}_M}\right]} \tag{10}$$

Heat -
$$\frac{T_M}{T_N} = 2 \left(\frac{V_M}{V_N}\right)\left(\frac{b_V}{r_N}\right)^2 \frac{\Delta T_M}{\Delta T_N} \int_0^1 \frac{f_V f_T \eta_V d\eta_V}{\left[f_T + \frac{(1-f_T)}{\bar{T}_M}\right]} \tag{11}$$

where $\bar{T}_M = \frac{T_M}{T_A}$

Unfortunately, bringing the density into the integrands makes the profile integrals functions of the maximum centerline temperature ratio. Hence, simple geometrical similarity does not exist for non-isothermal jets. The velocity scale length $\eta_V$ is used in the integration since there can be no contribution to eq. (10) or eq. (11) beyond the dynamic (velocity) layer. The integrals in the above equations do not lend themselves necessarily to analytical integration, and are defined as:

$$C_M(\bar{T}_M) = \int_0^1 \frac{f_V^2 \eta_V d\eta_V}{\left[f_T + \frac{(1-f_T)}{\bar{T}_M}\right]} \tag{12}$$

$$C_T(\bar{T}_M) = \int_0^1 \frac{f_V f_T \eta_V d\eta_V}{\left[f_T + \frac{(1-f_T)}{\bar{T}_M}\right]} \tag{13}$$

Equations (10) and (11) can be rewritten simply as

$$\frac{T_M}{T_N} = 2\left(\frac{V_M}{V_N}\right)^2\left(\frac{b_V}{r_N}\right)^2 C_M(\bar{T}_M) \tag{14}$$

$$\frac{T_M}{T_N} = 2\left(\frac{V_M}{V_N}\right)\left(\frac{b_V}{r_N}\right)^2 \frac{\Delta T_M}{\Delta T_N} C_T(\bar{T}_M) \tag{15}$$

The values of the integrals $C_M$ and $C_T$ are also functions of the profile characteristics. In general, it is assumed that

$$\frac{V}{V_M} = f_V(\eta_V) = \left[1-\left(\frac{\eta_V-\eta_c}{1-\eta_c}\right)^{\alpha}\right]^2 \tag{16}$$

and

$$\frac{\Delta T}{\Delta T_M} = \left[1-\left(\frac{\eta_T-\eta_c}{1-\eta_c}\right)^{\alpha}\right]^2 = f_T(\eta_T) \tag{17}$$

where $\eta_C = r_C/b_V$.

Since the dimensionless velocity and temperature profile functions have the same form, then

$$\eta_T = \left(\frac{b_{VH}}{b_{TH}}\right) \eta_V \tag{18}$$

In general, it is assumed that

$$\lambda_T \equiv \frac{b_{TH}}{b_{VH}} > 1 \tag{19}$$

Hence:

$$\eta_T = \frac{\eta_V}{\lambda_T} \tag{20}$$

and the temperature scale length can be directly related to the scale length of the dynamic layer.

6.4.1 <u>Potential core region</u> - In the potential core region, the maximum temperature and velocity are known and are equal to the nozzle values. The momentum and heat equations, (14) and (15), can be reduced to,

$$\frac{1}{2} R_V{}^2(\alpha) - \left(\frac{b_{VH}}{r_N}\right)^2 C_M\ (\alpha, \lambda_T) = 0 \tag{21}$$

$$\frac{1}{2} R_V{}^2(\alpha) - \left(\frac{b_{VH}}{r_N}\right)^2 C_T\ (\alpha, \lambda_T) = 0 \tag{22}$$

where $R_V = \frac{b_{VH}}{b_v} = \eta_c - (1-\eta_c) \left(\frac{2-\sqrt{2}}{2}\right)^{\frac{1}{\alpha}}$

Equations (21) and (22) are solved simultaneously for the exponent $\alpha$ and the thermal-to-dynamic layer ratio $\lambda_T$. For simplicity, the thermal and dynamic cores are assumed identical.

6.4.2 <u>Transition and fully-developed regions</u> - The conservation equations can now be written as:

$$\frac{1}{2} R_V^2 \left(\frac{T_M}{T_N}\right) - \left(\frac{V_M}{V_N}\right)^2 \left(\frac{b_{VH}}{r_N}\right)^2 C_M(\bar{T}_M) = 0 \qquad (23)$$

$$\frac{1}{2} R_V^2 \left(\frac{T_M}{T_N}\right)\left(\frac{T_N}{T_A}-1\right) - \left(\frac{V_M}{V_N}\right)\left(\frac{T_M}{T_N}\cdot\frac{T_N}{T_A}-1\right)\left(\frac{b_{VH}}{r_N}\right)^2 C_T(\bar{T}_M) = 0 \qquad (24)$$

The above equations are solved simultaneously for the dimensionless maximum temperature ratio, $\frac{T_M}{T_N}$, and maximum velocity ratio, $\frac{V_M}{V_N}$, given values for the exponent $\alpha$ and $\lambda_T$. Suitable values based on empirical data are assigned to these parameters in the fully developed regions as

$$\alpha_{FD} = 1.5$$

$$\lambda_T = 1 + 0.185\, T_N^{\beta_\lambda} \text{ where } \beta_\lambda \sim 0.50,$$

and a linear variation from potential core values to the fully developed ones is assumed.

Some typical results are shown in Figures 53 through 57 and compared to the test data of Corrsin & Uberoi (Ref. 13) for low Mach number or basically incompressible jets. Figure 53 shows the relationship between the dimensionless velocity and temperature decay rates for a slightly-heated jet (NTR = 1.05) and a significantly-heated jet (NTR = 2.0). Both the velocity and temperature decay rates are enhanced due to an increase in heat content of the jet. The temperature decays faster than the velocity. Figure 54 shows the dynamic pressure or total pressure decay for the two different temperature ratios. The total pressure decays faster for the hotter jet. Figure 55 shows the relationship between the dynamic pressure and total temperature decay. Unlike the velocity and temperature, the pressure and temperature curves cross each other. The dynamic pressure is computed as $\left(\frac{V_M}{V_N}\right)^2 / (T_M/T_N)$. Figure 56a and b shows the relationship between the half dynamic pressure (q), half velocity ($V_M/V_N$) and half dimensionless temperature ($T_M-T_A/T_N-T_a$) boundaries for the two nozzle

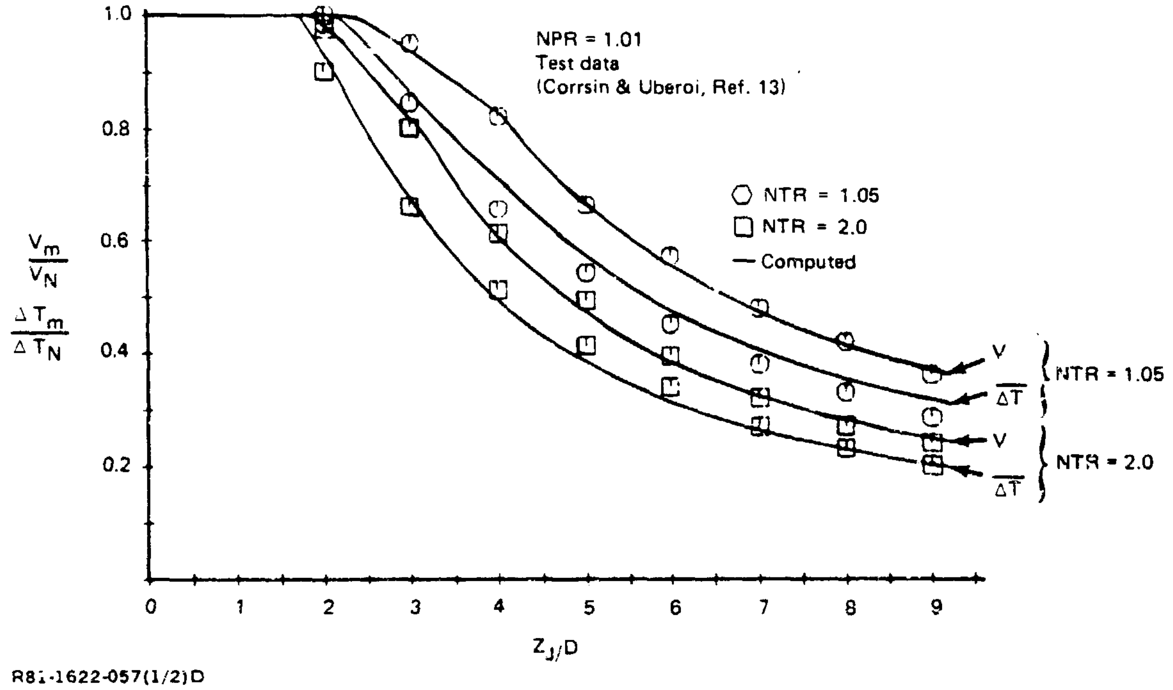


Figure 53 - Comparison of computed free-jet dimensionless velocity and temperature difference decay with test data.

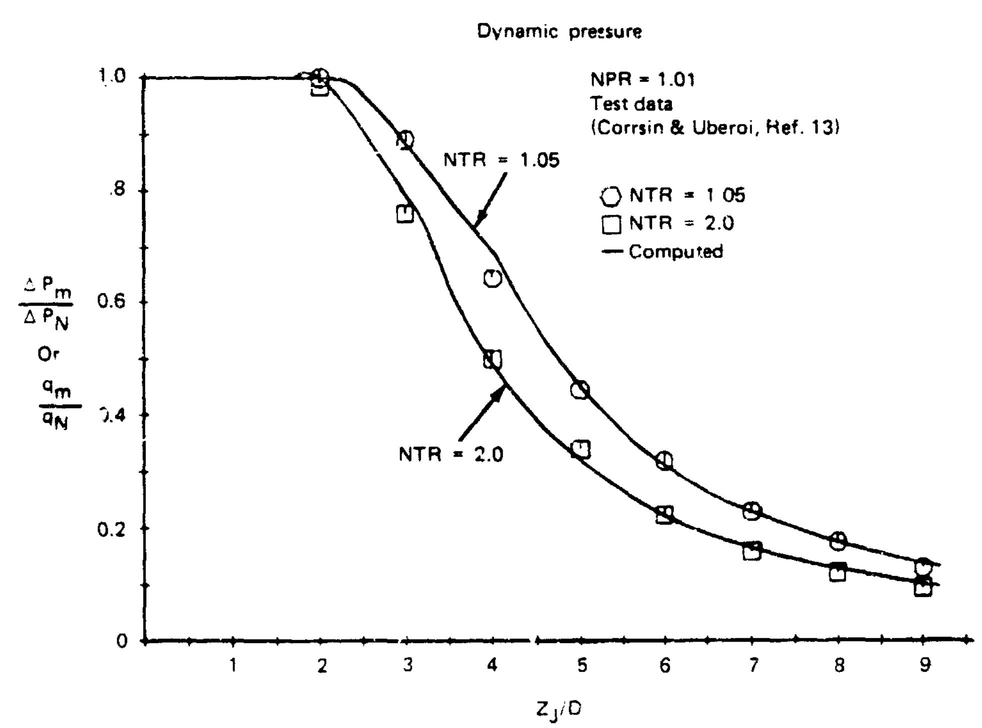


Figure 54 - Comparison of computed free-jet dimensionless dynamic pressure decay with test data.

ORIGINAL PAGE IS
OF POOR QUALITY

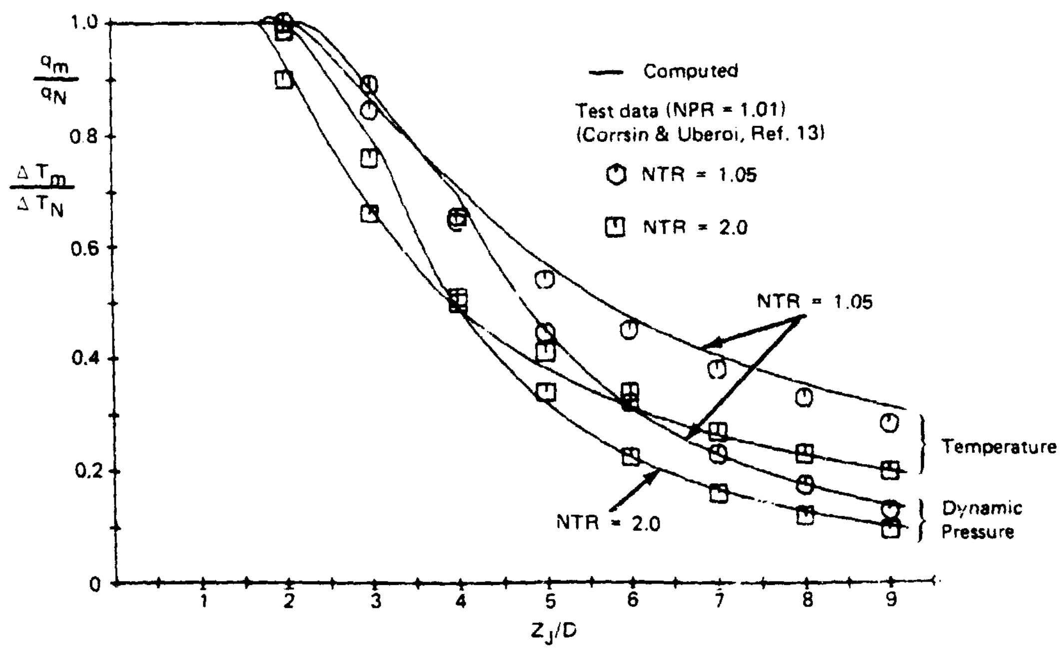


Figure 55 - Comparison of computed free-jet dimensionless dynamic pressure and temperature difference decay with test data.

temperature ratios. The half dynamic pressure boundary exhibits a contraction in the potential core region ($Z_{PC} \sim 4D$). The half velocity boundary lies between the half dynamic pressure and temperature boundaries. The half temperature boundary being significantly wider than the half velocity boundary as the nozzle temperature is increased. Figure 57 shows a comparison of the half q and half temperature boundaries for the two nozzle temperature ratios. Hence, heating the jets causes an increase in the jet half boundaries, which is consistent with the higher decay rate exhibited by the hotter jet in the previous figures.

6.5 Jet Deflection Region

A schematic of the wall jet impingement model is shown in Figure 58. The jet begins to stagnate at some ground effect height given by $\Delta_J$. Values for $\Delta_J$ are given in Ref. 14. The ground stagnation pressure and temperature is then determined by the jet properties at the ground effect height denoted by

ORIGINAL PAGE IS
OF POOR QUALITY

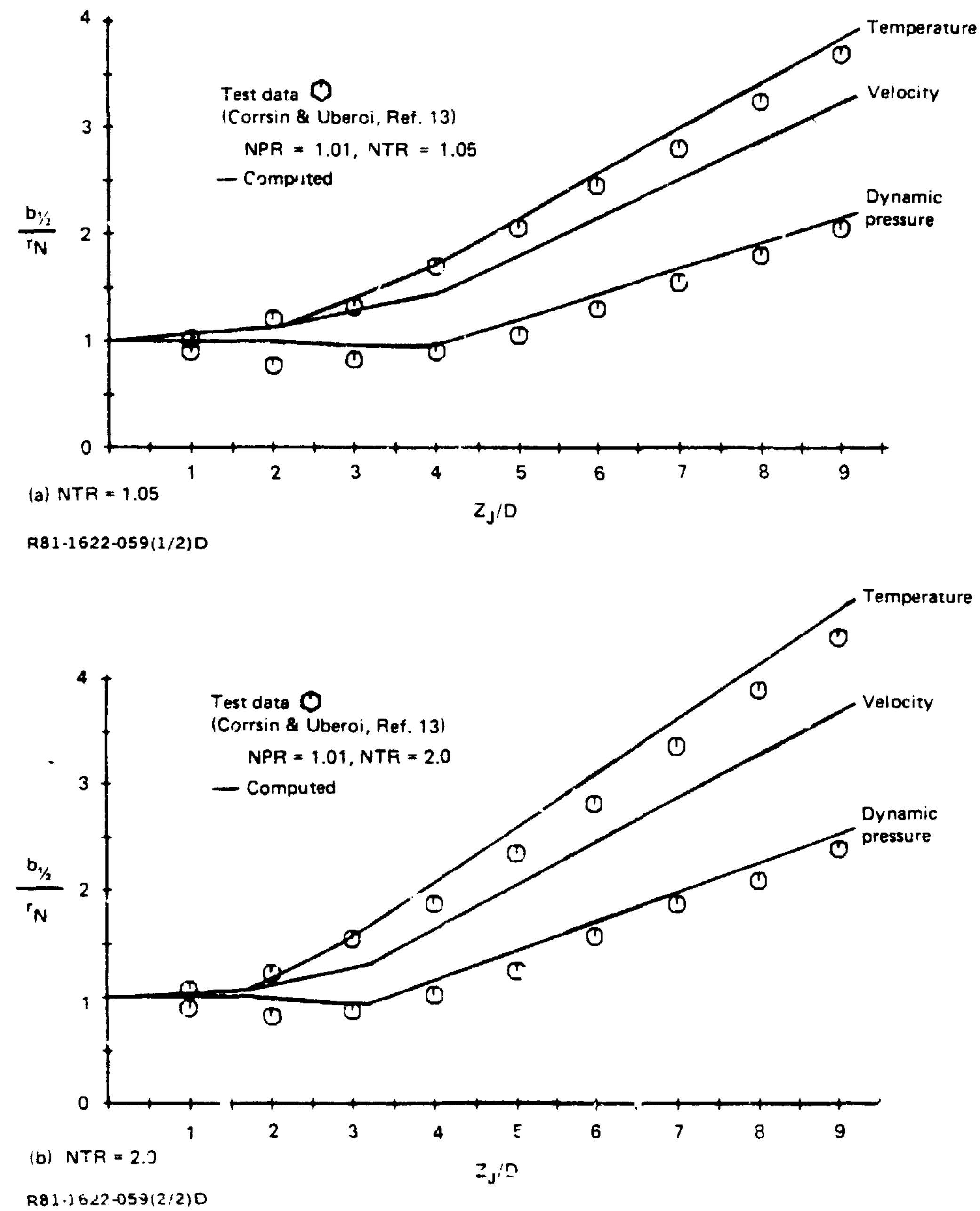


Figure 56 - Heated free-jet boundary growth characteristics.

ORIGINAL PAGE IS
OF POOR QUALITY

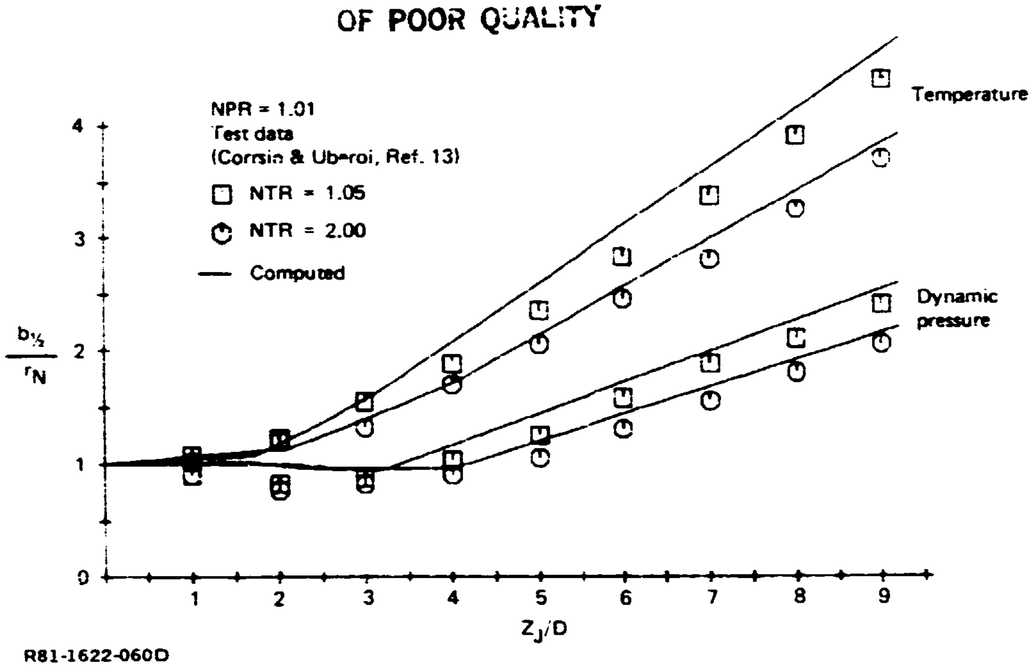


Figure 57 - Heated free-jet boundary growth characteristics.

the subscript (g), or:

$$\frac{\Delta P_S}{\Delta P_N} = \left(V_g/V_N\right)^2 \Big/ \left(T_g/T_N\right) ; \qquad (25)$$

$$\frac{T_S}{T_A} = \frac{T_g}{T_A}$$

The ground pressure distribution in the impingement region is obtained in the same fashion as for an isothermal jet. A momentum balance is performed with the integral of the ground pressure equal to the momentum or thrust of the incident jet.

$$\frac{M_J}{4} = \int_0^{r_o} \int_0^{\pi/2} \Delta P r dr d\varphi \qquad (26)$$

The ground pressure distribution is assumed to have the form:

$$\frac{\Delta P}{\Delta P_S} = f_g\left(\eta_W\right) = \left(1 - \eta_W^{\,a_g}\right)^4 \qquad (27)$$

where $\eta_W = \frac{r}{r_o}$.

L-2

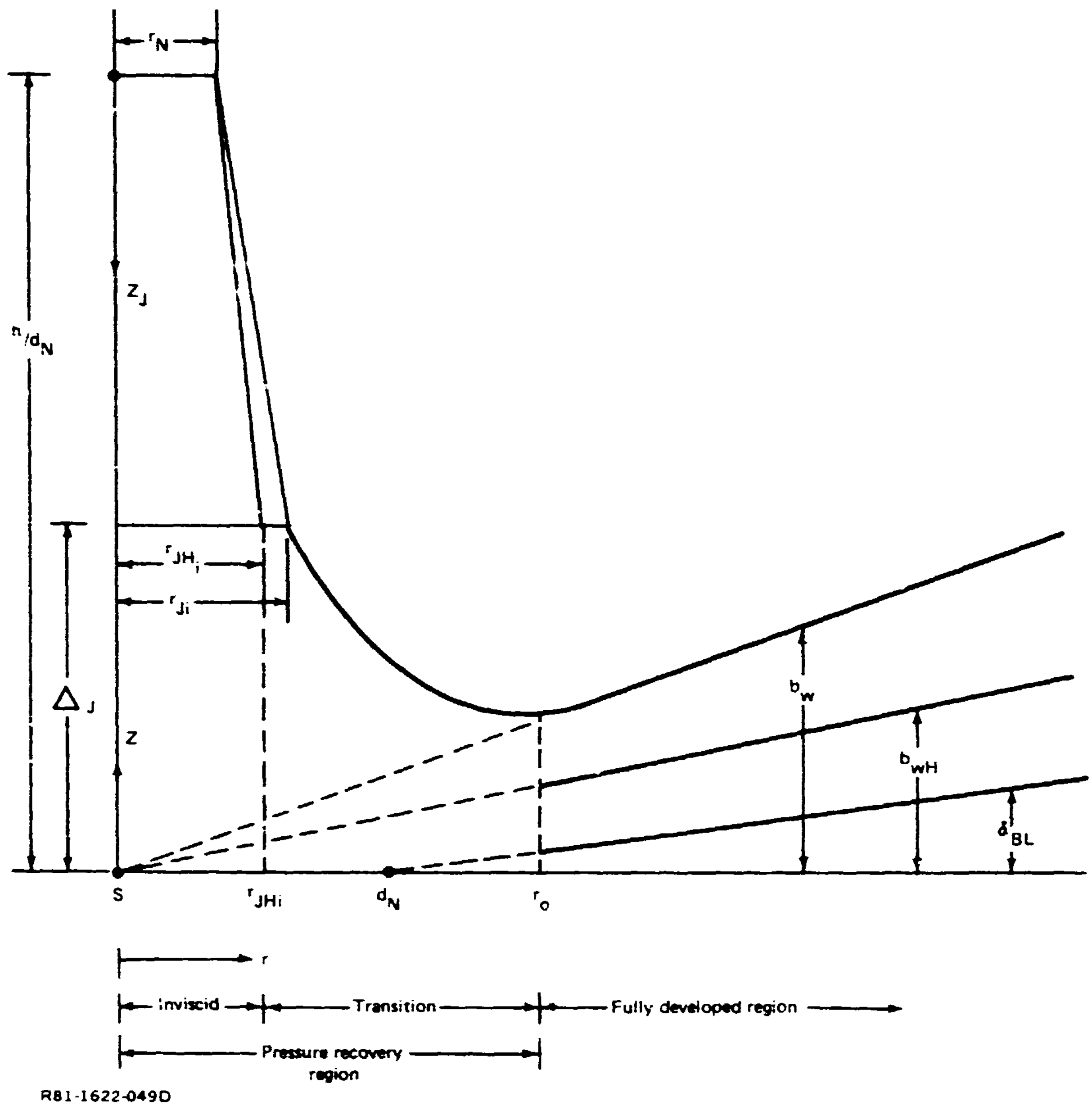


Figure 58 - Definition of scaling parameters for jet impingement and wall jet regions.

Equation (26) can be rewritten as,

$$1 = \left(\frac{r_o}{r_N}\right)^2 \left(\frac{V_g}{V_N}\right)^2 C_{sp}(\alpha_g) \Big/ (T_g / T_N) \tag{28}$$

where $C_{sp}(\alpha_g) = \int_0^1 f_g(\eta_W)\, \eta_W\, d\eta_W$.

Given the impingement radius $r_o$, equation (28) can be solved for the exponent $\alpha_g$ governing the shape of the ground pressure distribution. The deflection radius $r_o$ is estimated empirically and is based upon the incident half velocity radius ($b_{VHi}$) of the jet:

$$2.9 \le \frac{r_o}{b_{VHi}} \le 3.6 \;;\; 1.2 \le \frac{h}{D} \le 3.0$$

$$\frac{r_o}{b_{VHi}} = 3.6 \;:\; \frac{h}{D} > 3.0$$

6.6 Heated Wall-Jet Transition Model

Figure 58 shows a schematic of the wall-jet model. The wall-jet transition model developed in Ref. 3 consists of three subregions:

i) Inviscid deflection region where the effects of viscosity are assumed to be negligible except in a region close to the wall and near the edge of the deflected flow. In this region, the inner boundary layer is established as governed by axially-symmetric stagnation flow.

ii) Transition region where the effects of viscosity are beginning to dominate and the inner boundary layer and outer shear flow changes to the fully-developed turbulent wall-jet.

iii) Fully-developed flow, where the effects of turbulent viscosity dominate and the static pressure through the wall layer is considered ambient, or fully recovered. In this region, the nearly similar wall-jet develops.

The addition of heat to the wall-jet requires the introduction of a radial heat flux equation into the model of the isothermal wall-jet. The two conservation equations (assuming negligible losses) applied to the wall jet are:

<u>Momentum</u> -
$$M_F = \int_0^{b_W} (\rho V^2 + \Delta P)\, r dz \tag{29}$$

<u>Heat</u> -
$$H_F = \int_0^{b_W} \rho V \Delta T r dz \tag{30}$$

where $b_W$ is the height or thickness of the dynamic (velocity) layer.

Before being able to apply eqs. (29) and (30) to the wall layer, the velocity, pressure and temperature profile behavior must be approximated. Two sublayers are assumed, an inner boundary layer and an outer shear layer. Adiabatic wall conditions are assumed and the thermal and dynamic boundary layers are also assumed to coincide.

<u>Inner Boundary Layer</u>

$$\frac{V}{VM} = \left(\frac{\zeta_V}{K_\delta}\right)^{\frac{1}{N}} \quad \text{where } \zeta_V = \frac{Z}{b_W}, \; K_\delta = \frac{\delta_{bl}}{b_W} \tag{31}$$

$$\frac{\Delta P}{\Delta P_M} = 1 \quad \text{(constant pressure through boundary layer)}$$

$$\frac{\Delta T}{\Delta T_M} = 1 \quad \text{(adiabatic wall, constant temperature through boundary layer)}$$

where $7 \leqslant N \leqslant 15$.

<u>Outer Shear Layer</u>

$$\frac{V}{V_M} = f_V(\zeta_V) = \left[1 - \left(\frac{\zeta_V - K_\delta}{1 - K_\delta}\right)^\alpha\right]^2$$

$$\frac{\Delta P}{\Delta P_M} = f_p(\zeta_V) = f_V^2(\zeta_V) = \left[1 - \left(\frac{\zeta_V - K_\delta}{1 - K_\delta}\right)^\alpha\right]^4 \tag{32}$$

$$\frac{\Delta T}{\Delta T_M} = f_T(\zeta_T) = \left[1 - \left(\frac{\zeta_T - K_\delta}{1 - K_\delta}\right)^\alpha\right]^2$$

where $\zeta_T = \frac{Z}{b_T}$ and $b_T$ is the height or thickness of the thermal layer. The dynamic and thermal layers are assur ed to be related by:

$$\frac{b_{TH}}{b_{VH}} = \frac{b_T}{b_W} \equiv \lambda_T > 1 \tag{33}$$

The introduction of equations (30) and (31) into eqs. (28) and (29) lead to the development of several profile integral expressions.

The momentum integral has a velocity squared and a pressure term. The pressure term contributes to the momentum until pressure recovery occurs. Substitution of the profile expressions into the velocity term of the integral yields the following integrals for the two layers:

$$C_M\left(\overline{T}_M\right) = \int_0^{K_\delta} \left(\frac{\zeta_V}{K_\delta}\right)^{\frac{2}{N}} d\zeta_V + \int_{K_\delta}^{1} \frac{f_V^2(\zeta_V)\left[f_p(\zeta_V) + \left\langle 1 - \frac{f_p(\zeta_V)}{\overline{P}_M}\right\rangle\right]}{\left[f_T(\zeta_T) + \left(\frac{1-f_T(\zeta_T)}{\overline{T}_M}\right)\right]} d\zeta_V \tag{34}$$

where $\overline{T}_M = \frac{T_M}{T_A}$ and $\overline{P}_M = \frac{P_M}{P_A}$.

The pressure term leads to a simpler expression:

$$C_p = K_\delta + \int_{K_\delta}^{1} f_p \, d\zeta_V \tag{35}$$

which can be integrated analytically.

The heat equation leads to integrals similar to eq. (34):

$$C_T\left(\bar{T}_M\right)=\int_0^{K_\delta}\left(\frac{\zeta_V}{K_\delta}\right)^{\frac{1}{N}} d\zeta_V+\int_{K_\delta}^{1}\frac{f_V(\zeta_V)f_T(\zeta_T)\left\langle f_p(\zeta_V)+\left[1-f_p(\zeta_V)\right]\right\rangle d\zeta_V}{\left[f_T(\zeta_T)+\left\langle\frac{1-f_T(\zeta_T)}{\bar{\bar{T}}_M}\right\rangle\right]} \tag{36}$$

The pressure distribution along the wall was defined previously as:

$$\Delta P_M = \Delta P_S f_g\left(\eta_W\right) \tag{37}$$

Equations (29) and (30) can now be expressed as

Momentum -

$$F_M\left(\eta_W\right) F_{VIS}(r) = \left(\frac{r}{r_N}\right)\left(\frac{b_W}{r_N}\right)\left[\frac{2\bar{P}_M\left(\frac{V_M}{V_A}\right)^2}{\frac{T_M}{T_N}} C_M + \frac{\Delta P_S}{\Delta P_N} f_g\left(\eta_W\right) C_p\right] \tag{38}$$

Heat Flux -

$$F_T\left(\eta_W\right)=2\left(\frac{r}{r_N}\right)\left(\frac{b_W}{r_N}\right)\bar{P}_M\left(\frac{V_M}{V_N}\right)\left(\frac{\Delta T_M}{\Delta T_N}\right)C_T\Big/\left({T_M}/{T_N}\right) \tag{39}$$

The terms on the left side of eqs. (38) and (39), $F_M$ and $F_T$, reflect the gain in radial momentum or heat flux as the jet deflects and becomes parallel to the wall. These functions are made proportional to the pressure recovery function, or

$$F_M\left(\eta_W\right) = F_T\left(\eta_N\right) = 1-fg\left(\eta_W\right) \tag{40}$$

since little or no empirical data are available in the deflection region. Hence, the radial momentum and heat flux reach a maximum at pressure recovery, and for

$$\eta_W = \frac{r}{r_o} \geq 1\ ,\ F_M = F_T = 1$$

The term $F_{VIS}(r)$ reflects the loss of momentum due to frictional loses at the wall, and $F_{VIS}(r) = \frac{1}{\left(\frac{r}{D}\right)} \alpha_{VIS}$, where $\alpha_{VIS} = 0.15-0.25$. (41)

Equations (38) and (39) represent two simultaneous equations for the two unknowns, $V_M$ and $T_M$. The values of the integrals $C_M$, $C_p$ and $C_T$, which arise from the profile functions, are determined numerically and are, in general, a function of the maximum temperature ratio $\left(\frac{T_M}{T_A}\right)$.

The inviscid deflection region is assumed to occur under the half velocity width ($b_{VHi}$) of the incident jet profile. Constant total pressure and total temperature is assumed throughout the inviscid layer to be equal to the incident jet values. The wall-jet properties at the beginning of the wall-jet transition region are obtained from the inviscid values. The initial velocity at the end of the inviscid region is defined from the static pressure and Bernoulli's equation.

Equations (38) and (39) are used to determine the initial values of the exponent $\alpha$, governing the wall-jet profiles in the shear layer, and the initial ratio, $\lambda_{T_i}$, of the thermal-to-dynamic layer thickness. The wall layer is now completely initialized upon prescription of the initial boundary layer characteristics. Fully developed values for the exponent $\alpha$ and the ratio $\lambda_T$ are now prescribed and a linear variation between the initial values at the beginning of the transition to the fully developed region is assumed. Equations (38) and (39) can then be solved simultaneously for the maximum temperature and velocity throughout the wall-jet, given a prescribed behavior for the half-velocity thickness.

For the fully developed wall-jet region, the boundary and shear layers are assumed to have a simple linear behavior:

$$\frac{b_{WH}}{r_N} = a_{W_3} \left(\frac{r}{r_N}\right) \quad (42)$$

$$\frac{\delta_{bL}}{D} = a_{bL_3} \left(\frac{r}{D} - 1\right) \quad (43)$$

where $a_{W_3} = 0.9 \left[1 + \ln\left(\frac{2}{1 + \frac{1}{T_N \beta_W}}\right)\right]\left[1 - .16M_S\right]$ ; $\beta_W \sim 0.50$

$a_{bL_3} \cong 0.0175$

and $M_s$ is the stagnation Mach number of the jet. The wall jet thickness in the transition region is obtained by a linear variation between the initial and fully developed values. Some total pressure and temperature decay data is shown in Figure 59 for single circular jet impingement into a radial wall-jet. The wall-jet pressure decay is only slightly influenced by the nozzle temperature ratio for the range tested. The temperature decay shows a greater dependence on the nozzle temperature. Both the temperature and pressure decays more rapidly with an increase in nozzle temperature.

## 6.7 Two-Jet Interaction Model

Figure 60 shows a sketch of the ground plane coordinate systems for the two jet impingement interaction problem. The jets stagnate on the ground, de-

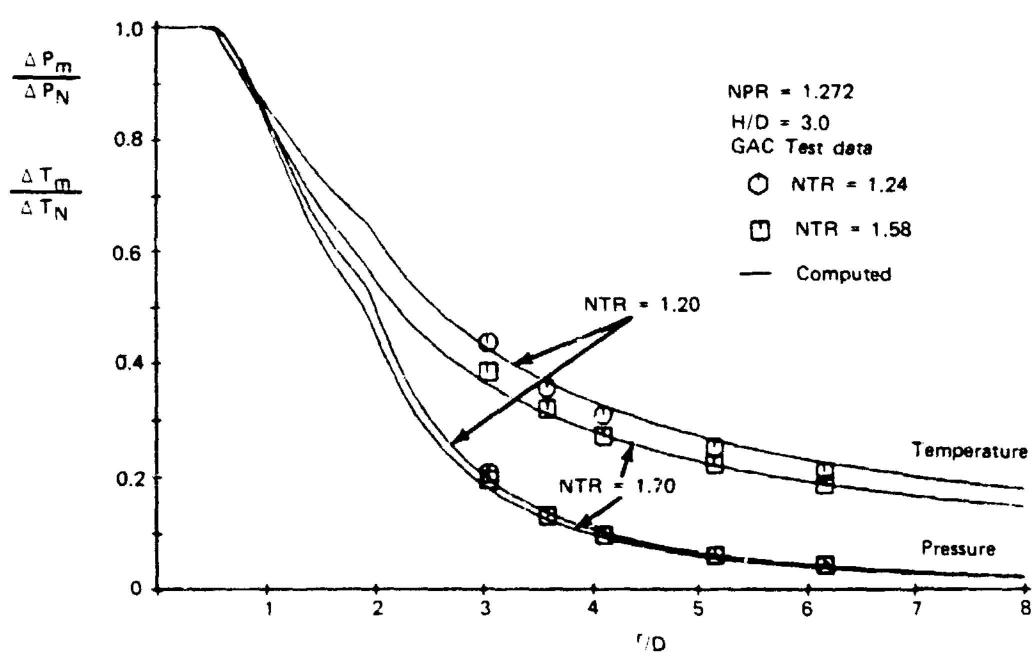


Figure 59 - Heated wall-jet dimensionless total pressure and temperature difference decay with ground radius.

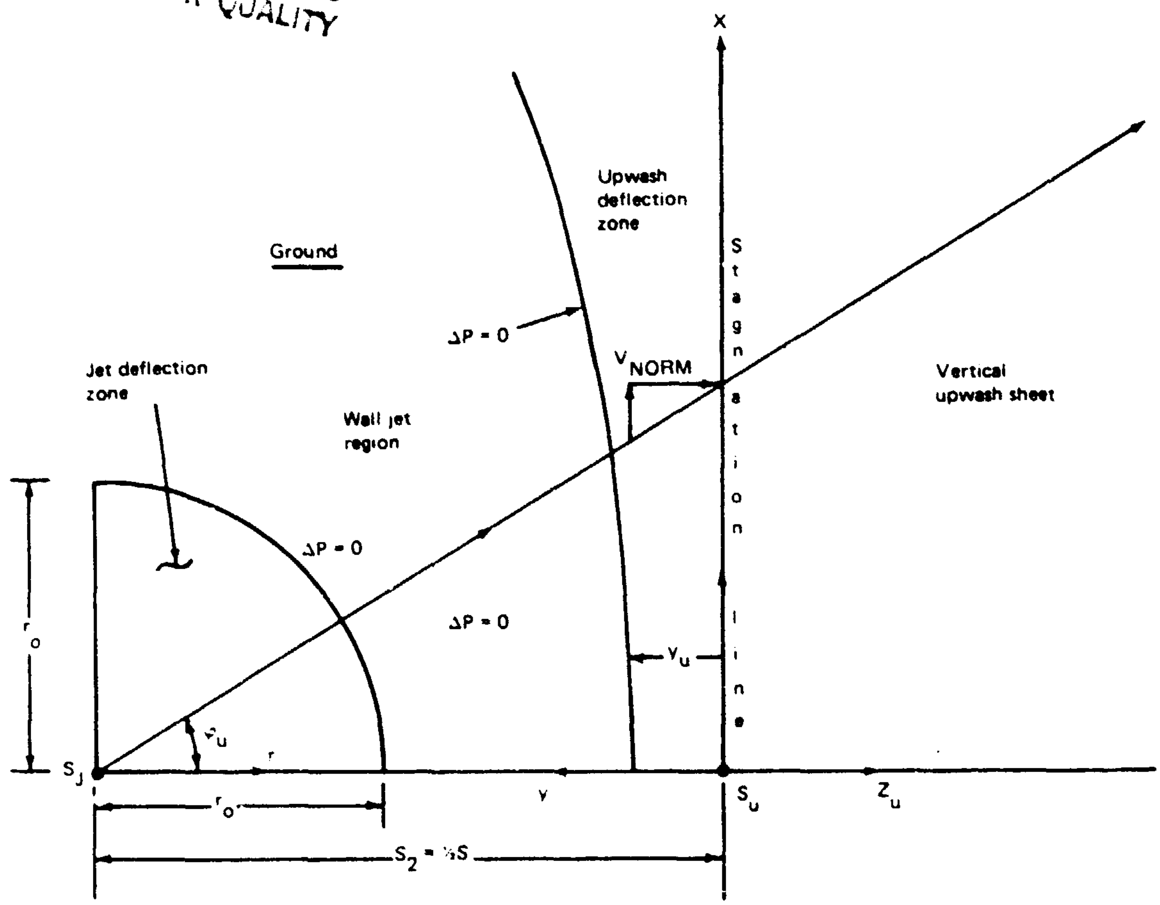


Figure 60 - Two-jet impingement without deflection zone interaction.

flect into radial wall jets and collide along their plane of symmetry. The formation of an upwash stagnation zone is a result of the upward deflection of the wall jet flow. The point $S_u$, on the line joining the jet centers, is the only true stagnation point where the flow comes to rest and deflects vertically. At points off of the center, the flow is deflected at an angle such that the pressure is representative of the stagnation of the normal component of the maximum wall jet velocity.

6.7.1 <u>Maximum pressure and temperature distribution along the upwash stagnation line</u> - To estimate the upwash stagnation line ground pressure and temperature distribution, the maximum velocity of the wall jet normal to the stagnation line is computed:

$$V_{NORM} = V_{MW} \cos \varphi_u \tag{44}$$

The maximum pressure along the stagnation line is computed from the static plus the contribution of the normal velocity of the wall jet.

Pressure -

$$\Delta P_{umg} = \Delta P_{MW} + \frac{1}{2} \frac{P_{MW}}{R_G T_{MW}} V_{MW}^2 \cos^2 \varphi_u \tag{45}$$

Dividing by the nozzle pressure given by

$$\frac{\Delta P_{SN}}{P_A} = NPR-1 = \frac{1}{2} \frac{V_N^2}{R_G T_N} \tag{46}$$

yields

$$\frac{\Delta P_{umg}}{\Delta P_{SN}} = \frac{\Delta P_{MW}}{\Delta P_{SN}} + \frac{\left(\frac{P_{MW}}{P_A}\right)\left(\frac{V_M}{V_N}\right)^2 \cos^2 \varphi u}{\left(\frac{T_M}{T_N}\right)} \tag{47}$$

Temperature -

$$\frac{T_{umg}}{T_A} = \frac{T_{MW}}{T_A} \tag{48}$$

The maximum temperature along the stagnation line is then just equal to the maximum temperature of the wall-jet at the stagnation line location, $X = \frac{S}{2}$

The pressure along the stagnation line given by eq. (47) uses the maximum temperature, velocity, and static pressure of the wall-jet evaluated at the stagnation line location.

6.7.2 Upwash momentum models - The upwash momentum model, including the effects of close jet spacing, remains unchanged in principle due to temperature effects and are those described in Ref. 3. The addition of temperature effects has a slight effect on the ground pressure distribution since the addition of heat to the flow somewhat affects the overall decay rates of the various regions. The overall upwash momentum can then be related to the integral of the upwash ground pressure distribution as described in detail in Ref. 3.

6.7.3 Heated upwash decay model - Figure 61 shows a schematic of the upwash sheet model and the characteristic scaling parameters. The upwash sheet is assumed to be a reflection of the wall-jet flow into the vertical plane of symmetry lying between the jets. The radial streamline pattern of the wall layer is assumed to continue into the upwash sheet and, to a first approximation, be unperturbed by the turning region. The wall-jet flow is assumed to enter the upwash deflection region with a characteristic profile, half velocity width and maximum velocity or total pressure. The characteristic length scale in the upwash sheet is the half velocity width of the incident wall-jet layer estimated at the wall location. The pressure recovery region in the upwash sheet is assumed to be approximately three times the half velocity width of the incident wall jet profile. The magnitude of the momentum flux in the resulting upwash streamline is assumed equal to that of the incident wall-jet. Hence, the upwash sheet is treated in a similar fashion as the wall-jet with a few exceptions.

Due to the high turbulence levels typically measured in the upwash sheet, the flow is considered to be fully turbulent and similar. The upwash velocity profile is taken to be that of a free shear profile with no internal momentum defect due to the wall layer. The upwash sheet growth rate is assumed to be

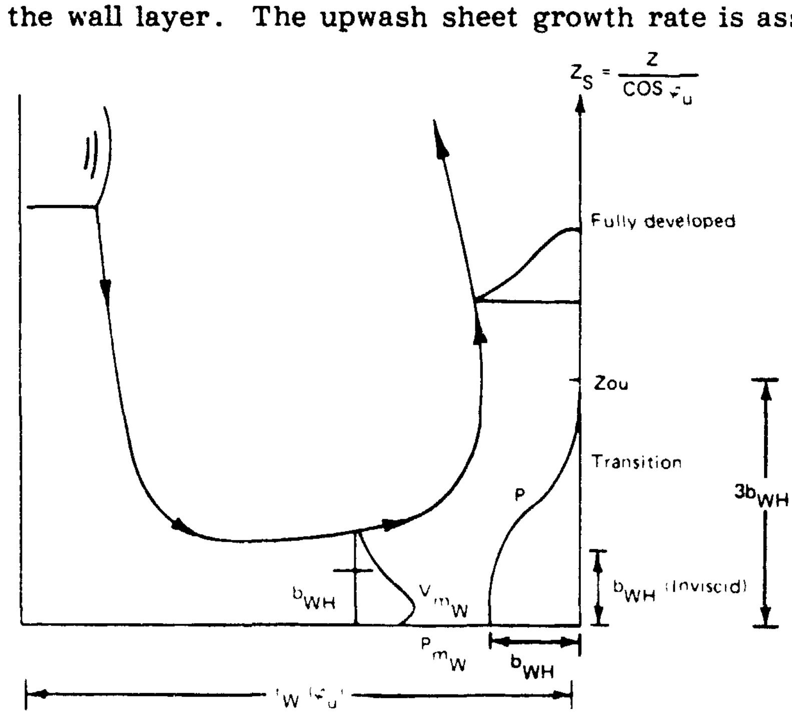


Figure 61 - Characteristic scaling parameters for upwash model.

constant without any initial transition phase. It is also assumed that the magnitude of the momentum flux distribution in the upwash sheet is given by the previously discussed momentum models. Expressions for the momentum and heat flux similar to those for the wall jet can be derived for the upwash flow:

Momentum -

$$f_{Mu}(\varphi)\left[1-f_{Pu}(\varphi)\right] = \left[\left(\frac{r_W + Z_S}{r_N}\right)\frac{b_u}{r_N}\right] \left[\frac{2\left(\frac{P_{uM}}{P_A}\right)\left(\frac{V_{Mu}}{V_N}\right)^2}{\left(\frac{T_{Mu}}{T_N}\right)} C_{Mu}\left(\overline{T}_{Mu}\right) + \frac{\Delta P_{uM}}{\Delta P_N} C_{Pu}\left(\overline{T}_{Mu}\right)\right] \quad (49)$$

where $\Delta P_{MU} = \Delta P_{MUG}(\varphi)\, f_{PU}^{-}(\varphi)$

Heat Flux -

$$f_{Mu}(\varphi)\left[1 - f_{Pu}(\varphi)\right] = 2\left(\frac{r_W + Z_S}{r_N}\right)\left(\frac{b_u}{r_N}\right)\left(\frac{P_{Mu}}{P_A}\right)\left(\frac{V_{Mu}}{V_N}\right)\left(\frac{\Delta T_{Mu}}{\Delta T_N}\right)\frac{C_{Tu}\ \overline{T}_{Mu}}{T_M / T_N} \quad (50)$$

where

$$C_{Mu} = \int_0^1 \frac{f_V{}^2\left[f_p + \frac{(1-f_P)}{\overline{P}_M}\right]}{\left[f_T + \frac{(1-f_T)}{\overline{T}_M}\right]} d\eta_V \quad (51)$$

$$C_{Pu} = \int_0^1 f_p\, d\eta_V \quad (52)$$

$$C_{Tu} = \frac{\int_0^1 f_V(\eta_V) f_T(\eta_T) \left[ f_p + \frac{(1-f_p)}{\bar{P}_M} \right] d\eta_V}{\left[ f_T + \frac{(1-f_T)}{\bar{T}_M} \right]} \qquad (53)$$

$$\zeta = \frac{Z_S}{Z_{SO}}, \quad \eta_V = \frac{Y}{b_u}, \quad \eta_T = \frac{Y}{b_{ut}}$$

The pressure terms in eqs. (49) and (50) only have a contribution in the upwash deflection regions. The above integrals, as with the wall-jet and jet flows, are carried out over the width of the dynamic layer given by $b_u$. The thermal layer is considered to be somewhat wider and is given by:

$$b_{uT} = \lambda_T b_u$$

The growth rate of the upwash flow is assumed to be approximately three times the rate of the wall-jet due to the higher turbulence. Equations (49) and (50) are then solved simultaneously for the temperature and velocity. Initial application of this model to the heated upwash led to the results shown in Figure 62 for the pressure and temperature decay. The pressure correlates well with the test data but the temperature decays too rapidly. The wall-jet and upwash temperature behavior for two interacting impinging jets is significantly different from a single isolated jet impinging to form a wall-jet. Recirculation effects dominate for multi-jet impingement. These effects are due to several aspects of the two-jet problem. Hot upwash flow tends to recirculate back into the free jet and wall jet regions, altering their effective temperature decay. Confinement of the region between the free jet and upwash flow tends to heat the ambient flow or restrict the influx of cooler ambient air into this region to be entrained by the wall jet and upwash flow. As a result of these effects, in order to be able to estimate the temperature behavior of wall-jets and upwash flow, a recirculation model must be established.

6.7.4 Recirculation model - As a preliminary attempt at estimating recirculation effects, a model was generated for both the wall-jet and upwash flows. The

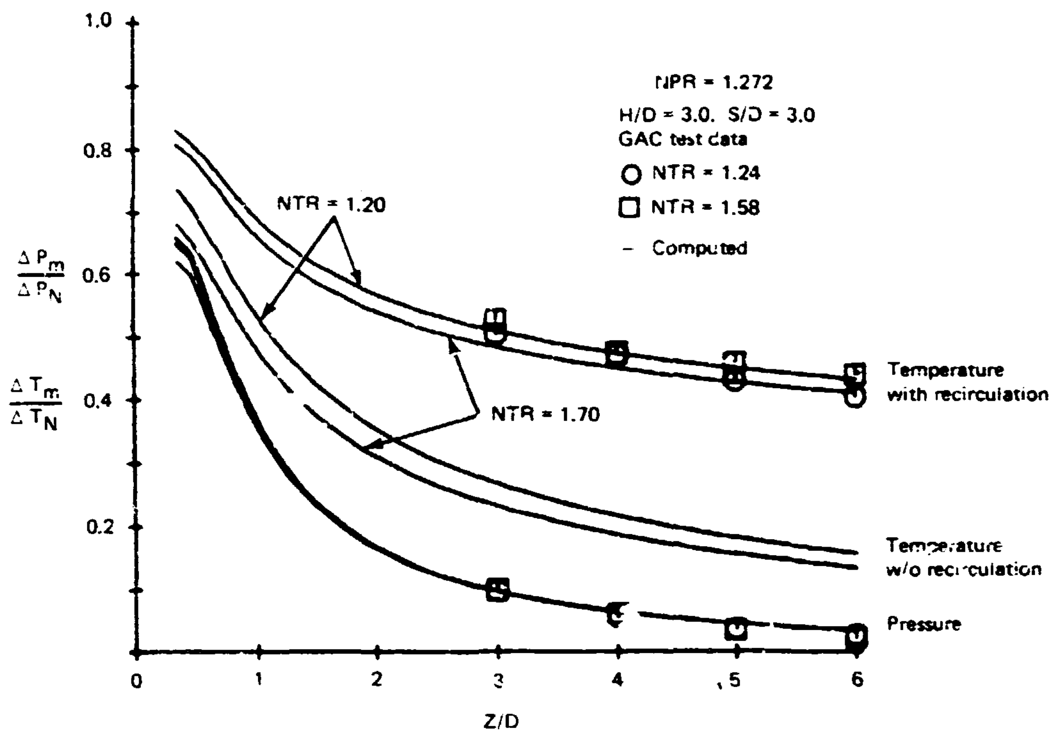


R81-1622-054(1/2)D

Figure 62 - Heated upwash centerline decay characteristics with recirculation effects.

basic principle of such a model is demonstrated in Figure 63. The model takes into account that the wall jet and upwash streamlines do not effectively entrain air at the reference ambient condition. This situation is most extreme along the inner wall-jet and upwash streamline ($\varphi=0^0$) and is enhanced as the jet spacing is reduced. The recirculation effect is also assumed to be negligible along the outermost ray ($\varphi=\pi$). In reality, the outermost ray may also be affected if the free jet decay has been altered. This is neglected in the present study. In order to quantify the recirculation effect, it is assumed that it results in a local change in ambient conditions represented by:

$$\frac{T_{Aeff}}{T_A} = 1 + A_{rec} \cos^2\left(\frac{\varphi}{2}\right) \Delta T_g \tag{54}$$

where

$$A_{rec} = \left[\frac{r_g}{(S/2)}\right]^{\alpha_{rec}}, \quad \alpha_{rec} \sim 1.30$$

and $\Delta T_g$ is the ground stagnation temperature of the incident jet.

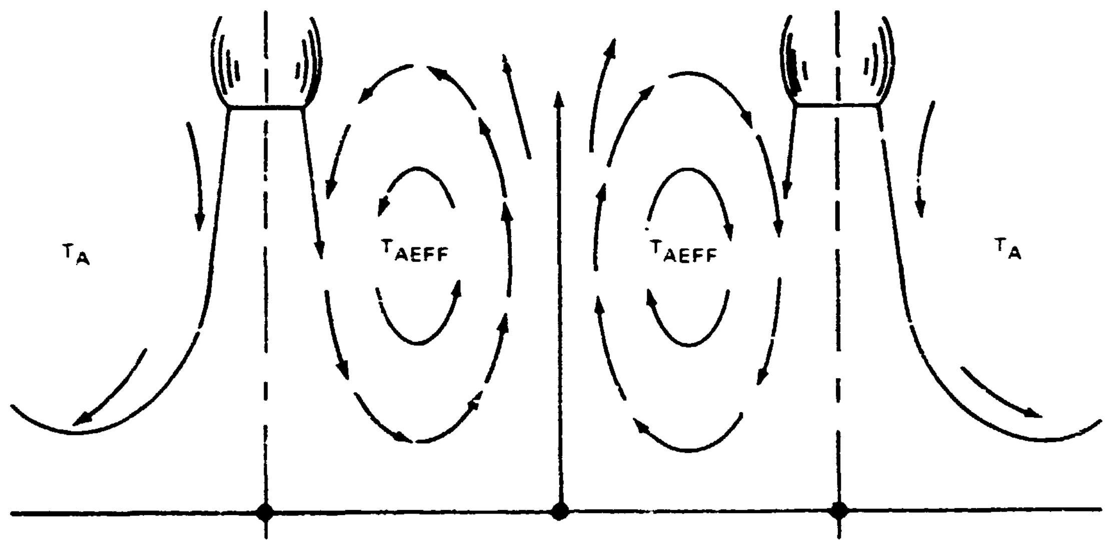


R81-1622-054(2/2)D

Figure 63 - Recirculation effects.

Essentially, the amount of excess heat flux in any given layer is then altered by the effective local ambient condition:

$$H_F - \Delta T_N = T_N - T_{Aeff}$$

Hence, if the effective or local ambient temperature is equal to the nozzle temperature, the excess heat flux will be zero and no temperature decay will take place as a result of the heat equation.

If the incident radius ($r_g$) of the impinging jet is equal to the half spacing of the jets, then the effective ambient temperature $\left(\frac{T_{Aeff}}{T_A}\right)$ becomes equal to the incident temperature ratio of the jet along the streamline $\varphi = 0°$ and no further temperature decay will occur. Figures 64a and 64b demonstrate the effect of this model on the wall jet decay rates for two jets with S/D = 3.0 and H/D = 3.0, and two different nozzle temperature ratios. In this figure, the decay is computed until the wall jet interacts with the stagnation line. For $\varphi > \pi/2$, the wall-jet decay is computed to a fixed radius of three diameters. The least temperature decay occurs along the inner ($\varphi = 0°$) streamline. The wall-jet decays more rapidly as the outermost ray is approached and, at $\varphi = \pi$, the decay of the wall-jet becomes equal to the isolated impingement value.

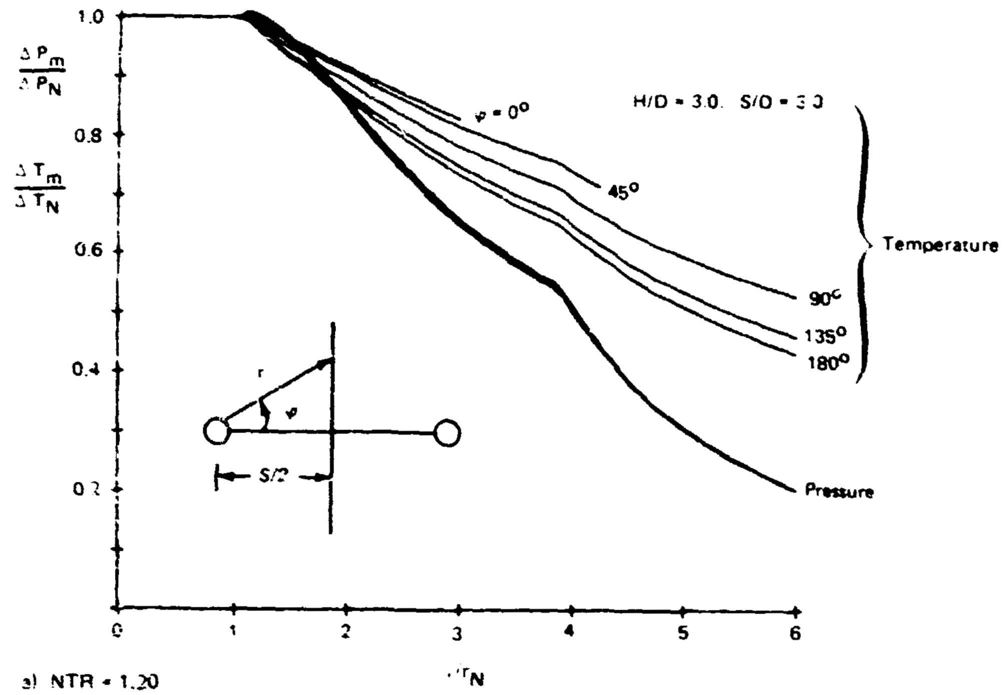


a) NTR = 1.20

R81-1622-055(1/2)D

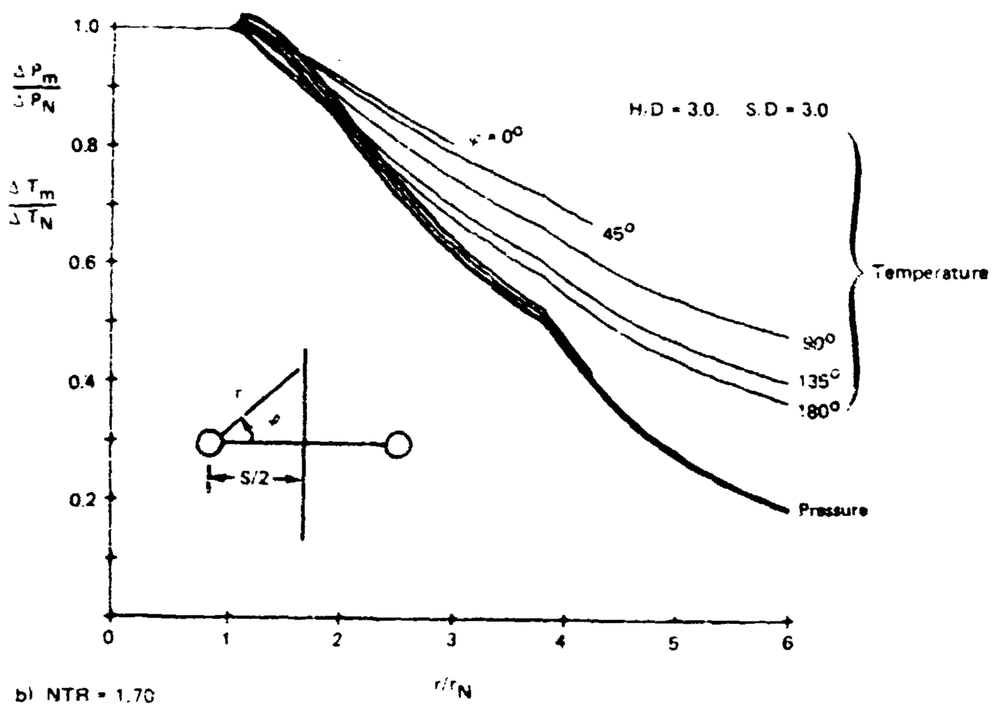


b) NTR = 1.70

R81-1622-055(2/2)D

Figure 64 - Heated wall jet decay characteristics with azimuthal recirculation model.

ORIGINAL PAGE IS
OF POOR QUALITY

A slight overshoot of the values occur at the end of the inviscid region due to a mismatch either in the radius of the inviscid region or in the thickness of the wall layer. Even though an effective change in ambient temperature conditions affects the temperature decay rate dramatically, it only affects the total pressure decay slightly as indicated by the figures. Figure 65 more clearly demonstrates the effect of the recirculation model as a function of jet spacing. The decay of the innermost streamline ($\psi$=0) is plotted as a function of jet spacing. As the spacing increases, the wall-jet temperature decays more rapidly and, as $S/D \rightarrow \infty$, the decay rate of the interacting wall jet approaches the isolated or single jet impingement behavior. The recirculation effect on the wall-jet feeds into the upwash as an alteration of the initial upwash temperature as well as changing the upwash decay rate. Figure 66 shows the improved correlation in the upwash temperature decay with the implementation of the recirculation model in comparison with Figure 62. Obviously, more detailed correlation is required really to be able to quantify this effect. It is also expected that the presence of a confining plate or vehicle will significantly alter or enhance the recirculation effects.

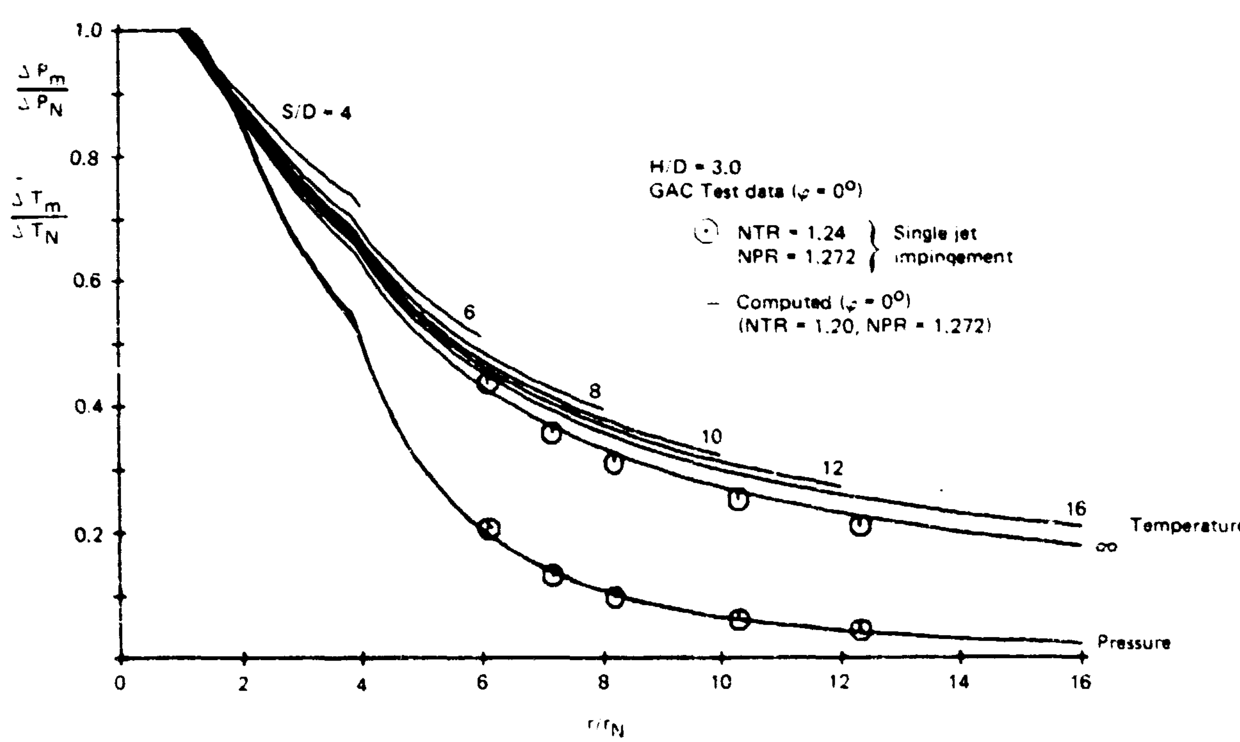


R81-1622-056(1/2)D

Figure 65 - Heated-wall jet decay characteristics ($\varphi$ = 0°) vs. jet spacing.

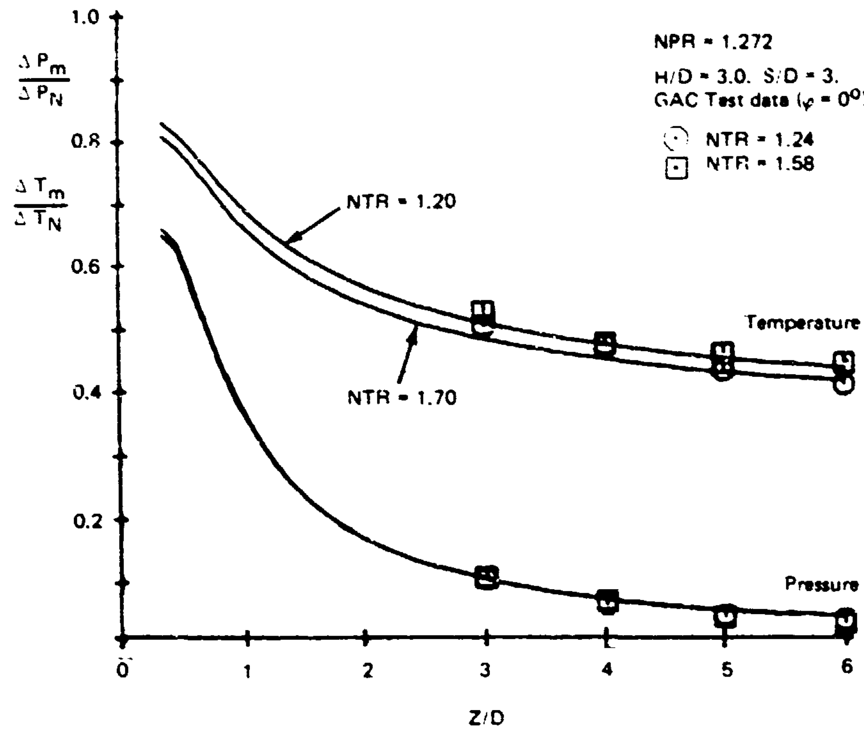


R81-1622-056(2/2)D

Figure 66 - Correleation of heated upwasn decay characteristics ( $\varphi$ = 0°) with recirculation model.

# 7 - CONCLUSIONS

For the configuration considered in this investigation, small-scale models can be used to predict full-scale induced forces. No scale effects were found, and jet temperature and pressure did not affect the nondimensionalized induced lift. The induced lift in-ground-effect was found to be higher for the uniform circular jets than for the simulated fan jets.

Modifications to an existing wall-jet transition model adequately predict the trends with height above ground of upwash temperatures and pressures. The addition of a recirculation model is necessary to predict upwash temperatures in the presence of an aircraft.

# APPENDIX

## COMPUTER PROGRAM DESCRIPTION

PROGRAM NAME: GRUMHOT2

PURPOSE: VTOL TWO-JET IMPINGEMENT INTERACTION PROBLEM

This program is designed to estimate the dynamic and thermal flow characteristics associated with two vertically-impinging and equal-strength hot jets. This program is specifically oriented towards the problem of closely-spaced jet interaction, where the deflection regions interact until eventually jet coalescence occurs.

Aside from the basic flow characteristics, the program assumes the symmetrical placement of a slender fuselage in the upwash flow. The upwash lift force is then computed for a cylindrical fuselage of constant cross-sectional shape. The body parameters, in terms of width and depth, do not vary longitudinally. The program estimates the force on the basis of a rectangular and a circular cross section. Two planes of symmetry are assumed and all output applies to one quadrant of the flow field (ie. equal jets and nozzles located at the midpoint of the fuselage). Jet entrainment effects may be significant but are neglected in this program. Hence, the force is only that due to upwash impingement. Some residual programming exists in the code for a parabolic body of revolution. These cards have been commented out but may be used if desired.

### INPUT DESCRIPTION

Note: All input parameters are in terms of nozzle diameters.

| Card No. | Code Names | Format |
|---|---|---|
| 1 | NPR, NTR | 2F10.5 |

| Name | Definition |
|---|---|
| NPR | Nozzle pressure ratio |
| NTR | Nozzle temperature ratio |

| Card No. | Code Names | Format |
|---|---|---|
| 2 | HD, SD, ZPLD, DZPL, ZFINAL | 5F10.5 |

| Name | Definition |
|---|---|
| HD | Nozzle height above ground |
| SD | Nozzle spacing |

Note: The program will compute one or several positions of the fuselage relative to the ground for a fixed nozzle height above ground.

| | |
|---|---|
| ZPLD | Initial fuselage height above ground |
| DZPL | Increment in fuselage $\Delta Z$ above ground |
| ZFINAL | Final Z coordinate of fuselage height relative to ground plane. |

| Card No. | Code Names | Format |
|---|---|---|
| 3 | XL2, WCON, ZCON | 3F10.5 |

| Names | Definition |
|---|---|
| XL2 | Fuselage Length |
| WCON | Fuselage Width |
| ZCON | Fuselage Depth |

Note: ZCON determines position of fuselage underside relative to its ZPLD location. Bottom of fuselage will be located at ZPLD-ZCON at first computed location. The upwash sheet properties are also computed at this Z location.

| Card No. | Code Names | Format |
|---|---|---|
| 4 | IPBAR | I1 |

| Name | Definition |
|---|---|
| IPBAR | Integer controlling the output of ground pressure pattern: IPBAR = 0, no pressure pattern output<br>IPBAR = 1, pressure pattern output is desired |

Note: Card No. 4 is not required if IPBAR = 0.

| Card No. | Code Name | Format |
|---|---|---|
| 5 | NU | I2 |

| Name | Definition |
|---|---|
| NU | Number of pressure values to be input for computation of ground isobar pattern NU < 25 |

Note: Card No. 5 is repeated NU times.

| Card No. | Code Name | Format |
|---|---|---|
| 6 | PU | F10.5 |

| Name | Definition |
|---|---|
| PU | Nondimensional pressure for isobar pattern $0.0 \leq PU < 1.0$ |

Figure 67 shows a typical input set.

```
TOF:
                                    INPUT DATA
*******************************************************************************

1.007     2.00
4.00      3.000     2.00      1.00      4.00
8.00      1.00      0.0
1
10
.9
.8
.7
.60
.50
.4
.3
.2
.10
.05

*******************************************************************************
EOF:
.
R81-1622-062D
```

Figure 67 Typical program input

## PRINTED OUTPUT DESCRIPTION

Figure 68 shows a typical computer printout. Most of the geometrical output quantities are nondimensionalized by the nozzle radius. All velocities and pressure are initially nondimensionalized by the nozzle exit velocity and stagnation pressure. All pressures are relative to ambient conditions.

Note: RN and D refer to nozzle exit radius and diameter. VN refers to nozzle exit velocity.

### Input Parameters

The first set of output echoes the input parameters.

| Output Titles | Definitions |
|---|---|
| NPR | Nozzle pressure ratio |
| NTR | Nozzle temperature ratio |
| Mach No. | Mach number computed from NPR and NTR |
| TN | Nozzle temperature ratio (NTR) relative to ambient or TN/TA |
| H/D | Nozzle height above ground |
| S/D | Nozzle spacing, distance between jet centerlines |
| Z/D | Initial fuselage height |
| DZ/D | Increment in fuselage position |
| ZFINAL/D | Final location of fuselage |
| L/D | Body Length |
| W/D | Body Width |
| ZB/D | Location of underside of body relative to specified fuselage location |

Note: If ZB = 0, underside location is coincident with specified fuselage position.

### Jet Decay Region

| Output Titles | Definitions |
|---|---|
| DELG/D | Jet ground effect height relative to ground plane |
| ZPC/RN | Length of potential core |
| ZFD/RN | Length of potential core and transition regions |
| Z/RN | Jet axial location measured from nozzle exit |

*** INPUT PARAMETERS ***

NPR= 1.0070 NTR= 2.0000
MACH NO.= 0.1000 TN/TA= 2.0000
H/D= 4.00000 S/D= 3.00000 Z/D= 2.00000

Z/D= 2.00000 DZ/D= 1.00000 ZFINAL/D= 4.00000

BODY LENGTH L/D= 8.00000 WIDTH W/D= 1.00000 DEPTH ZB/D= 0.0

***** JET DECAY REGION *****

JET DEFLECTION HEIGHT DELG/D = 1.19340
ZPC/RN= 6.81693 ZFD/RN= 12.78302

| Z/RN | RJH/RN | RJ/RN | ALPV | VJ/VN | RC/RN | ALPT | RJHT/RN | TM/TN | TM/TA | DTM/DTN | RJHQ/RN | QJ/QN |
|---|---|---|---|---|---|---|---|---|---|---|---|---|
| 0.0 | 1.0000 | 1.0000 | 0.0 | 1.0000 | 1.0000 | 1.5000 | 1.0000 | 1.0000 | 2.0000 | 1.0000 | 1.0000 | 1.0000 |
| 1.7016 | 1.0181 | 1.0673 | 6.0144 | 1.0000 | 0.8009 | 6.0144 | 1.0181 | 1.0000 | 2.0000 | 1.0000 | 1.0047 | 1.0000 |
| 3.4033 | 1.0363 | 1.1365 | 6.3209 | 1.0000 | 0.5691 | 6.3209 | 1.0363 | 1.0000 | 2.0000 | 1.0000 | 1.0088 | 1.0000 |
| 5.1049 | 1.0544 | 1.2085 | 6.5791 | 1.0000 | 0.3035 | 6.3791 | 1.0544 | 1.0000 | 2.0000 | 1.0000 | 1.0120 | 1.0000 |
| 6.8066 | 1.0726 | 1.2850 | 6.7837 | 1.0000 | 0.0019 | 6.7837 | 1.0726 | 1.0000 | 2.0000 | 1.0000 | 1.0138 | 1.0000 |

***** JET DEFLECTION REGION *****

RGH/RN= 1.07257 RG/RN= 1.28501 RO/RN= 3.86124 VG/VN= 1.00000

STAGNATION PRESSURE, DPS/DPTJ= 1.00000 GROUND MAX. TEMP., TGS/TA= 2.00000

STAGNATION MACH NUMBER OF JET= 0.10000

ALPG= 1.50462

SINGLE JET GROUND PRESSURES

| R/RGH | DPS/DPTG | R/RN | DPS/DPTJ |
|---|---|---|---|
| 0.0 | 1.00000 | 0.0 | 1.00000 |
| 0.15000 | 0.96689 | 0.16088 | 0.96689 |
| 0.30000 | 0.90821 | 0.32177 | 0.90821 |
| 0.45000 | 0.83608 | 0.48265 | 0.83608 |
| 0.60000 | 0.75619 | 0.64354 | 0.75619 |
| 0.75000 | 0.67257 | 0.80442 | 0.67257 |
| 0.90000 | 0.58832 | 0.96531 | 0.58832 |
| 1.05000 | 0.50592 | 1.12619 | 0.50592 |
| 1.20000 | 0.42734 | 1.28708 | 0.42734 |
| 1.35000 | 0.35409 | 1.44796 | 0.35409 |
| 1.50000 | 0.28731 | 1.60885 | 0.28731 |
| 1.65000 | 0.22775 | 1.76973 | 0.22775 |
| 1.80000 | 0.17586 | 1.93062 | 0.17586 |
| 1.95000 | 0.13175 | 2.09150 | 0.13175 |
| 2.10000 | 0.09528 | 2.25239 | 0.09528 |
| 2.25000 | 0.06606 | 2.41327 | 0.06606 |
| 2.40000 | 0.04350 | 2.57415 | 0.04350 |
| 2.55000 | 0.02685 | 2.73504 | 0.02685 |
| 2.70000 | 0.01524 | 2.89592 | 0.01524 |
| 2.85000 | 0.00771 | 3.05681 | 0.00771 |
| 3.00000 | 0.00331 | 3.21769 | 0.00331 |
| 3.14999 | 0.00110 | 3.37858 | 0.00110 |
| 3.29999 | 0.00023 | 3.53946 | 0.00023 |
| 3.44999 | 0.00001 | 3.70035 | 0.00001 |
| 3.59999 | 0.00000 | 3.86123 | 0.00000 |

***** WALL JET REGION *****

STAGNATION POINT BOUNDARY LAYER THICKNESS, DELS/RN= 0.03735
PMI/PA== 1.00373 (PTTOT/PA-1.)= 0.00700 (TOT/TA-1.)= 1.00000
TMI/TA= 2.00000 VMI/VN= 0.68210
VELOCITY AT START OF TURBULENT WALL JET, VM/VG= 0.68210
START OF WALL JET REGION, ALPWO= 0.60408 BWOH/RN= 0.34507 BWO/RN= 2.38600

R81-1622-063D(19 Sheets)

Figure 68 Typical program printout.

ISOLATED WALL JET PROPERTIES

| R/RN | VM/VG | VM/VN | BWH/RN | BW/RN | DELRL/RN | DELPJ | KDEL | TM/TN | TM/TA | BWHT/RN | DTM/DTN |
|---|---|---|---|---|---|---|---|---|---|---|---|
| 0.0 | 0.0 | 0.0 | 0.3451 | 2.3868 | 0.0374 | 1.0000 | 0.0156 | 1.0000 | 2.0000 | 0.3385 | 1.0000 |
| 0.2500 | 0.2512 | 0.2512 | 0.3451 | 2.3868 | 0.0374 | 1.0000 | 0.0156 | 1.0000 | 2.0000 | 0.3385 | 1.0000 |
| 0.5000 | 0.4138 | 0.4138 | 0.3451 | 2.3868 | 0.0374 | 1.0000 | 0.0156 | 1.0000 | 2.0000 | 0.3385 | 1.0000 |
| 0.7500 | 0.5455 | 0.5455 | 0.3451 | 2.3868 | 0.0374 | 1.0000 | 0.0156 | 1.0000 | 2.0000 | 0.3385 | 1.0000 |
| 1.0000 | 0.6542 | 0.6542 | 0.3451 | 2.3868 | 0.0374 | 1.0000 | 0.0156 | 1.0000 | 2.0000 | 0.3385 | 1.0000 |
| 1.2500 | 0.7258 | 0.7258 | 0.3483 | 2.0315 | 0.0370 | 0.9818 | 0.0182 | 0.9844 | 1.9687 | 0.3479 | 0.9687 |
| 1.5000 | 0.7622 | 0.7622 | 0.3529 | 1.6938 | 0.0366 | 0.9376 | 0.0216 | 0.9610 | 1.9219 | 0.3613 | 0.9219 |
| 1.7500 | 0.7764 | 0.7764 | 0.3575 | 1.4680 | 0.0362 | 0.8799 | 0.0247 | 0.9357 | 1.8715 | 0.3750 | 0.8715 |
| 2.0000 | 0.7741 | 0.7741 | 0.3620 | 1.3087 | 0.0358 | 0.8153 | 0.0273 | 0.9096 | 1.8193 | 0.3889 | 0.8193 |
| 2.2500 | 0.7597 | 0.7597 | 0.3666 | 1.1916 | 0.0353 | 0.7492 | 0.0297 | 0.8836 | 1.7673 | 0.4031 | 0.7673 |
| 2.5000 | 0.7367 | 0.7367 | 0.3712 | 1.1028 | 0.0349 | 0.6853 | 0.0316 | 0.8586 | 1.7173 | 0.4174 | 0.7173 |
| 2.7500 | 0.7081 | 0.7081 | 0.3758 | 1.0338 | 0.0345 | 0.6259 | 0.0333 | 0.8352 | 1.6704 | 0.4320 | 0.6704 |
| 3.0000 | 0.6764 | 0.6764 | 0.3803 | 0.9789 | 0.0340 | 0.5722 | 0.0348 | 0.8138 | 1.6276 | 0.4469 | 0.6276 |
| 3.2500 | 0.6439 | 0.6439 | 0.3849 | 0.9347 | 0.0336 | 0.5245 | 0.0360 | 0.7945 | 1.5889 | 0.4619 | 0.5889 |
| 3.5000 | 0.6123 | 0.6123 | 0.3895 | 0.8983 | 0.0332 | 0.4827 | 0.0369 | 0.7773 | 1.5545 | 0.4772 | 0.5545 |
| 3.7500 | 0.5830 | 0.5830 | 0.3941 | 0.8685 | 0.0328 | 0.4461 | 0.0377 | 0.7620 | 1.5239 | 0.4927 | 0.5239 |
| 4.0000 | 0.5476 | 0.5476 | 0.4103 | 0.8860 | 0.0350 | 0.4023 | 0.0395 | 0.7454 | 1.4907 | 0.5177 | 0.4907 |
| 4.2500 | 0.5071 | 0.5071 | 0.4360 | 0.9386 | 0.0394 | 0.3520 | 0.0419 | 0.7306 | 1.4612 | 0.5500 | 0.4612 |
| 4.5000 | 0.4718 | 0.4718 | 0.4616 | 0.9912 | 0.0437 | 0.3102 | 0.0441 | 0.7176 | 1.4352 | 0.5824 | 0.4352 |
| 4.7500 | 0.4409 | 0.4409 | 0.4873 | 1.0438 | 0.0481 | 0.2753 | 0.0461 | 0.7060 | 1.4120 | 0.6148 | 0.4120 |
| 5.0000 | 0.4135 | 0.4135 | 0.5129 | 1.0964 | 0.0525 | 0.2458 | 0.0479 | 0.6957 | 1.3913 | 0.6471 | 0.3913 |
| 5.2500 | 0.3892 | 0.3892 | 0.5386 | 1.1490 | 0.0569 | 0.2207 | 0.0495 | 0.6864 | 1.3727 | 0.6795 | 0.3727 |
| 5.5000 | 0.3674 | 0.3674 | 0.5642 | 1.2017 | 0.0613 | 0.1991 | 0.0510 | 0.6779 | 1.3558 | 0.7118 | 0.3558 |
| 5.7500 | 0.3477 | 0.3477 | 0.5899 | 1.2543 | 0.0656 | 0.1804 | 0.0523 | 0.6703 | 1.3405 | 0.7442 | 0.3405 |
| 6.0000 | 0.3300 | 0.3300 | 0.6155 | 1.3069 | 0.0700 | 0.1642 | 0.0536 | 0.6633 | 1.3265 | 0.7765 | 0.3265 |

***** TWO-JET INTERACTION PROBLEM *****

*** RECIRCULATION EFFECT ON WALL JETS ***

PHI= 0.0 DEGS.

TNEFF= 2.00000 TAEFF= 1.42834

| R | VM/VN | TM/TN | TM/TA | DPM/DPN | DTM/DTN |
|---|---|---|---|---|---|
| 0.0 | 0.0 | 1.00000 | 2.00000 | 1.00000 | 1.00000 |
| 0.12500 | 0.14993 | 1.00000 | 2.00000 | 1.00000 | 1.00000 |
| 0.25000 | 0.25116 | 1.00000 | 2.00000 | 1.00000 | 1.00000 |
| 0.37500 | 0.33728 | 1.00000 | 2.00000 | 1.00000 | 1.00000 |
| 0.50000 | 0.41383 | 1.00000 | 2.00000 | 1.00000 | 1.00000 |
| 0.62500 | 0.48281 | 1.00000 | 2.00000 | 1.00000 | 1.00000 |
| 0.75000 | 0.54548 | 1.00000 | 2.00000 | 1.00000 | 1.00000 |
| 0.87500 | 0.60245 | 1.00000 | 2.00000 | 1.00000 | 1.00000 |
| 1.00000 | 0.65416 | 1.00000 | 2.00000 | 1.00000 | 1.00000 |
| 1.12300 | 0.69741 | 0.99760 | 1.99520 | 0.99569 | 0.99520 |
| 1.25000 | 0.72787 | 0.99185 | 1.98369 | 0.98077 | 0.98369 |
| 1.37500 | 0.75098 | 0.98587 | 1.97175 | 0.96012 | 0.97175 |
| 1.50000 | 0.76785 | 0.97962 | 1.95925 | 0.93487 | 0.95925 |
| 1.62500 | 0.77938 | 0.97312 | 1.94623 | 0.90638 | 0.94623 |
| 1.75000 | 0.78629 | 0.96641 | 1.93281 | 0.87539 | 0.93281 |
| 1.87500 | 0.78918 | 0.95956 | 1.91913 | 0.84284 | 0.91913 |
| 2.00000 | 0.78859 | 0.95265 | 1.90530 | 0.80935 | 0.90530 |
| 2.12500 | 0.78458 | 0.94574 | 1.89147 | 0.77554 | 0.89147 |
| 2.25000 | 0.77877 | 0.93888 | 1.87776 | 0.74205 | 0.87776 |
| 2.37500 | 0.77036 | 0.93213 | 1.86425 | 0.70933 | 0.86425 |
| 2.50000 | 0.76008 | 0.92553 | 1.85106 | 0.67744 | 0.85106 |
| 2.62500 | 0.74829 | 0.91913 | 1.83825 | 0.64696 | 0.83825 |
| 2.75000 | 0.73528 | 0.91294 | 1.82589 | 0.61777 | 0.82589 |
| 2.87500 | 0.72135 | 0.90701 | 1.81402 | 0.59025 | 0.81402 |
| 3.00000 | 0.70679 | 0.90133 | 1.80266 | 0.56423 | 0.80266 |

Figure 68 - Continued

PHI= 45.0000 DEGS

TNEFF= 2.00000 TAEFF= 1.36561

| R | VM/VN | TM/TN | TM/TA | DPM/DPN | DTM/DTN |
|---|---|---|---|---|---|
| 0.0 | 0.0 | 1.00000 | 2.00000 | 1.00000 | 1.00000 |
| 0.17678 | 0.19461 | 1.00000 | 2.00000 | 1.00000 | 1.00000 |
| 0.35355 | 0.32347 | 1.00000 | 2.00000 | 1.00000 | 1.00000 |
| 0.53033 | 0.43124 | 1.00000 | 2.00000 | 1.00000 | 1.00000 |
| 0.70711 | 0.52460 | 1.00000 | 2.00000 | 1.00000 | 1.00000 |
| 0.88388 | 0.60628 | 1.00000 | 2.00000 | 1.00000 | 1.00000 |
| 1.06066 | 0.67759 | 1.00000 | 2.00000 | 1.00000 | 1.00000 |
| 1.23744 | 0.72490 | 0.99149 | 1.98298 | 0.98262 | 0.98298 |
| 1.41421 | 0.75632 | 0.98195 | 1.96390 | 0.95298 | 0.96390 |
| 1.59099 | 0.77578 | 0.97180 | 1.94360 | 0.91485 | 0.94360 |
| 1.76776 | 0.78556 | 0.96117 | 1.92233 | 0.87140 | 0.92233 |
| 1.94454 | 0.78744 | 0.95026 | 1.90051 | 0.82496 | 0.90051 |
| 2.12132 | 0.78287 | 0.93928 | 1.87857 | 0.77746 | 0.87857 |
| 2.29809 | 0.77309 | 0.92844 | 1.85688 | 0.73037 | 0.85688 |
| 2.47487 | 0.75920 | 0.91788 | 1.83577 | 0.68473 | 0.83577 |
| 2.65164 | 0.74215 | 0.90775 | 1.81550 | 0.64164 | 0.81550 |
| 2.82842 | 0.72284 | 0.89813 | 1.79626 | 0.60132 | 0.79626 |
| 3.00519 | 0.70210 | 0.88909 | 1.77818 | 0.56415 | 0.77818 |
| 3.18197 | 0.68068 | 0.88066 | 1.76132 | 0.53008 | 0.76132 |
| 3.35875 | 0.65927 | 0.87285 | 1.74570 | 0.49919 | 0.74570 |
| 3.53552 | 0.63844 | 0.86564 | 1.73128 | 0.47101 | 0.73128 |
| 3.71230 | 0.61861 | 0.85898 | 1.71796 | 0.44550 | 0.71796 |
| 3.88907 | 0.59812 | 0.85242 | 1.70484 | 0.41969 | 0.70484 |
| 4.06585 | 0.56866 | 0.84472 | 1.68944 | 0.38281 | 0.68944 |
| 4.24263 | 0.54030 | 0.83824 | 1.67648 | 0.34826 | 0.67648 |

PHI= 89.9999 DEGS.

TNEFF= 2.00000 TAEFF= 1.21417

| R | VM/VN | TM/TN | TM/TA | DPM/DPN | DTM/DTN |
|---|---|---|---|---|---|
| 0.0 | 0.0 | 1.00000 | 2.00000 | 1.00000 | 1.00000 |
| 0.25000 | 0.25116 | 1.00000 | 2.00000 | 1.00000 | 1.00000 |
| 0.50000 | 0.41383 | 1.00000 | 2.00000 | 1.00000 | 1.00000 |
| 0.75000 | 0.54548 | 1.00000 | 2.00000 | 1.00000 | 1.00000 |
| 1.00000 | 0.65416 | 1.00000 | 2.00000 | 1.00000 | 1.00000 |
| 1.25000 | 0.72690 | 0.98828 | 1.97656 | 0.98127 | 0.97656 |
| 1.50000 | 0.76518 | 0.97072 | 1.94144 | 0.93617 | 0.94144 |
| 1.75000 | 0.78159 | 0.95177 | 1.90354 | 0.87750 | 0.90354 |
| 2.00000 | 0.78170 | 0.93210 | 1.86419 | 0.81215 | 0.86419 |
| 2.25000 | 0.76971 | 0.91246 | 1.82472 | 0.74536 | 0.82492 |
| 2.50000 | 0.74898 | 0.89349 | 1.78699 | 0.68107 | 0.78699 |
| 2.75000 | 0.72238 | 0.87567 | 1.75135 | 0.62150 | 0.75135 |
| 3.00000 | 0.69239 | 0.85929 | 1.71858 | 0.56789 | 0.71858 |
| 3.25000 | 0.66122 | 0.84449 | 1.68897 | 0.52032 | 0.68897 |
| 3.50000 | 0.63070 | 0.83124 | 1.66249 | 0.47881 | 0.66249 |
| 3.75000 | 0.60216 | 0.81944 | 1.63888 | 0.44249 | 0.63888 |
| 4.00000 | 0.56726 | 0.80654 | 1.61307 | 0.39897 | 0.61307 |
| 4.25000 | 0.52658 | 0.79499 | 1.58998 | 0.34880 | 0.58998 |
| 4.50000 | 0.49105 | 0.78476 | 1.56952 | 0.30726 | 0.56952 |
| 4.75000 | 0.45976 | 0.77564 | 1.55128 | 0.27252 | 0.55128 |
| 5.00000 | 0.43202 | 0.76746 | 1.53491 | 0.24319 | 0.53491 |
| 5.25000 | 0.40726 | 0.76007 | 1.52014 | 0.21822 | 0.52014 |
| 5.50000 | 0.38504 | 0.75336 | 1.50673 | 0.19679 | 0.50673 |
| 5.75000 | 0.36499 | 0.74725 | 1.49450 | 0.17828 | 0.49450 |
| 6.00000 | 0.34682 | 0.74166 | 1.48331 | 0.16219 | 0.48331 |

Figure 68 - Continued

ORIGINAL PAGE IS
OF POOR QUALITY

PHI=134.9999 DEGS.

THEFF= 2.00000 TAEFF= 1.06273

| R | VM/VN | TM/TN | TM/TA | DPM/DPN | DTM/DTN |
|---|---|---|---|---|---|
| 0.0 | 0.0 | 1.00000 | 2.00000 | 1.00000 | 1.00000 |
| 0.25000 | 0.25116 | 1.00000 | 2.00000 | 1.00000 | 1.00000 |
| 0.50000 | 0.41383 | 1.00000 | 2.00000 | 1.00[illegible] | 1.00000 |
| 0.75000 | 0.54548 | 1.00000 | 2.00000 | 1.00000 | 1.00000 |
| 1.00000 | 0.65416 | 1.00000 | 2.00000 | 1.00000 | 1.00000 |
| 1.25000 | 0.72616 | 0.98555 | 1.97111 | 0.98166 | 0.97111 |
| 1.50000 | 0.76313 | 0.96392 | 1.92784 | 0.93718 | 0.92764 |
| 1.75000 | 0.77798 | 0.94060 | 1.88119 | 0.87914 | 0.88119 |
| 2.00000 | 0.77641 | 0.91642 | 1.83285 | 0.81436 | 0.83285 |
| 2.25000 | 0.76272 | 0.89235 | 1.78470 | 0.74799 | 0.78470 |
| 2.50000 | 0.74041 | 0.86916 | 1.73833 | 0.68397 | 0.73833 |
| 2.75000 | 0.71242 | 0.84743 | 1.69486 | 0.62450 | 0.69486 |
| 3.00000 | 0.68128 | 0.82750 | 1.65501 | 0.57087 | 0.65501 |
| 3.25000 | 0.64917 | 0.80954 | 1.61908 | 0.52317 | 0.61908 |
| 3.50000 | 0.61792 | 0.79351 | 1.58702 | 0.48147 | 0.58702 |
| 3.75000 | 0.58883 | 0.77925 | 1.55850 | 0.44494 | 0.55850 |
| 4.00000 | 0.55361 | 0.76375 | 1.52750 | 0.40128 | 0.52750 |
| 4.25000 | 0.51303 | 0.74993 | 1.49987 | 0.35097 | 0.49987 |
| 4.50000 | 0.47768 | 0.73774 | 1.47547 | 0.30930 | 0.4754[illegible] |
| 4.75000 | 0.44663 | 0.72688 | 1.45376 | 0.27443 | 0.45376 |
| 5.00000 | 0.41915 | 0.71716 | 1.43433 | 0.24497 | 0.43433 |
| 5.25000 | 0.39467 | 0.70840 | 1.41681 | 0.21988 | 0.41681 |
| 5.50000 | 0.37274 | 0.70047 | 1.40095 | 0.19835 | 0.40095 |
| 5.75000 | 0.35299 | 0.69325 | 1.38651 | 0.17974 | 0.38651 |
| 6.00000 | 0.33512 | 0.68666 | 1.37331 | 0.16355 | 0.3733[illegible] |

PHI=179.9999 DEGS.

THEFF= 2.00000 TAEFF= 1.00000

| R | VM/VN | TM/TN | TM/TA | DPM/DPN | DTM/DTN |
|---|---|---|---|---|---|
| 0.0 | 0.0 | 1.00000 | 2.00000 | 1.00000 | 1.00000 |
| 0.25000 | 0.25116 | 1.00000 | 2.00000 | 1.00000 | 1.00000 |
| 0.50000 | 0.41383 | 1.00000 | 2.00000 | 1.00000 | 1.00000 |
| 0.75000 | 0.54548 | 1.00000 | 2.00000 | 1.00000 | 1.00000 |
| 1.00000 | 0.65416 | 1.00000 | 2.00000 | 1.00000 | 1.00000 |
| 1.25000 | 0.72583 | 0.98437 | 1.96874 | 0.98183 | 0.96874 |
| 1.50000 | 0.76224 | 0.96097 | 1.92194 | 0.937[illegible]2 | 0.92194 |
| 1.75000 | 0.77641 | 0.93575 | 1.87149 | 0.87987 | 0.87149 |
| 2.00000 | 0.77409 | 0.90963 | 1.81925 | 0.81533 | 0.81925 |
| 2.25000 | 0.75967 | 0.88364 | 1.76727 | 0.74917 | 0.76727 |
| 2.50000 | 0.73667 | 0.85863 | 1.71726 | 0.68527 | 0.71726 |
| 2.75000 | 0.70807 | 0.83522 | 1.67044 | 0.62585 | 0.67044 |
| 3.00000 | 0.67641 | 0.81378 | 1.62755 | 0.5[illegible]222 | 0.62755 |
| 3.25000 | 0.64390 | 0.79447 | 1.58893 | 0.52447 | 0.58893 |
| 3.50000 | 0.61233 | 0.77725 | 1.55450 | 0.48268 | 0.55450 |
| 3.75000 | 0.58299 | 0.76196 | 1.52392 | 0.44606 | 0.52392 |
| 4.00000 | 0.54763 | 0.74536 | 1.49073 | 0.40235 | 0.49073 |
| 4.25000 | 0.50710 | 0.73061 | 1.46121 | 0.35197 | 0.46121 |
| 4.50000 | 0.47183 | 0.71759 | 1.43518 | 0.31024 | 0.43518 |
| 4.75000 | 0.44088 | 0.70602 | 1.41205 | 0.27531 | 0.41205 |
| 5.00000 | 0.41352 | 0.69567 | 1.39135 | 0.24580 | 0.39135 |
| 5.25000 | 0.38916 | 0.68636 | 1.37271 | 0.22066 | 0.37271 |
| 5.50000 | 0.36736 | 0.67792 | 1.35585 | 0.19907 | 0.35585 |
| 5.75000 | 0.34774 | 0.67026 | 1.34051 | 0.18042 | 0.34051 |
| 6.00000 | 0.33000 | 0.66325 | 1.32651 | 0.14419 | 0.3265[illegible] |

Figure 68 - Continued

MAXIMUM GROUND PRESSURE AND TEMPERATURE ALONG UPWASHGROUND STAGNATION LINE

| XW/RN | XW/S | DPMAX/DPJ | PMAX/PMAXO | DTMAX/DTJ | TMAX/TMAXO |
|---|---|---|---|---|---|
| 0.0 | 0.0 | 0.56423 | 1.00000 | 0.80266 | 1.00000 |
| 0.17473 | 0.02912 | 0.56128 | 0.99478 | 0.80208 | 0.99927 |
| 0.35065 | 0.05844 | 0.55263 | 0.97944 | 0.80031 | 0.99707 |
| 0.52698 | 0.08816 | 0.53952 | 0.95443 | 0.79734 | 0.99337 |
| 0.71101 | 0.11850 | 0.51902 | 0.91987 | 0.79315 | 0.98815 |
| 0.89814 | 0.14969 | 0.49183 | 0.87701 | 0.78771 | 0.98137 |
| 1.09191 | 0.18198 | 0.46621 | 0.82629 | 0.78096 | 0.97296 |
| 1.29407 | 0.21568 | 0.43380 | 0.76884 | 0.77286 | 0.96287 |
| 1.50665 | 0.25111 | 0.39862 | 0.70648 | 0.76335 | 0.95104 |
| 1.73205 | 0.28867 | 0.36127 | 0.64028 | 0.75241 | 0.93739 |
| 1.97313 | 0.32885 | 0.32275 | 0.57202 | 0.73994 | 0.92186 |
| 2.23341 | 0.37224 | 0.28402 | 0.50337 | 0.72591 | 0.90438 |
| 2.51770 | 0.41955 | 0.24282 | 0.43036 | 0.70873 | 0.88298 |
| 2.83035 | 0.47172 | 0.19617 | 0.34768 | 0.68737 | 0.85636 |
| 3.17981 | 0.52997 | 0.15346 | 0.27198 | 0.66515 | 0.82869 |
| 3.57525 | 0.59588 | 0.11645 | 0.20639 | 0.64119 | 0.79882 |
| 4.02969 | 0.67162 | 0.08535 | 0.15127 | 0.61545 | 0.76675 |
| 4.56127 | 0.76021 | 0.06009 | 0.10650 | 0.58796 | 0.73251 |
| 5.19614 | 0.86602 | 0.04034 | 0.07149 | 0.55874 | 0.69611 |
| 5.97346 | 0.99558 | 0.0255 | 0.04531 | 0.52781 | 0.65757 |
| 6.95473 | 1.15912 | 0.01506 | 0.02673 | 0.49520 | 0.61694 |
| 8.24235 | 1.37372 | 0.00811 | 0.01438 | 0.46093 | 0.57425 |
| 10.02056 | 1.67009 | 0.00385 | 0.00683 | 0.42503 | 0.52952 |
| 12.65775 | 2.10962 | 0.00153 | 0.00272 | 0.38750 | 0.48277 |
| 17.01334 | 2.83556 | 0.00046 | 0.00082 | 0.34829 | 0.43392 |

UPWASH MOMENTUM FUNCTION: JET RADIUS, INTERACTION CONSTANT, VERTICAL UPWASH SHEET MOMENTUM, AND COALES

RG/RN= 1.29501 ACON= 0.81653 XMOMZ= 0.93894 PHIO(DEGS)= 0.0

UPWASH WIDTH CONSTANT ESTIMATE , CU= 0.29758

*** CALL INTERG ***

SOLUTION OF GROUND PRESSURE DISTRIBUTION HAS BEEN FOUND
ITERATION CYCLE= 15 EPS= 0.03691 SIGMA= 0.91425
EPI= 0.03691 CUI= 0.29758 PHIUO= 49.43231 PHIO= 63.52774 DEGREES
PHI=0.0, DELPWO= 0.67723
PHI=0.0, PMIN= 0.11929
PHI=0.0, ALFUG= 2.73835
UPWASH THICKNESS CONSTANT, (CU) X (SIGMA)= 0.27206

*** COMPUTATION OF TWO-JET GROUND ISOBAR PATTERN ***

10 VALUES OF PRESSURE SPECIFIED FOR PATTERN

PBAR= 0.[illegible] 0.80000 0.70000 0.60000 0.50000 0.40000 0.30000 0.20000
0.10000 0.05000

Figure 68 - Continued

GROUND PATTERN IN JET CENTERED COORDINATE SYSTEM

FBAR= 0.90000

JET IMPINGEMENT REGION, IJET= 58 UPWASH DEFLECTION REGION, IU= 0

| XISOJ | YISOJ | XISOU | YISOU |
|---|---|---|---|
| 0.34791 | 0.0 | | |
| 0.34760 | 0.01472 | | |
| 0.34665 | 0.02941 | | |
| 0.34509 | 0.04402 | | |
| 0.34291 | 0.05852 | | |
| 0.34012 | 0.07269 | | |
| 0.33673 | 0.08707 | | |
| 0.33277 | 0.10105 | | |
| 0.32823 | 0.11479 | | |
| 0.32316 | 0.12827 | | |
| 0.31755 | 0.14145 | | |
| 0.31144 | 0.15431 | | |
| 0.30485 | 0.16683 | | |
| 0.29780 | 0.17899 | | |
| 0.29031 | 0.19076 | | |
| 0.28242 | 0.20214 | | |
| 0.27414 | 0.21310 | | |
| 0.26551 | 0.22363 | | |
| 0.25655 | 0.23374 | | |
| 0.24729 | 0.24339 | | |
| 0.23774 | 0.25260 | | |
| 0.22795 | 0.26135 | | |
| 0.21792 | 0.26965 | | |
| 0.20769 | 0.27748 | | |
| 0.19729 | 0.28486 | | |
| 0.18672 | 0.29178 | | |
| 0.17601 | 0.29824 | | |
| 0.16520 | 0.30425 | | |
| 0.15428 | 0.30981 | | |
| 0.15428 | 0.30981 | | |
| 0.13132 | 0.31999 | | |
| 0.10769 | 0.32846 | | |
| 0.08353 | 0.33519 | | |
| 0.05896 | 0.34013 | | |
| 0.03411 | 0.34328 | | |
| 0.00911 | 0.34461 | | |
| -0.01590 | 0.34453 | | |
| -0.04079 | 0.34184 | | |
| -0.06544 | 0.33775 | | |
| -0.08970 | 0.33189 | | |
| -0.11347 | 0.32429 | | |
| -0.13660 | 0.31501 | | |
| -0.15859 | 0.30408 | | |
| -0.18052 | 0.29157 | | |
| -0.20108 | 0.27755 | | |
| -0.22056 | 0.26209 | | |
| -0.23887 | 0.24527 | | |
| -0.25591 | 0.22719 | | |
| -0.27160 | 0.20794 | | |
| -0.28585 | 0.18761 | | |
| -0.29860 | 0.16633 | | |
| -0.30978 | 0.14418 | | |
| -0.31934 | 0.12130 | | |
| -0.32722 | 0.09779 | | |
| -0.33339 | 0.07379 | | |
| -0.33783 | 0.04941 | | |
| -0.34049 | 0.02477 | | |
| -0.34139 | 0.00060 | | |

Figure 68 - Continued

PBAR= 0.80000

JET IMPINGEMENT REGION, IJET= 58          UPWASH DEFLECTION REGION, IU= 0

| XISOJ | YISOJ | XISOU | YISOU |
|---|---|---|---|
| 0.56735 | 0.0 | | |
| 0.56684 | 0.02401 | | |
| 0.56530 | 0.04795 | | |
| 0.56275 | 0.07178 | | |
| 0.55919 | 0.09543 | | |
| 0.55464 | 0.11886 | | |
| 0.54912 | 0.14199 | | |
| 0.54265 | 0.16479 | | |
| 0.53526 | 0.18720 | | |
| 0.52698 | 0.20917 | | |
| 0.51784 | 0.23067 | | |
| 0.50788 | 0.25164 | | |
| 0.49712 | 0.27206 | | |
| 0.48563 | 0.29188 | | |
| 0.47342 | 0.31108 | | |
| 0.46055 | 0.32963 | | |
| 0.44705 | 0.34751 | | |
| 0.43298 | 0.36469 | | |
| 0.41837 | 0.38116 | | |
| 0.40326 | 0.39691 | | |
| 0.38770 | 0.41193 | | |
| 0.37172 | 0.42620 | | |
| 0.35537 | 0.43973 | | |
| 0.33869 | 0.45250 | | |
| 0.32172 | 0.46453 | | |
| 0.30449 | 0.47581 | | |
| 0.28703 | 0.48635 | | |
| 0.26939 | 0.49615 | | |
| 0.25159 | 0.50522 | | |
| 0.25159 | 0.50522 | | |
| 0.21415 | 0.52182 | | |
| 0.17562 | 0.53563 | | |
| 0.13621 | 0.54660 | | |
| 0.09614 | 0.55467 | | |
| 0.05562 | 0.55980 | | |
| 0.01485 | 0.56197 | | |
| -0.02593 | 0.56119 | | |
| -0.06652 | 0.55744 | | |
| -0.10671 | 0.55078 | | |
| -0.14628 | 0.54122 | | |
| -0.18503 | 0.52884 | | |
| -0.22276 | 0.51369 | | |
| -0.25928 | 0.49587 | | |
| -0.29439 | 0.47547 | | |
| -0.32791 | 0.45261 | | |
| -0.35968 | 0.42740 | | |
| -0.38954 | 0.39997 | | |
| -0.41732 | 0.37049 | | |
| -0.44290 | 0.33909 | | |
| -0.46615 | 0.30595 | | |
| -0.48694 | 0.27123 | | |
| -0.50517 | 0.23512 | | |
| -0.52075 | 0.19781 | | |
| -0.53361 | 0.15948 | | |
| -0.54358 | 0.12033 | | |
| -0.55090 | 0.08057 | | |
| -0.55526 | 0.04039 | | |
| -0.55671 | 0.00001 | | |

Figure 68 - Continued

ORIGINAL PAGE IS
OF POOR QUALITY

PBAR= 0.70000

JET IMPINGEMENT REGION, IJET= 58 UPWASH DEFLECTION REGION, IU= 0

| XISOJ | YISOJ | XISOU | YISOU |
|---|---|---|---|
| 0.76642 | 0.0 | | |
| 0.76573 | 0.03243 | | |
| 0.76365 | 0.06478 | | |
| 0.76020 | 0.09697 | | |
| 0.75540 | 0.12892 | | |
| 0.74925 | 0.16056 | | |
| 0.74179 | 0.19181 | | |
| 0.73306 | 0.22261 | | |
| 0.72307 | 0.25288 | | |
| 0.71189 | 0.28257 | | |
| 0.69954 | 0.31160 | | |
| 0.68608 | 0.33994 | | |
| 0.67155 | 0.36751 | | |
| 0.65602 | 0.39429 | | |
| 0.63953 | 0.42023 | | |
| 0.62214 | 0.44529 | | |
| 0.60392 | 0.46944 | | |
| 0.58490 | 0.49265 | | |
| 0.56516 | 0.51490 | | |
| 0.54475 | 0.53618 | | |
| 0.52373 | 0.55646 | | |
| 0.50215 | 0 57574 | | |
| 0.48007 | 0.59401 | | |
| 0.45753 | 0.61127 | | |
| 0.43460 | 0.62752 | | |
| 0.41133 | 0.64276 | | |
| 0.38775 | 0.65700 | | |
| 0.36391 | 0.67024 | | |
| 0.33987 | 0.68250 | | |
| 0.33987 | 0.68250 | | |
| 0.28929 | 0.70491 | | |
| 0.23724 | 0.72357 | | |
| 0.18401 | 0.73839 | | |
| 0.12989 | 0.74929 | | |
| 0.07513 | 0.75622 | | |
| 0.02007 | 0.75916 | | |
| -0.03503 | 0.75809 | | |
| -0.08987 | 0.75304 | | |
| -0.14415 | 0.74403 | | |
| -0 19761 | 0.73112 | | |
| -0.24996 | 0.71439 | | |
| -0.30093 | 0.69393 | | |
| -0.35025 | 0.66986 | | |
| -0.39768 | 0.64230 | | |
| -0.44297 | 0.61141 | | |
| -0.48589 | 0.57736 | | |
| -0.52622 | 0.54032 | | |
| -0.56375 | 0.50048 | | |
| -0.59831 | 0.45807 | | |
| -0.62971 | 0.41330 | | |
| -0.65779 | 0.36640 | | |
| -0.68242 | 0.31762 | | |
| -0.70347 | 0.26721 | | |
| -0.72084 | 0.21543 | | |
| -0.73444 | 0.16255 | | |
| -0.74420 | 0.10884 | | |
| -0.75008 | 0.05456 | | |
| -0.75204 | 0.00001 | | |

Figure 68 - Continued

PBAR= 0.60000

JET IMPINGEMENT REGION, IJET= 58 UPWASH DEFLECTION REGION, IU= 11

| XISOJ | YISOJ | XISOU | YISOU |
|---|---|---|---|
| 0.96092 | 0.0 | 2.75620 | 0.0 |
| 0.96005 | 0.04066 | 2.75724 | 0.09247 |
| 0.95745 | 0.08122 | 2.76042 | 0.18511 |
| 0.95313 | 0.12157 | 2.76592 | 0.27811 |
| 0.94710 | 0.16164 | 2.77408 | 0.37164 |
| 0.93939 | 0.20131 | 2.78552 | 0.46588 |
| 0.93004 | 0.24049 | 2.80128 | 0.56104 |
| 0.91909 | 0.27910 | 2.82348 | 0.65729 |
| 0.90657 | 0.31706 | 2.85749 | 0.75486 |
| 0.89254 | 0.35428 | 2.93572 | 0.85395 |
| 0.87706 | 0.39068 | 3.00000 | 0.86662 |
| 0.86018 | 0.42620 | | |
| 0.84198 | 0.46078 | | |
| 0.82250 | 0.49435 | | |
| 0.80183 | 0.52687 | | |
| 0.78003 | 0.55829 | | |
| 0.75717 | 0.58857 | | |
| 0.73333 | 0.61767 | | |
| 0.70859 | 0.64557 | | |
| 0.68300 | 0.67225 | | |
| 0.65664 | 0.69768 | | |
| 0.62958 | 0.72185 | | |
| 0.60189 | 0.74476 | | |
| 0.57364 | 0.76640 | | |
| 0.54489 | 0.78677 | | |
| 0.51571 | 0.80588 | | |
| 0.48615 | 0.82373 | | |
| 0.45626 | 0.84033 | | |
| 0.42612 | 0.85570 | | |
| 0.42612 | 0.85570 | | |
| 0.36270 | 0.88380 | | |
| 0.29744 | 0.90720 | | |
| 0.23070 | 0.92577 | | |
| 0.16283 | 0.93944 | | |
| 0.09420 | 0.94813 | | |
| 0.02516 | 0.95181 | | |
| -0.04392 | 0.95048 | | |
| -0.11267 | 0.94414 | | |
| -0.18074 | 0.93285 | | |
| -0.24776 | 0.91666 | | |
| -0.31339 | 0.89569 | | |
| -0.37729 | 0.87004 | | |
| -0.43914 | 0.83985 | | |
| -0.49860 | 0.80530 | | |
| -0.55538 | 0.76658 | | |
| -0.60919 | 0.72388 | | |
| -0.65976 | 0.67743 | | |
| -0.70682 | 0.62749 | | |
| -0.75014 | 0.57432 | | |
| -0.78951 | 0.51818 | | |
| -0.82472 | 0.45939 | | |
| -0.85560 | 0.39823 | | |
| -0.88199 | 0.33503 | | |
| -0.90377 | 0.27011 | | |
| -0.92082 | 0.20380 | | |
| -0.93306 | 0.13645 | | |
| -0.94043 | 0.06841 | | |
| -0.94289 | 0.00001 | | |

Figure 68 - Continued

ORIGINAL PAGE IS
OF POOR QUALITY

PBAR= 0.5000C

JET IMPINGEMENT REGION, IJET= 58 UPWASH DEFLECTION REGION, IU= 16

| XISOJ | YISOJ | XISOU | YISOU |
|---|---|---|---|
| 1.15977 | 0.0 | 2.65969 | 0.0 |
| 1.15872 | 0.04907 | 2.66023 | 0.09247 |
| 1.15558 | 0.09802 | 2.66189 | 0.18511 |
| 1.15036 | 0.14673 | 2.66471 | 0.27811 |
| 1.14308 | 0.19509 | 2.66877 | 0.37164 |
| 1.13379 | 0.24296 | 2.67421 | 0.46588 |
| 1.12250 | 0.29026 | 2.68121 | 0.56104 |
| 1.10928 | 0.33686 | 2.69003 | 0.65729 |
| 1.09417 | 0.38267 | 2.70102 | 0.75486 |
| 1.07724 | 0.42759 | 2.71472 | 0.85395 |
| 1.05856 | 0.47153 | 2.73192 | 0.95479 |
| 1.03819 | 0.51440 | 2.75392 | 1.05763 |
| 1.01621 | 0.55613 | 2.78312 | 1.16274 |
| 0.99271 | 0.59665 | 2.82518 | 1.27038 |
| 0.96775 | 0.63590 | 2.90661 | 1.38087 |
| 0.94144 | 0.67382 | 3.00000 | 1.40836 |
| 0.91386 | 0.71036 | | |
| 0.88509 | 0.74549 | | |
| 0.85522 | 0.77916 | | |
| 0.82433 | 0.81136 | | |
| 0.79252 | 0.84205 | | |
| 0.75986 | 0.87123 | | |
| 0.72645 | 0.89888 | | |
| 0.69235 | 0.92500 | | |
| 0.65765 | 0.94958 | | |
| 0.62243 | 0.97265 | | |
| 0.58675 | 0.99419 | | |
| 0.55068 | 1.01422 | | |
| 0.51430 | 1.03277 | | |
| 0.51430 | 1.03277 | | |
| 0.43775 | 1.06669 | | |
| 0.35900 | 1.09493 | | |
| 0.27844 | 1.11735 | | |
| 0.19653 | 1.13384 | | |
| 0.11369 | 1.14433 | | |
| 0.03036 | 1.14878 | | |
| -0.05301 | 1.14716 | | |
| -0.13599 | 1.13951 | | |
| -0.21814 | 1.12588 | | |
| -0.29903 | 1.10635 | | |
| -0.37824 | 1.08103 | | |
| -0.45537 | 1.05008 | | |
| -0.53001 | 1.01365 | | |
| -0.60178 | 0.97195 | | |
| -0.67031 | 0.92521 | | |
| -0.73525 | 0.87367 | | |
| -0.79628 | 0.81762 | | |
| -0.85308 | 0.75734 | | |
| -0.90537 | 0.69316 | | |
| -0.95289 | 0.62541 | | |
| -0.99538 | 0.55445 | | |
| -1.03265 | 0.48063 | | |
| -1.06451 | 0.40435 | | |
| -1.09079 | 0.32600 | | |
| -1.11137 | 0.24598 | | |
| -1.12615 | 0.16469 | | |
| -1.13504 | 0.08257 | | |
| -1.13801 | 0.00002 | | |

Figure 68 - Continued

ORIGINAL PAGE IS
OF POOR QUALITY

PBAR= 0.40000

JET IMPINGEMENT REGION, IJET= 58 UPWASH DEFLECTION REGION, IU= 20

| XISOJ | YISOJ | XISOU | YISOU |
|---|---|---|---|
| 1.37135 | 0.0 | 2.58414 | 0.0 |
| 1.37011 | 0.05802 | 2.58449 | 0.09247 |
| 1.36539 | 0.11590 | 2.58558 | 0.18511 |
| 1.36022 | 0.17350 | 2.58741 | 0.27811 |
| 1.35162 | 0.23067 | 2.59003 | 0.37164 |
| 1.34062 | 0.28729 | 2.59350 | 0.46588 |
| 1.32728 | 0.34321 | 2.59791 | 0.56104 |
| 1.31164 | 0.39832 | 2.60337 | 0.65729 |
| 1.29378 | 0.45248 | 2.61003 | 0.75486 |
| 1.27376 | 0.50559 | 2.61807 | 0.85395 |
| 1.25167 | 0.55755 | 2.62774 | 0.95479 |
| 1.22758 | 0.60824 | 2.63938 | 1.05763 |
| 1.20160 | 0.65759 | 2.65343 | 1.16274 |
| 1.17381 | 0.70550 | 2.67051 | 1.27038 |
| 1.14430 | 0.75191 | 2.69146 | 1.38087 |
| 1.11319 | 0.79675 | 2.71766 | 1.49454 |
| 1.08058 | 0.83996 | 2.75146 | 1.61176 |
| 1.04656 | 0.88149 | 2.79778 | 1.73292 |
| 1.01123 | 0.92131 | 2.87355 | 1.85848 |
| 0.97472 | 0.95937 | 3.00000 | 1.92118 |
| 0.93710 | 0.99567 | | |
| 0.89849 | 1.03017 | | |
| 0.85897 | 1.06286 | | |
| 0.81866 | 1.09374 | | |
| 0.77763 | 1.12282 | | |
| 0.73598 | 1.15009 | | |
| 0.69379 | 1.17556 | | |
| 0.65114 | 1.19925 | | |
| 0.60812 | 1.22118 | | |
| 0.60812 | 1.22118 | | |
| 0.51761 | 1.26129 | | |
| 0.42449 | 1.29468 | | |
| 0.32924 | 1.32119 | | |
| 0.23238 | 1.34069 | | |
| 0.13443 | 1.35304 | | |
| 0.03590 | 1.35835 | | |
| -0.06268 | 1.35644 | | |
| -0.16079 | 1.34740 | | |
| -0.25793 | 1.33128 | | |
| -0.35358 | 1.30819 | | |
| -0.44725 | 1.27825 | | |
| -0.53844 | 1.24164 | | |
| -0.62670 | 1.19857 | | |
| -0.71156 | 1.14926 | | |
| -0.79259 | 1.09399 | | |
| -0.86939 | 1.03306 | | |
| -0.94155 | 0.96678 | | |
| -1.00871 | 0.89551 | | |
| -1.07054 | 0.81962 | | |
| -1.12672 | 0.73951 | | |
| -1.17697 | 0.65560 | | |
| -1.22104 | 0.56832 | | |
| -1.25871 | 0.47812 | | |
| -1.28979 | 0.38547 | | |
| -1.31412 | 0.29085 | | |
| -1.33159 | 0.19474 | | |
| -1.34211 | 0.09763 | | |
| -1.34562 | 0.00002 | | |

Figure 68 - Continued

PBAR= 0.30000

JET IMPINGEMENT REGION, IJET= 58 UPWASH DEFLECTION REGION, IU= 24

| XISOJ | YISOJ | XISOU | YISOU |
|---|---|---|---|
| 1.60708 | 0.0 | 2.51121 | 0.0 |
| 1.60563 | 0.06800 | 2.51147 | 0.09247 |
| 1.60128 | 0.13583 | 2.51225 | 0.18511 |
| 1.59405 | 0.20333 | 2.51357 | 0.27811 |
| 1.58397 | 0.27033 | 2.51543 | 0.37164 |
| 1.57108 | 0.33667 | 2.51789 | 0.46588 |
| 1.55544 | 0.40221 | 2.52099 | 0.56104 |
| 1.53712 | 0.46679 | 2.52477 | 0.65729 |
| 1.51619 | 0.53026 | 2.52933 | 0.75484 |
| 1.49273 | 0.59251 | 2.53476 | 0.85395 |
| 1.46684 | 0.65339 | 2.54119 | 0.95479 |
| 1.43861 | 0.71280 | 2.54877 | 1.05763 |
| 1.40816 | 0.77063 | 2.55770 | 1.16274 |
| 1.37553 | 0.82678 | 2.56828 | 1.27038 |
| 1.34101 | 0.88116 | 2.58079 | 1.38087 |
| 1.30455 | 0.93371 | 2.59566 | 1.49454 |
| 1.26633 | 0.98435 | 2.61347 | 1.61173 |
| 1.22646 | 1.03302 | 2.63497 | 1.73292 |
| 1.18507 | 1.07968 | 2.66119 | 1.85848 |
| 1.14227 | 1.12429 | 2.69366 | 1.98892 |
| 1.09819 | 1.16682 | 2.73482 | 2.12481 |
| 1.05294 | 1.20725 | 2.78931 | 2.26676 |
| 1.00663 | 1.24557 | 2.87064 | 2.41548 |
| 0.95939 | 1.28176 | 3.00000 | 2.48979 |
| 0.91131 | 1.31583 | | |
| 0.86249 | 1.34779 | | |
| 0.81305 | 1.37764 | | |
| 0.76308 | 1.40540 | | |
| 0.71266 | 1.43110 | | |
| 0.71266 | 1.47110 | | |
| 0.60659 | 1.47810 | | |
| 0.49746 | 1.51723 | | |
| 0.38584 | 1.54830 | | |
| 0.27233 | 1.57116 | | |
| 0.15754 | 1.58569 | | |
| 0.04208 | 1.59185 | | |
| -0.07345 | 1.58962 | | |
| -0.18843 | 1.57902 | | |
| -0.30227 | 1.56013 | | |
| -0.41436 | 1.53306 | | |
| -0.52413 | 1.49798 | | |
| -0.63100 | 1.45508 | | |
| -0.73443 | 1.40461 | | |
| -0.83388 | 1.34682 | | |
| -0.92884 | 1.28205 | | |
| -1.01884 | 1.21064 | | |
| -1.10340 | 1.13297 | | |
| -1.18211 | 1.04945 | | |
| -1.25457 | 0.96051 | | |
| -1.32041 | 0.86663 | | |
| -1.37930 | 0.76830 | | |
| -1.43094 | 0.66601 | | |
| -1.47509 | 0.56021 | | |
| -1.51151 | 0.45174 | | |
| -1.54002 | 0.34085 | | |
| -1.56049 | 0.22821 | | |
| -1.57282 | 0.11441 | | |
| -1.57694 | 0.00002 | | |

Figure 68 - Continued

ORIGINAL PAGE IS
OF POOR QUALITY

PBAR= 0.20000

JET IMPINGEMENT REGION, IJET= 58        UPWASH DEFLECTION REGION, IU= 27

| XISOJ | YISOJ | XISOU | YISOU |
|---|---|---|---|
| 1.88819 | 0.0 | 2.42495 | 0.0 |
| 1.88648 | 0.07989 | 2.42521 | 0.09247 |
| 1.88137 | 0.15959 | 2.42596 | 0.18511 |
| 1.87287 | 0.23889 | 2.42722 | 0.27811 |
| 1.84103 | 0.31761 | 2.42898 | 0.37164 |
| 1.84589 | 0.39556 | 2.43124 | 0.46588 |
| 1.82751 | 0.47256 | 2.43399 | 0.56104 |
| 1.80598 | 0.54844 | 2.43725 | 0.65729 |
| 1.78139 | 0.62302 | 2.44103 | 0.75486 |
| 1.75382 | 0.69615 | 2.44538 | 0.85395 |
| 1.72341 | 0.76768 | 2.45034 | 0.95479 |
| 1.69024 | 0.83770 | 2.45600 | 1.05763 |
| 1.65446 | 0.90542 | 2.46244 | 1.16274 |
| 1.61620 | 0.97139 | 2.46983 | [illegible].27038 |
| 1.57557 | 1.03529 | 2.47830 | 1.38087 |
| 1.53274 | 1.09703 | 2.48809 | 1.49454 |
| 1.48783 | 1.15652 | 2.49947 | 1.61176 |
| 1.44099 | 1.21371 | 2.51281 | 1.73292 |
| 1.39235 | 1.26853 | 2.52855 | 1.85848 |
| 1.34207 | 1.32095 | 2.54727 | 1.98892 |
| 1.29028 | 1.37092 | 2.56971 | 2.12481 |
| 1.23711 | 1.41842 | 2.59680 | 2.26676 |
| 1.18271 | 1.46344 | 2.62976 | 2.41548 |
| 1.12720 | 1.50596 | 2.67830 | 2.57178 |
| 1.07071 | 1.54599 | 2.74376 | 2.73653 |
| 1.01336 | 1.58354 | 2.83529 | 2.91086 |
| 0.95527 | 1.61841 | 3.00000 | 3.07394 |
| 0.89655 | 1.65123 | | |
| 0.83731 | 1.68142 | | |
| 0.83731 | 1.68142 | | |
| 0.71270 | 1.73665 | | |
| 0.58447 | 1.78262 | | |
| 0.45333 | 1.81912 | | |
| 0.31997 | 1.84598 | | |
| 0.18510 | 1.86306 | | |
| 0.04944 | 1.87029 | | |
| -0.08630 | 1.86767 | | |
| -0.22140 | 1.85521 | | |
| -0.35514 | 1.83302 | | |
| -0.48684 | 1.80122 | | |
| -0.61581 | 1.76000 | | |
| -0.74137 | 1.70960 | | |
| -0.86289 | 1.65029 | | |
| -0.97974 | 1.58241 | | |
| -1.09131 | 1.50631 | | |
| -1.19705 | 1.42240 | | |
| -1.29640 | 1.33114 | | |
| -1.38888 | 1.23301 | | |
| -1.47401 | 1.12852 | | |
| -1.55137 | 1.01822 | | |
| -1.62056 | 0.90268 | | |
| -1.68124 | 0.78251 | | |
| -1.73310 | 0.65832 | | |
| -1.77589 | 0.53075 | | |
| -1.80940 | 0.40047 | | |
| -1.83345 | 0.26813 | | |
| -1.84793 | 0.13442 | | |
| -1.85277 | 0.00003 | | |

Figure 68 - Continued

ORIGINAL PAGE IS
OF POOR QUALITY

PBAR= 0.10000

JET IMPINGEMENT REGION, IJET= 50 UPWASH DEFLECTION REGION, IU= 50

| XISOJ | YISOJ | XISOU | YISOU |
|---|---|---|---|
| 2.14366 | 0.74971 | 2.25500 | 0.75486 |
| 2.11049 | 0.83772 | 2.28283 | 0.85395 |
| 2.07389 | 0.92380 | 2.30026 | 0.95479 |
| 2.03398 | 1.00779 | 2.31383 | 1.05763 |
| 1.99092 | 1.08955 | 2.32540 | 1.16274 |
| 1.94487 | 1.16894 | 2.33585 | 1.27038 |
| 1.89599 | 1.24584 | 2.34567 | 1.38087 |
| 1.84444 | 1.32013 | 2.35527 | 1.49454 |
| 1.79040 | 1.39172 | 2.36495 | 1.61176 |
| 1.73403 | 1.46054 | 2.37505 | 1.73292 |
| 1.67551 | 1.52651 | 2.38589 | 1.85848 |
| 1.61500 | 1.58958 | 2.39785 | 1.98892 |
| 1.55268 | 1.64971 | 2.41139 | 2.12481 |
| 1.48870 | 1.70688 | 2.42704 | 2.26676 |
| 1.42323 | 1.76105 | 2.44549 | 2.41548 |
| 1.35643 | 1.81222 | 2.47136 | 2.57178 |
| 1.28815 | 1.86039 | 2.50457 | 2.73655 |
| 1.21944 | 1.90557 | 2.54675 | 2.91086 |
| 1.14953 | 1.94778 | 2.59936 | 3.09591 |
| 1.07888 | 1.98703 | 2.66421 | 3.29313 |
| 1.00759 | 2.02337 | 2.74253 | 3.50416 |
| 1.00759 | 2.02337 | 2.74253 | 3.50416 |
| 0.85763 | 2.08Y82 | 2.74722 | 3.52268 |
| 0.70333 | 2.14515 | 2.75205 | 3.54132 |
| 0.54552 | 2.18907 | 2.75702 | 3.56008 |
| 0.38504 | 2.22138 | 2.76214 | 3.57895 |
| 0.22274 | 2.24193 | 2.76742 | 3.59793 |
| 0.05949 | 2.25064 | 2.77285 | 3.61704 |
| -0.10385 | 2.24748 | 2.77847 | 3.63627 |
| -0.26642 | 2.23250 | 2.78426 | 3.65562 |
| -0.42736 | 2.20579 | 2.79024 | 3.67509 |
| -0.58585 | 2.16753 | 2.79644 | 3.69469 |
| -0.74104 | 2.11793 | 2.80284 | 3.71441 |
| -0.89214 | 2.05727 | 2.80949 | 3.73426 |
| -1.03837 | 1.98590 | 2.81638 | 3.75424 |
| -1.17898 | 1.90421 | 2.82354 | 3.77435 |
| -1.31325 | 1.81263 | 2.83100 | 3.79459 |
| -1.44048 | 1.71167 | 2.83877 | 3.81497 |
| -1.56005 | 1.60185 | 2.84690 | 3.83548 |
| -1.67133 | 1.48376 | ~ 85541 | 3.85613 |
| -1.77378 | 1.35802 | 2.86436 | 3.87691 |
| -1.86636 | 1.22529 | 2.87379 | 3.89784 |
| -1.95012 | 1.08626 | 2.88380 | 3.91891 |
| -2.02314 | 0.94164 | 2.89446 | 3.94013 |
| -2.08555 | 0.79220 | 2.90592 | 3.96149 |
| -2.13704 | 0.63869 | 2.91838 | 3 98299 |
| -2.17736 | 0.48191 | 2.93216 | 4.00465 |
| -2.20631 | 0.32266 | 2.94785 | 4.02645 |
| -2.22373 | 0.16176 | 2.96686 | 4.04841 |
| -2.22955 | 0.00003 | 2.99881 | 4.07053 |

Figure 68 - Continued

PBAR= 0.05000

JET IMPINGEMENT REGION, IJET= 43 UPWASH DEFLECTION REGION, IU= 43

| XISOJ | YISOJ | XISOU | YISOU |
|---|---|---|---|
| 2.08715 | 1.49384 | 2.14019 | 1.49454 |
| 2.02600 | 1.57486 | 2.22838 | 1.61176 |
| 1.96221 | 1.65273 | 2.25469 | 1.73292 |
| 1.89599 | 1.72738 | 2.27276 | 1.85848 |
| 1.82752 | 1.79875 | 2.28751 | 1.98892 |
| 1.75699 | 1.86680 | 2.30084 | 2.12481 |
| 1.68460 | 1.93148 | 2.31384 | 2.26674 |
| 1.61051 | 1.99278 | 2.32739 | 2.41548 |
| 1.53492 | 2.05049 | 2.34467 | 2.57178 |
| 1.45800 | 2.10520 | 2.36596 | 2.73655 |
| 1.37990 | 2.15633 | 2.39259 | 2.91086 |
| 1.30080 | 2.20409 | 2.42590 | 3.09591 |
| 1.22084 | 2.24851 | 2.46759 | 3.29313 |
| 1.14018 | 2.28962 | 2.51904 | 3.50416 |
| 1.14018 | 2.28962 | 2.51904 | 3.50416 |
| 0.97049 | 2.36482 | 2.52380 | 3.55007 |
| 0.79588 | 2.42742 | 2.52886 | 3.59669 |
| 0.61730 | 2.47713 | 2.53426 | 3.64403 |
| 0.43570 | 2.51369 | 2.54001 | 3.69212 |
| 0.25205 | 2.53695 | 2.54615 | 3.74097 |
| 0.06732 | 2.54680 | 2.55269 | 3.79062 |
| -0.11752 | 2.54323 | 2.55967 | 3.84107 |
| -0.30148 | 2.52627 | 2.56712 | 3.89236 |
| -0.48360 | 2.49605 | 2.57508 | 3.94452 |
| -0.66294 | 2.45275 | 2.58360 | 3.99756 |
| -0.83855 | 2.39662 | 2.59270 | 4.05152 |
| -1.00954 | 2.32799 | 2.60246 | 4.10642 |
| -1.17501 | 2.24723 | 2.61291 | 4.16230 |
| -1.33412 | 2.15479 | 2.62414 | 4.21918 |
| -1.48606 | 2.05116 | 2.63621 | 4.27710 |
| -1.63004 | 1.93691 | 2.64922 | 4.33609 |
| -1.76533 | 1.81264 | 2.66325 | 4.39619 |
| -1.89126 | 1.67901 | 2.67844 | 4.45743 |
| -2.00719 | 1.53672 | 2.69493 | 4.51985 |
| -2.11252 | 1.38652 | 2.71290 | 4.58349 |
| -2.20674 | 1.22920 | 2.73257 | 4.64839 |
| -2.28936 | 1.06555 | 2.75423 | 4.71460 |
| -2.35999 | 0.89644 | 2.77828 | 4.78215 |
| -2.41826 | 0.72273 | 2.80529 | 4.8512[illegible] |
| -2.46388 | 0.54532 | 2.83615 | 4.92149 |
| -2.49664 | 0.36512 | 2.87247 | 4.99339 |
| -2.51635 | 0.18305 | 2.91795 | 5.06683 |
| -2.52294 | 0.00004 | 2.99761 | 5.14198 |

UPWASH DEFLECTION ZONE LINE, PBAR=0 OUTSIDE INTERACTION REGION

| XUP | YUP |
|---|---|
| 2.18381 | 0.0 |
| 2.17864 | 0.33802 |
| 2.17211 | 0.50972 |
| 2.16282 | 0.68473 |
| 2.15061 | 0.86428 |
| 2.13528 | 1.04974 |
| 2.11656 | 1.24264 |
| 2.09410 | 1.44472 |
| 2.06745 | 1.65804 |
| 2.03606 | 1.88502 |
| 1.99923 | 2.12861 |
| 1.95605 | 2.39247 |
| 1.90539 | 2.68096 |
| 1.84573 | 3.00000 |
| 1.77513 | 3.35700 |
| 1.69093 | 3.76187 |
| 1.58954 | 4.22810 |
| 1.46590 | 4.77446 |
| 1.31268 | 5.42806 |
| 1.11888 | 6.2295[illegible] |

Figure 68 - Continued

***** COMPUTATION OF UPWASH FLOW FIELD *****

COMPUTATION OF UPWASH STREAMLINE PROPERTIES

PHID= 0.0 DEGS

INV.VEL.= 0.54015 THI/TA= 1.80266 DELPWJ= 0.56423 DELTWJ= 0.80266 BWGH/RN= 0.38034
ZOU/RN= 1.14102 BUO/RN= 0.46750 BUOHN/RN= 0.20618 TLAMI= 1.22919

| Z/RN | VMU/VN | TM/TN | TM/TA | BUH/RN | BU/RN | DPU/DPJ | DTM/DTN |
|---|---|---|---|---|---|---|---|
| 0.38034 | 0.54015 | 0.90133 | 1.80266 | 0.20618 | 0.46750 | 0.56417 | 0.80266 |
| 0.53116 | 0.60399 | 0.89130 | 1.78261 | 0.25143 | 0.57009 | 0.53185 | 0.78261 |
| 0.68198 | 0.60919 | 0.87896 | 1.75791 | 0.29668 | 0.67268 | 0.46950 | 0.75791 |
| 0.83280 | 0.58224 | 0.86563 | 1.73125 | 0.34192 | 0.77527 | 0.40296 | 0.73125 |
| 0.98362 | 0.54169 | 0.85313 | 1.70625 | 0.38717 | 0.87786 | 0.34477 | 0.70625 |
| 1.13443 | 0.50113 | 0.84234 | 1.68467 | 0.43241 | 0 98045 | 0.29814 | 0.68467 |
| 1.28525 | 0.46613 | 0.83340 | 1.66679 | 0.47766 | 1.08304 | 0.26071 | 0.66679 |
| 1.43607 | 0.43608 | 0.82573 | 1.65146 | 0.52290 | 1.18563 | 0.23030 | 0.65145 |
| 1.58689 | 0.40994 | 0.81906 | 1.63812 | 0.56815 | 1.28822 | 0.20517 | 0.63812 |
| 1.73771 | 0.38696 | 0.81319 | 1.62639 | 0.61340 | 1.39081 | 0.18414 | 0.62639 |
| 1.88853 | 0.36659 | 0.80799 | 1.61598 | 0.65864 | 1.49340 | 0.16632 | 0.61598 |
| 2.03935 | 0.34837 | 0.80334 | 1.60668 | 0.70389 | 1.59599 | 0.15107 | 0.60668 |
| 2.19017 | 0.33198 | 0.79915 | 1.59830 | 0.74913 | 1.69858 | 0.13791 | 0.59830 |
| 2.34099 | 0.31713 | 0.79536 | 1.59071 | 0.79438 | 1.80117 | 0.12645 | 0.59071 |
| 2.49180 | 0.30362 | 0.79190 | 1.58381 | 0.83962 | 1.90376 | 0.11641 | 0.58381 |
| 2.64262 | 0.29126 | 0.78875 | 1.57749 | 0.88487 | 2.00635 | 0.10755 | 0.57749 |
| 2.79344 | 0.27991 | 0.78584 | 1.57169 | 0.93012 | 2.10894 | 0.09970 | 0.57169 |
| 2.94426 | 0.26944 | 0.78317 | 1.56634 | 0.97536 | 2.21153 | 0.09270 | 0.56634 |
| 3.09508 | 0.25976 | 0.78069 | 1.56139 | 1.02061 | 2.31411 | 0.08643 | 0.56139 |
| 3.24590 | 0.25077 | 0.77839 | 1.55679 | 1.06585 | 2.41670 | 0.08079 | 0.55679 |
| 3.39672 | 0.24240 | 0.77626 | 1.55251 | 1.11110 | 2.51929 | 0.07570 | 0.55251 |
| 3.54754 | 0.23459 | 0.77426 | 1.54852 | 1.15634 | 2.62188 | 0.07108 | 0.54852 |
| 3.69835 | 0.22729 | 0.77239 | 1.54478 | 1.20159 | 2.72447 | 0.06688 | 0.54478 |
| 3.84917 | 0.22043 | 0.77064 | 1.54127 | 1.24683 | 2.82706 | 0.06305 | 0.54127 |
| 3.99999 | 0.21399 | 0.76899 | 1.53798 | 1.29208 | 2.92965 | 0.05955 | 0.53798 |

PHID= 60.0000 DEGS

INV.VEL.= 0.26871 THI/TA= 1.55874 DELPWJ= 0.16135 DELTWJ= 0.55874 BWGH/RN= 0.61550
ZOU/RN= 1.84649 BUO/RN= 1.11853 BUOHN/RN= 0.49331 TLAMI= 1.05924

| Z/RN | VMU/VN | TM/TN | TM/TA | BUH/RN | BU/RN | DPU/DPJ | DTM/DTN |
|---|---|---|---|---|---|---|---|
| 0.61550 | 0.26871 | 0.77937 | 1.55874 | 0.49331 | 1.11853 | 0.16122 | 0.55874 |
| 0.92319 | 0.32788 | 0.77604 | 1.55207 | 0.55858 | 1.26653 | 0.16662 | 0.55207 |
| 1.23087 | 0.33782 | 0.76938 | 1.53876 | 0.62385 | 1.41452 | 0.15529 | 0.53876 |
| 1.53856 | 0.32358 | 0.76089 | 1.52178 | 0.68912 | 1.56251 | 0.13801 | 0.52178 |
| 1.84625 | 0.30302 | 0.75283 | 1.50566 | 0.75439 | 1.71051 | 0.12197 | 0.50566 |
| 2.15393 | 0.28421 | 0.74712 | 1.49424 | 0.81966 | 1.85850 | 0.10812 | 0.49424 |
| 2.46162 | 0.26772 | 0.74211 | 1.48422 | 0.88493 | 2.00649 | 0.09658 | 0.48422 |
| 2.76931 | 0.25312 | 0.73768 | 1.47536 | 0.95020 | 2.15449 | 0.08685 | 0.47536 |
| 3.07699 | 0.24009 | 0.73372 | 1.46744 | 1.01547 | 2.30248 | 0.07857 | 0.46744 |
| 3.38468 | 0 22840 | 0.73017 | 1.46033 | 1.08074 | 2.45047 | 0.07144 | 0.46033 |
| 3.69237 | 0.21782 | 0.72695 | 1.45391 | 1.14601 | 2.59846 | 0.06527 | 0.45391 |
| 4.00005 | 0.20822 | 0.72403 | 1.44807 | 1.21128 | 2.74646 | 0.05988 | 0.44807 |
| 4.30774 | 0.19946 | 0.72137 | 1.44274 | 1.27655 | 2.89445 | 0.05515 | 0.44274 |
| 4.61543 | 0.19142 | 0.71893 | 1.43785 | 1.34182 | 3.04244 | 0.05097 | 0.43785 |
| 4.92311 | 0.18402 | 0.71668 | 1.43335 | 1.40709 | 3.19044 | 0.04725 | 0.43335 |
| 5.23080 | 0.17719 | 0.71460 | 1.42920 | 1.47237 | 3.33843 | 0.04394 | 0.42920 |
| 5.53849 | 0.17086 | 0.71267 | 1.42534 | 1.53763 | 3.48642 | 0.04096 | 0.42534 |
| 5.84617 | 0.16497 | 0.71088 | 1.42176 | 1.60291 | 3.63442 | 0.03829 | 0.42176 |
| 6.15386 | 0.15949 | 0.70921 | 1.41843 | 1.66818 | 3.78241 | 0.03587 | 0.41843 |
| 6.46155 | 0.15437 | 0.70765 | 1.41531 | 1.73345 | 3.93040 | 0.03367 | 0.41531 |
| 6.76923 | 0.14957 | 0.70619 | 1.41239 | 1.79972 | 4.07840 | 0.03168 | 0.41239 |
| 7.07692 | 0.14506 | 0.70482 | 1.40965 | 1.86399 | 4.22639 | 0.02986 | 0.40965 |
| 7.38461 | 0.14083 | 0.70353 | 1.40707 | 1.92926 | 4.37438 | 0.02819 | 0.40707 |
| 7.69230 | 0.13683 | 0.70232 | 1.40464 | 1.99453 | 4.52238 | 0.02666 | 0.40464 |
| 7.99998 | 0.13307 | 0.70117 | 1.40235 | 2.05980 | 4.67037 | [illegible] | 0.40235 |

Figure 68 - Continued

ORIGINAL PAGE IS
OF POOR QUALITY

UPWASH PROPERTIES COMPUTED AT Z LOCATION OF UNDERSIDE OF BODY

BODY CENTERLINE LOCATION AT Z/RN= 4.00000

| ZU/RN | RW/RN | PHIB | X/RN | VMU/VN | DPU/PN | BUH/RN | DPU/PUO | DPU/PJS | TM/TA | DTSM/DTN | PBS/PN |
|---|---|---|---|---|---|---|---|---|---|---|---|
| 4.0000 | 3.0000 | 0.0 | 0.0 | 0.2140 | 0.0595 | 1.2921 | 1.0000 | 0.0595 | 1.5380 | 0.5380 | 0.05955 |
| 4.0000 | 3.0024 | 2.7263 | 0.3333 | 0.2139 | 0.0595 | 1.2931 | 0.9991 | 0.0595 | 1.5377 | 0.5377 | 0.05936 |
| 4.0000 | 3.0136 | 5.4403 | 0.6667 | 0.2136 | 0.0593 | 1.2960 | 0.9965 | 0.0593 | 1.5370 | 0.5370 | 0.05881 |
| 4.0000 | 3.0305 | 8.1301 | 1.0000 | 0.2130 | 0.0591 | 1.3009 | 0.9923 | 0.0591 | 1.5357 | 0.5357 | 0.05791 |
| 4.0000 | 3.0539 | 10.7843 | 1.3333 | 0.2122 | 0.0587 | 1.3076 | 0.9863 | 0.0587 | 1.5340 | 0.5340 | 0.05668 |
| 4.0000 | [illegible] | 13.3925 | 1.6667 | 0.2113 | 0.0583 | 1.3161 | 0.9785 | 0.0583 | 1.5319 | 0.5319 | 0.05515 |
| 4.0000 | [illegible] | 15.9454 | 2.0000 | 0.2101 | 0.0577 | 1.3263 | 0.9692 | 0.0577 | 1.5293 | 0.5293 | 0.05336 |
| 4.0000 | 3.1623 | 18.4349 | 2.3333 | 0.2087 | 0.0571 | 1.3379 | 0.9582 | 0.0571 | 1.5263 | 0.5263 | 0.05135 |
| 4.0000 | 3.2103 | 20.8544 | 2.6667 | 0.2071 | 0.0563 | 1.3512 | 0.9456 | 0.0563 | 1.5230 | 0.5230 | 0.04917 |
| 4.0000 | 3.2639 | 23.1986 | 3.0000 | 0.2053 | 0.0555 | 1.3656 | 0.9316 | 0.0555 | 1.5194 | 0.5194 | 0.04687 |
| 4.0000 | 3.3228 | 25.4633 | 3.3333 | 0.2033 | 0.0546 | 1.3813 | 0.9163 | 0.0546 | 1.5155 | 0.5155 | 0.04448 |
| 4.0000 | 3.3866 | 27.6460 | 3.6667 | 0.2012 | 0.0536 | 1.3981 | 0.8997 | 0.0536 | 1.5114 | 0.5114 | 0.04204 |
| 4.0000 | 3.4553 | 29.7448 | 4.0000 | 0.1990 | 0.0525 | 1.4157 | 0.8822 | 0.0525 | 1.5071 | 0.5071 | 0.03960 |
| 4.0000 | 3.5283 | 31.7594 | 4.3333 | 0.1966 | 0.0514 | 1.4344 | 0.8636 | 0.0514 | 1.5027 | 0.5027 | 0.03718 |
| 4.0000 | 3.6055 | 33.6900 | 4.6667 | 0.1941 | 0.0503 | 1.4536 | 0.8445 | 0.0503 | 1.4981 | 0.4981 | 0.03482 |
| 4.0000 | 3.6867 | 35.5376 | 5.0000 | 0.1915 | 0.0491 | 1.4735 | 0.8248 | 0.0491 | 1.4935 | 0.4935 | 0.03252 |
| 4.0000 | 3.7715 | 37.3039 | 5.3333 | 0.1889 | 0.0479 | 1.4938 | 0.8047 | 0.0479 | 1.4888 | 0.4888 | 0.03032 |
| 4.0000 | 3.8598 | 38.9910 | 5.6667 | 0.1862 | 0.0467 | 1.5147 | 0.7843 | 0.0467 | 1.4840 | 0.4840 | 0.02821 |
| 4.0000 | 3.9512 | 40.6013 | 6.0000 | 0.1833 | 0.0454 | 1.5384 | 0.7626 | 0.0454 | 1.4792 | 0.4792 | 0.02618 |
| 4.0000 | 4.0457 | 42.1376 | 6.3333 | 0.1803 | 0.0441 | 1.5631 | 0.7407 | 0.0441 | 1.4744 | 0.4744 | 0.02425 |
| 4.0000 | 4.1429 | 43.6028 | 6.6667 | 0.1773 | 0.0428 | 1.5892 | 0.7185 | 0.0428 | 1.4696 | 0.4696 | 0.02243 |
| 4.0000 | 4.2426 | 45.0000 | 7.0000 | 0.1743 | 0.0415 | 1.6157 | 0.6966 | 0.0415 | 1.4648 | 0.4648 | 0.02074 |
| 4.0000 | 4.3448 | 46.3322 | 7.3333 | 0.1713 | 0.0402 | 1.6427 | 0.6750 | 0.0402 | 1.4601 | 0.4601 | 0.01916 |
| 4.0000 | 4.4493 | 47.6025 | 7.6667 | 0.1683 | 0.0389 | 1.6701 | 0.6538 | 0.0389 | 1.4554 | 0.4554 | 0.01770 |
| 4.0000 | 4.5558 | 48.8140 | 8.0000 | 0.1654 | 0.0377 | 1.6979 | 0.6331 | 0.0377 | 1.4509 | 0.4509 | 0.01635 |

FLAT BOTTOM VEHICLE WITH SHARP CORNERS

UPWASH LIFT FORCE LU/2TJ= 0.08718

BODY WITH CIRCULAR CROSS SECTION

UPWASH LIFT FORCE LU/2TJ= 0.02366

Figure 68 - Continued

ORIGINAL PAGE IS
OF POOR QUALITY

UPWASH PROPERTIES COMPUTED AT Z LOCATION OF UNDERSIDE OF BODY

BODY CENTERLINE LOCATION AT Z/RN= 6.00000

| ZU/RN | RW/RN | PHIB | Y/RN | VMU/VN | DPU/PN | BUH/RN | DPU/PUO | DPU/PJS | TH/TA | DTSH/DTN | PBS/PN |
|---|---|---|---|---|---|---|---|---|---|---|---|
| 6.0000 | 3.0000 | 0.0 | 0.0 | 0.1546 | 0.0317 | 1.8921 | 1.0000 | 0.0317 | 1.5076 | 0.5076 | 0.03170 |
| 6.0000 | 3.0021 | 2.1211 | 0.3333 | 0.1545 | 0.0317 | 1.8928 | 0.9995 | 0.0317 | 1.5074 | 0.5074 | 0.03165 |
| 6.0000 | 3.0082 | 4.2364 | 0.6667 | 0.1544 | 0.0316 | 1.8953 | 0.9981 | 0.0316 | 1.5070 | 0.5070 | 0.03147 |
| 6.0000 | 3.0185 | 6.3402 | 1.0000 | 0.1542 | 0.0316 | 1.8992 | 0.9957 | 0.0316 | 1.5062 | 0.5062 | 0.03118 |
| 6.0000 | 3.0327 | 8.4270 | 1.3333 | 0.1539 | 0.0315 | 1.9047 | 0.9923 | 0.0315 | 1.5052 | 0.5052 | 0.03078 |
| 6.0000 | 3.0510 | 10.4915 | 1.6667 | 0.1535 | 0.0313 | 1.9118 | 0.9879 | 0.0313 | 1.5039 | 0.5039 | 0.03028 |
| 6.0000 | 3.0732 | 12.5288 | 2.0000 | 0.1530 | 0.0312 | 1.9203 | 0.9826 | 0.0312 | 1.5023 | 0.5023 | 0.02969 |
| 6.0000 | 3.0992 | 14.5344 | 2.3333 | 0.1524 | 0.0310 | 1.9302 | 0.9763 | 0.0310 | 1.5005 | 0.5005 | 0.02900 |
| 6.0000 | 3.1289 | 16.5043 | 2.6667 | 0.1517 | 0.0307 | 1.9414 | 0.9690 | 0.0307 | 1.4985 | 0.4985 | 0.02824 |
| 6.0000 | 3.1623 | 18.4349 | 3.0000 | 0.1510 | 0.0305 | 1.9539 | 0.9608 | 0.0305 | 1.4962 | 0.4962 | 0.02741 |
| 6.0000 | 3.1992 | 20.3231 | 3.3333 | 0.1501 | 0.0302 | 1.9677 | 0.9516 | 0.0302 | 1.4938 | 0.4938 | 0.02653 |
| 6.0000 | 3.2394 | 22.1663 | 3.6667 | 0.1492 | 0.0299 | 1.9826 | 0.9416 | 0.0299 | 1.4911 | 0.4911 | 0.02560 |
| 6.0000 | 3.2830 | 23.9625 | 4.0000 | 0.1482 | 0.0295 | 1.9984 | 0.9308 | 0.0295 | 1.4883 | 0.4883 | 0.02464 |
| 6.0000 | 3.3296 | 25.7099 | 4.3333 | 0.1471 | 0.0291 | 2.0[illegible]3 | 0.9191 | 0.0291 | 1.4854 | 0.4854 | 0.02365 |
| 6.0000 | 3.3793 | 27.4075 | 4.6667 | 0.1460 | 0.0287 | 2.0330 | 0.9067 | 0.0287 | 1.4823 | 0.4823 | 0.02266 |
| 6.0000 | 3.4319 | 29.0546 | 5.0000 | 0.1448 | 0.0283 | 2.0515 | 0.8937 | 0.0283 | 1.4791 | 0.4791 | 0.02165 |
| 6.0000 | 3.48[illegible] | 30.6506 | 5.3333 | 0.1435 | 0.0279 | 2.0709 | 0.8801 | 0.0279 | 1.4758 | 0.4758 | 0.02065 |
| 6.0000 | 3.54[illegible]1 | 32.1957 | 5.6667 | 0.1422 | 0.0275 | 2.0908 | 0.8659 | 0.0275 | 1.4725 | 0.4725 | 0.01966 |
| 6.0000 | 3.6[illegible]5 | 33.6900 | 6.0000 | 0.1400 | 0.0270 | 2.1114 | 0.8514 | 0.0270 | 1.4691 | 0.4691 | 0.01869 |
| 6.0000 | 3.6683 | 35.1342 | 6.3333 | 0.1394 | 0.0265 | 2.1325 | 0.8364 | 0.0265 | 1.4657 | 0.4657 | 0.01774 |
| 6.0000 | 3.7334 | 36.5288 | 6.6667 | 0.1380 | 0.0260 | 2.1541 | 0.8212 | 0.0260 | 1.4622 | 0.4622 | 0.01681 |
| 6.0000 | 3.8006 | 37.8749 | 7.0000 | 0.1365 | 0.0255 | 2.1761 | 0.8057 | 0.0255 | 1.4588 | 0.4588 | 0.01592 |
| 6.0000 | 3.8698 | 39.1736 | 7.3333 | 0.1350 | 0.0250 | 2.1988 | 0.7901 | 0.0250 | 1.4553 | 0.4553 | 0.01505 |
| 6.0000 | 3.9409 | 40.4260 | 7.6667 | 0.1334 | 0.0245 | 2.2234 | 0.7737 | 0.0245 | 1.4518 | 0.4518 | 0.01421 |
| 6.0000 | 4.0139 | 41.6335 | 8.0000 | 0.1319 | 0.0240 | 2.2486 | 0.7573 | 0.0240 | 1.4483 | 0.4483 | 0.01341 |

FLAT BOTTOM VEHICLE WITH SHARP CORNERS

UPWASH LIFT FORCE LU/2TJ= 0.05623

BODY WITH CIRCULAR CROSS SECTION

UPWASH LIFT FORCE LU/2TJ= 0.01440

Figure 68 - Continued .

UPWASH PROPERTIES COMPUTED AT Z LOCATION OF UNDERSIDE OF BODY

BODY CENTERLINE LOCATION AT Z/RN= 8.00000

| ZU/RN | RW/RN | PHIB | X/RN | VMU/VN | DFU/FN | BUH/RN | DFU/PUO | DFU/PJS | TM/TA | DTSM/DTM | PBS/PN |
|---|---|---|---|---|---|---|---|---|---|---|---|
| 8.0000 | 3.0000 | 0.0 | 0.0 | 0.1212 | 0.0197 | 2.4921 | 1.0000 | 0.0197 | 1.4905 | 0.4905 | 0.01972 |
| 8.0000 | 3.0014 | 1.7357 | 0.3333 | 0.1212 | 0.0197 | 2.4928 | 0.9997 | 0.0197 | 1.4904 | 0.4904 | 0.01970 |
| 8.0000 | 3.0055 | 3.4682 | 0.6667 | 0.1211 | 0.0197 | 2.4947 | 0.9988 | 0.0197 | 1.4901 | 0.4901 | 0.01962 |
| 8.0000 | 3.0124 | 5.1944 | 1.0000 | 0.1210 | 0.0197 | 2.4981 | 0.9972 | 0.0197 | 1.4896 | 0.4896 | 0.01950 |
| 8.0000 | 3.0220 | 6.9112 | 1.3333 | 0.1209 | 0.0196 | 2.5028 | 0.9951 | 0.0196 | 1.4889 | 0.4889 | 0.01934 |
| 8.0000 | 3.0342 | 8.6156 | 1.6667 | 0.1207 | 0.0196 | 2.5088 | 0.9922 | 0.0196 | 1.4880 | 0.4880 | 0.01913 |
| 8.0000 | 3.0492 | 10.3048 | 2.0000 | 0.1204 | 0.0195 | 2.5160 | 0.9888 | 0.0195 | 1.4870 | 0.4870 | 0.01888 |
| 8.0000 | 3.0668 | 11.9761 | 2.3333 | 0.1201 | 0.0194 | 2.5245 | 0.9847 | 0.0194 | 1.4858 | 0.4858 | 0.01858 |
| 8.0000 | 3.0869 | 13.6270 | 2.6667 | 0.1198 | 0.0193 | 2.5342 | 0.9800 | 0.0193 | 1.4844 | 0.4844 | 0.01825 |
| 8.0000 | 3.1096 | 15.2551 | 3.0000 | 0.1194 | 0.0192 | 2.5451 | 0.9747 | 0.0192 | 1.4828 | 0.4828 | 0.01789 |
| 8.0000 | 3.1347 | [illegible]584 | 3.3333 | 0.1189 | 0.0191 | 2.5570 | 0.9687 | 0.0191 | 1.4811 | 0.4811 | 0.01750 |
| 8.0000 | 3.1623 | 18.4349 | 3.6667 | 0.1185 | 0.0190 | 2.5699 | 0.9622 | 0.0190 | 1.4793 | 0.4793 | 0.01708 |
| 8.0000 | 3.1922 | 19.9831 | 4.0000 | 0.1179 | 0.0188 | 2.5840 | 0.9550 | 0.0188 | 1.4773 | 0.4773 | 0.01663 |
| 8.0000 | 3.2244 | 21.5014 | 4.3333 | 0.1174 | 0.0187 | 2.5990 | 0.9472 | 0.0187 | 1.4752 | 0.4752 | 0.01617 |
| 8.0000 | 3.2588 | 22.9887 | 4.6667 | 0.1168 | 0.0185 | 2.6150 | 0.9389 | 0.0185 | 1.4730 | 0.4730 | 0.01569 |
| 8.0000 | 3.2954 | 24.4439 | 5.0000 | 0.1161 | 0.0183 | 2.6318 | 0.9299 | 0.0183 | 1.4707 | 0.4707 | 0.01520 |
| 8.0000 | 3.3340 | 25.8663 | 5.3333 | 0.1154 | 0.0182 | 2.6494 | 0.9205 | 0.0182 | 1.4683 | 0.4683 | 0.01470 |
| 8.0000 | 3.3747 | 27.2553 | 5.6667 | 0.1147 | 0.0180 | 2.6678 | 0.9105 | 0.0180 | 1.4658 | 0.4658 | 0.01419 |
| 8.0000 | 3.4173 | 28.6104 | 6.0000 | 0.1140 | 0.0178 | 2.6868 | 0.9002 | 0.0178 | 1.4633 | 0.4633 | 0.01368 |
| 8.0000 | 3.4617 | 29.9315 | 6.3333 | 0.1132 | 0.0175 | 2.7065 | 0.8994 | 0.0175 | 1.4607 | 0.4607 | 0.01317 |
| 8.0000 | 3.5080 | 31.2184 | 6.6667 | 0.1124 | 0.0173 | 2.7268 | 0.8783 | 0.0173 | 1.4581 | 0.4581 | 0.01267 |
| 8.0000 | 3.5559 | 32.4712 | 7.0000 | 0.1115 | 0.0171 | 2.7478 | 0.8668 | 0.0171 | 1.4554 | 0.4554 | 0.01217 |
| 8.0000 | 3.6055 | 33.6900 | 7.3333 | 0.1107 | 0.0169 | 2.7691 | 0.8550 | 0.0169 | 1.4527 | 0.4527 | 0.01167 |
| 8.0000 | 3.6568 | 34.8753 | 7.6667 | 0.1098 | 0.0166 | 2.7910 | 0.8430 | 0.0166 | 1.4500 | 0.4500 | 0.01119 |
| 8.0000 | 3.7095 | 36.0273 | 8.0000 | 0.1089 | 0.0164 | 2.8134 | 0.8307 | 0.0164 | 1.4472 | 0.4472 | 0.01071 |

FLAT BOTTOM VEHICLE WITH SHARP CORNERS

UPWASH LIFT FORCE LU/2TJ= 0.03891

BODY WITH CIRCULAR CROSS SECTION

UPWASH LIFT FORCE LU/2TJ= 0.00970

Figure 68 – Concluded.

| Output Titles | Definitions |
|---|---|
| RJH/RN | Half-velocity radius of jet measured from jet centerline |
| RJ/RN | Half width of jet |
| ALPV | Exponent of velocity profile |
| VJ/VN | Centerline velocity |
| RC/RN | Potential core radius |
| ALPT | Exponent of temperature profile |
| RJNT/RN | Half temperature radius |
| TM/TN | Center line temperature non-dimensionalized by nozzle temperature |
| TM/TA | Centerline temperature nondimensionalized by ambient temperature |
| DTM/DTN | (TM-TA)/(TN-TA) |
| RJHQ/RN | Half dynamic pressure radius |
| QJ/QN | Centerline dynamic pressure |

Note: RN, VN, TN, and QN denote nozzle radius, velocity, temperature, and dynamic pressure. TA denotes ambient temperature.

Jet Deflection Region

Single jet impingement characteristics are printed.

| Output Titles | Definitions |
|---|---|
| RGH/RN | Half-velocity radius of jet at ground-effect height |
| RG/RN | Jet half width at ground-effect height |
| RO/RN | Deflection zone or pressure recovery radius |
| VG/VN | Square root of jet ground stagnation pressure |
| DPS/DPTJ | Jet ground stagnation pressure nondimensionalized by nozzle stagnation pressure |
| TGS/TA | Stagnation temperature of incident jet at ground-effect height. |
| ALPG | Exponent of ground pressure distribution |
| R/RGH | Radial location in deflection region relative to ground stagnation point. Nondimensionalized by ground-effect half-velocity radius of jet |

| | |
|---|---|
| DPS/DPTG | Ground pressure nondimensionalized by ground stagnation pressure |
| R/RN | Radial location in deflection region nondimensionalized by nozzle radius |
| DPS/DPTJ | Ground pressure nondimensionalized by nozzle stagnation pressure |

Wall Jet Region

Isolated wall jet properties are printed in this set of output.

| Output Titles | Definitions |
|---|---|
| DELS/RN | Boundary layer thickness at stagnation point |
| VMI/VG<br>VMI/VN | Inviscid maximum velocity at jet half width (RGH) radial location or start of transition to turbulent wall jet |
| ALPWO | Exponent of velocity profile at start of wall jet |
| BWOH/RN | Half velocity thickness at start of wall jet |
| BWO/RN | Initial thickness of wall layer |
| PMI/PR | Initial static pressure in wall layer |
| TMI/TA | Initial temperature of wall layer |
| (PTTOT/PR-1.) | Initial total pressure of wall layer |
| (TOT/TA-1.) | Initial total temperature of wall layer |
| R/RN | Radial location in wall jet measured from ground stagnation point |
| VM/VG | Maximum velocity in wall layer nondimensionalized by square root of ground stagnation pressure |
| VM/VN | Maximum velocity in wall layer referenced to nozzle exit velocity. |
| BWH/RN | Half velocity thickness of wall layer |
| BW/RN | Thickness of wall layer |
| DELBL/RN | Boundary layer thickness |
| DELPJ | Maximum stagnation pressure in wall layer |
| KDEL | Ratio of boundary layer to total wall layer thickness |
| TM/TN<br>TM/TA | Maximum temperature in wall layer profile |
| BWNT/RN | Half temperature thickness of wall layer |
| DTM/DTN | (TM-TA)/(TN-TA) |

## TWO-JET IMPINGEMENT INTERACTION OUTPUT

### Recirculation Effect on Wall Jets

Note: This set of output recomputes the wall jet properties accounting for the interaction of two hot jets.

| Output Titles | Definitions |
|---|---|
| PHI | Azimuthal angle in jet-centered ground polar coordinate system |
| TNEFF<br>TAEFF | Effective nozzle and ambient temperature ratios with recirculation effects taken into account. |
| R | Radial location in wall jet, measured from ground stagnation point |
| VM/VN | Maximum velocity in wall layer |
| TM/TN<br>TM/TA | Maximum temperature in wall layer |
| DPM/DPN | (PM-PA)/(PN-PA) or (PM-1.)/(NPR-1.) |
| DTM/DTN | (TM-TA)/(TN-TA) or (TM-1.)/(NTR-1.) |

### Maximum Ground Pressures along Upwash Ground Stagnation Line

| Output Titles | Definitions |
|---|---|
| XW/RN<br>XW/S | Coordinate along stagnation line measured from upwash stagnation point |
| DPMAX/DPJ | Stagnation line pressure nondimensionalized by nozzle stagnation pressure $(P_{MAX}-P_A)/(P_N-P_A)$ |
| PMAX/PMAXO | Stagnation line pressure nondimensionalized by upwash stagnation point pressure |
| DTMAX/DTJ | Stagnation line temperature nondimensionalized by nozzle stagnation temperature |
| TMAX/TMAXO | Stagnation line temperature nondimensionalized by upwash stagnation point temperature |

### Upwash Momentum Function

| Output Titles | Definitions |
|---|---|
| RG/RN | Radius of jet at ground effect height |
| ACON | Constant in momentum function |

| | |
|---|---|
| XMOMZ | Total vertical momentum in upwash sheet non-dimensionalized by the optimum value of $M_J/2\pi$ |
| PHIO | Coalescence angle used in upwash momentum model<br>If PHIO = 0 jets are not coalesced<br>If PHIO > 0 jets have begun to coalesce |

Note: Depending on the value of PHIO (i.e. zero or non-zero) the constant ACON applies to the appropriate upwash momentum model.

| | |
|---|---|
| CU | Nondimensional upwash deflection region width constant |

Note: There are two possible outputs that can occur at this point. If the jets are spaced far enough apart the comment:

JET AND UPWASH DEFLECTION REGIONS DO NOT

INTERACT, CU ESTIMATE IS CORRECT

In this case the value of CU is correct and the jet impingement and upwash deflection regions are independent. The perturbation parameters are then defined as:

EPS = 0.0
SIG = 1.0
PHIUO = 0.0
PHIO = 0.0
PMIN = 0.0 along upwash line
ALPUG = 1.50

If the nozzle spacing and height above ground are such that the deflection regions interact, the subroutine INTERG will be called and

***CALL INTERG***

will be displayed. The following output will be printed.

Note: The ground pressure distributions are computed without temperature effects.

| Output Titles | Definitions |
|---|---|
| Iteration cycle | Number of iterations required to find solution using Newton's method |

| | |
|---|---|
| EPS or EPI | Perturbation parameter for jet impingement pressure distribution |
| SIGMA or SIG | Perturbation parameter for upwash deflection region pressure distribution |
| CU or CUI | Upwash width estimate prior to iterative solution |
| PHIUO<br>PHIO | Angles defining the intersection of jet and upwash deflection regions |

Note: The following values apply along the line connecting the jet stagnation points on the ground (i.e. x = 0).

| | |
|---|---|
| DELPWO | Pressure at upwash stagnation point nondimensionalized by nozzle stagnation pressure |
| PMIN | Minimum pressure between jet and upwash deflection regions nondimensionalized by nozzle stagnation pressure |
| ALPUG | Exponent of upwash ground pressure distribution function |
| (CU) x (SIGMA) | Final value of upwash thickness constant |

Note: If IPBAR = 0, the following output will occur.

Computation of Two-Jet Ground Isobar Pattern

| Output Titles | Definitions |
|---|---|
| PBAR | Input values of pressure, nondimensionalized by nozzle stagnation pressures, will be echoed. |

Note: The following will be repeated NU times.

| Output Titles | Definitions |
|---|---|
| IJET | Number of points on jet impingement region isobar |
| IU | Number of points on upwash deflection region isobar |

If IJET = 0 or IU = 0, the specified value of PBAR was not found in ground pressure distribution.

Note: The following coordinates are referenced to the jet stagnation point on the ground.

| Output Titles | Definitions |
|---|---|
| XISOJ | X coordinate of jet isobar |
| YISOJ | Y coordinate of jet isobar |

| | |
|---|---|
| XISOU | X coordinate upwash region isobar |
| YISOU | Y coordinate of upwash region isobar |

The final set of output in this section is the upwash deflection zone line. If the deflection zones do not interact, ambient conditions exist along this line.

| | |
|---|---|
| XUP | X coordinate of upwash line |
| YUP | Y coordinate of upwash line |

## COMPUTATION OF UPWASH FLOW FIELD

### Upwash Streamline Properties

Note: Two streamlines are printed

| Output Titles | Definitions |
|---|---|
| PHID | Azimuthal angle of upwash streamline referenced to jet ground coordinate system |
| INV. VEL. | Inviscid turning region maximum velocity |
| TMI/TA | Inviscid turning region maximum temperature |
| DELPWJ | Maximum pressure on upwash stagnation line on the ground where upwash streamline orginated |
| BWGH/RN | Half velocity width of incident wall jet streamline |
| ZOU/RN | Upwash turning region height above ground |
| BUO/RN | Initial upwash width |
| BUOHN/RN | Initial upwash half velocity width |

### Upwash Streamline Decay Properties

| Output Titles | Definitions |
|---|---|
| Z/RN | Upwash Streamline coordinate (ZS) |
| VMU/VN | Upwash maximum or centerline velocity |
| TM/TN<br>TM/TA | Upwash maximum or centerline temperature |
| BUH/RN | Half velocity width |
| BU/RN | Half width of upwash |
| DPU/DPJ | Upwash maximum or centerline total pressure non-dimensionalized by nozzle stagnation pressure or $(P_{MU}-P_A)/(P_N-P_A)$ |

Upwash Properties Computed At Z Location of Underside of Body

If ZB = 0, the output will yield the upwash properties at Z = constant plane above ground.

| Output Titles | Definitions |
|---|---|
| ZU/RN | Upwash coordinate measured from ground plane |
| RW/RN | Radial coordinate from jet ground stagnation point to upwash stagnation line |
| PHIB | Azimuthal location of upwash streamline referenced to jet coordinate system |
| X/RN | X coordinate in upwash sheet or X coordinate on fuselage |
| VMU/VN | Maximum or centerline upwash velocity |
| DPU/PN | Maximum or centerline upwash total pressure nondimensionalized by nozzle stagnation pressure $(P_{MU}-P_A)/(P_N-P_A)$ |
| BUH/RN | Half-velocity width of upwash |
| DPU/PUO | Upwash total pressure nondimensionalized by total pressure on streamline originating from upwash stagnation point (X = 0, Y = 0) |
| DPU/PJS | Upwash total pressure nondimensionalized by jet ground stagnation pressure |
| TM/TA | Maximum or centerline upwash temperature |
| DTSM/DTN | (TM-TA)/(TN-TA) |
| PBS/PN | Stagnation pressure on underside of fuselage placed in upwash sheet |

Upwash Lift Force

Two values are printed:

FLAT BOTTOM VEHICLE WITH SHARP CORNERS

BODY WITH CIRCULAR CROSS SECTION

| Output Title | Definition |
|---|---|
| LU/2TJ | Upwash lift force nondimensionalized by the total thrust of the two jets |

COMPUTER PROGRAM LISTING

Figure 69 shows a Fortran listing of the computer program

```
C*************************************************************************
C
C     VTOL TWO-JET IMPINGEMENT INTERACTION COMPUTER PROGRAM
C                FOR CLOSELY SPACED JETS
C                  BY M.J.SICLARI
C                   516 575-2207
C            GRUMMAN AEROSPACE CORPORATION
C             BETHPAGE,NEW YORK 11714
C
C*************************************************************************
C
C   PROGRAM GRUMHOT2
C
      REAL KDELFD,KDELO,NFD,NO,N,KDEL
      REAL MACH,NPR,NTR
      COMMON/WALL/DELS,NO,KDELO,ALPG,ALPWO,ALPWFD,RO,RGH,VG,BWHO
      COMMON/WALLT/ TLAMI,DELPS,DELTSB,PSBAR
      COMMON/NOZZLE/NPR,NTR,TN,GAM,MACH,ACHS,TAEFF,TNEFF
      COMMON/JET/SD,RGU
      COMMON/HEIGHT/ HD,IPBAR
      FETAWB(ETA,A)=ETA-(4./(A+1.))*ETA**(A+1.)+(6./(2.*A+1.))*ETA**(2.*
     1A+1.)-(4./(3.*A+1.))*ETA**(3.*A+1.)+(1./(4.*A+1.))*ETA**(4.*A+1.)
C
C   BODY SHAPE FUNCTIONS FOR FORCE PREDICTION
C     W2...HALF-WIDTH IN NOZZLE RADII
C     ZBODY...HALF DEPTH IN NOZZLE RADII
C     DZDXB...AXIAL SLOPES
C     THNOSE...NOSE ANGLE OF PARABOLIC BODY
C
C
C  PARABOLIC BODY WITH CONSTANT CROSS SECTIONAL SHAPE
C
C     W2(XB)=.5*TAN(THNOSE)*(XL2**2-XB**2)/XL2
C     ZBODY(XB)=.5*TAN(THNOSE)*(XL2**2-XB**2)/XL2
C     DZDXB(XB)=TAN(THNOSE)*XB/XL2
C
C  CYLINDRICAL BODY WITH CONSTANT CROSS SECTIONAL SHAPE
C
      W2(XB)=WCON
      ZBODY(XB)=ZCON
      DZDXB(XB)=ZSCON
C
C  CYLINDRICAL BODY PARAMETERS IN TERMS OF NOZZLE DIAMTERS
C
C
      ZSCON=0.0
     THNOSE=14.0362*PI/180.
C
C  CIRCULAR CROSS SECTION
C     POINT OF FLOW SEPARATION
C
      PI=3.14159265
      GAM=1.4
      PHISEP=135.*PI/180.
      READ (5,1) NPR,NTR
      READ (5,1) HD,SD,ZPLD,DZPL,ZFINAL
    1 FORMAT (5F10.5)
      READ (5,1) XL2,WCON,ZCON
      WRITE (6,21)
   21 FORMAT ('1',///30X,'***   INPUT PARAMETERS   ***'//)
      MACH=SQRT(2.*(NPR-1.)/GAM)
      TN=NTR
      WRITE (6,17) NPR,NTR
   17 FORMAT (20X,'NPR=',F8.4,2X,'NTR=',F8.4)
      WRITE (6,27) MACH,TN
   27 FORMAT (20X,'MACH NO.=',F10.4,2X,'TN/TA=',F10.4)
      WRITE (6,9) HD,SD,ZPLD
    9 FORMAT (20X,'H/D=',F10.5,2X,'S/D=',F10.5,2X,'Z/D=',F10.5)
      WRITE (6,907) ZPLD,DZPL,ZFINAL
```

R81-1622-064D(30 Sheets)

Figure 69 Program FORTRAN Listing

```
  907 FORMAT (/20X,'Z/D=',F10.5,2X,'DZ/D=',F10.5,2X,'ZFINAL/D=',F10.5/)
      WRITE (6,908) XL2,WCON,ZCON
  908 FORMAT (/20X,'BODY LENGTH L/D=',F10.5,2X,'WIDTH W/D=',F10.5,2X,'DE
     1PTH ZB/D=',F10.5/)
      ZPLANE=2.*ZPLD
C
C  COMPUTE JET STANDOFF DISTANCE AND EFFECTIVE JET DECAY HEIGHT
C  (GIRALT ET AL)
C
      IF (HD.LE.6.8) DELG=0.153*7.8
      IF (HD.GT.6.8) DELG=0.153*(1.+HD)
      ZEND=(HD-.50*DELG)*2.
      WRITE (6,22)
   22 FORMAT (///30X,'*****      JET DECAY REGION      *****'//)
      WRITE (6,7) DELG
    7 FORMAT (10X,'JET DEFLECTION HEIGHT DELG/D =',F10.5)
C
C  COMPUTE JET DECAY
C
C  ALL DIMENSIONS NONDIMENSIALIZED BY NOZZLE RADIUS
C
C   SET EMPIRICAL CONSTANTS FOR HALF-WIDTH BEHAVIOR AND LENGTH OF
C  POTENTIAL CORE (KRYCAK,ET AL)
C
      A2=.040
      B2=.800
      FM=1.
      A3=.09*(1.+ALOG(2./(1.+1./TN**.5)))*(1.0-.16*FM*MACH)
      B3=0.
      ZPC0=8.55
      FM=0.0
      ZPC=.5*ZPC0*(1.+1./(TN**.75))*(1.0+.16*FM*MACH)
      A1=A2+(B2-1.)/ZPC
      ZFD=B2/(A3-A2)
      ALPFD=1.5
      WRITE (6,23) ZPC,ZFD
   23 FORMAT (10X,'ZPC/RN=',F10.5,2X,'ZFD/RN=',F10.5)
      WRITE (6,12)
   12 FORMAT (//3X,'Z/RN',3X,'RJH/RN',3X,'RJ/RN',2X,'ALPV',4X,'VJ/VN',4X
     1,'RC/RN',3X,'ALPT',3X,'RJHT/RN',2X,'TM/TN',2X,'TM/TA',4X,'DTM/DTN'
     2,2X,'RJHO/RN',2X,'QJ/QN')
C
C  REGION I...POTENTIAL CORE REGION OF JET..
C
      NJPC=5
      DNPC=NJPC-1
      IF (ZEND.GE.ZPC) DZPC=ZPC/DNPC
      IF (ZEND.LT.ZPC) DZPC=ZEND/DNPC
      Z=0.
      DO 100 I=1,NJPC
      IF (I.EQ.1) GO TO 102
      GO TO 103
  102 VJ=1.
      RJH=1.
      RJHT=1.
      RJ=1.
      ALPVC=0.
      ALPTC=1.5
      CV2=.5
      RJPC=1.
      TM=1.
      DELPMN=1.
      TMB=TN
      DELTMN=1.0
      RC=1.
      RJHO=1.
      GO TO 104
  103 ETAC=1.-Z/ZPC
      RJH=A1*Z+1.
      CALL JETFCT (TN,ETAC,RJH,ALPVC,TLAM,CV2,CT,RV,RT)
      TLAMPC=TLAM
      RJ=RJH/RV
      RJHT=TLAM*RJH
      TM=1.
      TMB=TN
      DELTMN=1.
      DELPMN=1.
```

Figure 69 - Continued

```
      RJPC=RJ
      RJHTPC=RJHT
      VJ=1.
      RC=ETAC*RJ
      ALPTC=ALPVC
      CALL QHALF (TMB,ETAC,ALPVC,TLAM,RQ)
      RJHQ=RJ*RQ
      VQ=1.
      TQ=1.
      TMSTAG=TMB+VJ*VJ*(NTR-TN)
      DTSTAG=(TMSTAG-1.)/(NTR-1.)
  104 WRITE (6,11) Z,RJH,RJ,ALPVC,VJ,RC,ALPTC,RJHT,TM,TMB,DELTMN,RJHQ,
     1DELPMN
   11 FORMAT (1X,4(F7.4,1X),6(F7.4,1X),4(F8.4,1X))
      Z=Z+DZPC
  100 CONTINUE
C
C  TRANSITION REGION II AND FULLY DEVELOPED REGION OF JET
C
      IF (ZEND.LE.ZPC) GO TO 998
      NJFD=25
      DNFD=NJFD-1
      ALPVFD=1.5
      ALPTFD=1.50
      TLAMFD=1.+.185*TN**.5
      RCON=(2.-SQRT(2.))/2.
      RVFD=RCON**(1./ALPVFD)
      RJFD=(A3*ZFD+B3)/RVFD
      RTFD=RVFD
      RJHTFD=TLAMFD*(A3*ZFD+B3)
      DZ=(ZEND-ZPC)/DNFD
      Z=ZPC+DZ
      DO 200 I=2,NJFD
      IF (Z.GT.ZFD) GO TO 201
      RJ=RJPC+((RJFD-RJPC)/(ZFD-ZPC))*(Z-ZPC)
      RJH=A2*Z+B2
      RV=RJH/RJ
      ALPV=ALOG(RCON)/ALOG(RV)
      ALPT=ALPV
      TLAM=TLAMPC+((TLAMFD-TLAMPC)/(ZFD-ZPC))*(Z-ZPC)
      GO TO 202
  201 ALPV=ALPVFD
      ALPT=ALPTFD
      RJH=A3*Z+B3
      TLAM=TLAMFD
  202 CALL VTSOLV(TN,RJH,ALPV,TLAM,VJ,TM,RV,RT)
      RJ=RJH/RV
      RJHT=TLAM*RJH
      TMB=TM*TN
      IF (ABS(TN-1.).LT.1.E-5) DELTMN=1.0
      IF (ABS(TN-1.).GT.1.E-5) DELTMN=(TMB-1.)/(TN-1.)
      DELPMN=VJ*VJ/TM
      CALL QHALF (TMB,0.,ALPV,TLAM,RQ)
      RJHQ=RQ*RJ
      TQ=TM
      VQ=VJ
      TMSTAG=TMB+VJ*VJ*(NTR-TN)
      DTSTAG=(TMSTAG-1.)/(NTR-1.)
      WRITE (6,11) Z,RJH,RJ,ALPV,VJ,RC,ALPT,RJHT,TM,TMB,DELTMN,RJHQ
     1,DELPMN
      Z=Z+DZ
  200 CONTINUE
C
C  JET DEFLECTION REGION
C  JET IMPINGEMENT PRESSURES
C
  998 AOCON=-.032026
      BOCON=.3354248
      COCON=2.8
      IF (HD.GT.3.) AO=3.6
      AOSLH=(3.6-2.9)/(3.-1.2)
      IF (HD.LE.3.) AO=2.9+AOSLH*(HD-1.2)
      WRITE (6,79)
   79 FORMAT (///30X,'*****     JET DEFLECTION REGION      *****'/)
   80 FORMAT (10X,'ROH/RN=',F10.5,2X,'RG/RN=',F10.5,2X,'PO/RN=',F10.5,2X
     1,'VG/VN=',F10.5/)
C
```

Figure 69 - Continued

```
C  SET CHARACTERISTIC SCALE LENGTHS FOR IMPINGEMENT REGION
C
      RGH=RJH
      RG=RJ
      RO=AO*RGH
      ETAWG=RGH/RO
      IF (2.*HD.LE.ZPC) GO TO 454
C
C  DETERMINE STAGNATION POINT PRESSURE
C
  454 WRITE (6,80) RGH,RG,RO,VG
C
C  STAGNATION PRESSURE NONDIMENSIONALIZED BY JET TOTAL PRESSURE
C
      RGU=RG
      DELPS=(VG**2)/TG
      PSBAR=1.+DELPS*(NPR-1.)
      ACHS=SQRT(2.*(PSBAR-1.)/GAM)
      TGB=TG*TN
      TGBS=TGB+(NTR-TN)*VG*VG
      WRITE (6,81) DELPS,TGBS
   81 FORMAT (10X,'STAGNATION PRESSURE, DPS/DPTJ=',F10.5,2X,2X,'GROUND M
     1AX. TEMP., TGS/TA=',F10.5)
      WRITE (6,801) ACHS
  801 FORMAT (/10X,'STAGNATION MACH NUMBER OF JET=',F10.5/)
      CALL GPREST(RO,VG,TO,ALPG,R,CV2)
      WRITE (6,82) ALPG
   82 FORMAT (10X,'ALPG=',F10.5)
      NG=25
      RNGM=NG-1
      DR=RO/(RNGM*RGH)
      DETA=1./(RNGM)
      ETA=0.
      R=0.
      WRITE (6,83)
   83 FORMAT (30X,'SINGLE JET GROUND PRESSURES'//25X,'R/RGH',6X,'DPS/DPT
     1G',8X,'R/RN',7X,'DPS/DPTJ'/)
      DO 300 I=1,NG
      DPTG=(1.-ETA**ALPG)**4.
      DPTJ=DPTG*DELPS
      RRN=R*RGH
      WRITE (6,84) R,DPTG,RRN,DPTJ
   84 FORMAT (20X,4(F10.5,5X))
      R=R+DR
      ETA=ETA+DETA
  300 CONTINUE
C
C  INITIALIZE WALL JET REGION
C
      AW3=.09*(1.+ALOG(2./(1.+1./TN**.5)))*(1.-.16*ACHS)
      TLAMFD=1.+.185*TN**.5
      ALPWFD=1.5
      KDELFD=?0962
      ALPUG=1.5
      NFD=7.
      CALL SIMW(KDELFD,NFD,ALPWFD,RATW,CSV2W,CPW)
      CALL SIMUG(ALPUG,RATUG,CSPUG)
      CU=2.*AW3*CSV2W/(RATW*CSPUG)
      AS1=.015638
      AS2=.128035
      DELS=2.*AS1*(HD)**AS2
      WRITE (6,26)
   26 FORMAT (///30X,'*****     WALL JET REGION     *****'//)
      WRITE (6,86) DELS
   86 FORMAT (5X,'STAGNATION POINT BOUNDARY LAYER THICKNESS, DELS/RN=',
     1F10.5)
      NO=14
      KDELO=DELS/(2.*DELG)
      FETAG=(1.-ETAWG**ALPG)**4
      PMBI=1.+(NPR-1.)*DELPS*FETAG
      DELPSB=(NPR-1.)*DELPS
      ACHI=SQRT(2.*(PSBAR/PMBI-1.)/GAM)
      TMBI=TGBS
      VMI=(ACHI/MACH)*SQRT(TMBI/TN)
      DELTSB=?BS-1.0
      WRITE (6,89) PMBI,DELPSB,DELTSB
```

Figure 69 - Continued

ORIGINAL PAGE IS
OF POOR QUALITY

```
   89 FORMAT (1X,'PMI/PA==',F10.5,2X,'(PTTOT/PA-1.)=',F10.5,2X,'(TOT/TA-
     11.)=',F10.5)
      WRITE (6,92) T    VMI
   92 FORMAT (2X,'TMI  A=',F10.5,2X,'VMI/VN=',F10.5)
      TMI=TMBI/TN
      CALL GMATT(TN,RGH,DELPS,PMBI,TMI,VMI,ALPG,KDELO,NO,ETAWG,DELS,
     1ALPWO,R,BWO,BWHO,TLAMI)
      RATWO=R
      DELSM=BWO*KDELO
      VMG1=VMI/VG
      WRITE (6,91) VMG1
   91 FORMAT (5X,'VELOCITY AT START OF TURBULENT WALL JET, VM/VG=',F10.5
     1)
C     WRITE (6,87) TLAMFD
   87 FORMAT (5X,'TLAMFD=',F10.5)
      WRITE (6,85) ALPWO,BWHO,BWO
   85 FORMAT (10X,'START OF WALL JET REGION, ALPWO=',F10.5,2X,'BWOH/RN='
     1,F10.5,2X,'BWO/RN=',F10.5)
C
C  MAXIMUM VELOCITY DISTRIBUTION IN DEFLECTION REGION
C
      NWPT=25
      XNWPT=NWPT-1
      REND=2*SD
      BR=REND/XNWPT
      BW3HO=AW3*RO
      DELBRH=(BW3HO-BWHO)/(RO-RGH)
      DELNR=(NFD-NO)/(RO-RGH)
      DELAR=(ALPWFD-ALPWO)/(RO-RGH)
      ADELBT=.0175
      ADELBL=(ADELBT*(RO-2.)-DELS)/(RO-RGH)
      R=0.
      TLAMSL=(TLAMFD-TLAMI)/(RO-RGH)
      WRITE (6,107)
  107 FORMAT(//40X,'ISOLATED WALL JET PROPERTIES'//)
      WRITE (6,97)
   97 FORMAT (//5X,'R/RN',5X,'VM/VG',5X,'VM/VN',5X,'BWH/RN',3X,
     1'BW/RN',3X,'DELBL/PN',3X,'DELPJ',3X,'KDEL',3X'TM/TN'
     2,1X,'TM/TA',1X,'BWHT/FN',1X,'DTM/DTN'/)
      DO 400 I=1,NWPT
      IF (R.GE.RGH) TLAM=TLAMI+TLAMSL*(R-RGH)
      IF (R.LT.RGH) TLAM=TLAMI
      IF (R.LE.RO) FETA=(1.-(R/RO)**ALPG)**4
      IF (R.GT.RO) FETA=0.0
      IF (R.GT.RO) TLAM=TLAMFD
      PMB=1.+(NPR-1.)*DELPS*FETA
      IF (R.GT.RGH) GO TO 402
      ACH=SQRT(2.*(PSBAR/PMB-1.)/GAM)
      TMB=TOBS
      VMN=(ACH/MACH)*SQRT(TMB/TN)
      TM=TMB/TN
      DELPJ=DELPS
      DELTA=KDELO*BWO
      N=14
      KDEL=KDELO
      BW=BWO
      BWH=RATWO*BWO
      VMG=VMN/VG
      BWHT=TLAMI*BWH
      DELTMN=(TMB-1.)/(TN-1.)
      TMSTAG=TMB+VMN*VMN*(NTR-TN)
      DTSTAG=(TMSTAG-1.)/(NTR-1.)
      GO TO 401
  402 IF (R.GT.RO) GO TO 403
      BWH=BWHO+DELBRH*(R-RGH)
      ALPW=ALPWO+DELAR*(R-RGH)
      DELBL=DELS+ADELBL*(R-RGH)
      N=NO+DELNR*(R-RGH)
      GO TO 405
  403 BWH=AW3*R
      DELBL=ADELBT*(R-2.)
      N=NFD
      ALPW=ALPWFD
```

Figure 69 - Continued

ORIGINAL PAGE IS
OF POOR QUALITY

```
  405 ALAM=((2.-SQRT(2.))/2.)**(1./ALPW)
      KDEL=DELBL/(DELBL+(BWH-DELBL)/ALAM)
      IF (R.LE.4.) FVIS=1.0
      IF (R.GT.4.) FVIS=1./(R/4.)**.24
      FMOM=1.-FETA
      DELPM=DELPS*FETA
      TAEFF=1.
      TNEFF=TN
      CALL VTWALL (R,BWH,FVIS,FMOM,DELPM,TN,TLAM,PMB,KDEL,N,ALPW,
     1VMN,TM,TNEFF,TAEFF)
      VMG=VMN/VG
      DELPJ=(PMB-1.)/(NPR-1.)+PMB*VMN*VMN/TM
      RCON=(2.-SQRT(2.))/2.
      RAT=KDEL+(1.-KDEL)*RCON**(1./ALPW)
      BW=BWH/RAT
      DELTA=KDEL*BW
      TMB=TM*TN
      BWHT=TLAM*BWH
      DELTMN=(TMB-1.)/(TN-1.)
      TMSTAG=TMB+VMN*VMN*(NTR-TN)
      DTSTAG=(TMSTAG-1.)/(NTR-1.)
  401 WRITE (6,95) R,VMG,VMN,BWH,BW,DELTA,DELPJ,KDEL,TM,TMB
     1,BWHT,DELTMN
      R=R+DR
   95 FORMAT (1X,5(F8.4,2X),8(F7.4,1X))
  400 CONTINUE
C
C     UPWASH GROUND MAXIMUM PRESSURE DISTRIBUTION
C
      WRITE (6,24)
   24 FORMAT (////30X,'*****      TWO-JET INTERACTION PROBLEM      *****'/
     1//)
C
C     WALL JET RECIRCULTAION EFFECTS
C
      IRAY=5
      AREC=1.
      OMEG=(TGBS-1.)*((RG/SD)**AREC)
      IF (RG.GT.SD) OMEG=TGBS-1.
      DRAY=IRAY-1
      DPHI=PI/DRAY
      PHI=0.
      WRITE (6,710)
  710 FORMAT (//30X,'***  RECIRCULATION EFFECT ON WALL JETS  ***'///)
      DO 750 IW=1,IRAY
      PHID=PHI*180./PI
      WRITE (6,711) PHID
  711 FORMAT (/50X,'PHI=',F8.4,' DEGS.'/)
      CPHI2=COS(.5*PHI)
      TAEFF=1.+OMEG*CPHI2*CPHI2
      TNEFF=TN+(TAEFF-1.)*(TGBS-TN)/(TGBS-1.)
      WRITE (6,740) TNEFF,TAEFF
  740 FORMAT (/40X,'TNEFF=',F10.5,2X,'TAEFF=',F10.5/)
      IF (PHI.GE..5*PI) GO TO 701
      XW=SD*TAN(PHI)
      RW=SQRT(XW**2+SD**2)
      IF (RW.GT.2.*SD) RW=2.*SD
      GO TO 702
  701 RW=2.*SD
  702 NWPT=25
      XNWPT=NWPT-1
      DR=RW/XNWPT
      R=0.
      WRITE (6,713)
  713 FORMAT (/37X,'R',7X,'VM/VN',7X,'TM/TN',7X,'TM/TA',7X,'DPM/DPN',5X,
     1'DTM/DTN'/)
      DO 703 IR=1,NWPT
      CALL WALLJT (R,VMN,BWH,DELPW,TM,TMB,PMB,DELTMN,DTSTAG)
      WRITE (6,704) R,VMN,TM,TMB,DELPW,DTSTAG
  704 FORMAT (30X,6(F10.5,2X))
      R=R+DR
  703 CONTINUE
      PHI=PHI+DPHI
  750 CONTINUE
      WRITE (6,460)
```

Figure 69 - Continued

```
  460 FORMAT (//5X,'MAXIMUM GROUND PRESSURE AND TEMPERATURE ALONG UPWASH
     1GROUND STAGNATION LINE'//)
      WRITE (6,470)
  470 FORMAT (14X,'XW/RN',6X,'XW/S',6X,'DPMAX/DPJ',3X,'PMAX/PMAXO',3X,'D
     1TMAX/DTJ',3X,'TMAX/TMAXO'/)
      PHI=0.
      PHIM=80.*PI/180.
      DPHI=PHIM/24.
      DO 450 IL=1,25
      XW=SD*TAN(PHI)
      RW=SQRT(XW**2+SD**2)
      XWS=XW/(2.*SD)
      CPHI2=COS(.5*PHI)
      TAEFF=1.+OMEG*CPHI2*CPHI2
      TNEFF=TN+(TAEFF-1.)*(TGBS-TN)/(TGBS-1.)
      CALL WALLJT (RW,VMN,BWH,DELPW,TH,THB,PHB,DELTHN,DTSTAG)
      PMAXG=(PMB-1.)/(HPR-1.)+PHB*VMN*VMN*COS(PHI)*COS(PHI)/TM
      TSG=THB+(NTR-TN)*VMN*VMN*COS(PHI)*COS(PHI)
      TMAXG=(TSG-1.)/(NTR-1.)
      IF (IL.EQ.1) DELPWO=PMAXG
      IF (IL.EQ.1) DELTWO=TMAXG
      PMAXND=PMAXG/DELPWO
      TMAXND=TMAXG/DELTWO
      WRITE (6,455) XW,XWS,PMAXG,PMAXND,TMAXG,TMAXND
  455 FORMAT (10X,8(F10.5,2X))
      PHI=PHI+DPHI
  450 CONTINUE
      ACON=1.-(RG/SD)**2
      PHIOD=0.0
      IF (ACON.GE.0.) PHIO=0.0
      IF (ACON.GE.0.) GO TO 667
      PHIO=ARCOS((SD/RG)**.20)
      PHIOD=PHIO*180./PI
      ACON=2./(SIN(.5*PI-PHIO)**2)
      XMOMZ=ACON*(1.0+SIN(PHIO)*(SIN(PHIO)-2.0))/3.
      GO TO 668
  667 XMOMZ=ACON+2.*(1.-ACON)/3.
  668 WRITE (6,553)
  553 FORMAT (//5X,'UPWASH MOMENTUM FUNCTION: JET RADIUS, INTERACTION
     1CONSTANT, VERTICAL UPWASH SHEET MOMENTUM, AND COALESCENCE ANGLE'/)
      WRITE (6,551) RG,ACON,XMOMZ,PHIOD
  551 FORMAT (15X,'RG/RN=',F10.5,2X,'ACON=',F10.5,2X,'XMOMZ=',F10.5,2X,'
     1PHIO(DEGS)=',F10.5/)
      CPHI2=1.
      TAEFF=1.+OMEG*CPHI2*CPHI2
      TNEFF=TN+(TAEFF-1.)*(TGBS-TN)/(TGBS-1.)
      CALL WALLJT(SD,VMN,BWH,DELPW,TK,THB,PHB,DELTHN,DTSTAG)
      CALL PGUMAT(CJ,DELPS,DELPW,RO,SD,ALPG,ALFUG)
      CALL SIMW(KDELFI,NFD,ALPUFD,RATW,CSV2W,CFW)
      CALL SIMUG(ALPUG,RATUG,CSPUG)
      CU=2.*AW3*CSV2W/(RATW*CSPUG)
      WRITE (6,557) CU
  557 FORMAT (25X,'UPWASH WIDTH CONSTANT ESTIMATE , CU=',F10.5)
      READ (5,661) IPBAR
  661 FORMAT (I1)
C
C   TEST FOR INTERACTION OF DELFLECTION REGIONS
C
      IF (CU*SD+RO.LE.SD) GO TO 222
C
C  COMPUTATION OF DEFLECTION REGION INTERACTION
C
      CALL INTERQ(XMOMZ,DELPS,SD,RO,ALPG,EPS,CU,SIG)
C
      GO TO 223
  222 EPS=0.0
      SIG=1.0
      PHIUO=0.
      PHIO=0.0
      WRITE (6,28) EPS,SIG,PHIUO,PHIO
   28 FORMAT (//20X,'JET AND UPWASH DEFLECTION REGIONS DO NOT INTERACT,
     1 CU ESTIMATE IS CORRECT'/
     1/35X,'EPS=',F10.5,2X,'SIG=',F10.5,2X,'PHIUO=',F10.5,2X,'PHIO=',F10
     1.5)
      WRITE (6,29) ALPUG
```

Figure 69 - Continued

```
 29 FORMAT (30X,'PMIN=0.0 ALONG UPWASH  LINE, ALPUG=',F8.4,1X,' IN UPW
   1ASH DEFLECTION REGION'/)
    IF (IPBAR.NE.0) CALL GPLOT (ALPG,DELPS,SD,RO,EPS,CU,SIG,PHIUO,PHIG
   1)
C
C
223 WRITE (6,111)
111 FORMAT (//30X,'*****      COMPUTATION OF UPWASH FLOW FIELD      ****
   1*'//)
    WRITE (6,112)
112 FORMAT (//35X,'COMPUTATION OF UPWASH STREAMLINE PROPERTIES'/)
    DPHI=20.*PI/180.
    PHI=0.
114 FORMAT (//30X,'PHID=',F8.4,' DEGS'//)
    DO 600 I=1,2
    PHID=PHI*180./PI
    WRITE (6,114) PHID
    ZEND=ZPLANE/COS(PHI)
    Y=SD*TAN(PHI)
    RW=SQRT(SD**2+Y**2)
    IF (RW.LE.RO) BWH=BWHO+DELBRH*(RW-RGH)
    IF (RW.GT.RO) BWH=AW3*RW
    CPHI2=COS(.5*PHI)
    TAEFF=1.+OMEG*CPHI2*CPHI2
    TNEFF=TN+(TAEFF-1.)*(TGBS-TN)/(TGBS-1.)
    CALL WALLJT(RW,VMN,BWHG,DELPWS,TM,TMB,PMB,DELTMN,DELTWS)
    IWR=1
    CALL UPWAST(RO,RW,PHI,ZEND,BWHG,DELPS,DELPWS,DELTWS,VUN,DELPUJ
   1,TM,TMB,DELTMN,DSTAG,BUH,ZOUS,IWR)
    PHI=PHI+DPHI
600 CONTINUE
    NUPT=25
    XNUPT=NUPT-1
    ALPU=1.5
C
C  CIRCULAR CYLINDER DRAG FUNCTION
C
    DRAG=SIN(PHISEP)*(1.-(4./3.)*(SIN(PHISEP)**2))
    DO 700  J=1,23
    SUMF=0.0
    SUMFC=0.0
    XB=0.
    DXB=XL2/XNUPT
    WRITE (6,116)
116 FORMAT (/////30X,'UPWASH PROPERTIES COMPUTED AT Z LOCATION OF UNDE
   1RSIDE OF BODY'//)
    WRITE (6,118) ZPLANE
118 FORMAT (/35X,'BODY CENTERLINE LOCATION AT Z/RN=',F10.5//)
    WRITE (6,78)
 78 FORMAT (//1X,'ZU/RN',5X,'RW/RN',5X,'PHIB',5X,'X/RN',5X,'VMU/VN',
   13X,'DPU/PN',4X,'BUH/RN',2X,'DPU/PUO',1X,'DPU/PJS',3X,'TM/TA',3X,'D
   2TSM/DTN',1X,'PBS/PN'/)
    IWR=0
    DO 500 I=1,NUPT
    FACT=2.0
    IF (I.EQ.1) FACT=1.0
    IF (I.EQ.NUPT) FACT=1.
    ZB=ZBODY(XB)
    PHIB=ATAN(XB/(SD+ZPLANE-ZB))
    XW=SD*TAN(PHIB)
    RW=SQRT(SD**2+XW**2)
    CPHI2=COS(.5*PHIB)
    TAEFF=1.+OMEG*CPHI2*CPHI2
    TNEFF=TN+(TAEFF-1.)*(TGBS-TN)/(TGBS-1.)
    CALL WALLJT(RW,VMN,BWHG,DELPWS,TM,TMB,PMB,DELTMN,DELTWS)
    ZU=ZPLANE-ZB
    ZEND=ZU/COS(PHIB)
    CALL UPWAST (RO,RW,PHIB,ZEND,BWHG,DELPS,DELPWS,DELTWS,VUN,
   1DELPUJ,TM,TMB,DELTMN,DTSTAG,BUH,ZOUS,IWR)
    THETB=ATAN(DZDXB(XB))
    ETAWB=W2(XB)/(3.6*BUH)
    IF (ETAWB.GT.1.) ETAWB=1.
    FB=FETAWB(ETAWB,ALPU)
    DCYL=W2(XB)*DRAG
    DFLAT=3.6*BUH*FB
    SUMF=SUMF+.5*DXB*FACT*DFLAT*(VUN**2)*(COS(PHIB+THETB)**2)/TM
```

Figure 69 - Continued

```
      SUMFC=SUMFC+.5*DXB*FACT*DCYL*(VUN**2)*(COS(PHIB+THETB)**2)/TM
      ZOU=ZOUS*COS(PHIB)
      PHID=PHIB*180./PI
      IF (ABS(PHIB).LT.1.E-4) DELPM=DELPUJ
      IF (DELPM.NE.0.) DELPB=DELPUJ/DELPM
       IF (DELPM.EQ.0.) DELPB=DELPUJ
      DELPUS=DELPUJ/DELPS
      PBS=((VUN*COS(PHIB+THETB))**2)/TM
      WRITE (6,77) ZU,RW,PHID,XB,VUN,DELPUJ,BUH,DELPB,DELPUS,TMB,DTSTAG,
     1PBS
   77 FORMAT (1X,11(F8.4,1X),F8.5)
      XB=XB+DXB
  500 CONTINUE
C
C  FLAT BOTTOM LIFT FORCE
C
      XLUT=(1./PI)*SUMF
      WRITE (6,778)
  778 FORMAT (//30X,'FLAT BOTTOM VEHICLE WITH SHARP CORNERS'/)
      WRITE (6,771) XLUT
  771 FORMAT (35X,'UPWASH LIFT FORCE',5X,'LU/2TJ=',F10.5//)
C
C  UPWASH LIFT FORCE FOR CIRCULAR CROSS SECTION
C
      XLUT=(1./PI)*SUMFC
      WRITE (6,773)
  773 FORMAT (//30X,'BODY WITH CIRCULAR CROSS SECTION'/)
      WRITE (6,771) XLUT
      ZPLANE=ZPLANE+2.*DZPL
      IF (ZPLANE.GT.2.*ZFINAL) STOP
  700 CONTINUE
      END




      SUBROUTINE VTSOLV (TN,BVH,ALPV,TLAM,VM,TM,RV,RT)
      RCON=(2.-SQRT(2.))/2.
C     WRITE (6,200) TN,BVH,ALPV,ALPT
  200 FORMAT (1X,'TN=',F10.5,2X,'BVH=',F10.5,2X,'ALPV=',F10.5,2X,'ALPT='
     1,F10.5)
      DTN=TN-1.
      REL=.5
      DELMIN=1.E-5
      RV=(RCON)**(1./ALPV)
      RT=RV
      ALPT=ALPV
      VM=1.
      TM=1.
      DO 100 I=1,500
      CALL SIMTV(TN,TM,ALPV,TLAM,CM,CT,CMTM,CTTM)
C     WRITE (6,203) CM,CT,CMTM,CTTM
  203 FORMAT (1X,'CM=',F10.5,2X,'CT=',F10.5,2X,'CMTM=',F10.5,2X,
     1'CTTM=',F10.5)
      F=RV*RV*TM-2.*VM*VM*BVH*BVH*CM
      G=DTN*TM*RV*RV-2.*VM*(TM*TN-1.)*BVH*BVH*CT
      FTM=TM-2.*VM*VM*BVH*BVH*CMTM
      FVM=-4.*VM*BVH*BVH*CM
      GTM=DTN*RV*RV-2.*VM*(TM*TN-1.)*BVH*BVH*CTTM-2.*VM*BVH*BVH*CT*TN
      GVM=-2.*(TM*TN-1.)*BVH*BVH*CT
      DET=FVM*GTM-GVM*FTM
      DELVM=(G*FTM-F*GTM)/DET
      DELTM=(F*GVM-G*FVM)/DET
      VM=VM+REL*DELVM
      TM=TM+REL*DELTM
C     WRITE (6,505) VM,DELVM,TM,DELTM,F,G
  505 FORMAT (1X,'VM=',F10.5,1X,'DELV=',F10.5,1X,'TM=',F10.5,2X,'DTM=',F
     110.5,1X,'F=',F10.5,1X,'G=',F10.5)
      IF (ABS(F).LT.DELMIN.AND.ABS(G).LT.DELMIN) GO TO 101
  100 CONTINUE
      STOP
  101 RETURN
      END
```

Figure 69 - Continued

```
      SUBROUTINE WALLJT (R,VMN,BWH,DELPJ,TM,TMB,PMB,DELTMN,DTSTAG)
      REAL KDELO,NO,KDELFD,NFD,N,KDEL,NPR,NTR,MACH
      COMMON/WALL/ DELS,NO,KDELO,ALPG,ALPWO,ALPWFD,RO,RGH,VG,BWHO
      COMMON/WALLT/TLAMI,DELPS,DELTSB,PSBAR
      COMMON /NOZZLE/ NPR,NTR,TN,GAM,MACH,ACHS,TAEFF,TNEFF
      RCON=(2.-SQRT(2.))/2.
      NFD=7.0
      KDELFD=1./9.
      BW3HO=AW3*RO
      AW7=.09*(1.+ALOG(2./(1.+1./TN**.5)))*(1.-.16*ACHS)
      B' 3''D=AW3*RO
      DELBRH=(BW3HO-BWHO)/(RO-RGH)
      DELNR=(NFD-NO)/(RO-RGH)
      DELAR=(ALPWFD-ALPWO)/(RO-RGH)
      ADELBT=.0175
      ADELBL=(ADELBT*(RO-2.)-DELS)/(RO-RGH)
      TLAMFD=1.+.185*TN**.5
      TLAMSL=(TLAMFD-TLAMI)/(RO-RGH)
      IF (R.GE.RGH) TLAM=TLAMI+TLAMSL*(R-RGH)
      IF (R.LT.RGH) TLAM=TLAMI
      IF (R.LE.RO) FETA=(1.-(R/RO)**ALPG)**4
      IF (R.GT.RO) FETA=0.0
      IF (R.GT.RO) TLAM=TLAMFD
      PMB=1.+(NPR-1.)*DELPS*FETA
      IF (R.GT.RGH) GO TO 402
      TMB=1.+DELTSB
      TM=TMB/NTR
      ACHI=SQRT(2.*(PSBAR/PMB-1.)/GAM)
      VMN=(ACHI/MACH)*SQRT(TMB/NTR)
      DELPJ=DELPS
      DELTA=KDELO*BWO
      N=14
      KDEL=KDELO
      BW=BWO
      BWH=RATWO*BWO
      VMG=VMN/VG
      BWHT=TLAMI*BWH
      DELTMN=(TMB-1.)/(NTR-1.)
      TMSTAG=TMB
      DTSTAG=(TMSTAG-1.)/(NTR-1.)
      GO TO 401
  402 IF (R.GT.RO) GO TO 403
      BWH=BWHO+DELBRH*(R-RGH)
      ALPW=ALPWO+DELAR*(R-RGH)
      DELBL=DELS+ADELBL*(R-RGH)
      N=NO+DELNR*(R-RGH)
      GO TO 405
  403 BWH=AW3*R
      DELBL=ADELBT*(R-2.)
      N=NFD
      ALPW=ALPWFD
  405 ALAM=((2.-SQRT(2.))/2.)**(1./ALPW)
      KDEL=DELBL/(DELBL+(BWH-DELBL)/ALAM)
      IF (R.LE.4.) FVIS=1.0
      IF (R.GT.4.) FVIS=1./(R/4.)**.24
      FMOM=1.-FETA
      DELPM=DELPS*FETA
      CALL VTWALL (R,BWH,FVIS,FMOM,DELPM,TN,TLAM,PMB,KDEL,N,ALPW,
     1VMN,TM,TNEFF,TAEFF)
      VMG=VMN/VG
      RCON=(2.-SQRT(2.))/2.
      RAT=KDEL+(1.-KDEL)*RCON**(1./ALPW)
      BW=BWH/RAT
      DELTA=KDEL*BW
      DELPJ=(PMB-1.)/(NPR-1.)+PMB*VMN*VMN/TM
      TMB=TM*NTR
      BWHT=TLAM*BWH
      DELTMN=(TMB-1.)/(NTR-1.)
      TMSTAG=TMB
      DTSTAG=(TMSTAG-1.)/(NTR-1.)
C 401 WRITE (6,95) R,VMG,VMN,BWH,BW,DELTA,DELPJ,KDEL,TM,TMB
C    1,BWHT,DELTMN,DTSTAG
  401 CONTINUE
      R=R+DR
   95 FORMAT (1X,5(F8.4,2X),6(F7.4,1X))
      RETURN
      END
```

Figure 69 - Continued

ORIGINAL PAGE IS
OF POOR QUALITY

```
      SUBROUTINE VTWALL (R,BWH,FVIS,FMOM,DPM,TN,TLAM,PMB,KDEL,N,ALPV,VM,
     1TM,TNEFF,TAEFF)
      REAL KDEL,N
      VM=1.
      TM=1.
      DELMIN=1.E-5
      REL=.5
      DO 100 I=1,500
      TMB=TM*TN
      CALL SIMUTV (TN,TM,TLAM,PMB,KDEL,N,ALPV,CV2,CP,CT,CV2TM,CTTM,
     1RV)
      F=RV*FMOM*FVIS-R*BWH*(2.*PMB*VM*VM*CV2/TM+DPM*CP)
      G=RV*FMOM*(TNEFF-TAEFF)*TM-2.*PMB*VM*(TMB-TAEFF)*R*BWH*CT
      FVM=-4.*R*BWH*(PMB*VM*CV2/TM)
      FTM=2.*R*BWH*PMB*VM*VM*(CV2/(TM*TM)-CV2TM/TM)
      GVM=-2.*PMB*(TMB-TAEFF)*R*BWH*CT
      GTM=RV*FMOM*(TNEFF-TAEFF)-2.*PMB*VM*R*BWH*(CT*TN+(TMB-TAEFF)*CTTM)
      DET=FVM*GTM-GVM*FTM
      DELVM=(G*FTM-F*GTM)/DET
      DELTM=(F*GVM-G*FVM)/DET
      VM=VM+REL*DELVM
      TM=TM+REL*DELTM
C     WRITE (6,705) F,G,VM,TM
  705 FORMAT (1X,'F=',F10.5,2X,'G=',F10.5,1X,'VM=',F10.5,1X,'TM=',F10.5)
      IF (ABS(F).LT.DELMIN.AND.ABS(G).LT.DELMIN) GO TO 101
  100 CONTINUE
      STOP
  101 CONTINUE
      RETURN
      END




      SUBROUTINE UPWAST (RO,RWALL,PHI,ZEND,BWGH,DELPS,DELPWS,DELTWS,
     1VMUN,DELPUJ,TM,TMB,DELTMN,DTSTAG,BWH,ZOU,IWR)
      REAL NPR,NTR,MOMU
      COMMON /JET/ SD,RGH
      COMMON/NOZZLE/NPR,NTR,TN,GAM,MACH,ACHS,TAEFF,TNEFF
      REAL MACH
C
C THIS ROUTINE COMPUTES THE UPWASH STREAMLINE PROPERTIES
C
      AOU=3.
      PI=3.14159265
      ALPUP=1.5
      ALPUM=1.5
      ACON=1.-(RGH/SD)**2
      IF (ACON.GE.0.) GO TO 907
      PHIO=ARCOS((SD/RGH)**.20)
      ACON=2./(SIN(.5*PI-PHIO)**2)
      PHIOD=PHIO*180./PI
      IF (PHI.GE.PHIO) MOMU=ACON*SIN(PHI-PHIO)**2
      IF (PHI.LT.PHIO) MOMU=0.
      GO TO 909
  907 MOMU=ACON+2.*(1.-ACON)*SIN(PHI)**2
  909 CONTINUE
  773 FORMAT (1X,'ACON=',F10.5,2X,'MOMU=',F10.5)
      AU3=.30
      ALU1=.5
      ALU2=.8
      ZOU=AOU*BWGH
C     WRITE (6,108) SD,RGH,ZOU
  108 FORMAT (1X,'JET',3F10.5)
      ZV=ZOU*COS(PHI)
      ALU=.5
      ALPU=1.5
      CALL SIMU(ALPU,RAT,CV2U)
C     WRITE (6,111) CV2U
  111 FORMAT (1X,'SIMU',F10.5)
C
C   DETERMINE DEPATURE FROM INVISCID DEFLECTION
```

Figure 69 - Continued

ORIGINAL PAGE IS
OF POOR QUALITY

```
C  DETERMINE INITIAL UPWASH WIDTH
C
      DELPWJ=DELPWS
      ZETAG=BWGH/ZOU
      FETAGP=(1.-ZETAG**ALPUP)**4
C     WRITE (6,117) ZETAG,FETAGP
  117 FORMAT (1X,'ZETAG=',F10.5,2X,'FETAGP=',F10.5)
      FETAGM=(1.-ZETAG**ALPUM)**4
      FMOMU=MOMU*(1.-FETAGM)
      PMBI=1.+(NPR-1.)*DELPWJ*FETAGP
      DELPWB=(NPR-1.)*DELPWJ
      PSB=1.+DELPWB
      DELTSB=(NTR-1.)*DELTWS
C     WRITE (6,107) DELPWB,DELTSB
  107 FORMAT (1X,'DTP=',F10.5,2X,'DTT=',F10.5)
      ACHI=SQRT(2.*(PSB/PMBI-1.)/GAM)
      TMBI=1.+DELTSB
      VMNUI=(ACHI/MACH)*SQRT(TMBI/NTR)
      TMI=TMBI/NTR
      IF (IWR.NE.0) WRITE (6,55) VMNUI,TMBI,DELPWJ,DELTWS,BWGH
   55 FORMAT (1X,'INV.VEL.=',F10.5,3X,'TMI/TA=',F10.5,2X,'DELPWJ=',F10.5
     1,2X,'DELTWJ=',F10.5,2X,'BWGH/RN=',F10.5)
      RAY=RWALL+BWGH
      CALL SIMUM (TN,TMI,TLAMI,FMBI,ALPU,FETAGP,DELPWJ,VMNUI,BUON,RAY,
     1RAT,FMOMU,TNEFF,TAEFF)
      BUOHN=RAT*BUON
      IF (ABS(MOMU).LT.1.E-5) BUON=1.E-5
      IF (ABS(MOMU).LT.1.E-5) BUOHN=1.E-5
      IF (IWR.NE.0) WRITE (6,10) ZOU,BUON,BUOHN,TLAMI
   10 FORMAT (15X,'ZOU/RN=',F10.5,2X,'BUO/RN=',F10.5
     1,2X,'BUOHN/RN=',F10.5,2X,'TLAMI=',F10.5//)
      NUPT=25
      XNUPT=NUPT-1
      DZ=(ZEND-BWGH)/XNUPT
      Z=BWGH
      IF (IWR.NE.0) WRITE (6,12)
   12 FORMAT (7X,'Z/RN',7X,'VMU/VN',7X,'TM/TN',7X,'TM/TA',7X,'BUH/RN',6
     1X,'BU/RN',6X,'DPU/DPJ',6X,'DTM/DTN'/)
      TLAMFD=1.+.185*TN**.5
      TLAMSL=(TLAMFD-TLAMI)/(ZOU-BWGH)
      TM=TMI
      VMUN=VMNUI
      DO 100 I=1,NUPT
      BUH=BUOHN+AU3*(Z-BWGH)*(COS(PHI)**ALU1)
      BU=BUH/RAT
      ZETA=Z/ZOU
      IF (Z.GE.ZOU) ZETA=1.
      IF (Z.GT.ZOU) TLAM=TLAMFD
      IF (Z.LE.ZOU) TLAM=TLAMI+TLAMSL*(Z-BWGH)
      FETAP=(1.-ZETA**ALPUP)**4
      FETAM=(1.-ZETA**ALPUM)**4
      RAY=RWALL+Z
      FMOM=MOMU*(1.-FETAM)
      DPM=DELPWJ*FETAP
      PMB=1.+(NPR-1.)*DPM
      CALL VTUPW (RAY,BUH,FMOM,DPM,TN,TLAM,PMB,ALPU,VMUN,TM,TNEFF,TAEFF)
  905 DELPUJ=(PMB-1.)/(NPR-1.)+PMB*VMUN*VMUN/TM
      TMB=TM*NTR
      DELTMN=(TMB-1.)/(NTR-1.)
      TMSTAG=TMB
      DTSTAG=(TMSTAG-1.)/(NTR-1.)
      IF (IWR.EQ.0) DELPUJ=DELPUJ/DELPS
      IF (IWR.NE.0) WRITE (6,11) Z,VMUN,TM,TMB,BUH,BU,DELPUJ,DELTMN
   11 FORMAT (2X,9(F10.5,2X))
      Z=Z+DZ
  100 CONTINUE
      RETURN
      END
```

Figure 69 - Continued

```
      SUBROUTINE VTUPW (R,BUH,FMOM,DFM,TN,TLAM,PMB,ALPV,VM,TM,TNEFF,
     1TAEFF)
      DELMIN=1.E-5
      REL=.5
      DO 100 I=1,500
      TMB=TM*TN
      CALL SIMUTV (TN,TM,TLAM,PMB,ALPV,CV2,CF,CT,CV2TM,CTTM,RV)
      F=RV*FMOM-R*BUH*(2.*PMB*VM*VM*CV2/TM+DFM*CP)
      G=RV*FMOM*(TN-1.)*TM-2.*PMB*VM*(TMB-1.)*R*BUH*CT
C     WRITE (6,111) F,G,TM,VM
  111 FORMAT (1X,'F=',F10.5,2X,'G=',F10.5,2X,'TM=',F10.5,2X,'VM=',F10.5)
      FVM=-4.*R*BUH*(PMB*VM*CV2/TM)
      FTM=2.*R*BUH*PMB*VM*VM*(CV2/(TM*TM)-CV2TM/TM)
      GVM=-2.*PMB*(TMB-1.)*R*BUH*CT
      GTM=RV*FMOM*(TN-1.)-2.*PMB*VM*R*BUH*(CT*TN+(TMB-1.)*CTTM)
      DET=FVM*GTM-GVM*FTM
      DELVM=(G*FTM-F*GTM)/DET
      DELTM=(F*GVM-G*FVM)/DET
      VM=VM+REL*DELVM
      TM=TM+REL*DELTM
C     WRITE (6,705) F,G,VM,TM
  705 FORMAT (1X,'F=',F10.5,2X,'G=',F10.5,1X,'VM=',F10.5,1X,'TM=',F10.5)
      IF (ABS(F).LT.DELMIN.AND.ABS(G).LT.DELMIN) GO TO 101
  100 CONTINUE
      STOP
  101 CONTINUE
      RETURN
      END




      SUBROUTINE INTERG (XLAM,DELPS,SD,RO,ALPB,EPS,CU,SIG)
C
C  MAIN ROUTINE FOR COMPUTING GROUND PRESSURE DISTRIBUTION
C   THIS ROUTINE FINDS THE SOLUTION FOR THE UPWASH THICKNESS AND
C   JET IMPINGEMENT PERTURBATION PARAMETERS SIGMA AND EPS BY
C   MATCHING PRESSURE INTEGRALS
C
      COMMON /HEIGHT/ HD,IPBAR
      DIMENSION EP(200),C(200),PHIU(200),PHI(200),CSJ(200),FUI(4),FJI(4)
      CSPJ(ETA,A)=.5*ETA**2-(4./(A+2.))*ETA**(A   )+(3./(A+1.))*ETA**(2.
     1*A+2.)-(4./(3.*A+2.))*ETA**(3.*A+2.)+(   (4.*A+2.))*ETA**(4.*A+2.)
      FETA(ETA,A)=(1.-ETA**A)**4
      EP(1)=.0
      WRITE (6,777)
  777 FORMAT (///1X,'*** CALL INTERG ***'//)
      IFLAG=0
      C(1)=1.
      PI=3.14159265
      SIG1=1.0
      CUI=CU
      ALU=1.0
      PARM=.01
      DO 900 J=1,100
      EPI=EP(J)
      SIGI=C(J)
      DO 1000 ITR=1,4
      IF (ITR.EQ.2) EPI=EP(J)+PARM
      IF (ITR.EQ.3) EPI=EP(J)
      IF (ITR.EQ.4) SIGI=C(J)+PARM
C
C   SOLVE FOR INTERSECTION OF PRESSURE BOUNDARIES
C
      DO 100 I=1,99
      IF (I.EQ.1) PHIU(1)=1.42
      XU=SD*TAN(PHIU(I))
      XUP=SD/(COS(PHIU(I))**2)
      YU=CUI*SIGI*SD/(COS(PHIU(I))**ALU)
      YUP=-CUI*SIGI*SD*ALU/(COS(PHIU(I))**(ALU+1.))
      RUSQ=XU**2+(SD-YU)**2
      RU=SQRT(RUSQ)
      ROP=RO+EPI*(1.+((SD-YU)/RU))
      ROPSQ=ROP**2
      F=RUSQ-ROPSQ
      FP=2.*XU*XUP-2.*(SD-YU)*YUP-2.*EPI*ROP*(SD-YU)*
     1(YUP/RU+(2.*XU*XUP-2.*(SD-YU)*YUP)/RUSQ)
      PHIU(I+1)=PHIU(I)-F/FP
      IF (ABS(PHIU(I+1)-PHIU(I)).LT.1.E-5) GO TO 101
```

Figure 69 - Continued

ORIGINAL PAGE IS
OF POOR QUALITY

```
  100 CONTINUE
      STOP
  101 PHIUO=PHIU(I+1)
      PHIUOD=PHIUO*180./PI
      YUO=CUI*SIGI*SD/(COS(PHIUO)**ALU)
      PHIO=ATAN2(SD*TAN(PHIUO),SD-YUO)
      PHIOD=PHIO*180./PI
      IF (IFLAG.EQ.1) WRITE (6,10) EPI,CUI,PHIUOD,PHIOD
   10 FORMAT (15X,'EPI=',F10.5,2X,'CUI=',F10.5,2X,'PHIUO=',F10.5
     1,2X,'PHIO=',F10.5,2X,'DEGREES')
C
C DETERMINE MOMENTUM INTEGRAL FOR IMPINGEMENT REGION
C
      NUPTS=99
      IF (J.GT.20) NUPTS=198
      XPTS=NUPTS-1.
      DPHIU=PHIUO/XPTS
      PHIU(1)=0.
      SUMU1=0.
      DO 200 IJ=1,NUPTS
      FACT=2.0
      IF (IJ.EQ.1) FACT=1.0
      IF (IJ.EQ.NUPTS) FACT=1.0
      RW=SD/COS(PHIU(IJ))
      CALL WALLJ (RW,VMN,DUM2,DUM3,DUM4,DELPW)
      IF (IJ.EQ.1.AND.IFLAG.EQ.1) WRITE (6,111) DELPW
  111 FORMAT (35X,'PHI=0.0, DELPWO=',F10.5)
      YU=CUI*SIGI*SD/COS(PHIU(IJ))
      XU=SD*TAN(PHIU(IJ))
      PHI(IJ)=ATAN2(XU,SD-YU)
      RU=(SD-YU)/COS(PHI(IJ))
      ROP=RO+EPI*(1.+COS(PHI(IJ)))
      ETAM=RU/ROP
      IF (ETAM.GT.1.) FETAG=0.0
      IF (ETAM.GT.1.) GO TO 1011
      FETAG=FETA(ETAM,ALPG)
 1011 PMIN=DELPS*FETAG
      IF (IJ.EQ.1.AND.IFLAG.EQ.1) WRITE (6,775) PMIN
  775 FORMAT (35X,'PHI=0.0, PMIN=',F10.5)
      PMAX=DELPW-VMN**2+(VMN*COS(PHIU(IJ)))**2
      CALL PMATCH (PMIN,PMAX,ALPUG)
      IF (IJ.EQ.1.AND.IFLAG.EQ.1) WRITE (6,1055) ALPUG
 1055 FORMAT (35X,'PHI=0.0, ALPUO=',F10.5)
      CALL SIMUO(ALPUO,RATU,CSPUG)
      PMAX=DELPW-VMN**2+(VMN*COS(PHIU(IJ)))**2
      FU=DELPS*FETAG+CSPUG*(PMAX-DELPS*FETAG)
      FUT=SIGI*FU/(COS(PHIU(IJ))**3)
      SUMU1=SUMU1+.5*DPHIU*FACT*FUT
      IF (ETAM.GT.1.) ETAM=1.0
      CSJ(IJ)=CSFJ(ETAM,ALPG)
      PHIU(IJ+1)=PHIU(IJ)+DPHIU
  200 CONTINUE
      XI1UG=CUI*SUMU1*SD**2
      SUMI=0.
      NUPTSM=NUPTS-1
      DO 300 IJ=1,NUPTSM
      ROPP=RO+EPI*(1.+COS(PHI(IJ+1)))
      ROPPSQ=ROPP**2
      ROPM=RO+EPI*(1.+COS(PHI(IJ)))
      ROPMSQ=ROPM**2
      FM=ROPMSQ*CSJ(IJ)
      FP=ROPPSQ*CSJ(IJ+1)
      DPHI=PHI(IJ+1)-PHI(IJ)
      SUMI=SUMI+.5*DPHI*(FM+FP)
  300 CONTINUE
      XI1JG=DELPS*SUMI
      CALL SIM(0.0,ALPG,R[illegible]3,CSPJG)
      XI2JG=CSPJG*DELPS*((PI-PHIO)*(RO*(RO+2.*EPI)+1.5*EPI**2)
     1-2.*EPI*(RO+EPI)*SIN(PHIO)-.25*SIN(2.*PHIO)*EPI**2)
      XJI=XI1JG+XI2JG
      FJI(ITR)=XJI-PI
      DPHIU=(.5*PI-PHIUO)/XPTS
      SUMU2=0.0
      PH=PHIUO
      XI2UG=SIGI*(1.-SIN(PHIUO))
      FUI(ITR)=XI1UG+XI2UG-XLAM
```

Figure 69 - Continued

```
      IF (IFLAG.EQ.1) GO TO 907
      IF (ITR.EQ.1) GO TO 1000
      RELAX=.5
      DEPI=PARM
      DCUI=PARM
      IF (ITR.EQ.2) FUIE=(FUI(ITR)-FUI(ITR-1))/DEPI
      IF (ITR.EQ.4) FUIC=(FUI(ITR)-FUI(ITR-1))/DCUI
      IF (ITR.EQ.2) FJIE=(FJI(ITR)-FJI(ITR-1))/DEPI
      IF (ITR.EQ.4) FJIC=(FJI(ITR)-FJI(ITR-1))/DEPI
 1000 CONTINUE
      DET=FUIE*FJIC-FJIE*FUIC
      DELE=(FJI(1)*FUIC-FUI(1)*FJIC)/DET
      DELC=(FUI(1)*FJIE-FJI(1)*FUIE)/DET
      EP(J+1)=EP(J)+RELAX*DELE
      C(J+1)=C(J)+RELAX*DELC
  905 FORMAT (15X,'ITERATION CYCLE=',I3,2X,'EPS=',F10.5,2X,'SIGMA=',F10.
     15)
      IF (ABS(DELE).LT.1.E-5.AND.ABS(DELC).LT.1.E-5) IFLAG=1
      IF (IFLAG.EQ.1) WRITE (6,909)
  909 FORMAT (20X,'SOLUTION OF GROUND PRESSURE DISTRIBUTION HAS BEEN FOU
     1ND')
      IF (IFLAG.EQ.1) WRITE (6,905) J,EP(J+1),C(J+1)
  900 CONTINUE
      STOP
  907 SIG=C(J)
      EPS=EP(J)
      CUU=SIG*CUI
      WRITE (6,13) CUU
   13 FORMAT (20X,'UPWASH THICKNESS CONSTANT, (CU) X (SIGMA)=',F10.5)
      IF (IPBAR.NE.0) CALL GPLOT(ALPG,DELPS,SD,RO,EPS,CUI,SIG,PHIUO,PHIO
     1)
      RETURN
      END




      SUBROUTINE GPLOT (ALPG,DELPS,SD,RO,EPS,CUI,SIGI,PHIUO,PHIO)
      DIMENSION PU(25),RWALL(102),ERR(102),XPLOTU(202),YPLOTU(
     1202),XPLOTJ(202),YPLOTJ(202),XAXIS(30),YAXIS(30),XDATA(10),YDATA(1
     20)
      COMMON /HEIGHT/ HD,IPBAR
C
C  THIS ROUTINE COMPUTES THE GROUND ISOBAR PATTERN FOR THE TWO-JET
C   IMPINGEMENT FLOW FIELD
C
      FETA(ETA,A)=(1.-ETA**A)**4
C
C   INPUT NUMBER OF ISOBAR VALUES
C
      READ(5,51) NU
   51 FORMAT (I2)
      WRITE (6,53) NU
   53 FORMAT ('1',//30X,'***  COMPUTATION OF TWO-JET GROUND ISOBAR PATTE
     1RN ***'///32X,I2,' VALUES OF PRESSURE SPECIFIED FOR PATTERN'
     2//)
C
C   INPUT NU ISOBAR VALUES FOR GROUND PATTERN
C
      READ(5,1) (PU(I),I=1,NU)
    1 FORMAT (F10.5)
      WRITE (6,112) (PU(I),I=1,NU)
  112 FORMAT (10X,'PBAR=',8(F10.5,2X))
      WRITE (6,121)
  121 FORMAT (//25X,'GROUND PATTERN IN JET CENTERED COORDINATE SYSTEM'//
     1)
      NUPTS=29
C     CALL PLOT(6.,0.,-3)
      XLMAX=RO+SD
C     XSC=XLMAX/8.
      XSC=1.0
      XMIN=0.
      DXMIN=-1.
      DO 801 IP=1,100
      IF (XMIN.LT.-RO) GO TO 802
      XMIN=XMIN+DXMIN
  801 CONTINUE
```

Figure 69 - Continued

ORIGINAL PAGE IS
OF POOR QUALITY

```
  802 XMAX=SD
      DXAXIS=SD-XMIN
      NAPTS=DXAXIS+1
      XAXIS(1)=XMIN/XSC
      YAXIS(1)=0.
      DO 809 IP=2,NAPTS
      XAXIS(IP)=XAXIS(IP-1)+1./XSC
      YAXIS(IP)=YAXIS(IP-1)
  809 CONTINUE
      DYAX=1./XSC
      XAXIS(NAPTS+1)=SD/XSC
      YAXIS(NAPTS+1)=0.
      DO 805 IP=2,NAPTS
      XAXIS(NAPTS+IP)=SD/XSC
      YAXIS(NAPTS+IP)=YAXIS(NAPTS+IP-1)+DYAX
  805 CONTINUE
      NPLOT=2*NAPTS
C     CALL LINE (XAXIS,YAXIS,NPLOT,1,1,-3,1,.1)
C     CALL SYMBL4 (-3.,8.,.2,'H/D=14.0, S/D=2.00',0.,18)
      PI=3.14159265
      XPTS=NUPTS-1.
      RELAX=.5
      DO 500 I-1,NU
      WRITE (6,66) PU(I)
   66 FORMAT (///45X,'PBAR=',F10.5)
      IFLAG=1
      XPUF=0.
      IJET=1
      IU=1
      RW=SD
      ALPUG=1.5
      CALL WALLJ (RW,VMN,DUM2,DUM3,DUM4,DELPW)
      PMAXO=DELPW
      IF (PMAXO.LT.PU(I)) IFLAG=0
      RW=SD/COS (PHIUO)
      CALL WALLJ (RW,VMN,DUM2,DUM3,DUM4,DELPW)
      PMAXF=DELPW-VMN**2+(VMN*COS(PHIUO))**2
      IF (IFLAG.EQ.0) GO TO 502
      RWALL(1)=SD
      RWALL(2)=SD+.1
      DO 400 K=1,100
      CALL WALLJ(RWALL(K),VMN,DUM2,DUM3,DUM4,DELPW)
      XU=SQRT(RWALL(K)**2-SD**2)
      PHIU=ATAN2(XU,SD)
      PMAX=DELPW-VMN**2+(VMN*COS(PHIU))**2
      ERR(K)=PU(I)-PMAX
      IF (K.EQ.1) GO TO 400
      IF (ABS(ERR(K)).LT.1.E-5) GO TO 501
      DRDE=(RWALL(K)-RWALL(K-1))/(ERR(K)-ERR(K-1))
      RWALL(K+1)=RWALL(K)-RELAX*DRDE*ERR(K)
  400 CONTINUE
      STOP
  501 RW=RWALL(K)
      XPUF=SQRT(RW**2-SD**2)
      PUF=ATAN2(XPUF,SD)
      YUF=CUI*SIGI*SD/COS(PUF)
      PUFD=PUF*180./PI
  502 DPHIU=PHIUO/XPTS
      IF (PHIUO.EQ.0.) GO TO 201
      PHIU=0.
      DO 200 IJ=1,NUPTS
      RW=SD/COS(PHIU)
      CALL WALLJ (RW,VMN,DUM2,DUM3,DUM4,DELPW)
      YU=CUI*SIGI*SD/COS(PHIU)
      XU=SD*TAN(PHIU)
      PHI=ATAN2(XU,SD-YU)
      RU=(SD-YU)/COS(PHI)
      ROP=RO+EPS*(1.+COS(PHI))
      ETAM=RU/ROP
      IF (ETAM.GT.1.) FETAG=0.0
      IF (ETAM.GT.1.) GO TO 1011
      FETAG=FETA(ETAM,ALPG)
 1011 PMIN=DELPS*FETAG
      PMAX=DELPW-VMN**2+(VMN*COS(PHIU))**2
      CALL PMATCH (PMIN,PMAX,ALPUG)
      PBAR=(PU(I)-PMIN)/(PMAX-PMIN)
```

Figure 69 - Continued

```
      IF (PMIN.GT.PU(I)) GO TO 509
      PBARJ=PU(I)/DELPS
      IF (PBARJ.GT.1.) GO TO 509
      ETAJ=(1.-PBARJ**.25)**(1./ALPG)
      XPLOTJ(IJET)=ROP*ETAJ*COS(PHI)
      YPLOTJ(IJET)=ROP*ETAJ*SIN(PHI)
      XPLOTJ(IJET)=XPLOTJ(IJET)/XSC
      YPLOTJ(IJET)=YPLOTJ(IJET)/XSC
      IJET=IJET+1
  509 IF (PBAR.GT.1..OR.PBAR.LT.0.) GO TO 506
      ETAU=(1.-PBAR**.25)**(1./ALPUG)
      XPLOTU(IU)=SD-YU*ETAU
      YPLOTU(IU)=XU
      XPLOTU(IU)=XPLOTU(IU)/XSC
      YPLOTU(IU)=YPLOTU(IU)/XSC
      IU=IU+1
  506 PHIU=PHIU+DPHIU
  200 CONTINUE
  201 DPHI=(PI-PHIO)/XPTS
      PHI=PHIO
      DO 600 IK=1,NUPTS
      PBARJ=PU(I)/DELPS
      IF (PBARJ.GT.1.) GO TO 600
      ETAJ=(1.-PBARJ**.25)**(1./ALPG)
      ROP=RO+EPS*(1.+COS(PHI))
      XPLOTJ(IJET)=ROP*ETAJ*COS(PHI)
      YPLOTJ(IJET)=ROP*ETAJ*SIN(PHI)
      XPLOTJ(IJET)=XPLOTJ(IJET)/XSC
      YPLOTJ(IJET)=YPLOTJ(IJET)/XSC
      IJET=IJET+1
      PHI=PHI+DPHI
  600 CONTINUE
      IF (IFLAG.EQ.0) GO TO 513
      IF (PU(I).EQ.0.) GO TO 513
      IF(PUF.LT.PHIUO) GO TO 510
      GO TO 511
  510 XPLOTU(IU)=SD
      YPLOTU(IU)=XPUF
      XPLOTU(IU)=XPLOTU(IU)/XSC
      YPLOTU(IU)=YPLOTU(IU)/XSC
      GO TO 800
  511 DPHIU=(PUF-PHIUO)/XPTS
      PHIU=PHIUO
      DO 700 IJ=1,NUPTS
      YU=CUI*SIGI*SD/COS(PHIU)
      XU=SD*TAN(PHIU)
      RW=SD/COS(PHIU)
      CALL WALLJ(RW,VMN,DUM2,DUM3,DUM4,DELPW)
      PMAX=DELPW-VMN**2+(VMN*COS(PHIU))**2
      PBAR=PU(I)/PMAX
      ETAU=(1.-PBAR**.25)**(1./ALPUG)
      XPLOTU(IU)=SD-YU*ETAU
      YPLOTU(IU)=XU
      XPLOTU(IU)=XPLOTU(IU)/XSC
      YPLOTU(IU)=YPLOTU(IU)/XSC
      IU=IU+1
      PHIU=PHIU+DPHIU
  700 CONTINUE
  513 IU=IU-1
  800 IJET=IJET-1
      WRITE (6,11) IJET,IU
   11 FORMAT (//15X,'JET IMPINGEMENT REGION,  IJET=',I4,10X,'UPWASH DEFL
     1ECTION REGION, IU=',I4//)
      IF (IJET.GT.0.OR.IU.GT.0) WRITE (6,552)
  552 FORMAT (//34X,'XISOJ',6X,'YISOJ',8X,'XISOU',8X,'YISOU'/)
      IMIN=IU
      IMAX=IJET
      IF (IU.GT.IJET) IMAX=IU
      IF (IU.GT.IJET) IMIN=IJET
      DO 803 IM=1,IMAX
      IF (IM.LE.IMIN) WRITE(6,12) XPLOTJ(IM),YPLOTJ(IM),XPLOTU(IM),YPLOT
     1U(IM)
   12 FORMAT (30X,4(F10.5,2X))
      IF (IM.GT.IMIN.AND.IMIN.EQ.IU) WRITE (6,15) XPLOTJ(IM),YPLOTJ(IM)
   15 FORMAT (30X,2(F10.5,2X))
      IF (IM.GT.IMIN.AND.IMIN.EQ.IJET) WRITE (6,16) XPLOTU(IM),YPLOTU(IM
     1)
   16 FORMAT (54X,2(F10.5,2X))
```

Figure 69 - Continued

```
  803 CONTINUE
C     CALL LINE (XPLOTU,YPLOTU,IU,1,1,1,1,.1)
C     CALL LINE (XPLOTJ,YPLOTJ,IJET,1,1,1,1,.1)
  500 CONTINUE
      DPHIU=.5*PI/XPTS
      PHIU=0.
      DO 900 IJ=1,NUPTS
      YU=CUI*SIGI*SD/COS(PHIU)
      XU=SD*TAN(PHIU)
      IF (XU.GT.XLMAX) GO TO 901
      XPLOTU(IJ)=SD-YU
      YPLOTU(IJ)=XU
      XPLOTU(IJ)=XPLOTU(IJ)/XSC
      YPLOTU(IJ)=YPLOTU(IJ)/XSC
      PHIU=PHIU+DPHIU
  900 CONTINUE
  901 IU=IJ-1
      WRITE (6,807)
  807 FORMAT (///15X,'UPWASH DEFLECTION ZONE LINE, PBAR=0 OUTSIDE INTERA
     1CTION REGION'//)
      WRITE (6,808)
  808 FORMAT (35X,'XUP',8X,'YUP'//)
      DO 813 IM=1,IU
      WRITE (6,811) XPLOTU(IM),YPLOTU(IM)
  813 CONTINUE
  811 FORMAT (30X,2(F10.5,2X))
C     CALL LINE (XPLOTU,YPLOTU,IU,1,1,1,1,.1)
C     CALL ADRAW
C     CALL PLOT (-99.,-99., 3)
C     READ (5,101) PAUSE
  101 FORMAT (1X,F10.5)
      RETURN
      END




      SUBROUTINE WALLJ(R,VMN,BWH,BW,CV2,DELPW)
      REAL KDELO,NO,KDELFD,NFD,N,KDEL
C
C   THIS COMPUTES THE WALL JET PROPERTIES GIVEN A WALL RADIUS
C
      COMMON/WALL/ DELS,NO,KDELO,ALPG,ALPWO,ALPWFD,RO,RGH,VG,BWHO
C
C  MAXIMUM VELOCITY DISTRIBUTION IN DEFLECTION REGION
C
      AW3=.09
      NFD=7.
      KDELFD=1./9.
      BW3HO=AW3*RO
      DELBRH=(BW3HO-BWHO)/(RO-RGH)
      ALPWFD=1.5
      DELAR=(ALPWFD-ALPWO)/(RO-RGH)
      DELNR=(NFD-NO)/(RO-RGH)
      ADELBT=.0175
      ADELBL=(ADELBT*(RO-2.)-DELS)/(RO-RGH)
      DKDELR=(KDELFD-KDELO)/(RO-RGH)
      IF (R.LE.RO) FETA=(1.-(R/RO)**ALPG)**4
      IF (R.GT.RO) FETA=0.0
      IF (R.LE.RGH) VMG=SQRT(1.-FETA)
      IF (R.LE.RGH) VMN=VMG*VG
      IF (R.LE.RGH) GO TO 401
      IF (R.LE.RO) BWH=BWHO+DELBRH*(R-RGH)
      IF (R.GT.RO) BWH=AW3*R
      IF (R.LE.RO) ALPW=ALPWO+DELAR*(R-RGH)
      IF (R.GT.RO) ALPW=ALPWFD
      IF (R.LE.RO) N=NO+DELNR*(R-RGH)
      IF (R.GT.RO) N=NFD
      IF (R.LE.RO) DELBL=DELS+ADELBL*(R-RGH)
      IF (R.GT.RO) DELBL=ADELBT*(R-2.)
      ALAM=((2.-SQRT(2.))/2.)**(1./ALPW)
      KDEL=DELBL/(DELBL+(BWH-DELBL)/ALAM)
      CALL SIMW(KDEL,N,ALPW,RAT,CV2,CP)
      IF (R.LE.4.) VISMOM=1.0
      IF (R.GT.4.) VISMOM=1./(R/4.)**.24
      F1=VISMOM*RAT*(1.-FETA)/(R*BWH)
      F2=CP*FETA*VG**2
```

Figure 69 - Continued

```
      VMN=SQRT((F1-F2)/(2.*CV2))
      VMG=VMN/VG
      DELFW=FETA*VG**2+VMN**2
      BW=BWH/RAT
      DELTA=KDEL*BW
  401 CONTINUE
      IF (R.LT.RGH) DELFW=VG**2
      IF (R.LT.RGH) BWH=BWHO
      RETURN
      END




      SUBROUTINE JETPCT (TM,ETAC,BVH,ALPV,TLAM,CM,CT,RV,RT)
      DELMIN=1.E-5
      CALL JETPCN(ETAC,BVH,ALPVI,RVI,CV2)
C     WRITE (6,555) CV2,ALPVI
C     CALL JETPC (ETAC,BVH,ALPVI,RVI,CV2)
C     WRITE (6,555) CV2,ALPVI
  555 FORMAT (1X,'CV2=',F10.6,2X,'ALPVI=',F10.6)
C     WRITE (6,123) TM,ETAC,BVH
  123 FORMAT (1X 3F13.6)
      ALPV=1.*ALPVI
      TLAM=1.
      R2=(SQRT(2.)-1.)/SQRT(2.)
      REL=.1000000
      DO 100 I=1,999
      RV=ETAC+(1.-ETAC)*R2**(1./ALPV)
      RVAV=(ETAC-1.)*((RV-ETAC)/(1.-ETAC))*ALOG((RV-ETAC)/(1.-ETAC))/
     1ALPV
      CALL SIMTPC(TM,ETAC,ALPV,TLAM,CM,CT,CMAV,CMAT,CTAV,CTAT)
      F=2.*BVH*BVH*CT-RV*RV
      G=2.*BVH*BVH*CM-RV*RV
      FAV=2.*BVH*BVH*CTAV-2.*RV*RVAV
      FAT=2.*BVH*BVH*CTAT
      GAV=2.*BVH*BVH*CMAV-2.*RV*RVAV
      GAT=2.*BVH*BVH*CMAT
      DET=FAV*GAT-GAV*FAT
      DALPV=(G*FAT-F*GAT)/DET
      DLAM=(F*GAV-G*FAV)/DET
C     WRITE (6,800) BVH,CT,RV,CM,ALPV,ALPT,F,G
  800 FORMAT (1X,8F14.6)
C     WRITE (6,700) I,DALPV,DALPT
  700 FORMAT (1X,I3,2X,2F15.6)
      ALPV=ALPV+REL*DALPV
      TLAM=TLAM+REL*DLAM
      IF (ABS(F).LT.DELMIN.AND.ABS(G).LT.DELMIN) GO TO 200
  100 CONTINUE
      STOP
C 200 WRITE (6,500) I,ALPV,ALPT
  200 CONTINUE
  500 FORMAT (1X,I3,2X,'ALPV=',F10.6,2X,'ALPT=',F10.6)
      RT=RV
      RETURN
      END



      SUBROUTINE JETPCN (ETAC,RJH,ALPC,R,CV2)
C
C     THIS ROUTINE COMPUTES THE EXPONENT OF THE JET VELOCITY PROFILE
C     IN THE POTENTIAL CORE REGION
C
      ALP=4.0
      DELMIN=1.E-5
      REL=.50
      DO 100 I=1,500
      CALL SIMN(ETAC,ALP,R,CV2,CV2A,RALP)
      FUNC=CV2-.5*(R/RJH)**2
      FUNCD=CV2A-(R*RALP)/(RJH**2)
      ALFN=ALP-FUNC/FUNCD
C     WRITE (6,700) ALFN,FUNC
  700 FORMAT (1X,'ALF=',F10.5,2X,'FUNC=',F10.5)
      ALP=ALP+REL*(ALFN-ALP)
      IF (ABS(FUNC).LT.DELMIN) GO TO 101
```

Figure 69 - Continued

ORIGINAL PAGE IS
OF POOR QUALITY

```
  100 CONTINUE
      STOP
  101 ALPC=ALPN
      RETURN
      END



      SUBROUTINE SIMN(ETAC,ALP,R,CV2,CV2A,RALP)
C
C   INTEGRAL OF JET VELOCITY PROFILE FUNCTION=CV2
C    R=RATIO OF RJH TO RJ
C
      A1=.5-4./(ALP+2.)+3./(ALP+1.)-4./(3.*ALP+2.)+1./(4.*ALP+2)
      A2=1.-4./(ALP+1.)+6./(2.*ALP+1.)-4./(3.*ALP+1.)+1./(4.*ALP+1.)
      CV2=.5*ETAC**2+A1*(1.-ETAC)**2+ETAC*(1.-ETAC)*A2
      A1ALP=4./((ALP+2.)**2)-3./((ALP+1)**2)+12./((3.*ALP+2.)**2)
     1-4./((4.*ALP+2.)**2)
      A2ALP=4./((ALP+1)**2)-12./((2.*ALP+1.)**2)+12./((3.*ALP+1.)**2)
     1-4./((4.*ALP+1.)**2)
      ETAB1=(1.-ETAC)**2
      ETAB2=ETAC*(1.-ETAC)
      CV2A=ETAB1*A1ALP+ETAB2*A2ALP
      R=ETAC+(1.-ETAC)*((2.-SQRT(2.))/2.)**(1./ALP)
      RALP=((ETAC-R)/ALP)*ALOG((R-ETAC)/(1.-ETAC))
      RETURN
      END



      SUBROUTINE SIKTFC (TM,ETAC,ALPV,TLAM,CM,CT,CMALP,CMTLAM,CTALP,
     1CTTLAM)
      FVP(ETAP)=(1.-ETAP**ALPV)**2
      FTP(ETAPT)=(1.-ETAPT**ALPT)**2
      FVAVP(ETAP,FV)=2.*SQRT(FV)*(SQRT(FV)-1.)*ALOG(ETAP)
      FTATP(ETAPT,FT)=2.*SQRT(FT)*(SQRT(FT)-1.)*ALOG(ETAPT)
      FTLAM(ETAPT,ETAP,TLAM)=2.*ALPT*(1.-ETAPT**ALPT)*(ETAPT**(ALPT-1.
     1))*(ETAP TLAM*TLAM))
      FUNC(FV,FT)=FV/(FT+(1.-FT)/TM)
      FUN(FT)=FT/(FT+(1.-FT)/TM)
      FUNCT(FV,FT)=FV/((FT+(1.-FT)/TM)**2)
      N=24
C     WRITE (6,800) TM,ETAC,ALPV,TLAM
  800 FORMAT (5X,4F11.5)
      DTM=(1.-TM)/TM
      N1=N-1
      ALPT=ALPV
      N2=N-2
      DETA=(1.-ETAC)/N1
      ETA=ETAC+DETA
      SUMOM=0.
      SUMOMA=0.
      SUMOMT=0.
      SUMOTA=0.
      SUMOTT=0.
      SUMOT=0.
      DO 100 I=1,N1,2
      ETAP=(ETA-ETAC)/(1.-ETAC)
      ETAPT=ETAP/TLAM
      FV=FVP(ETAP)
      FT=FTP(ETAPT)
      FVAV=FVAVP(ETAP,FV)
      FTAT=FTATP(ETAPT,FT)
      FTTLAM=FTLAM(ETAPT,ETAP,TLAM)
      SUMOM=SUMOM+FV*ETA*FUNC(FV,FT)
      SUMOT=SUMOT+FT*ETA*FUNC(FV,FT)
      SUMOMA=SUMOMA+2.*FVAV*ETA*FUNC(FV,FT)+FV*FTAT*ETA*DTM*FUNCT(FV,FT)
      SUMOMT=SUMOMT+FV*FTTLAM*ETA*FUNCT(FV,FT)
      SUMOTA=SUMOTA+FVAV*ETA*FUN(FT)+FTAT*ETA*FUNC(FT,FV)+FTAT*DTM*FUNCT
     1(FV,FT)*ETA
      SUMOTT=SUMOTT+FTTLAM*ETA*(FUNC(FV,FT)+DTM*FUNCT(FV,FT))
      ETA=ETA+2.*DETA
```

Figure C? - Continued

```
  100 CONTINUE
      ETA=ETAC+2.*DETA
      SUMEM=0.
      SUMET=0.
      SUMEMA=0.
      SUMEMT=0.
      SUMETA=0.
      SUMETT=0.
      DO 200 I=3,N2,2
      ETAP=(ETA-ETAC)/(1.-ETAC)
      ETAPT=ETAP/TLAM
      FV=FVP(ETAP)
      FT=FTP(ETA
      FVAV=FVAVP(ETAP,FV)
      FTAT=FTATP(ETAPT,FT)
      FTTLAM=FTLAM(ETAPT,ETAP,TLAM)
      SUMEM=SUMEM+FV*CTA*FUNC(FV,FT)
      SUMET=SUMET+FT*ETA*FUNC(FV,FT)
      SUMEMA=SUMEMA+2.*FVAV*ETA*FUNC(FV,FT)+FV*FTAT*ETA*DTM*FUNCT(FV,FT)
      SUMEMT=SUMEMT+FV*FTTLAM*ETA*FUNCT(FV,FT)
      SUMETA=SUMETA+FVAV*ETA*FUN(FT)+FTAT*ETA*FU.C(FT,FV)+FTAT*DTM*FUNCT
     1(FV,FT)*ETA
      SUMETT=SUMC   TLAM*ETA*(FUNC(FV,FT)+DTM*FUNCT(FV,FT))
      ETA=ETA+2.*DETA
  200 CONTINUE
      CM=.5*ETAC*ETAC+(DETA/3.)*(ETAC+4.*SUMOM+2.*SUMEM)
      CT=.5*ETAC*ETAC+(DETA/3.)*(ETAC+4.*SUMOT+2.*SUMET)
      CMALP=(DETA/3.)*(4.*SUMOMA+2.*SUMEMA)
      CMTLAM=(DETA/3.)*(4.*SUMOMT+2.*SUMEMT)*DTM
      CTALP=(DETA/3.)*(4.*SUMOTA+2.*SUMETA)
      CTTLAM=(DETA/3.)*(4.*SUMOTT+2.*SUMETT)
C     WRITE (6,700) TM,ETAC,ALPV,TLAM,CM,CT,CMALP,CMTLAM,CTALP,CTTLAM
  700 FORMAT (1X,10F11.5)
      RETURN
      END



      SUBROUTINE QHALF (TMB,ETAC,ALPV,TLAM,QQ)
      FVP(ETAP)=(1.-ETAP**ALPV)**2
      FTP(ETAP)=(1.-(ETAP/TLAM)**ALPT)**2
      FVETAP(ETAP)=-2.*(1.-ETAP**ALPV)*ALPV*ETAP**(ALPV-1.)
      FTETAP(ETAP)=-2.*(1.-(ETAP/TLAM)**ALPT)*ALPT*((ETAP/TLAM)**(ALPT-1
     1.))*(1./TLAM)
      REL=.5
      ALPT=ALPV
C     WRITE (6,700) TMB,ETAC,ALPV,ALPT
  700 FORMAT (1X,'TMB=',F10.5,2X,'ETAC=',F10.5,2X,'ALPV=',F10.5,2X,'ALPT
     1=',F10.5)
      ETAP=0.
      DETAP=1./24.
      DO 300 I=1,25
      FV=FVP(ETAP)
      FT=FTP(ETAP)
      QOLD=Q
      Q=FV*FV*TMB/(1.+FT*(TMB-1.))
      IF (Q.LT..5.AND.QOLD.GT..5) GO TO 367
      ETAP=ETAP+DETAP
  300 CONTINUE
      STOP
C 367 WRITE (6,557) QOLD,Q
  557 FORMAT (2X,'QO=',F10.5,2X,'Q=',F10.5)
  367 DEDQ=DETAP/(Q-QOLD)
      ETAP=ETAP+DEDQ*(.5-Q)
C     WRITE (6,375) ETAP
  375 FORMAT (2X,'ETAP=',F10.5)
      DELMIN=1.E-5
      DO 100 I=1,500
      FV=FVP(ETAP)
      FT=FTP(ETAP)
      FVETA=FVETAP(ETAP)
      FTETA=FTETAP(ETAP)
      DEN=1.+FT*(TMB-1.)
      FUNC=.5-FV*FV*TMB/DEN
      FUNCD=FV*FV*TMB*(TMB-1.)*FTETA/(DEN*DEN)-2.*FV*FVETA*TMB/DEN
      ETAN=ETAP-FUNC/FUNCD
      ETAP=ETAP+REL*(ETAN-ETAP)
C     WRITE (6,500) ETAP,FUNC
```

Figure 69 - Continued

ORIGINAL PAGE IS
OF POOR QUALITY

```
  500 FORMAT (1X,2F10.5)
      IF (ABS(FUNC).LT.1.E-5) GO TO 200
  100 CONTINUE
      STOP
  200 RO=ETAC+(1.-ETAC)*ETAP
      RETURN
      END



      SUBROUTINE SIMTV (TN,TM,ALPV,TLAM,CM,CT,CMTM,CTTM)
      FVP(ETA)=(1.-ETA**ALPV)**2
      FTP(ETA)=(1.-(ETA/TLAM)**ALPT)**2
      FUNC(ETA,FV,FT)=FV*ETA/(FT+(1.-FT)/TMB)
      FUNCD(ETA,FV,FT)=FV*ETA*((1.-FT)/(TMB*TM))/((FT+(1.-FT)/TMB)**2)
      N=24
      ALPT=ALPV
C     WRITE (6,777) TN,TM,ALPV,ALPT,CM,CT
      TMB=TM*TN
      N1=N-1
      N2=N-2
      DETA=1./N1
      ETA=DETA
      SUMOM=0.
      SUMOT=0.
      SUMOTM=0.
      SUMOCM=0.
      DO 100 I=1,N1,2
      FV=FVP(ETA)
      FT=FTP(ETA)
      SUMOM=SUMOM+FV*FUNC(ETA,FV,FT)
      SUMOT=SUMOT+FT*FUNC(ETA,F  ,FT)
      SUMOCM=SUMOCM+FV*FUNCD(ET ,FV,FT)
      SUMOTM=[illegible]+FT*FUNCD(ETA,FV,FT)
      ETA=ETA+2.*DETA
  100 CONTINUE
      ETA=2.*DETA
      SUMEM=0.
      SUMET=0.
      SUMECM=0.
      SUMETM=0.
      DO 200 I=3,N2,2
      FV=FVP(ETA)
      FT=FTP(ETA)
      SUMEM=SUMEM+FV*FUNC(ETA,FV,FT)
      SUMET=SUMET+FT*FUNC(ETA,FV,FT)
      SUMECM=SUMECM+FV*FUNCD(ETA,FV FT)
      SUMETM=SUMETM+FT*FUNCD(ETA,FV,F )
      ETA=ETA+2.*DETA
  200 CONTINUE
      CM=(DETA/3.)*(4.*SUMOM+2.*SUMEM)
      CT=(DETA/3.)*(4.*SUMOT+2.*SUMET)
      CMTM=(DETA/3.)*(4.*SUMOCM+2.*SUMECM)
      CTTM=(DETA/3.)*(4.*SUMOTM+2.*SUMETM)
C     WRITE (6,777) TN,TM,ALPV,ALPT,CM,CT
  777 FORMAT (1X,6F10.5)
      RETURN
      END



      SUBROUTINE GPREST (RO,VG,THG,ALPG,R,CPG)
      FUNC(ALP)=.5-4./(ALP+2.)+3./(ALP+1.)-4./(3.*ALP+2.)+1./(4.*ALP
     1+2.)
      FUNCD(ALP)=4./((ALP+2.)**2)-3./((ALP+1.)**2)+12./((3.*ALP+2.)**2)
     1-4./((4.*ALP+2.)**2)
C
C  THIS ROUTINE SOLVES GROUND PRESSURE INTEGRAL FOR GROUND PRESSURE
C   EXPONENT
C
      ALPG=1.5
      REL=.5
      DELMIN=1.E-5
      DO 100 I=1,99
      CPG=FU C(ALPG)
      CPGP=F NCD(ALPG)
      F=THG-RO*RO*VG*VG*CPG
      FP=-RO*RO*VG*VG*CPGP
      ALPG=ALPG-REL*F/FP
C     WRITE (6,500) ALPG,CPG,CPGP,
```

Figure 69 - Continued

```
  500 FORMAT (1X,4F15.5)
      IF (ABS(F).LT.DELMIN) GO TO 101
  100 CONTINUE
      STOP
  101 RETURN
      END



      SUBROUTINE SIMW(KDEL,N,ALPW,R,CV2,CP)
C
C   THIS ROUTINE COMPUTES THE INTEGRAL OF THE VELOCITY SQUARED PROFILE
C   AND STATIC PRESSURE PROFILE FOR WALL JET FUNCTIONS
C     CV2=VELOCITY SQUARED INTEGRAL
C     CP=STATIC PRESSURE INTEGRAL
C     R=RATIO OF BWH TO BW
C
      REAL KDEL,N
      XN=N
      XI1=1.-4./(ALPW+1.)+6./(2.*ALPW+1.)-4./(3.*ALPW+1.)+1./(4.*ALPW+1.
     1)
      CV2=(XN/(2.+XN))*KDEL+(1.-KDEL)*XI1
      CP=KDEL+(1.-KDEL)*XI1
      F=((2.-SQRT(2.))/2.)**(1./ALPW)
      R=KDEL+(1.-KDEL)*F
C     WRITE (6,500) CV2,CP
  500 FORMAT (1X,'CV2=',F10.5,2X,'CP=',F10.5)
      RETURN
      END



      SUBROUTINE SIMUG(ALPU,R,CV2U)
C
C   THIS ROUTINE COMPUTES VELOCITY  QUARED INTEGRAL FOR UPWASH
C
      CV2U=1.-4./(ALPU+1.)+6./(2.*ALPU+1.)-4./(3.*ALPU+1.)+1./(4.*ALPU+1
     1.)
      F=(SQRT(2.)-1.)/SQRT(2.)
      R=F**(1./ALPU)
      RETURN
      END



      SUBROUTINE GMATT (TN,RG,DELPS,PMBI,TMI,VMI,ALPG,KDEL,N,ETAWG,DELS
     1,ALPW,R,BWO,BWOH,TLAM)
C
C   THIS ROUTINE IS USED FOR INITIATING WALL JET REGION
C     COMPUTES THE INTIAL INVISCID EXPONENT FOR WALL JET PROFILE
C
      REAL KDEL,N
      BWO=DELS/KDEL
      TLAM=1.1
      ALPW=.5
      CALL SIMWH (TN,TMI,TLAM,PMBI,KDEL,N,ALPW,ALPG,ETAWG,DELPS,VMI,
     1BWO,RG)
      RCON=(2.-SQRT(2.))/2.
      R=KDEL+(1.-KDEL)*RCON**(1./ALPW)
      BWOH=R*BWO
C     WRITE (6,709) TLAM,ALPW,BWO,BWOH
  709 FORMAT (1X,'TLAM=',F10.5,2X,'ALPW=',F10.5,2X,'BWO=',F10.5,2X,'BWOH
     1=',F10.5)
      RETURN
      END



      SUBROUTINE SIMWH(TN,TM,TLAM,PMB,KDEL,N,ALPW,ALPG,ETAWG,DELPS,VM,
     1BW,RG)
      REAL KDEL,N
      TMB=TM*TN
      REL=.5
      DELMIN=1.E-5
      FETAG=(1.-ETAWG**ALPG)**4
      FMOM=1.-FETAG
C     WRITE (6,400) FETAG,FMOM,BW,RG
```

Figure 69 - Continued

ORIGINAL PAGE IS
OF POOR QUALITY

```
  400 FORMAT (1X,'FETAG',4F10.5)
      DO 100 I=1,200
      CALL SIMUTI (TN,TM,TLAM,PMB,KDEL,N,ALPW,CV2,CP,CT,CV2A,CV2L
     1,CPA,CTA,CTL,R,RALP)
C     WRITE (6,740) CV2,CP,CT,CV2A,CV2L,CPA,CTA,CTL,R
  740 FORMAT (1X,9F10.5)
      F=FMOM-RG*BW*(2.*PMB*VM*VM*CV2/TM+DELPS*FETAG*CP)
      G=FMOM*TM*(TN-1.)-2.*PMB*VM*(TMB-1.)*RG*BW*CT
      FALP=-RG*BW*(2.*PMB*VM*VM*CV2A/TM+DELPS*FETAG*CPA)
      FLAM=-RG*BW*(2.*PMB*VM*VM*CV2L/TM)
      GALP=-2.*PMB*VM*(TMB-1.)*RG*BW*CTA
      GLAM=-2.*PMB*VM*(TMB-1.)*RG*BW*CTL
C     WRITE (6,750) FALP,FLAM,GALP,GLAM
  750 FORMAT (1X,'FA=',F10.5,1X,'FL=',F10.5,1X,'GA=',F10.5,1X,'GL=',F10.
     15)
      DET=FALP*GLAM-FLAM*GALP
      DALP=(G*FLAM-F*GLAM)/DET
      DLAM=(F*GALP-G*FALP)/DET
      ALPW=ALPW+REL*DALP
      TLAM=TLAM+REL*DLAM
C     WRITE (6,500) F,G,ALPW,TLAM
      IF (ABS(F).LT.DELMIN.AND.ABS(G).LT.DELMIN) GO TO 101
  500 FORMAT (1X,4F15.5)
  100 CONTINUE
      STOP
  101 CONTINUE
      RETURN
      END



      SUBROUTINE SIMUTI (TN,TM,TLAM,PMB,KDEL,N,ALPV,CV2,CP,CT,CV2A,CV2L
     1,CPA,CTA,CTL,R,RALP)
      REAL KDEL,N
      FVP(ETAP)=(1.-ETAP**ALPV)**2
      FTP(ETAP)=(1.-(ETAP/TLAM)**ALPT)**2
      FVA(ETAP)=-2.*(ETAP**ALPV)*(1.-ETAP**ALPV)*ALOG(ETAP)
      FTA(ETAPT)=-2.*(ETAPT**ALPT)*(1.-ETAPT**ALPT)*ALOG(ETAPT)
      FPA(ETAP)=-4.*(ETAP**ALPV)*((1.-ETAP**ALPV)**3)*ALOG(ETAP)
      FTL(ETAPT)=2.*(1.-ETAPT**ALPT)*ALPT*(ETAPT**ALPT)/TLAM
      FUNC(FV,FT,FP)=FV*(FP+(1.-FP)/PMB)/(FT+(1.-FT)/TMB)
      FUNCD(FV,FT,FP)=FV*(FP+(1.-FP)/PMB)/((FT+(1.-FT)/TMB)**2)
      FUN(FV,FT)=FT*(FP+(1.-FP)/PMB)/(FT+(1.-FT)/TMB)
      FUNT(FV,FT)=FV*FT/(FT+(1.-FT)/TMB)
      NPTS=24
      ALPT=ALPV
C     WRITE (6,777) TN,TM,ALPV,ALPT,CM,CT
      TMB=TM*TN
      DTM=(1.-TMB)/TMB
      DPM=(PMB-1.)/PMB
      N1=NPTS-1
      N2=NPTS-2
      XN1=N1
      DETA=(1.-KDEL)/XN1
      ETA=KDEL+DETA
      SUMOM=0.
      SUMOT=0.
      SCV2AO=0.
      SCV2LO=0.
      SCTAO=0.
      SCTLO=0.
      DO 100 I=1,N1,2
      ETAP=(ETA-KDEL)/(1.-KDEL)
      ETAPT=ETAP/TLAM
      IF (ETAPT.GT.1.) ETAPT=1.
      FV=FVP(ETAP)
      FT=FTP(ETAP)
      FP=FV*FV
      FVALP=FVA(ETAP)
      FTALP=FTA(ETAPT)
      FPALP=FPA(ETAP)
      FTLAM=FTL(ETAPT)
      SUMOM=SUMOM+FV*FUNC(FV,FT,FP)
      SUMOT=SUMOT+FT*FUNC(FV,FT,FP)
```

Figure 69 - Continued

```
      SCV2AO=SCV2AO+FUNC(FV,FT,FP)*(2.*FVALP+FV*FPALP*DPM)
     1+FUNCD(FV,FT,FP)*FV*FTALP*DTM
      SCV2LO=SCV2LO+FUNCD(FV,FT,FP)*FV*FTLAM*DTM
      SCTAO=SCTAO+FVALP*FUN(FT,FP)+FUNC(FV,FT,FP)*FTALP
     1+FUNT(FV,FT)*FPALP*DPM+FUNCD(FV,FT,FP)*FT*FTALP*DTM
      SCTLO=SCTLO+FUNC(FV,FT,FP)*FTLAM+FUNCD(FV,FT,FP)*FT*FTLAM*DTM
      ETA=ETA+2.*DETA
  100 CONTINUE
      ETA=KDEL+2.*DETA
      SUMEM=0.
      SUMET=0.
      SCV2AE=0.
      SCV2LE=0.
      SCTAE=0.
      SCTLE=0.
      DO 200 I=3,N2,2
      ETAP=(ETA-KDEL)/(1.-KDEL)
      ETAPT=ETAP/TLAM
      IF (ETAPT.GT.1.) ETAPT=1.
      FV=FVP(ETAP)
      FT=FTP(ETAP)
      FP=FV*FV
      FVALP=FVA(ETAP)
      FTALP=FTA(ETAPT)
      FPALP=FPA(ETAP)
      FTLAM=FTL(ETAPT)
      SUMEM=SUMEM+FV*FUNC(FV,FT,FP)
      SUMET=SUMET+FT*FUNC(FV,FT,FP)
      SCV2AE=SCV2AE+FUNC(FV,FT,FP)*(2.*FVALP+FV*FPALP*DPM)
     1+FUNCD(FV,FT,FP)*FV*FTALP*DTM
      SCV2LE=SCV2LE+FUNCD(FV,FT,FP)*FV*FTLAM*DTM
      SCTAE=SCTAE+FVALP*FUN(FT,FP)+FUNC(FV,FT,FP)*FTALP
     1+FUNT(FV,FT)*FPALP*DPM+FUNCD(FV,FT,FP)*FT*FTALP*DTM
      SCTLE=SCTLE+FUNC(FV,FT,FP)*FTLAM+FUNCD(FV,FT,FP)*FT*FTLAM*DTM
      ETA=ETA+2.*DETA
  200 CONTINUE
      CV2=N*KDEL/(2.+N)+(DETA/3.)*(1.+4.*SUMOM+2.*SUMEM)
      CT=N*KDEL/(1.+N)+(DETA/3.)*(1.+4.*SUMOT+2.*SUMET)
      CV2A=(DETA/3.)*(4.*SCV2AO+2.*SCV2AE)
      CV2L=(DETA/3.)*(4.*SCV2LO+2.*SCV2LE)
      CTA=(DETA/3.)*(4.*SCTAO+2.*SCTAE)
      CTL=(DETA/3.)*(4.*SCTLO+2.*SCTLE)
      CPF=1.-4./(ALPV+1.)+6./(2.*ALPV+1.)-4./(3.*ALPV+1.)+1./(4.*ALPV+1.
     1)
      CPFD=4./((ALPV+1.)**2)-12./((2.*ALPV+1.)**2)+12./((3.*ALPV+1.)**2)
     1-4./((4.*ALPV+1.)**2)
      CP=KDEL+(1.-KDEL)*CPF
      CPA=(1.-KDEL)*CPFD
      RCON=(2.-SDRT(2.))/2.
      R=KDEL+(1.-KDEL)*RCON**(1./ALPV)
      RP=(R-KDEL)/(1.-KDEL)
      RALP=(KDEL-1.)*RP*ALOG(RP)/ALPV
C     WRITE (6,777) TN,TM,ALPV,ALPT,CV2,CP,CT
  777 FORMAT (1X,7F10.5)
      RETURN
      END



      SUBROUTINE SIMWTV (TN,TM,TLAM,PMB,KDEL,N,ALPV,CV2,CP,CT,CV27M,CTTM
     1,R)
      REAL KDEL,N
      FVP(ETAP)=(1.-ETAP**ALPV)**2
      FTP(ETAP)=(1.-(ETAP/TLAM)**ALPT)**2
      FUNC(FV,FT,FP)=FV*(FP+(1.-FP)/PMB)/(FT+(1.-FT)/TMB)
      FUNCD(FV,FT,FP)=FV*((1.-FT)/(TMB*TM))*(FP+(1.-FP)/PMB)/((FT+(1.-FT
     1)/TMB)**2)
      NPTS=24
      ALPT=ALPV
C     WRITE (6,777) TN,TM,ALPV,ALPT,CM,CT
      TMB=TM*TN
      DTM=(1.-TMB)/TMB
      DPM=(PMB-1.)/PMB
      N1=NPTS-1
      N2=NPTS-2
      XN1=N1
      DETA=(1.-KDEL)/XN1
      ETA=KDEL+DETA
      SUMOM=0.
```

Figure 69 - Continued

```
      SUMOT=0.
      SCV2TO=0.
      SCTMO=0.
      DO 100 I=1,N1,2
      ETAP=(ETA-KDEL)/(1.-KDEL)
      ETAPT=ETAP/TLAM
      IF (ETAPT.GT.1.) ETAPT=1.
      FV=FVP(ETAP)
      FT=FTP(ETAP)
      FP=FV*FV
      SUMOM=SUMOM+FV*FUNC(FV,FT,FP)
      SUMOT=SUMOT+FT*FUNC(FV,FT,FP)
      SCV2TO=SCV2TO+FUNCD(FV,FT,FP)*FV
      SCTMO=SCTMO+FUNCD(FV,FT,FP)*FT
      ETA=ETA+2.*DETA
  100 CONTINUE
      ETA=KDEL+2.*DETA
      SUMEM=0.
      SUMET=0.
      SCV2TE=0.
      SCTME=0.
      DO 200 I=3,N2,2
      ETAP=(ETA-KDEL)/(1.-KDEL)
      ETAPT=ETAP/TLAM
      IF (ETAPT.GT.1.) ETAPT=1.
      FV=FVP(ETAP)
      FT=FTP(ETAP)
      FP=FV*FV
      SUMEM=SUMEM+FV*FUNC(FV,FT,FP)
      SUMET=SUMET+FT*FUNC(FV,FT,FP)
      SCV2TE=SCV2TE+FUNCD(FV,FT,FP)*FV
      SCTME=SCTME+FUNCD(FV,FT,FP)*FT
      ETA=ETA+2.*DETA
  200 CONTINUE
      CV2=N*KDEL/(2.+N)+(DETA/3.)*(1.+4.*SUMOM+2.*SUMEM)
      CT=N*KDEL/(1.+N)+(DETA/3.)*(1.+4.*SUMOT+2.*SUMET)
      CV2TM=(DETA/3.)*(4.*SCV2TO+2.*SCV2TE)
      CTTM=(DETA/3.)*(4.*SCTMO+2.*SCTME)
      CPF=1.-4./(ALPV+1.)+6./(2.*ALPV+1.)-4./(3.*ALPV+1.)+1./(4.*ALPV+1.
     1)
      CP=KDEL+(1.-KDEL)*CPF
      RCON=(2.-SQRT(2.))/2.
      R=KDEL+(1.-KDEL)*RCON**(1./ALPV)
C     WRITE (6,777) TN,TM,ALPV,ALPT,CV2,CP,CT
  777 FORMAT (1X,7F10.5)
      RETURN
      END


      SUBROUTINE PGUMAT(CUFD,DELPS,DELPW,RO,SD,ALPG,ALPUG)
      DIMENSION ERR(101),SIG(101)
C
C   THIS ROUTINE COMPUTES EXPONENT OF UPWASH GROUND PRESSURE PROFILE
C
      SIG(1)=.10
       SIG(2)=1.0
      ALPUFD=1.5
      DO 100 I=1,100
      PB=(DELPS/DELPW)**(.25)
      ETAG=SD*(1.-SIG(I))/RO
      ETAU=SIG(I)/CUFD
      F1=PB*(1.-ETAG**ALPG)
      F2=1.-ETAU**ALPUFD
      ERR(I)=F1-F2
      IF (I.EQ.1) GO TO 100
      S=(SIG(I)-SIG(I-1))/(ERR(I)-ERR(I-1))
      IF (ABS(ERR(I)).LT.1.E-5) GO TO 101
      SIG(I+1)=SIG(I)-S*ERR(I)
  100 CONTINUE
      STOP
  101 SIGUO=SIG(I)
      ETAM=SIGUO/CUFD
      IF (ETAM.GT.1.0) ETAM=1.0
      PMIN=DELPW*(1.-ETAM**ALPUFD)**4
      CALL PMATCH (PMIN,DELPW,ALPUG)
      RETURN
      END
```

Figure 69 - Continued

```
      SUBROUTINE PMATCH (PMIN,PMAX,ALPUG)
      DIMENSION ERR(101),AL(101)
C
C    THIS ROUTINE COMPUTES THE EXPONENT OF THE PRESSURE PROFILE FOR
C    THE UPWASH DEFLECTION ZONE
C
      ALPUFD=1.
      PB=PMIN/PMAX
      ETAM=(1.-PB**.25)**(1./ALPUFD)
      CALL SIMUF(ALPUFD,ETAM,CSPUFD)
      AL(1)=1.5
      AL(2)=3.0
      DO 100 I=1,100
      CALL SIMUF(AL(I),1.0,CSPU)
      X1=ETAM*(PB+(1.-PB)*CSPU)
      X2=CSPUFD
      ERR(I)=X1-X2
      IF (ABS(ERR(I)).LT.1.E-5) GO TO 101
      IF (I.EQ.1) GO TO 100
      S=(AL(I)-AL(I-1))/(ERR(I)-ERR(I-1))
      AL(I+1)=AL(I)-S*ERR(I)
  100 CONTINUE
      STOP
  101 ALPUG=AL(I)
      RETURN
      END


      SUBROUTINE SIMUF(ALPU,ETA,CSPU)
      A1=ETA
      A2=-(4./(ALPU+1.))*ETA**(ALPU+1.)
      A3=(6./(2.*ALPU+1.))*ETA**(2.*ALPU+1.)
      A4=-(4./(3.*ALPU+1.))*ETA**(3.*ALPU+1.)
      A5=(1./(4.*ALPU+1.))*ETA**(4.*ALPU+1.)
      CSPU=A1+A2+A3+A4+A5
      RETURN
      END


      SUBROUTINE SIM(ETAC,ALP,R,CV2)
C
C   INTEGRAL OF JET VELOCITY PROFILE FUNCTION=CV2
C    R=RATIO OF BJH TO BJ
C
      A1=.5-4./(ALP+2.)+3./(ALP+1.)-4./(3.*ALP+2.)+1./(4.*ALP+2)
      A2=1.-4./(ALP+1.)+6./(2.*ALP+1.)-4./(3.*ALP+1.)+1./(4.*ALP+1.)
      CV2=.5*ETAC**2+A1*(1.-ETAC)**2+ETAC*(1.-ETAC)*A2
      R=ETAC+(1.-ETAC)*((2.-SQRT(2.))/2.)**(1./ALP)
      RETURN
      END


      SUBROUTINE SIMU(ALPU,R,CV2U)
      CV2U=1.-4./(ALPU+1.)+6./(2.*ALPU+1.)-4./(3.*ALPU+1.)+1./(4.*ALPU+
     1.)
      F=(SQRT(2.)-1.)/SQRT(2.)
      R=F**(1./ALPU)
      RETURN
      END


      SUBROUTINE SIMUM(TN,TM,TLAM,FMB,ALPU,FETAG,DELPWS,VM,BU,RG,R,FM
     1TNEFF,TAEFF)
C     WRITE (6,111) PMB,VM
  111 FORMAT (1X,'PMB=',F10.5,2X, VM=',F10.5)
      TMB=TM*TN
      REL=.5
      IFLAG=0
      DELMIN=1.E-5
      TLAM=1.0
      TLAMI=TLAM
C     WRITE (6,400) FETAG,FMOM,BU,RG
```

Figure 69 - Continued

```
  400 FORMAT (1X,'FETAG',4F10.5)
      DO 100 I=1,50
      CALL SIMUTI (TN,TM,TLAM,PMB,ALPU,CV2,CP,CT,CV2L,CTL,R)
      IF (I.EQ.1) BU=FMOM/(RG*CV2*(2.
     1*VM**2+DELPUS*FETAG))
      IF (I.EQ.1) BUI=BU
C     WRITE (6,740) CV2,CP,CT,CV2L,CTL,R
  740 FORMAT (1X,6F10.5)
C     IF (I.EQ.1) WRITE (6,103) BU
  103 FORMAT (1X,'BU EST.=',F10.5)
      F=FMOM-RG*(2.*PMB*VM*VM*CV2/TM+DELPUS*FETAG*CP)
      G=FMOM*TM*(TM-1.)-2.*PMB*VM*(TMB-1.)*RG*BU*CT
      FBU=-RG*(2.*PMB*VM*VM*CV2/TM+DELPUS*FETAG*CP)
      FLAM=-RG*BU*(2.*PMB*VM*VM*CV2L/TM)
      GBU=-2.*PMB*VM*(TMB-1.)*RG*CT
      GLAM=-2.*PMB*VM*(TMB-1.)*RG*BU*CTL
C     WRITE (6,750) FBU,FLAM,GBU,GLAM
  750 FORMAT (1X,'FA=',F10.5,1X,'FL=',F10.5,1X,'GA=',F10.5,1X,'GL=',F10.
     15)
      DET=FBU*GLAM-FLAM*GBU
      IF (ABS(DET).LT.1.E-10) ILFAG=1
      IF (ABS(DET).LT.1.E-10) GO TO 101
      DBU=(G*FLAM-F*GLAM)/DET
      DLAM=(F*GBU-G*FBU)/DET
      BU=BU+REL*DBU
      TLAM=TLAM+REL*DLAM
      IF (TLAM.LT.0.) IFLAG=1
      IF (TLAM.LT.0.) GO TO 101
C     WRITE (6,500) F,G,BU,TLAM
      IF (ABS(F).LT.DELMIN.AND.ABS(G).LT.DELMIN) GO TO 101
  500 FORMAT (1X,4F15.5)
  100 CONTINUE
      STOP
  101 IF (IFLAG.EQ.1) BU=BUI
      IF (IFLAG.EQ.1) TLAM=TLAMI
      RETURN
      END



      SUBROUTINE SIMUTI (TN,TM,TLAM,PMB,ALFV,CV2,CP,CT,CV2L,CTL,R)
      FVP(ETAP)=(1.-ETAP**ALFV)**2
      FTP(ETAP)=(1.-(ETAP/TLAM)**ALPT)**2
      FTL(ETAPT)=2.*(1.-ETAPT**ALPT)*ALPT*(ETAPT**ALPT)/TLAM
      FUNC(FV,FT,FP)=FV*(FP+(1.-FP)/PMB)/(FT+(1.-FT)/TMB)
      FUNCD(FV,FT,FP)=FV*(FP+(1.-FP)/PMB)/((FT+(1.-FT)/TMB)**2)
      NPTS=24
      ALPT=ALFV
C     WRITE (6,777) TN,TM,ALFV,ALPT,CM,CT
      TMB=TM*TN
      DTM=(1.-TMB)/TMB
      DPM=(PMB-1.)/PMB
      N1=NPTS-1
      N2=NPTS-2
      XN1=N1
      DETA=1./XN1
      ETA=DETA
      SUMOM=0.
      SUMOT=0.
      SCV2LO=0.
      SCTLO=0.
      DO 100 I=1,N1,2
      ETAP=ETA
      ETAPT=ETAP/TLAM
      IF (ETAPT.GT.1.) ETAPT=1.
      FV=FVP(ETAP)
      FT=FTP(ETAP)
      FP=FV*FV
      FTLAM=FTL(ETAPT)
      SUMOM=SUMOM+FV*FUNC(FV,FT,FP)
      SUMOT=SUMOT+FT*FUNC(FV,FT,FP)
      SCV2LO=SCV2LO+FUNCD(FV,FT,FP)*FV*FTLAM*DTM
      SCTLO=SCTLO+FUNC(FV,FT,FP)*FTLAM+FUNCD(FV,FT,FP)*FT*FTLAM*DTM
      ETA=ETA+2.*DETA
```

Figure 69 - Continued

```
  100 CONTINUE
      ETA=2.*DETA
      SUMEM=0.
      SUMET=0.
      SCV2LE=0.
      SCTLE=0.
      DO 200 I=3,N2,2
      ETAP=ETA
      ETAPT=ETAP/TLAM
      IF (ETAPT.GT.1.) ETAPT=1.
      FV=FVP(ETAP)
      FT=FTP(ETAP)
      FP=FV*FV
      FTLAM=FTL(ETAPT)
      SUMEM=SUMEM+FV*FUNC(FV,FT,FP)
      SUMET=SUMET+FT*FUNC(FV,FT,FP)
      SCV2LE=SCV2LE+FUNCD(FV,FT,FP)*FV*FTLAM*DTM
      SCTLE=SCTLE+FUNC(FV,FT,FP)*FTLAM+FUNCD(FV,FT,FP)*FT*FTLAM*DTM
      ETA=ETA+2.*.
  200 CONTINUE
      CV2=(DETA/3.)*(1.+4.*SUMOM+2.*SUMEM)
      CT=(DETA/3.)*(1.+4.*SUMOT+2.*SUMET)
      CV2L=(DETA/3.)*(4.*SCV2LO+2.*SCV2LE)
      CTL=(DETA/3.)*(4.*SCTLO+2.*SCTLE)
      CP=1.-4./(ALPV+1.)+6./(2.*ALPV+1.)-4./(3.*ALPV+1.)+1./(4.*ALPV+1.
     .)
      RCON=(2.-SQRT(2.))/2.
      R=RCON**(1./ALPV)
C     WRITE (6,777) TN,TM,ALPV,ALPT,CV2,CP,CT
  777 FORMAT (1X,7F10.5)
      RETURN
      END



      SUBROUTINE SIMUTV (TN,TM,TLAM,PMB,ALPV,CV2,CP,CT,CV2TM,CTTM,R)
      FVP(ETAP)=(1.-ETAP**ALPV)**2
      FTP(ETAP)=(1.-(ETAP/TLAM)**ALPT)**2
      FUNC(FV,FT,FP)=FV*(FP+(1.-FP)/PMB)/(FT+(1.-FT)/TMB)
      FUNCD(FV,FT,FP)=FV*((1.-FT)/(TMB*TM))*(FP+(1.-FP)/PMB)/((FT+(1.-FT
     1)/TMB)**2)
      NPTS=24
      ALPT=ALPV
C     WRITE (6,777) TN,TM,ALPV,ALPT,CM,CT
      TMB=TM*TN
      DTM=(1.-TMB)/TMB
      DPM=(PMB-1.)/PMB
      N1=NPTS-1
      N2=NPTS-2
      XN1=N1
      DETA=1./XN1
      ETA=DETA
      SUMOM=0.
      SUMOT=0.
      SCV2TO=0.
      SCTMO=0.
      DO 100 I=1,N1,2
      ETAP=ETA
      ETAPT=ETAP/TLAM
      IF (ETAPT.GT.1.) ETAPT=1.
      FV=FVP(ETAP)
      FT=FTP(ETAP)
      FP=FV*FV
      SUMOM=SUMOM+FV*FUNC(FV,FT,FP)
      SUMOT=SUMOT+FT*FUNC(FV,FT,FP)
      SCV2TO=SCV2TO+FUNCD(FV,FT,FP)*FV
      SCTMO=SCTMO+FUNCD(FV,FT,FP)*FT
      ETA=ETA+2.*DETA
```

Figure 69 - Continued

```
  100 CONTINUE
      ETA=2.*DETA
      SUMEM=0.
      SUMET=0.
      SCV2TE=0.
      SCTME=0.
      DO 200 I=3,N2,2
      ETAP=ETA
      ETAPT=ETAP/TLAM
      IF (ETAPT.GT.1.) ETAPT=1.
      FV=FVP(ETAP)
      FT=FTP(ETAP)
      FP=FV*FV
      SUMEM=SUMEM+FV*FUNC(FV,FT,FP)
      SUMET=SUMET+FT*FUNC(FV,FT,FP)
      SCV2TE=SCV2TE+FUNCD(FV,FT,FP)*FV
      SCTME=SCTME+FUNCD(FV,FT,FP)*FT
      ETA=ETA+2.*DETA
  200 CONTINUE
      CV2=(DETA/3.)*(1.+4.*SUMOM+2.*SUMEM)
      CT=(DETA/3.)*(1.+4.*SUMOT+2.*SUMET)
      CV2TM=(DETA/3.)*(4.*SCV2TO+2.*SCV2TE)
      CTTM=(DETA/3.)*(4.*SCTMO+2.*SCTME)
      CPF=1.-4./(ALPV+1.)+6./(2.*ALPV+1.)-4./(3.*ALPV+1.)+1./(4.*ALPV+1.
     1)
      CP=CPF
      RCON=(2.-SQRT(2.))/2.
      R=RCON**(1./ALPV)
C     WRITE (6,777) TN,TM,ALPV,ALPT,CV2,CP,CT
  777 FORMAT (1X,7F10.5)
      RETURN
      END
```

Figure 69 - Concluded.

## 8 - REFERENCES


1. Full-Scale Tests of Grumman Design 698-411 Tilt-Nacelle V/STOL Model at the NASA-Ames Research Center, Grumman Report PDR 698-53, December, 1981.

2. Hill, W.G., Jr., and Jenkins, R.C., "Experimental Investigation of Multiple Jet Impingement Flows Applicable to VTOL Aircraft in Ground Effect", Grumman Research Department Memorandum RM-605, November 1975.

3. Migdal, D., Hill, W.G., Jr., Jenkins, R.C. and Siclari, M.J., "VTOL in Ground Effect Flows for Closely Spaced Jets", NASA CR 152321, Dec. 1979.

4. Jenkins, R.A. and Hill, W.G., Jr., "Investigation of VTOL Upwash Flows Formed by Two Impinging Jets," Grumman Research Department RE-548, November 1977.

5. Platzer, M.F. and Margason, R.J., "Prediction Methods for Jet V/STOL Propulsion Aerodynamics", Jr. of Aircraft, Vol. 15, No. 2, pp. 69-77, Feb. 1978.

6. Siclari, M.J., Migdal, D., and Palcza, J.L., "The Development of Theoretical Models for Jet-Induced Effects on V/STOL Aircraft", AIAA Paper No. 75-1216, AIAA/SAE 11th Propulsion Conference, Anaheim, Cal., Sept. 29-Oct. 1, 1975.

7. Siclari, M.J., Hill W.G., Jr., and Jenkins, R.C., "Investigation of Stagnation Line and Upwash Formation", AIAA Paper No. 77-615, AIAA/NASA, Ames V/STOL Conference, June 1977.

8. Schlicting, H., Boundary Layer Theory, McGraw Hill, 1960

9. Reichardt, H., Gesetzmer Bigkeiten der freien Turbulenz, VDI - Forschungsheft, 414 (1942), 2 ed. 1951.

10. Abramovich, G.H., The Theory of Turbulent Jets, MIT Press, 1963.

11. Harsha, P.T., "Free Turbulent Mixing: A Critical Evaluation of Theory and Experiment", AEDC-TR-71-36, Feb. 1971.

12. Schauer, J.J., and Eustis, R.H., "The Flow Development and Heat Transfer Characteristics of Plane Turbulent Impinging Jets", NSF 69705, Sept. 1963.

13. Corrsin, S. and Uberoi, M., "Further Experiments on the Flow and Heat Transfer in a Heated Turbulent Air Jet", NACA Report 998, 1947.

14. Giralt, F.G., Chia, C.J., and Trass, O., "Characterization of the Impingement Region in an Axisymmetric Turbulent Jet", Industrial Engineering Chemistry, Fundamentals, Vol. 16, No. 1, 1977.